2005

Implementation of manifold bridge tuning for noise control of an automotive intake system.

Colin Novak
University of Windsor

IMPLEMENTATION OF MANIFOLD BRIDGE TUNING FOR NOISE CONTROL OF AN AUTOMOTIVE INTAKE SYSTEM

by

Colin Novak

A Dissertation
Submitted to the
Faculty of Graduate Studies and Research
through the Department of
Mechanical, Automotive and Materials Engineering
in Partial Fulfilment of the Requirements for the
Degree of Doctor of Philosophy
at the University of Windsor

Windsor, Ontario, Canada
2005

0-494-09724-8

Your file Votre référence
ISBN:
Our file Notre référence
ISBN:

ABSTRACT

The considerable effort invested by automobile manufacturers to attenuate various noise sources within the passenger compartment has resulted in other sources such as induction noise having become more noticeable. This study was undertaken to investigate the feasability of using a non conventional noise cancellation technique to improve the acoustic performance of the induction system by introducing exhaust noise into the intake system through a manifold bridge.

The effectiveness of this technique was first investigated using Ricardo Wave, a computational, engine simulation, software program. Using a one-dimensional, finite-difference approach to analyse the dynamics of the pressure waves, mass flows, and energy losses within the ducts, an optimized bridge configuration was determined. A physical model incorporating the design of the optimized bridge was installed and tested on a motored engine for comparison to the numerical results.

The realized attenuation of induction noise due to the manifold bridge was evaluated using 1/12th octave frequency spectra and three-dimensional colour maps of both the unmodified and bridged engine for steady state and transient engine cases. A sound quality analysis was also performed using various psychoacoustic metrics including loudness, sharpness, roughness and fluctuation strength.

Both the numerical and experimental models demonstrated reductions in the overall sound level measured at the intake opening with the experimental results being more favourable. While the results of the sound quality analysis correlated well between the numerical and experimental models, the success of the bridging technique was somewhat

ambiguous, depending on the sound quality metric used. As with the traditional analysis techniques, the reported loudness was lower for the numerical and experimental bridged engines. Sharpness was found not to be a relevant metric in this study due to a lack of high frequency content to the noise. Depending on the engine speed, values for roughness and fluctuation strength were either improved or diminished with the implementation of the manifold bridge.

For the conditions tested, implementation of the manifold bridge has demonstrated promise. Before it can be declared commercially viable, however, further considerations such as the effects of exhaust gas recirculation and fired engine tests, are warranted.

DEDICATION

Dedicated to my family and friends for all their support and patience..

ACKNOWLEDGEMENTS

I would like to express gratitude to my advisor and friend, Dr. Robert Gaspar for his kindness, direction and technical assistance throughout the period of this study. Thanks is also extended to my committee members, Dr. E. Tam, Dr. M. Zheng and Dr. P. Henshaw and to my friend Stewart McLellan for all their assistance. Special recognition is given to Helen Ule for which a successful outcome to this project would not have been possible without her assistance and support.

TABLE OF CONTENTS

LIST OF TABLES

LIST OF FIGURES

NOMENCLATURE

A	area of resonator neck (m^3)
AC/DC	alternating current/direct current
ANC	active noise control
BDC	bottom dead centre
c	speed of sound (m/s)
cc	cubic centimetres (cm^3)
dB	decibel
dBA	A- weighted decibel
D	diameter of the duct (m)
DC	direct current
DFT	discrete Fourier transform
EGR	exhaust gas recirculation
F_F	face area of silencer (m^2)
f_n	natural frequency of resonator (Hz)
FEM	finite element modelling
FFT	fast Fourier transform
hp	horsepower
Hz	hertz (cycles per second)
kHz	kilohertz (1000 cycles per second)
kPa	kilopascal
L	length of resonator connecting pipe (m)
L_W	overall flow-generated noise power level (dB)
mm	millimetres
NVH	noise, vibration and harshness
p	pressure (Pa)
Pa	pascals
p_0	initial pressure (Pa)
P_{amb}	atmospheric pressure (Pa)
P_{area}	percentage of open area of the silencer cross section (%)
PC	personal computer
p_{tot}	total pressure (Pa)
PWL_{oct}	octave band sound power level (dB)
RMS	root mean square

rpm	revolutions per minute
S	cross section (m^2)
SPL	sound pressure level
t	time (s)
T	mean gas temperature (^0F)
TDA	time domain averaging
TDC	top dead centre
u	particle velocity (m/s)
V	volume of the resonator (m^3)
Δt	sampling width (s)
η_W	efficiency factor (dB)
μ_f	mean face velocity in silencer (m/s)
π	pi
ρ	density (kg/m^3)
ρ_0	initial density (kg/m^3)
ρ_{tot}	total density (kg/m^3)

I. INTRODUCTION

The competitive nature of the automotive industry has increasingly focussed on the need for better crash, emissions and acoustic performance of automobiles in the past 10 to 15 years. The end-consumers have influenced this focus through demands for improved performance in terms of efficiency, acceleration as well as comfort. It has been accepted that not only is the amount of noise generated by a car important, but also the perceived quality of that noise plays an important role in the satisfaction of the end user. Thus, many challenges exist in refining the acoustic comfort of today's automobiles.

Today's internal combustion powered vehicles have many moving parts and associated processes. Due to these influences, one should not be surprised at the amount of noise that can be heard within the passenger compartment of the vehicle. Sources of this noise include exterior wind noise at higher speeds, tire noise, and the combustion process in the engine with its attendant exhaust and intake noise. Automotive manufacturers have continued to improve the acoustic performance through the use of stiffer and better acoustically insulated vehicle bodies, more aerodynamic body designs, improved tire technology and quieter air induction and exhaust system designs. These efforts have improved the acoustic environment by reducing the overall sound level within the passenger compartment. Unfortunately the improvements have made some of the other potential noise sources such as air induction noise more noticeable. The comment: "Investigations have shown that, depending on the car, up to 11% of the overall sound level is caused by the air intake system" by Pricken [37] is an example of the acknowledgement of the existence of this problem. Presently, a greater effort is being directed toward the study of induction noise and what may be done to lessen its impact on the overall comfort of the passenger compartment occupants.

The advent of smaller vehicles with less space under the hood, coupled with the increased number of engine components, largely due to emissions controls, has imposed significant limitations on design engineers in the area of noise control. This has increased the difficulty of installing traditional acoustic attenuators to dampen induction system noise at the intake orifice. Two examples of these controls are a simple Helmholtz resonator and an adaptive passive system which allow the acoustic resonator volume to react according to the rotational speed of the engine. Such limitations make it evident that it is not always possible to design an induction manifold to be as quiet as possible while maintaining minimum flow requirement objectives as well as achieving the target space and weight allocation under the hood. In answer to this, automotive engineers may perhaps choose to 'tune' the manifold to alter the acoustic properties to achieve a more pleasing sound as opposed to reducing its overall sound level.

All sound levels can be measured empirically by engineers. Customers, however, may be more concerned with the quality, and not the quantity of sound, within reason. If attenuation efforts have been maximized to their potential, then efforts can be made to produce a more pleasing sound [31]. The inclination of the consumer to appreciate the quality of a sound is illustrated by the positive influence of the solid thud of a car door or the muscular purr of a sports car at idle and its effect on vehicle demand. While such sounds are not related to the intrinsic qualities of the car, sound quality analysis has become an important subjective parameter used for the evaluation of vehicle performance.

In order to achieve an improvement of the above, efforts have been taken in the development of new design approaches for induction system attenuation. Active noise cancellation is one such approach where preliminary work has shown promising results. To understand how such methods can be applied, a review of the causes of inlet noise is needed.

The causes of inlet noise include the influence on the intake air by the movement of the intake valves, the physical parameters of the manifold ducting and any other attached accessories. This inlet noise is the audible result of the oscillation of intake air at the natural frequency of the inlet passage column. This oscillation is caused by a sharp pulse which occurs when the intake valve opens to the cylinder which is at a higher pressure than the intake manifold runner at the instant of opening. At the same time, a high frequency noise is also generated at approximately 1000 Hz by the intake air travelling across the valve seat at a high velocity. These noise impulses, however, are usually reduced significantly to the 80 - 150 Hz frequency range, associated with the engine firing frequency, due to the influence of the manifold ducting and air cleaner. A second oscillation occurs when the intake valve closes [30]. The sequence of these oscillations with respect to piston position is illustrated in Figure 1.1.

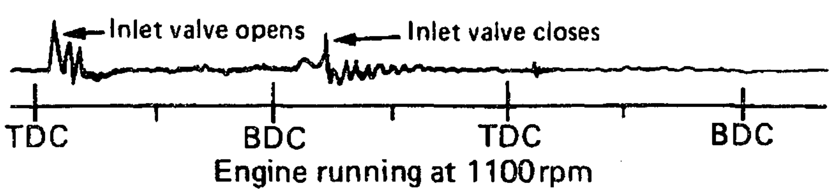

Figure 1.1: Illustration of Inlet Noise Oscillogram Caused by the Movement of the Intake Valve [30]

As commented on by Sacks et al, "A secondary source of induction noise is turbulent flow through the induction system and intake manifold. This source tends to produce a broad spectrum at frequencies above 1 kHz. These frequencies are effectively attenuated by both the air cleaner and the transmission path between the engine and passenger compartment. Consequently, this source does not produce sound levels in the passenger compartment that would warrant concern." [43]

The objective of this study was to investigate the feasibility of attenuating automotive intake noise through the implementation of tuned exhaust feedback to the intake system. Specifically, it was proposed that an open physical bridge be inserted between the exhaust and intake manifold of the engine in hopes of reducing, or cancelling, some of the acoustical energy of the intake system. This investigative process involved the numerical modelling of the bridge on an engine followed by experimental verification.

The realization of this feasibility study began with the determination of a number of engine related operating parameters that would be needed as input to the analytical model of the engine. The engine chosen for this work was a Toyota 4A-GE used in North America in the MR2 Mark I (1985 - 1989) and Corolla GTS (1988 -1991) applications. The modelling software chosen to model the engine was Ricardo WAVE. The outputs from WAVE were compared to the results measured on the dynamometer motored, unmodified engine located within a semi anechoic environment. Once the WAVE model was validated, the inclusion of the bridging components on the modelled engine was investigated. Given the variety of diameters and lengths of connecting piping that could be selected, the connection locations on the intake and exhaust system components, and the pairings of cylinder exhaust numbers with corresponding cylinder intake numbers, the development of the model became very complex. A number of system models were developed and eventually four variations of bridging configurations were constructed. The physical models were tested on the motored engine located in the instrumented semi-anechoic chamber.

The design and the results of the most effective model are presented in this study. The results include the measurement of sound levels at the same physical location as is used in the WAVE model. A variety of Sound Quality metrics available in the instrumentation are also reported. This includes a discussion of the validity of each of them for the application of induction noise measurements.

Given the approach outlined above, it is also the goal that this study provides a major contribution to the current state of the art. To ensure this, the planned attenuation technique is both unique and nontraditional as an acoustic attenuation technique. Further, while the implementation of psychoacoustic metrics is still relatively new, these metrics are not totally unique to the automotive industry. The application of the metrics used in this study will be applied to a noise source not normally evaluated using sound quality techniques. As such, the investigation of the applicability of this approach will be included. Since this is a new technique, it is anticipated to perhaps open new avenues of research which may involve applications in materials engineering or the development of psychoacoustic metrics better suited to induction noise applications.

II. NUMERICAL AND PRACTICAL TECHNIQUES

The focus of this work is to attenuate the pressure pulses at the outlet of an intake manifold through the application of an interactive noise control technique. This noise is the result of the complex interaction of two individual, yet simultaneously occurring phenomena. The first event is caused by the valve action of the engine which generates pressure pulses which propagate to the open end of the intake duct. The second event is flow generated noise caused by the mean flow in the duct. In order to fully appreciate the complexity of this research, a review of the numerical and actual behaviour of the air induction system is presented in this chapter. Further, a review of active noise control in general along with some discussion of its limitations is given as essential background prior to discussion of the interactive noise control techniques used in this work.

2.1 Acoustics of Air Induction Systems

The noise emitted from the intake system of an automotive engine is the result of a combination of two processes. The first process is the propagation of pressure pulses through the intake system which are generated by the periodic charging and discharging of gases through the intake valves. Also, flow generated, or gas flow noise, is the result of turbulence of the mean flow generated at the geometrical discontinuities of the intake system. These causes of noise will result in radiation of noise from the intake opening as well as shell noise radiation from the walls of the intake manifold, air filter box and inlet ducting.

It should be noted that the intake noise is certainly not the exclusive source of noise from an internal combustion engine. Other sources include combustion and mechanical noise from the engine block as well as both pulse and flow generated noise through the exhaust system. Figure 2.1 is a schematic illustration of acoustic radiation from the various engine noise sources.

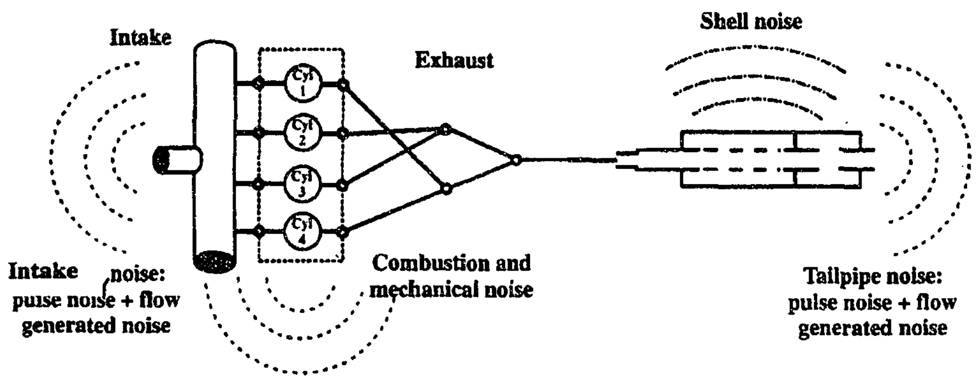

Figure 2.1: Schematic of Acoustic Radiation from Various Engine Noise sources [55]

The propagation of noise inside the intake system ducting is frequently assumed to be a one-dimensional plane wave. This assumption is valid for the frequency range of interest because the noise at the air intake orifice is primarily low in frequency. As explained by Pricken, the wavelengths are large relative to the equivalent diameters of the ducting. The fact that the geometric dimensions of the typical intake system ducts involve small duct diameters and long duct lengths helps to minimize the presence of high frequency cross-duct modes while fostering the development of "organ pipe" low frequency modes [37]. It has been shown by Chiatti et al, that the "hypothesis of plane acoustic propagation" is able to provide reliable predictions of the pressure propagation of intake systems [9].

2.1.1 The One-Dimensional Wave Equation for Pulse Noise

A derivation of the equation which illustrates the way acoustic pressure fluctuations, or pulse noise, propagate with respect to a co-ordinate direction x and with respect to time t can be found as examples in many textbooks on acoustics [29] [25]. For a simple harmonic wave motion such as that shown in Figure 2.2, the acoustic variables consisting of pressure p, density ρ, and particle velocity u, vary continuously in space and time.

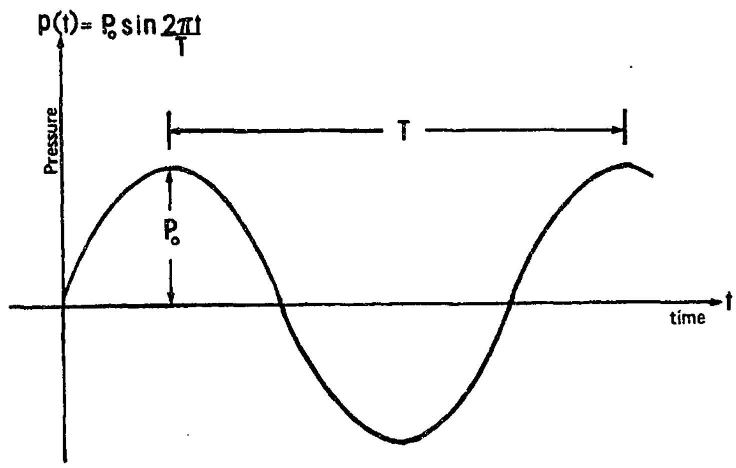

Figure 2.2: Simple Harmonic Motion of Sound Wave Illustrating the Pressure Amplitude and Time Period of the Cyclic Wave [4]

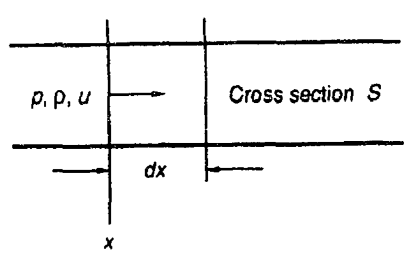

Figure 2.3: Illustration of the Variables used to Represent the Propagation of a Wave through a Duct Represented by a Control Volume [29]

Consider a fixed volume of a duct as shown in figure 2.3 with a cross section S and an arbitrary length dx in the x direction. Through analysis, the one-dimensional wave equation for the propagation of acoustic pressure fluctuations in a duct and can be presented as:

$$\frac{\partial^2 p}{\partial x^2} - \frac{1}{c^2}\frac{\partial^2 p}{\partial t^2} = 0 \qquad (2.1)$$

Where c is the speed of sound and can be expressed as:

$$p = c_o{}^2 \rho \qquad (2.2)$$

This relationship illustrates the way that acoustic pressure fluctuations act with respect to the co-ordinate distance x and with respect to time.

2.1.2 Gas Flow Noise

Air flowing through the inlet of an automotive induction system can be considered, to a degree, to be a high velocity flow, particularly at high engine speeds. This results in the generation of gas flow noise. Simply stated, gas flow noise is defined as the result of generated turbulence as the intake air travels through any geometric discontinuities in the air induction system. These areas of discontinuity are the locations of vortex shedding and turbulence which is responsible for self generated broadband noise. In fact, traditional methods of pulse noise attenuation such as silencers and Helmholtz resonators can themselves behave as noise sources whose resulting noise levels can be comparable to that of the realized attenuation of pulse noise.

The cause and mechanisms of gas flow noise are well understood; however, its prediction through the use of fluid dynamic, numerical models is difficult. Such models are not very well adapted to the determination of the complex three-dimensional turbulent flow field which is present. Instead, the usual approach is to use semi-empirical formulas to determine the sound power radiated by the gas flow noise. Such an approach can then be easily included in the one-dimensional fluid dynamic model described in the previous section in order to evaluate the overall intake noise as the sum of both pulse and aerodynamic noise. This is the approach that is used by the modelling software package, Ricardo WAVE. This software is used by automobile manufacturers and their suppliers to design intake, exhaust and engine systems.

A simple empirical prediction equation was described by Ver [55] [53] which was derived from experimental data on gas flow noise generated by an expansion chamber. This formula, based on Imperial units, is given as:

$$PWL_{oct} = -145 + 55\log u_f + 10\log F_F - 45\log\left(\frac{P_{area}}{100}\right) - 20\log\left(\frac{460 + T}{530}\right) \tag{2.3}$$

The output of the above formula predicts the octave band sound power level by using the mean flow velocity through the discontinuity, the face area of the chamber, the percentage of open cross section area and the temperature of the gas as input variables. The advantage of this equation is its simplicity since no consideration of the internal geometry of the expansion volume is required.

Green and Smith [55] [14] developed an equation to determine the overall sound power level across the frequency spectrum and is given as follows:

$$L_w = \eta_w + 10\log P_{amb} - 17.5\log T + 20\log D + 45\log u - 26.9 \quad (2.4)$$

Here, η_w is the efficiency factor which is determined experimentally. Figure 2.4 shows the efficiency factor for a simple expansion chamber. The variables used in the equation are the atmospheric pressure P_{amb}, the temperature T, the duct diameter D, and the flow velocity u.

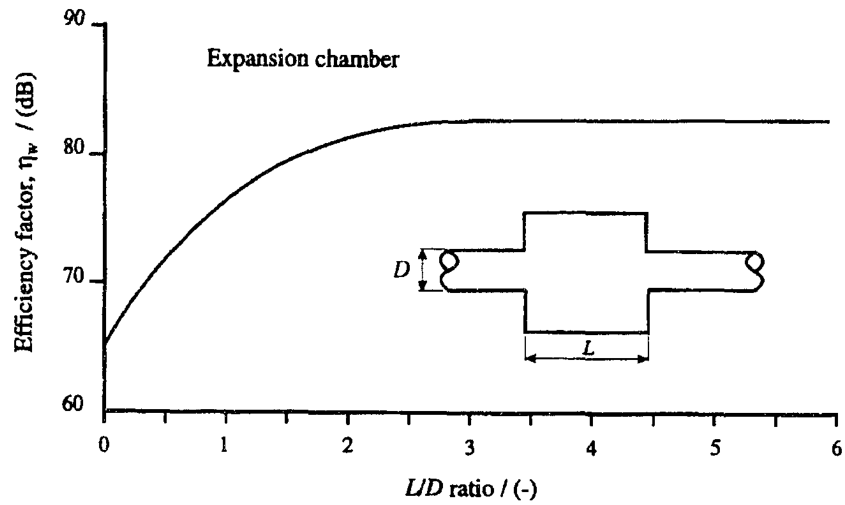

Figure 2.4: Experimental Efficiency Factor in decibels versus Aspect Ratio for the Simple Expansion Chamber Muffler [55]

As previously stated, once the gas flow noise has been determined, these results can be combined with a one-dimensional fluid dynamic analysis to calculate the overall flow generated noise level at the intake system orifice. Figure 2.5 illustrates contributions of the modelled pulse noise and the calculated gas flow noise to the resulting overall noise level produced at the tailpipe of an engine for various engine speeds. A similar approach could have been used to illustrate the effect of the intake for an induction system where the air filter housing acts as the simple expansion chamber.

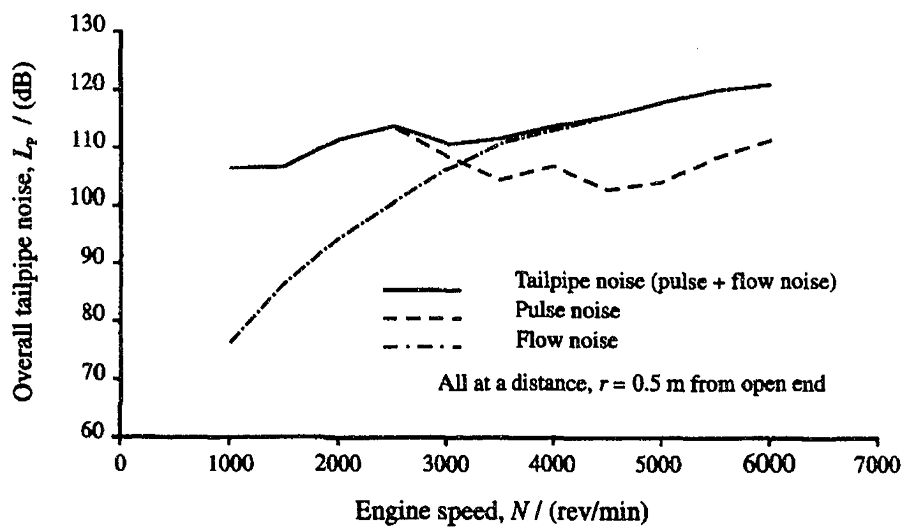

Figure 2.5: Calculated Tailpipe Sound Pressure Levels in Decibels of Flow Noise, Pulse Noise and Total Noise versus Engine Speed at 0.5 Metres [55]

2.2 Active Noise Control

Active noise control (ANC) is a technique which is used to attenuate an unwanted acoustical disturbance by generating a second acoustical waveform which is equal in amplitude but opposite in phase to the original acoustical signal. Traditionally, the application of ANC consists of an electronically generated sound field using one or more loudspeakers to cancel the existing sound field. Although the idea of active noise control dates back more than 60 years, the commercial and practical implementations of the concept has only more recently been made possible because of the availability of fast microprocessors [49].

While most noise control efforts involve the use of passive attenuation techniques, certain applications do exist where active noise control techniques can be more effective. This section will review the more common ANC methods as well as provide a more thorough review of the circumstances required for the successful implementation of active noise control along with its pros and cons.

2.2.1 Adaptive Feedforward Active Noise Control

The most common configurations of active noise control systems are the adaptive feedforward, the adaptive feedback and wave synthesis. The latter of which is a type of feedforward control suited for periodic noise [15]. With the exception of sensor positioning and controller algorithms, the fundamentals are similar for each system. The following discussion will be limited to the most common system, the adaptive feedforward active noise control system.

A typical adaptive feedforward active noise control system is shown in Figure 2.6. There are four components which make up a feedforward ANC system. A reference microphone is placed upstream of any control components and will measure the unwanted noise as illustrated in Figure 2.6, in this case, fan noise. An electronic controller, or control system, will receive the reference signal measured by the reference microphone and calculate the required opposing noise signal prior to the physical arrival of the unwanted noise. The opposing acoustic signal is generated by the control source. This control source is typically a loudspeaker which is powered by the control system. If the control system performed its duties flawlessly, the unwanted noise signal would be totally cancelled. In spite of this, given the complexities of the duties required of the control system, as well as any time varying fluctuations in the unwanted noise, some degree of residual noise is likely to propagate further downstream of the position of the active noise control system. In order this error signal to be measured, an error microphone is employed that will sample the remaining residual noise downstream of the control source. This error signal is then sent back to the control source where corrections can be made to improve the noise cancellation process.

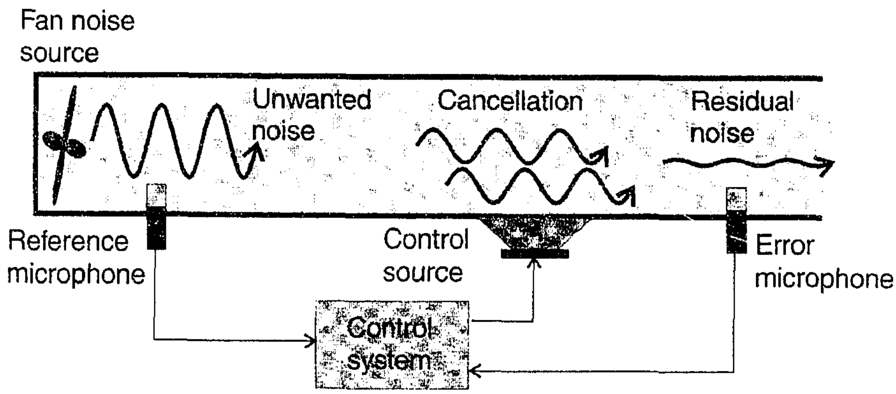

Figure 2.6: Schematic of the Adaptive Feedforward Active Noise Control System Process in a Simple Duct with a Fan Noise Source [49]

Although this whole process appears to be rather primitive, the computation of the cancelling sound field can be a rather demanding task. Many variables play a role in dictating the success of an ANC system.

The nature of the environment in which the sound field exists plays a role in the system's effectiveness. Consideration must include how this environment affects the noise signal as it propagates downstream of the reference microphone position but before reaching the control source location. This is particularly important for active control of sources that cause noise propagation through ducts. The influences of the geometry of the duct can vary the acoustic signal between these two locations resulting in an ineffective reference signal being sent to the control system.

The quality of the reference signal is directly proportional to the quality of the microphone. Its associated cabling is also important. Similarly, the change in the controller signal as it passes through the amplifier and loudspeaker must also be considered. Further, the effect of these changes themselves will vary over time as the properties of the microphones and speaker alter due to exposure to any harsh environmental effects or to natural aging of the components. Even air speed and temperature fluctuations are important variables that can significantly influence the overall quality of the reference signal sent to the control module.

To accommodate these considerations, the controller system's algorithm must be adaptive in order to adjust the control calculations to best suit the varying environment. This is implemented using the error signal such that the goal is a resultant sound field with total cancellation at the error microphone position. In doing so, the designer of such a system must be cognitive of the physical acoustics of the problem environment. According to Snyder, "The controller can only work within the bounds defined by the fundamental physics" [49] associated with the wave propagation through the duct.

2.2.2 Active Noise Control of Sound Propagation in Ducts

Noise propagation through an automotive intake system can be considered synonymous to the propagation of a sound field through a duct. Simply put, a duct can be likened to an enclosure where one of the dimensions of the enclosure is very long. This enclosure most often terminates into an open space. In the case of an automotive induction system, the termination would be the air intake opening at the upstream end of the duct. In any case, the fundamental implication of the duct on a travelling sound wave is that the acoustic front of the wave is constrained in two dimensions while being allowed to propagate freely in the third.

The following observation by Hansen regarding Active Noise Control provides the reader with some appreciation of its applicability. "Active control of noise propagating in ducts is well suited for the control of low frequency noise where the amount of attenuation which can be achieved using conventional passive silencers may be inadequate. Elements of active systems are usually small and can be mounted in the duct wall, thus minimising air flow pressure losses. This application of active noise control is the oldest and is now the most commercially successful with numerous systems installed in industry in the USA. Typical results achieved are 15 - 20 dB over two octaves of random noise and 20 to 30 dB for tonal noise. Typical frequencies which are controlled range from 40 Hz to 400 Hz." [15] This further reinforces the argument for active noise control for automotive intake applications since this falls well within the frequency range of interest. Figure 2.7 illustrates the effectiveness of ANC on a broadband noise source propagating through a duct from 0 to 200 Hz. Both the uncontrolled noise signal and the attenuated noise source after the application of active control are shown. The effectiveness of the active noise cancellation is particularly evident in the frequency range from approximately 45 Hz to 170 Hz for the specific example illustrated.

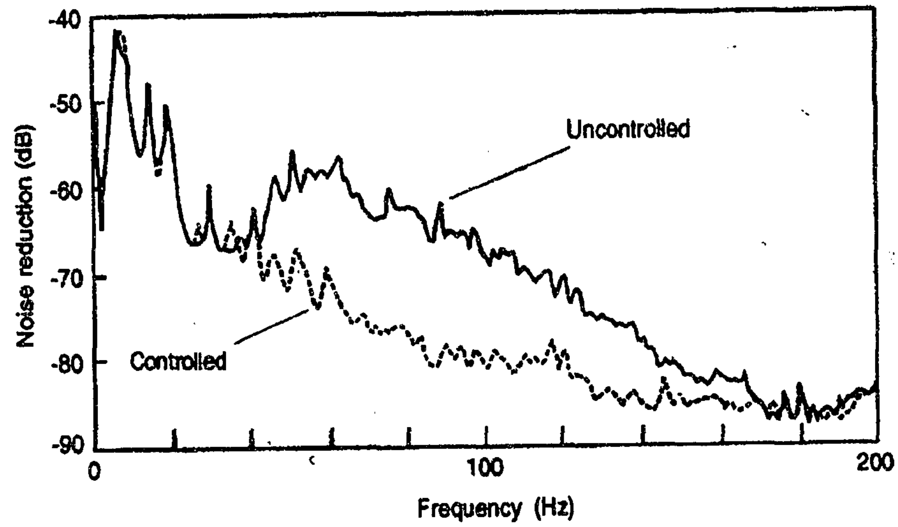

Figure 2.7: Attenuated and Uncontrolled Broadband Sound Propagation in a Duct with Implementation of an Active Control System [15]

Since the sound field in the duct is constrained on two sides, a modal response will be present in either one or two dimensions, depending on the geometry of the duct. These duct modes will travel in the downstream direction of the duct. As stated by Snyder, the open end of the duct will "have a response similar to that associated with free space radiation." [49] Since there are no restricting boundaries, the acoustic energy will dissipate outward with no modal response associated with this third dimension of the duct.

The fundamental frequency, or mode, in a duct is referred to as the plane wave mode. This mode has a uniform pressure distribution across the cross section of the duct and does not lose its pressure amplitude along the length of the duct. Figure 2.8 illustrates the uniform pressure distribution as the pressure peaks and troughs propagate through the duct at the speed of sound.

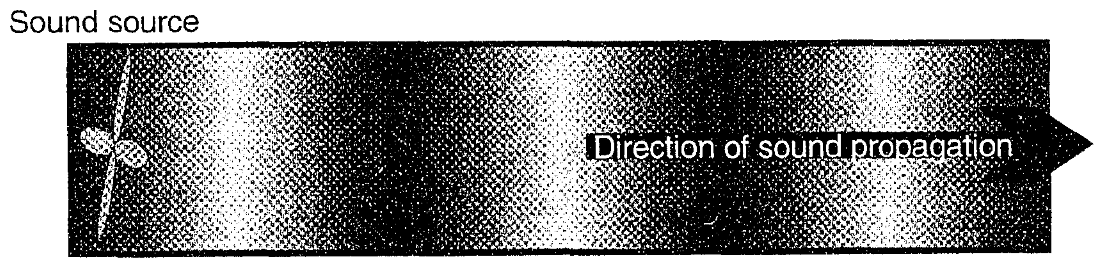

Figure 2.8: Plane Wave Sound Propagation in a Duct Illustrating the Pressure Peaks and Troughs of the Pressure Distribution Moving at the Speed of Sound [49]

As stated earlier, the active noise control technology is most commonly used in applications involving ducts. In fact, the technology was initially patented more than 60 years ago [49] with the fundamental limitations being associated with the signal processing technology of the time. In order to implement a successful application of active noise control in a duct, several key elements of the overall system must be considered to ensure performance benefits. Each of these considerations will be discussed in greater detail.

2.2.2.1 Reference/Error Signal Quality

The reference microphone measures the sound field in the upstream section of the duct which is ultimately to be cancelled by the active control system. With this signal, the controller will calculate the required cancellation output to be sent to the control source. If care is not taken to acquire an accurate representation of the signal from the reference microphone, it is difficult for the controller to fulfill its requirements. The adage of 'garbage in, garbage out' is appropriate to the circumstance. The same discussion holds true for the error microphone.

The most common difficulty in accurately measuring the reference and error signals is differentiating the actual sound field from any existing air flow noise which is commonly present in duct flow. Using a common microphone often results in measuring the pseudo noise caused by turbulence effects from the air flow passing over the microphone. To overcome this obstacle, anti-turbulence microphones are usually employed. A schematic of an anti-turbulence microphone is illustrated in Figure 2.9. The microphones utilize the concept that the sound energy of interest and the unwanted wind noise travel at different speeds. Therefore, as the noise of interest enters the slit along the length of the microphone, the acoustic energy will increase. The wind noise, however, will not since the wind noise inside the tube will travel at a different speed to that of the wind noise outside the tube. As the outside wind noise enters the tube at different locations, it is not related to the wind noise inside and does not amplify to the same degree compared to the target noise to be eliminated. This results in a much improved signal to noise ratio [49].

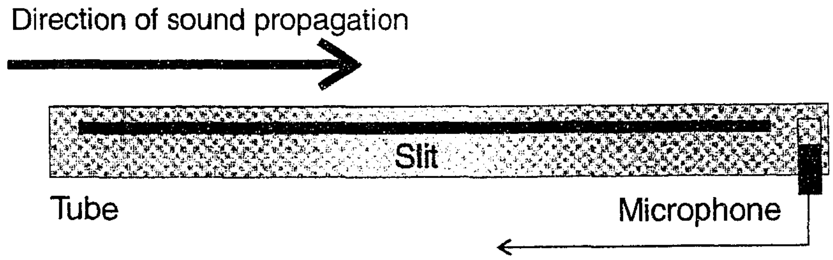

Figure 2.9: Anti-Turbulence Microphone Probe which enables the Measurement of a Sound Field in a Duct Without the Influence of Flow Noise [49]

The use of piezoelectric film bonded sensors in place of conventional microphones provides an alternative measurement option for the case of noise radiating structures such as flexible heating ducts which can 'rumble' like a drum. These sensors measure the structural vibration and relate this information to the contributing radiating sound [15].

2.2.2.2 Distance between Reference Sensor and Control Source

In a feedforward active noise control system, several activities take place before the control source signal is generated. The reference microphone must measure the noise from the source and send this signal to the control system where a suitable opposing signal is generated. This signal is then sent to the control source where it is transformed into an acoustic signal. This entire process requires a finite period of time called the system's 'group delay' and can be as long as several milliseconds. The sound wave travelling from the reference sensor position to the location of the control source also requires a finite amount of time. This can be roughly estimated at 1 metre every 2.9 milliseconds. Care must be taken to ensure that there exists enough separation distance between the sensing microphone and the control source such that the wave front does not reach the speaker before the controlling noise is produced.

2.2.2.3 Position of the Control Source in a Duct

A typical passive noise control technique for ducts is the side branch or Helmholtz resonator. It is a carefully chosen volume placed off the main duct. The volume or length of the resonator is chosen to correspond to one-quarter of the wavelength of the target frequency. If the side branch has negligible impedance, the unwanted acoustic energy will flow into the volume and not continue down the duct. To be most effective, the resonator should be placed in the duct at a location where the acoustic pressure is at a maximum. The most advantageous locations are typically at odd multiples of one quarter of a wavelength from the noise source. At these locations, the pressure will be most sensitive to an impedance change [49]. The same notion applies to the placement of the control source in an active noise control system in ducts. That is, the control source should be placed at a location where the amplitude of the sound pressure is at its peak.

2.2.2.4 Response Characteristics of the Duct

It is common practice to use passive noise control techniques in ducts when there are multiple modes of sound propagation through the duct because it is a most effective method to used in these circumstances. Specifically, these passive techniques are very effective at attenuating the higher order modes. On the other hand, active noise control techniques are best suited where there is only one mode, or only on the plane, or fundamental mode, for the cases where there are multiple modes of sound propagating through the duct. In this case, a combination of active and passive techniques work extremely well where the active portion attenuates the low frequency noise and the passive method takes care of the higher frequencies.

For the situation where the duct diameter is very large, the higher orders cut-on at lower frequencies. That is, the applicable frequency range for these larger ducts begins at lower frequencies. To better apply active noise control techniques at higher frequencies, the cut-on frequencies can be raised by dividing the duct diameter into several smaller ducts. By doing so, the propagating sound wave is forced to travel through the smaller ducts in the plane mode for which active control techniques are well-disposed to handle.

III. LITERATURE SURVEY

The following literature survey was undertaken to determine if any such or similar work has already been conducted by others using the proposed noise control technique documented in this study. The search was unsuccessful in finding any literature which indicates this specific project has been carried out in the past. It is apparent from the review of related literature that much research has been undertaken in both the study of induction noise attenuation as well the application of active noise cancellation, including examples of the attenuation of automotive engine noise. A review of these studies is essential to accumulate both an understanding of the fundamental analysis tools available as well as to gain a better comprehension of what can be achieved by continuing this type of research.

Additionally, since a fundamental portion of this research involves the numeric modelling and analysis of the problem using Ricardo WAVE, a software modelling program, a review of its application through publications will also be included.

3.1 Passive Attenuation of Induction Noise

The manner in which the attenuation of automotive intake noise has been traditionally approached has been through the application of passive control techniques. These techniques are usually the simplest and least expensive form of attenuation but do not always yield the best results. Two primary categories of passive noise control exist. The first category aims at redirecting the path of the acoustic energy, such as in the implementation of a noise barrier. The second category reduces the acoustic energy flow, usually through either absorption with acoustic insulation or by changing the acoustic impedance of the power output, perhaps through the use of a sudden cross section change. An obvious example of this would be an automotive muffler. Much research has been conducted and many papers have been written studying the various applications and implementations of passive control techniques of automotive induction systems. The following sections provide a review of these passive techniques.

3.1.1 Helmholtz Resonator

One of the most common passive noise control techniques used in automotive induction systems is the Helmholtz resonator. When acoustic energy travels down a tube or pipe, a specifically chosen attached volume can be used to attenuate the travelling noise [2]. This technique is particularly effective when the unwanted noise consists of a narrow frequency band and the volume, or resonator, is tuned to the target frequency. A schematic of a Helmholtz resonator in an automotive induction system is provided in Figure 3.1 which illustrates the resonator volume attached to the intake duct by a narrow tube or orifice section.

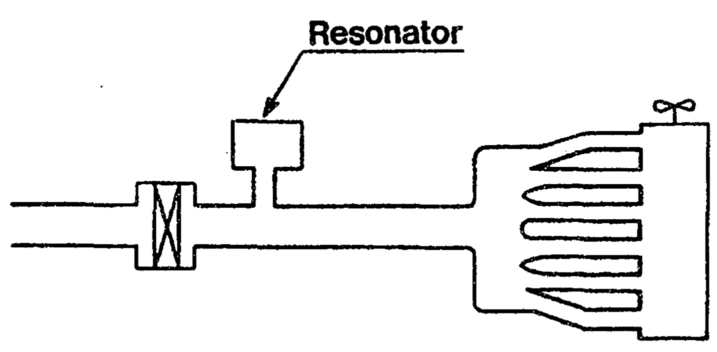

Figure 3.1: Schematic of Helmholtz Resonator in Automotive Intake System Located between the Air Filter Box and the Intake Manifold [31]

The resonator volume is chosen so as to offer the sound wave in the main pipe an alternative path of negligible impedance at a target frequency. A reflected acoustic wave results which bounces back toward the source and effectively attenuates the unwanted noise. The resonant frequency of the Helmholtz resonator is given as:

$$fn = \frac{c}{2\pi}\sqrt{\frac{A}{LV}} \tag{3.1}$$

where fn is the natural frequency of the resonator, c is the speed of sound, A is the cross-sectional area of the neck, L is the length of the connecting pipe and V is the volume of the resonator.

A more realistic illustration of two differing, yet typical, resonator configurations are shown in Figure 3.2. The detailed diagram of resonator B clearly shows the throat tube leading into the resonator volume.

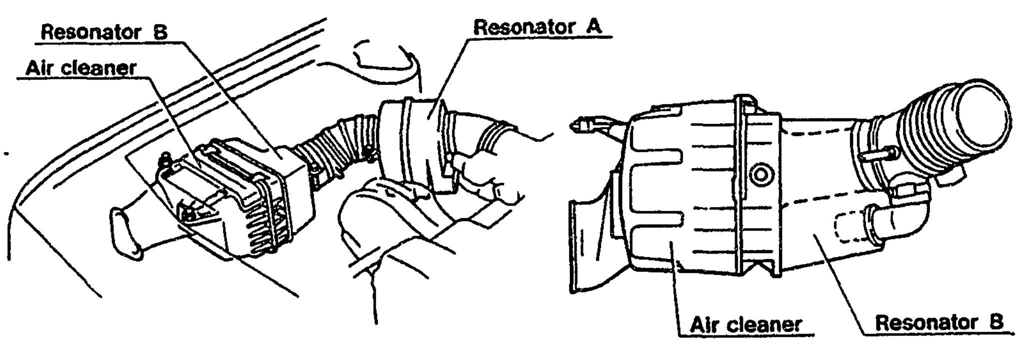

Figure 3.2: Application of Two Different Configurations of Helmholtz Resonators Installed on a Typical Automotive Air Intake System [31]

Kostek [18] investigated ways to further develop this passive technique into an adaptive-passive method of attenuation. Kostek stated that to change the resonator characteristics, one of the resonator parameters must be altered. "For example, heating elements could change the temperature in the resonator, thereby changing fn via the speed of sound" [18]. Care must be taken since this can cause irreparable process disturbances on the intake system. Kostek proposed a variable volume resonator achieved by attaching the neck to a pneumatic air cylinder. A control system fed by a microphone was used to tune the resonator's volume position so as to achieve the best possible performance.

Nishio [31] investigated the effect of resonator position on attenuation performance in an automobile induction system. Figure 3.3 shows the realized intake noise reduction for two resonator positions. It is shown that position A results in the lowest sound pressure level measured at the intake orifice. Snyder explained this behaviour with the following reasoning, "for the resonator to be most effective in providing sound attenuation, it should be placed at a point in the duct where the acoustic pressure is maximum. Intuitively, the pressure will then be most sensitive to an impedance change. This is commonly an odd multiple of one-quarter wavelengths downstream from the noise source." [49]

Lu [20] also investigated the effectiveness of various resonator designs and placements through the use of a test rig. A specific design was bench evaluated by using a shaker as the sound source instead of an actual engine or speaker. It was determined that a relatively simple and inexpensive test rig technique was an effective tool in evaluating a given Helmholtz resonator's ability to achieve a given NVH development goal.

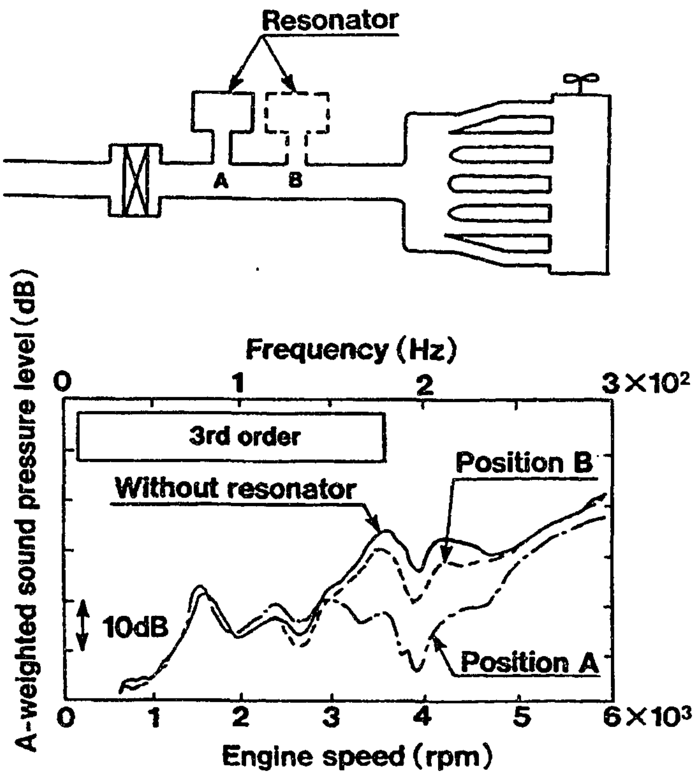

Figure 3.3:Illustartion of Realized Intake Noise Reduction through the Implementation of a Resonator at Positions A and B in the Intake System [31]

Birdsong [6] made a similar attempt at a tunable resonator. Whereas a traditional resonator is designed to target a single frequency noise, his system included a conventional Helmholtz resonator which was electronically tunable to effectively attenuate tonal noise with a time varying frequency. This was achieved by sampling the noise in the duct and any noticed change in the target frequency was noted and a change was generated by a control system which would send a compensated signal to a speaker located within the resonator cavity. This speaker acted as the compensation source to permit the resonant frequency to vary over a range of frequencies instead of normal, fixed, resonator frequency. A schematic of this apparatus is shown in Figure 3.4.

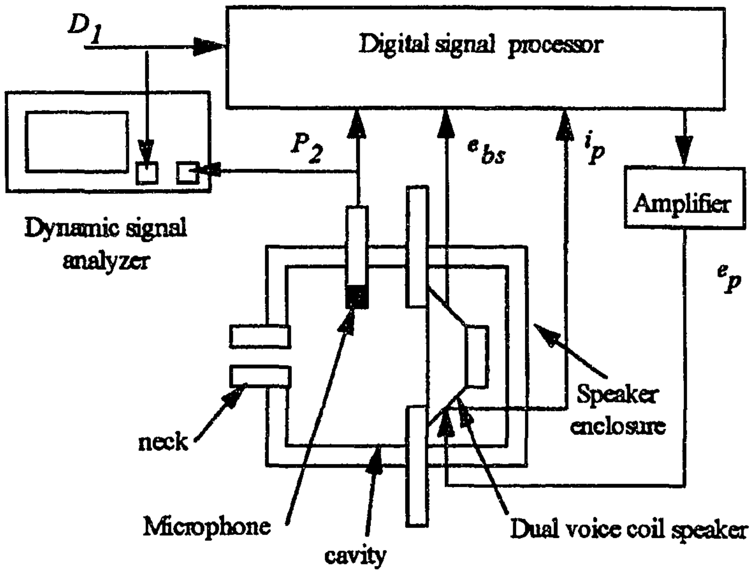

Figure 3.4: Schematic of Birdsong's Experimental Apparatus Designed to Attenuate Intake Noise with an Actively Controlled Tunable Helmholtz Resonator [6]

Since the eventual conclusions in this study will be based on both numerical and experimental comparisons, it was felt prudent to discuss similar comparisons that have been investigated regarding Helmholtz resonators.

Selament compared experimental results of the realized insertion loss of a Helmholtz resonator in an automotive induction system to the predicted results of a nonlinear fluid dynamic model. The insertion loss measurements were presented in both the time domain and the order domain for an engine operating range of 1000 to 5000 rpm. The numerical technique employed was "a quasi one dimensional time domain approach to solve the balance equations for mass, momentum and internal energy in ducts of variable cross section." [46]. Selament found that the predictions of the fluid dynamic model compared reasonably well with the experiments. He concluded that the use of such a model to predict the trends in terms of amplitudes and frequency components of the presence of the resonator would accelerate the development process of an intake system.

Selament continued his work by comparing the results of a one dimensional and multidimensional analysis to experimental results. Specifically, Selament investigated the effect of specific cavity dimensions of resonators with consideration of the wave motion which is neglected by the classical approach of Helmholtz theory. It was determined that "the one dimensional analytical expression and numerical simulation demonstrate well the basic behaviour observed in the experiments. It should be noted that at low *l/d* ratios, these results start deviating from the experimental data due to a degree of multi-dimensionality in the physics, as illustrated by the three-dimensional numerical prediction." [46]

3.1.2 Mufflers

Another common passive noise control technique is the use of an expansion chamber muffler with or without the inclusion of absorptive elements. A muffler without the presence of absorbing material is called a reactive muffler. Here, the performance of the muffler is dependant on the geometrical shape of the muffler. If the attenuating performance of the muffler depends on the presence of sound absorbing material, the muffler is referred to as a dissipative muffler. Each of these muffler types is to be discussed in the following sections. It should be noted that mufflers are generally best suited for controlling frequencies of higher magnitude where the lower limit on the effective range is 500 Hz.

3.1.2.1 Reactive Mufflers

A simple reactive muffler is essentially a large opening in a pipe system as is schematically illustrated in Figure 3.5. It is this sudden increase in cross sectional area which creates an impedance mismatch for the acoustical energy travelling along the duct. As explained by Beranek, "This impedance mismatch results in a reflection of part of the acoustic energy back toward the source of sound" [5], thus preventing some of the energy from being transmitted past the muffler.

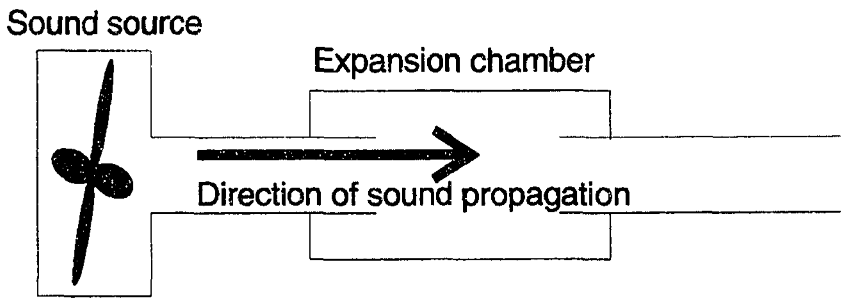

Figure 3.5: Schematic of a Simple Reactive Muffler Designed to Attenuate Noise by Initiating an Impedance Mismatch by a Sudden Increase in Cross Sectional Area [49]

In studies by Novak and Ule [33][49], the feasability of using simplified numerical modelling equations as a preliminary step in the design process of muffler systems was presented. The results of the theoretical equations for a simple expansion chamber muffler were compared to the results of a computer model. Further, the results of this relatively simple computer model were then compared to the results of a very complex computer simulation model of the muffler with a modelled internal combustion engine as the source. This study successfully demonstrated the merits of using these fundamental equations for preliminary design considerations of reactive muffler systems by demonstrating a computational transmission loss of 14 dB, which closely matched that predicted using the theory. Transmission loss is defined as the ratio of sound power incident on the muffler to the sound power transmitted by the muffler. It was also shown that a significant insertion loss can be achieved with the addition of the muffler in both the simple and complex computational model. Insertion loss is the difference between sound pressure levels measured in space before and after a muffler has been inserted.

Bai [1] conducted a similar study where he experimentally compared the realized theoretical insertion loss of a reactive muffler to experimental results. Using the transfer function method described by Munjal [28], Bai predicted the insertion loss of his reactive concentric perforated tube muffler. These results were found to favourably compare to the results obtained by the play back of a 2000 cc automobile engine operating at 4000 rpm through the muffler.

3.1.2.2 Dissipative Mufflers

In the reactive muffler, the realized attenuation is the result of an impedance change causing acoustic energy to reflect back to the noise source, whereas a dissipative muffler dissipates the acoustic energy in the form of minute amounts of heat. This is accomplished by lining the muffler with sound absorbing material. This lining is usually isolated from the flow by a perforated metal enclosure. According to Snyder, "Provided that the open area provided by the holes is approximately 25% or more of the total panel area, the effect on the acoustic performance of the liner is negligible." [49]

The sound absorption properties and characteristics of various fibre materials are well established in the literature by Cofer [11]. According to Selament, "The recent improvements in their properties combined with their broadband acoustic dissipation characteristics make such materials potentially desirable for implementation in silencers. The use of fibres may prove particularly effective when their dissipative characteristics are combined with the reactive silencers, leading to hybrid configurations." [45]

Selament compared the acoustic attenuation performance of a perforated concentric silencer filled with continuous strand fibres both experimentally and analytically. Selament varied the perforated duct porosity and fibre density and applied a one dimensional analytical and three dimensional boundary element method, both in the absence of flow. While good agreement was achieved between the experimental and numerical results, it was found that the multidimensional analysis was required at the higher frequencies.

In addition to the reactive muffler experiments, as discussed earlier, Bai [1] also conducted a study where he experimentally compared the realized numerical insertion loss of a dissipative muffler to experimental results. Bai's predicted insertion loss of his dissipative lined expansion chamber was found to favourably compare to the experimental results obtained by the play back of a 2000 cc automobile engine operating at 4000 rpm through the muffler.

3.2 Active Attenuation of Induction Noise

As was stated earlier, the traditional manner in which the attenuation of automotive intake noise has been approached has been through the application of passive control techniques. While inexpensive, these techniques work well for noise at medium and high frequencies. They are not well suited for low frequency sources [22]. This is where active noise control techniques can be successfully applied. Much research has been conducted and many papers have been written studying various applications and implementations of active noise control techniques in ducts as well as in automotive applications. The goal here is to investigate some of these techniques.

McLean [24] used a source coupling technique to control automotive intake noise by placing a conventional loudspeaker coaxially inside the air intake. Here, the speaker diaphragm was coplanar with the termination of the air intake duct. A sketch of the speaker system inside the intake duct is shown in Figure 3.6.

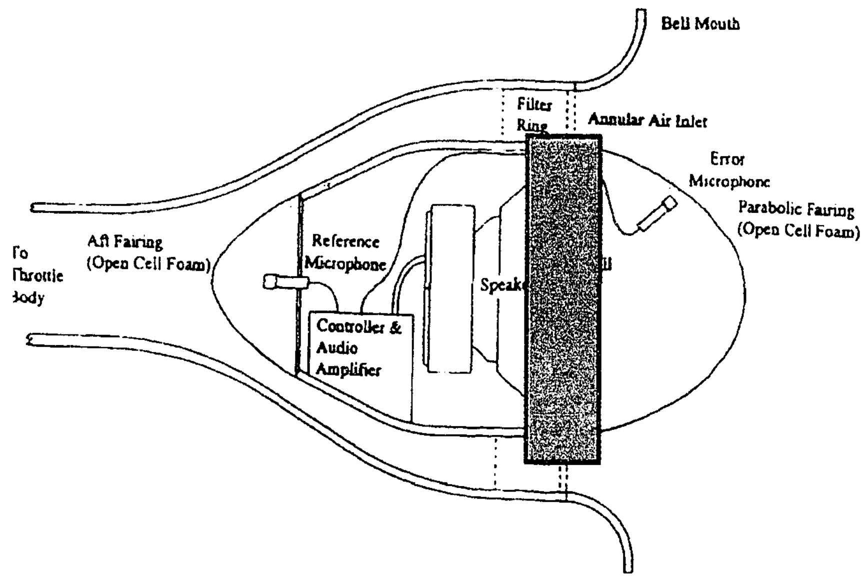

Figure 3.6: Sketch of Air Induction ANC Module via Source Coupling where the Speaker is Located Coplanar with the Air Intake Opening [48]

It was found that placing the speaker in the coaxal configuration provided at least an intake pipe noise attenuation of better than 20 dB when compared to configurations where the speaker was aligned with the pipe axis and the speaker was pointed into the pipe inlet or where the speaker and pipe axes were orthogonal.

A schematic of the active noise control feedforward components showing the layout of the system is illustrated in Figure 3.7.

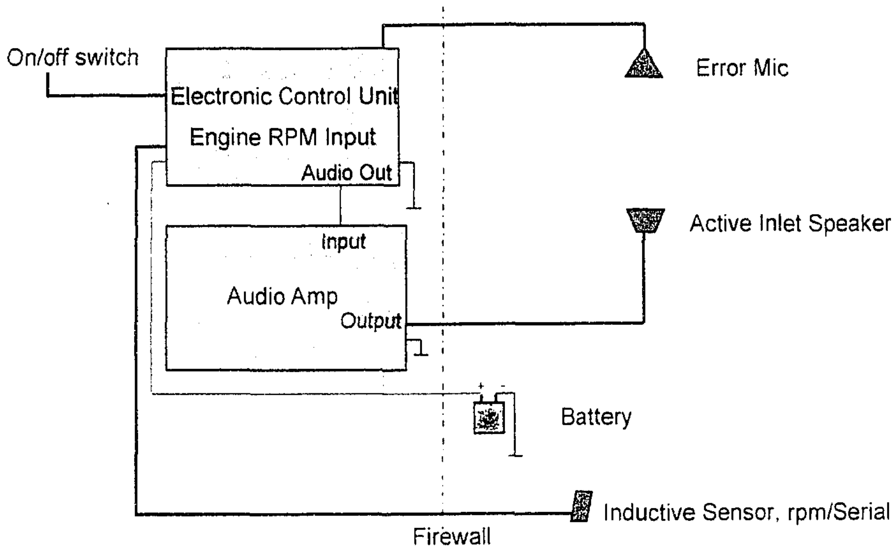

Figure 3.7: Electrical Schematic of the Active Noise Control Components used by McLean in his Attenuator [48]

The approach taken by McLean was a global noise control strategy where the total radiated sound power of the source is targeted for reduction. This would result in both a reduction of noise transmitted into the passenger compartment as well as a reduction in exterior noise such as in a pass-by noise test. To achieve a global reduction, the secondary noise source was placed in near proximity to the primary source resulting in the two sources coupling. If the two sources have similar impedances, this results in the generation of an ideal dipole pressure field which according to Kido [17] is the optimal noise control strategy when using the source coupling technique.

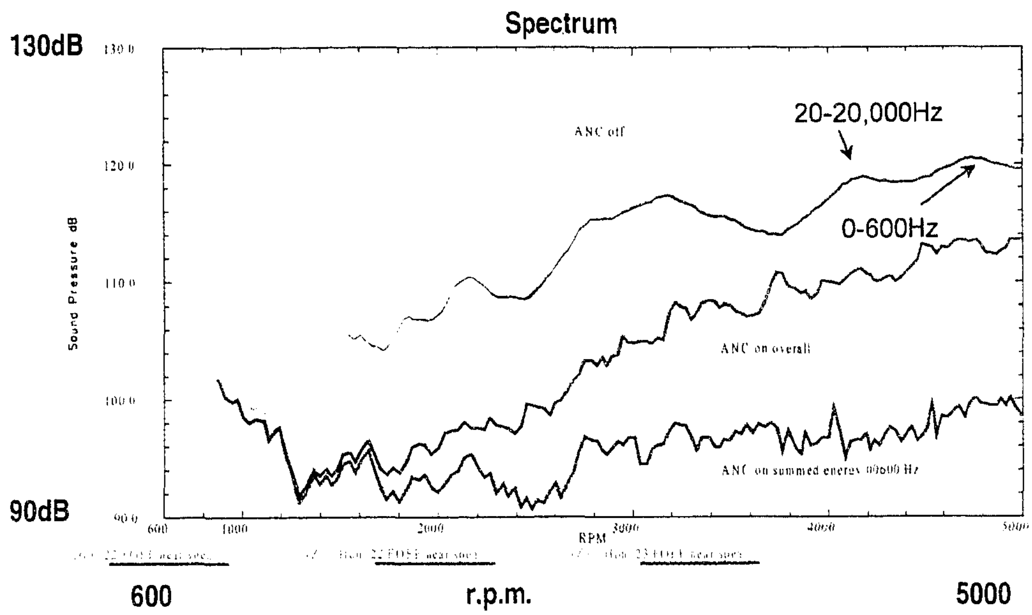

Figure 3.8: McLean's Measured SPL Results of a Honda V6 with his Active Noise Control System Turned both On and Off [48]

Figure 3.8 shows the results of McLean's experiment applied to a Honda V6 engine. The yellow and blue curves show the sound pressure levels measured at engine speeds up to 5000 rpm without the active noise control operating. The green and red curves show the resulting sound pressure levels at the indicated frequency ranges with the active noise control system activated. A significant degree of attenuation is realized through the implementation of the control system. McLean did note that the system was found to be successful on six and eight cylinder applications but not on four cylinder engines. This was due to the large acoustic power demanded of the secondary source to eliminate the high amplitude, low frequency spectral lines associated with the second and fourth engine orders.

Pricken [37] described his active noise control system as "a single loudspeaker placed in the dirty air side duct of an air intake system. An electronic control unit calculates the signal driving the loudspeaker. The control unit gets a reference signal from an rpm sensor in the engine and an error signal from an acoustic sensor at the orifice of the intake system." A schematic of this system is shown in Figure 3.9.

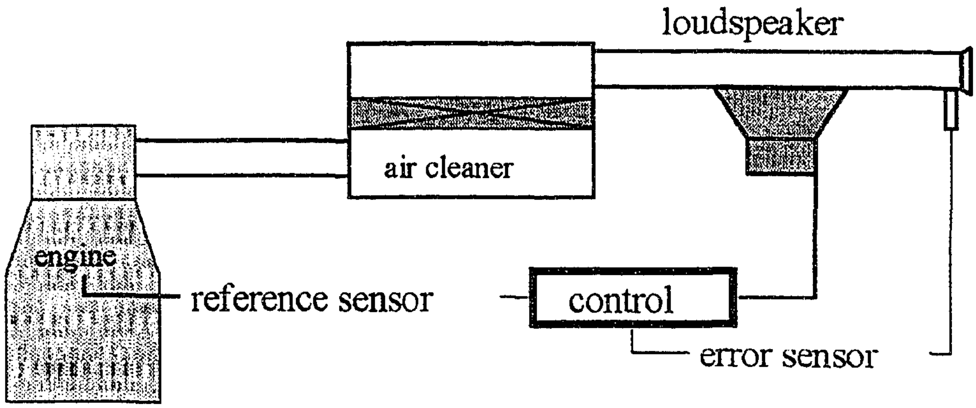

Figure 3.9: Schematic of Pricken's Active Noise Cancellation System Using a Single Speaker Installed in the Dirty Air Side of the Intake System [37]

Pricken was able to attenuate the overall measured unweighted sound pressure level at the intake orifice by six to ten dB for engine speeds above 1500 rpm. The results were even more substantial for single engine orders with the non-dominant engine orders being reduced to the system's residual noise level.

Chaves [8] did some work with Volkswagen where he implemented an electronic feedforward system utilizing an LMS algorithm. While he did not go into much detail of the experimental apparatus, instead focussing on the control theory aspects of his design, Chaves did present a good graphical representation of his results as is presented in Figure 3.10.

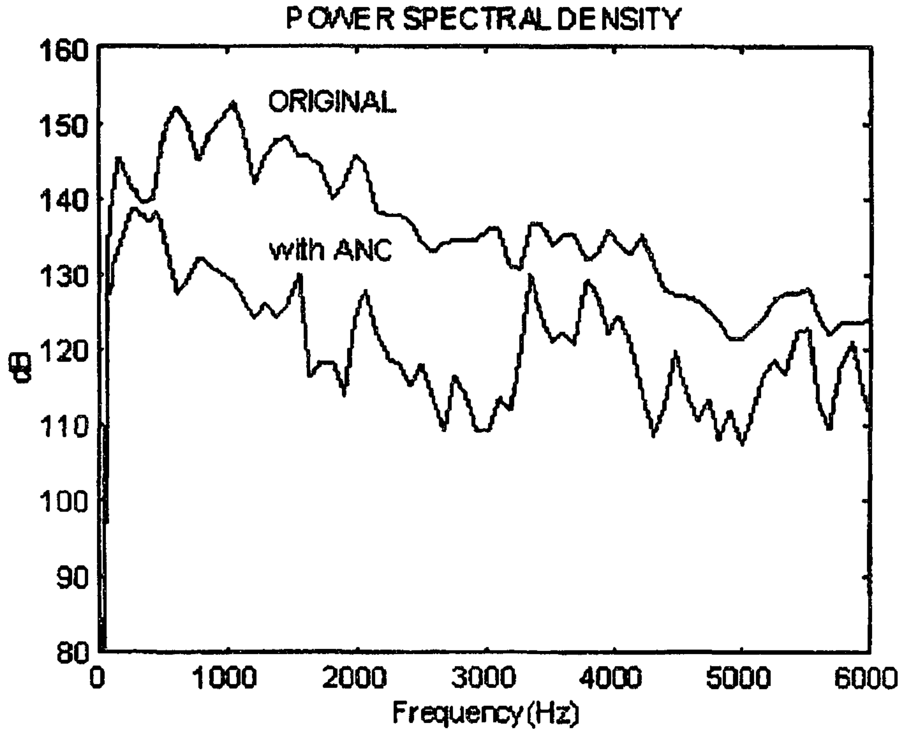

Figure 3.10: Chaves's Experimental Results Using an LMS Algorithm to Control a Feedforward Active Noise Control System on Intake Noise [8]

Most of the applications of active noise control in ducts to date have used a speaker as the secondary noise source for cancellation. These have proven to be successful and are commercially available for ventilation systems and ducts. It was stated earlier that active noise cancellation techniques are particularly useful for low frequency noise where passive techniques fail. The implication of this is that the speaker must also be capable of producing high power, low frequency signals. Depending on the nature of the unwanted noise, this may require very large diameter speakers and massive amounts of amplification as described by Beeson [3]. Also, for automotive applications, the extreme conditions under the hood including temperature variations and dirt and chemical contaminants, can play havoc with the efficiency and reliability of a conventional speaker system. To combat this, some system designers have implemented horn speakers, which produce their own set of limitations. Others have used high sound power electro-pneumatic loudspeakers which require a source of compressed air.

Boonen [7] took a unique active noise control approach to attenuate automotive exhaust noise without the use of a speaker system. Boonen's device consisted of an electrically driven valve in the exhaust pipe which is also downstream of a buffering volume. The idea is to constantly vary the valve opening such that, in conjunction with the buffering volume, only the mean flow passes through the exhaust outlet. In other words, the fluctuations of the flow are temporarily buffered resulting in a decrease in the emitted exhaust noise.

Using a cold engine simulator, Boonen was able to achieve a reduction in exhaust noise of 13 dBA with a feedforward controller algorithm and a reduction of 16 dBA with a feedback control. The introduction of the buffering volume and valve was found to increase the back pressure to the engine by 10 kPa. A schematic of Boonen's active silencer with the cold engine simulator is illustrated in Figure 3.11.

While it is not a focus of this research, it is considered worthwhile to mention how the area of Sound Quality is beginning to play an important role in noise control research. The analysis of sound quality is the psychoacoustic discipline which attempts to quantify an objective evaluation of a sound or vibration source. Here, instead of just measuring the level or spectrum of a source, as is done in the classical acoustic approach, a quantification of how pleasant, or for that matter, how unpleasant a source is perceived is pursued. Sound quality criteria are often used to measure the success, or effectiveness, of many active control techniques [21].

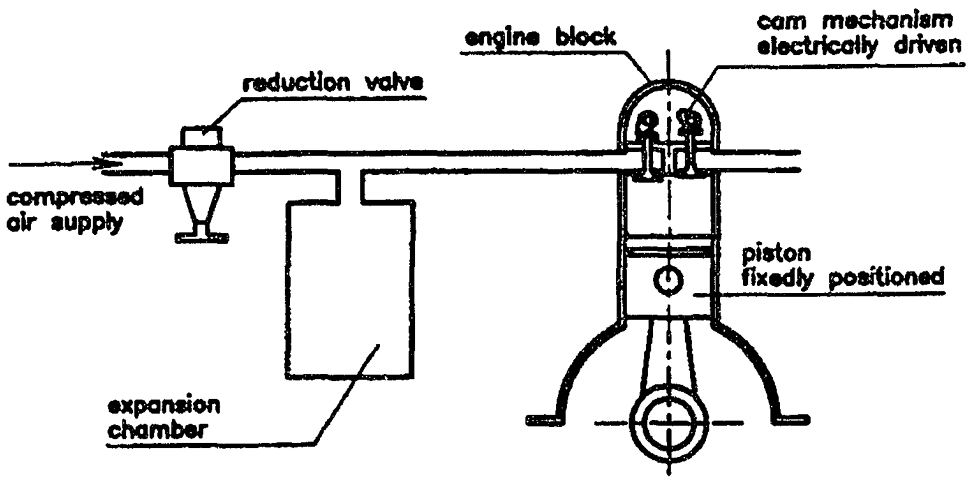

Figure 3.11: Boonen's Active Noise Silencer with Cold Engine Simulator Used to Control Exhaust Noise by Controlling Mean Flow [7]

Scheuren [44] used several accepted sound quality metrics to evaluate the effectiveness of active noise control techniques aimed at improving automotive cabin noise. Here the goal is not necessarily to simply attenuate the noise within the automobile, but also to measure the qualitative improvements realized by the implementation of the active noise control techniques. Scheuren was able to not only demonstrate an improvement in the overall sound levels as a result of active control, but he showed how, "such devices are capable to help in experimentally determining the optimal sound for a given vehicle." [44]

3.3 Applications of Ricardo WAVE

A fundamental portion of this work involves the numeric modelling and analysis of the proposed manifold bridge using Ricardo WAVE, a software modelling program. A review of applications of WAVE through publications is included here.

Ciocci [10] used WAVE to perform an analysis of the intake system of a 12-cylinder Ferrari 550 Maranello. The results of the analysis were also correlated with experimental data.

Ciocci stated that, "Since Ferrari cars are characterized by their performance and their engine sound (the "roar" of a Ferrari is legendary) it is natural that Ferrari is using state-of-the art simulation techniques in order to design their intake and exhaust systems." [10] The goal was to duplicate this distinctive sound with WAVE such that a benchmark model was created that could be used to investigate potential future engine modifications.

Using a postprocessor module of WAVE, the intake sound pressure levels at the intake orifice were generated at various engine rpms and are shown in Figure 3.12. Comparing these results to experimental measurements, the model was further refined by calibrating the wall friction coefficients and discharge coefficients. As a result, a successfully calibrated engine model was created that is capable of predicting engine performance and noise data as well as providing a good baseline for further analysis.

Hetherington [16] investigated a problem with a V-10 Dodge Viper which had a high level of 2.5 order exhaust noise which was due to the odd firing engine sequence. To solve this problem, WAVE was used to design and test an asymmetric exhaust system which is illustrated in Figure 3.13. The idea was to delay one bank of exhaust pulses by adding length to one side of the exhaust system. As will be discussed later, a similar approach is used in this work to modify the timing of the introduction of an exhaust pulse into an engine's intake manifold.

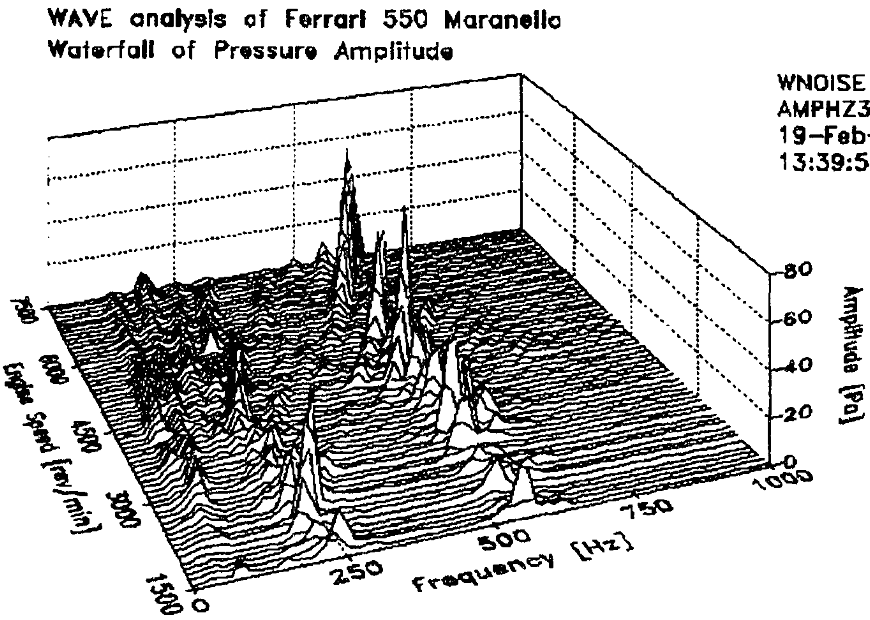

Figure 3.12: Waterfall Analysis of Ferrari 550 Intake Noise Measured at the Intake Orifice versus Engine Speed using Ricardo WAVE Software [10]

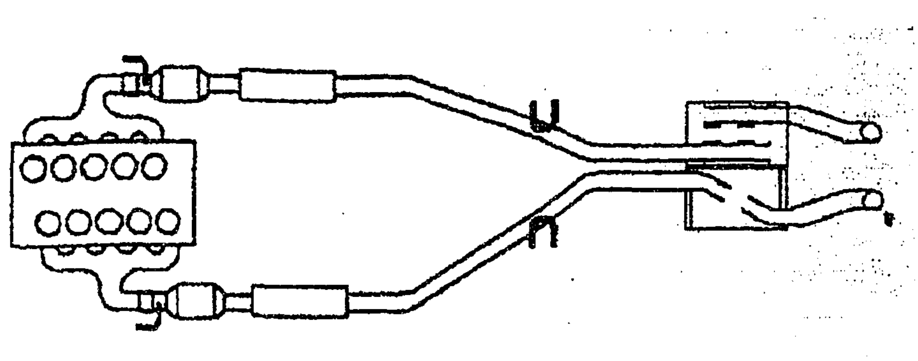

Figure 3.13: Proposed Asymmetric Exhaust System for a Viper V-10 with One Exhaust Bank Lengthened to Delay the Exhaust Noise Emission for Optimum Output [16]

A WAVE model of the original exhaust system was built and calibrated to engine dynamometer data to provide a baseline system to which a sound quality assessment using measurements gathered with a binaural head provided excellent results. The proposed exhaust system was then modelled using WAVE which created an audio output file for playback. It was determined by Hetherington that while the WAVE model provided good numerical results, "the direct play back of the noise files generated by WAVE did not sound realistic enough to be used for a general, non-specialized audience. It was concluded though, that it was good enough to be used by exhaust design or development engineers when they need to assess the relative sound quality of different designs." [16]

Wirtz [56] of Ducati described the application of using WAVE to optimize the engine performance and intake and exhaust noise emissions in the early prototyping stage of the new 900 Super Sport Ducati engine. The goal was to increase the engine performance by 5 hp and lower the noise emissions by 2 dBA and to change from a carburetted to a fuel injected system. This needed to be accomplished without any major modifications of the technical components such as the cylinder head. Also, this all needed to be accomplished in the short time of three months which eliminated the option of building any prototypes.

WAVE was used to create a model of a proposed fuel injected intake system and investigate the best performance through variation of the intake duct length and valve timing. In doing so, an optimized design for performance was achieved. Using this design, modifications were then needed to improve the pass-by noise emissions. Wirtz found that using the WNOISE module of WAVE, a pseudo pass-by simulation showed a "major frequency peak at 265 Hz evident in the spectra due to the resonating air column of the characteristic intake duct length." [56] To solve this problem, a Helmholtz resonator, designed for this frequency, was modelled and was shown to absorb this 265 Hz noise. WAVE was also used to design a new exhaust silencer to further improve pass-by noise emissions. A complex WAVE model with small discretization lengths of 10 mm were used in order to achieve accurate results. Comparing the results of the improved silencer to the original, an attenuation of about 5 dB between the major spectral peaks was achieved.

In the end, an improvement of engine performance from five to seven percent of maximum power with increased torque at lower rpms was achieved. In addition to this, the target reduction of pass-by noise of 2 dBA was also realized, thus satisfying all of the design objectives.

3.4 Summary

Various methods of controlling intake noise have been presented in the literature review. These control methods include both passive and active attenuation techniques. A review of published applications of Ricardo WAVE has also been included given that this software modelling program has a significant contribution to this study. While these discussions give light to both past and present technology, unresolved issues still exist in solving the problem of induction noise which this study hopes to partially remedy.

Passive attenuation of intake noise is not a new technology. In the discussions presented by Nishio [31] and Snyder [49], it is pointed out that the application of the Helmholtz resonator is effective for the attenuation of a narrow band of acoustic energy only. Here, the resonator is tuned to the target frequency which severely limits its application. The focus in the present study is to develop a control technique that is effective in the attenuation of a much broader frequency range.

Attempts were made to overcome the frequency limitations of the fixed volume resonator by the likes of Kostek [18] and Birdsong [6]. The approach taken by Kostek was to vary the volume by means of a pneumatic air cylinder regulated by a control system fed by a microphone. While this system does have the advantage of a greater frequency range of effectiveness, it is still limited by the confines of the volume extremes as well as the increased costs of the control electronics. Birdsong's approach also made attempts to compensate for varying tonal components through application of a speaker in the resonator cavity which allowed for the resonant frequency to vary over a greater range. This system, while shown effective, still had limitations of the effective range. Also, due to the speaker and employed electronics, practical limitations in the implementation of such an approach in a production vehicle is suspect.

The application of mufflers as a control device was also discussed. Also reviewed were studies by Novak [33], Ule [51] and Bai [1] involving reactive mufflers where experimental and numerical predictions of insertion loss were investigated. Similar studies were conducted by Selament [45] and Bai [1] for dissipative mufflers. While the application of these types of muffler systems are somewhat inadvertently applied to intake systems by the various changes in ducting diameter and inclusion of the air filter, the application of reactive and dissipative mufflers is not usually employed in the automotive induction system. The fundamental reason being the subsequent flow restrictions and resulting back pressures from these types of control devices. The approach used in this study does not have these same limitations.

The application of active noise control techniques for the attenuation of intake noise was also discussed. A very effective technique was demonstrated by McLean where attenuation values of up to 20 dB were realized for six and eight cylinder applications. This approach was not very effective for four cylinder engines due to the higher order harmonics associated with these types of engines. The other disadvantage of this system is the very high cost associated with the implementation of this type of control device in a production vehicle. A similar study by Chaves [8] was also reviewed. Another disadvantage of this type of control system is that it is only effective for the control of low frequency noise, and not higher frequencies. It is also best suited for steady, or non transient sources.

Given that a substantial amount of this study makes use of and relies on the application of Ricardo WAVE for the numeric modelling and analysis of the proposed control device, a discussion of some of the previous studies using this software has been included. The purpose behind its inclusion was not necessarily to provide a critical insight to specific work done by others, but instead to demonstrate both the suitability and acceptance of this software for the type of experimental procedures pursued in this study. While the works have been cited previously, those citations were with regard to the modelling results and the software used was of peripheral importance.

Ciocci [10] used WAVE to numerically benchmark the intake system of a Ferrari to allow for future studies. This numerical analysis resulted in a good correlation with experimental results. A similar study was successfully demonstrated by Wirtz [56] of Ducati to improve engine performance while simultaneously reducing noise emissions. Hetherington [16] used WAVE to design an exhaust system which in conjunction with the other referenced works demonstrated WAVE's ability and acceptance by industry to be a useful tool for the design and evaluation of induction engines and associated systems for both performance and acoustical characteristics. Caution should be noted though that care must be taken in the design of any system with a modelling program such as WAVE. The quality of the results are extremely dependant on the care given to the input of the various required variables for the modelled system. Because of this, a substantial amount of time was given in this study to tune the WAVE model to best represent the actual engine used in the experimental portion of this work.

IV. MODELLING SOFTWARE

This study involved the experimental verification of a software modelling study. It was the intent that the problem first be thoroughly investigated using software modelling techniques that are based on the theoretical one-dimensional equations reviewed earlier. The results of this approach were then verified with experimental measurements. The following sections will describe the modelling software used as well as the design of the specific model used in this study. A detailed section describing the specific modelling output descriptors used is also included.

4.1 Modelling Software

The modelling software program used in this study is Ricardo WAVE. It has become one of the automotive industry preferred choices for engine simulation. "WAVE is a computer-aided engineering code developed by Ricardo to analyse the dynamics of pressure waves, mass flows and energy losses in ducts, plenums and the intake and exhaust manifolds of various systems" [41]. This is accomplished by applying a one-dimensional finite difference approach of the theoretical thermo-fluid equations of the working fluids of the defined system.

The following sections provide a discussion of the fundamental equations and formulations used by WAVE in the modelling of the various processes associated with a basic engine model. It should be noted that some of these equations are not applicable for this study given that only a motored engine is investigated. Also included is a discussion of the numerical acoustic approach and simplifying assumptions used by WAVE's noise post-processor, WNOISE, for the prediction of noise radiation.

4.1.1 Fluid Dynamics

Formulation of the fluid dynamic flow in the defined ducts is the solution of quasi-one dimensional compressible flow equations which include the conservation of mass, energy and momentum. These equations written in an explicitly conservative from are given as equations 4.1, 4.2 and 4.3 respectively.

$$mass = \frac{dm}{dt} = \sum \dot{m} \tag{4.1}$$

$$energy = \frac{dme}{dt} = \sum \dot{m}\, h + sources \tag{4.2}$$

$$momentum = \frac{dmu}{dt} = -A\frac{dp}{dx}dx + \sum \dot{m}\, u - losses \tag{4.3}$$

The above governing equations are written in a finite difference form for a series of elementary volumes. These are created by the user through the discretization of the duct system into a series of small volumes. The equations of mass and energy are solved for each volume and the momentum equation is solved for the boundaries between each of these volumes.

The perfect gas equations are used for the thermodynamic properties of the gaseous fluids while real gas equations are used for fluids such as freon and oils. These fluids requiring real gas equations are not present in the model created for this study.

A finite difference technique using the finite volume approach to the discretization of the partial differential equations is employed to find the solution of the governing equations. The time steps are governed by the Courant condition which according to Ricardo is said to be superior to the method of characteristics. Specifically, this method, which automatically adjusts the time step during the run to achieve minimum run time, is better suited to deal with the terms of heat transfer, friction, distributed losses and boundary conditions in cases of an abrupt area change, junctions of multiple ducts and bends. [41]

4.1.1.1 Wall Friction

To predict wall friction, WAVE calculates the local Reynolds number (Re) using the instantaneous flow velocity, density, viscosity and pipe diameter. Depending on whether the flow is laminar or turbulent, the boundary layer thickness (δ) is then calculated which then permits the prediction of the wall friction coefficient (C_f) for either case. Equations 4.4 and 4.5 illustrate the laminar and turbulent friction coefficients respectively.

$$\frac{C_f}{2} = 0.027 \mathrm{Re}_\delta^{-0.25} \tag{4.4}$$

$$\frac{C_f}{2} = \frac{4}{\mathrm{Re}_\delta} \tag{4.5}$$

To account for the pressure loss coefficients due to bends in the ducts, handbook values are usually applied. These are usually acceptable except for circumstances of large radius curves which can have larger frictional losses. These cases are adjusted accordingly by WAVE.

4.1.2 Thermodynamics

The simulation of the engine processes is a model of the time dependent in-cylinder processes which are based on the solution of the equations for mass and energy. The mass equation accounts for the changes of mass through valves and fuel injection as well as changes due to the combustion process. The energy equation is based on the first law of thermodynamics and equates the changes of internal energy to the net enthalpy, heat transfer and piston work as given in equation 4.6.

$$\Delta mu = \sum_i \Delta m_i h_i - Q - p\Delta V \tag{4.6}$$

4.1.3 Combustion Model

For a model representing a fired engine, the standard spark ignition combustion model employed is the Wiebe model. This model uses the Wiebe function relationship to define the rate of mass burned as a function of crank angle. This correlation is represented by equation 4.7.

$$W = 1 - EXP(-AWI(\frac{\Delta\theta}{BDUR})^{(WEXP+1)}) \qquad (4.7)$$

where:
W	=	cumulative mass fraction burned
$\Delta\theta$	=	crank angle after start of combustion
BDUR	=	user defined crank angle for 10 to 90% burn duration
WEXP	=	Wiebe exponent
AWI	=	internally calculated parameter to allow BDUR to cover the 10 to 90 % range

Note: Also required by WAVE is the user defined 50% burn point of the total heat release.

4.1.4 Noise Prediction Model

Once a WAVE model representing an engine design has been created and successfully run, noise measurement predictions can be made from the resulting data using the WAVE post-processor program WNOISE. This program uses noise radiation models to predict the source strength radiation of the potential noise sources associated with the WAVE model. WNOISE also includes acoustic processing and analysis tools.

Two fundamental sources of noise are simulated by a WAVE model. These are flow noise from sources such as exhaust and intake orifices as well as pressure sources. Flow sources radiate noise to the free field and can be measured by any number of simulated free field microphones which are positioned at any defined location and distance from the vehicle. Pressure sources can be measured by placing pressure sensors inside the duct and junctions in the WAVE model.

The noise radiation model employed by WNOISE is given as equation 4.8. This linear model assumes that all the sources are point sources which are subsequently measured in the far field. Hemispherical radiation is predicted by WNOISE by simply doubling the radiated pressure. Similarly, the ground reflection is modelled by adding a second source of the same strength at the location of plane of ground reflection.

$$P(t) = \frac{\rho}{4\pi R}\frac{dS(t - R/c)}{dt} \tag{4.8}$$

Where,	P	=	Sound pressure at microphone
	S	=	Source strength (volumetric flow rate of gas)
	R	=	instantaneous distance between source and microphone
	c	=	Speed of Sound
	t	=	Time
	ρ	=	Air Density

WAVE can also simulate flow generated noise through implementation of an empirical flow noise correlation developed by A.J. Green and P.N. Smith. The correlation is given by equation 4.9.

$$L_W = E_W + 10\log(Pat) - 17.5\log(T + 273) + 20\log(D) + 45\log(U) - 26.9 \tag{4.9}$$

Where,	Lw	=	Acoustic power	dB re 1pW
	Ew	=	Efficiency	dB re 1pW (empirically defined constant - model specific)
	Pat	=	Atmospheric pressure	mmHg
	T	=	Temperature	°C
	D	=	Source Diameter	m
	U	=	Flow velocity	m/s

If the flow noise simulation option is chosen for a given source, a white noise velocity source is added to the WAVE predicted velocity to simulate the flow noise. It should be noted that the flow noise is derived from a correlation and is not a prediction. To be used responsibly, good information regarding the real flow source should be known so as to allow for post validation. As such, the flow noise option was not used in this study.

The accuracy and effectiveness of WAVE as an analytical tool for engine simulation has been extensively tested by both Ricardo and independent researchers and academics. Such verifications were illustrated through publications discussed in the previous chapter.

Before a model of a working system, such as an engine, can be analyzed, a representation of the subject components must first be synthesized to a rendering of the system at hand. In order to facilitate this, specific information related to the engine design and operation must be obtained. This information consists of three categories being geometric data, engine data and the operating conditions of the engine. A detailed discussion of each of these areas follows.

4.1.5 Geometric Engine Data

The geometric data required for the engine model consist of the dimensions of the intake and exhaust systems including the pipe lengths, port sizes and muffler and air filter box volumes. The manifold pipe lengths are very important since these play a key role in the tuning of the performance curves of the engine. Likewise, the various system volumes also help determine the performance characteristics of the engine as well as being very important in noise prediction work. Examples of these might include the air filter housing or the volumes that make up the various duct junctions.

The geometric dimensions used in the model must be as accurate as possible to assure the best possible predictions from the numerical results. The geometric data can either be acquired from engineering drawings or measured directly from the physical engine components if available. In fact, actual parts can provide additional information such as the presence of moulding seams in a plastic component or burrs at the leading edge of a pipe which can reduce the effective diameter of the entrance and thus affect the realized flow. The component materials and surface finishes may also be important. Also, a rough surface may cause increased flow losses due to an increase in wall friction; thus affecting the accuracy of the modelled results. The variation in thermal properties of the materials used in the construction of the system components will affect the analysis results.

4.1.6 Engine Data

The engine data includes the dimensions and other quantitative information associated with the cylinder head and engine block. For the cylinder head, the typical information required includes the valve diameters, timing and lift profiles. If available, port flow coefficients measured using a flow bench under steady flow test conditions will increase the accuracy found in the numerical results. For the engine block, the fundamental cylinder dimensions are necessary. These include the bore and stroke, the connecting rod length and pin offset, the compression ratio, firing order and frictional details.

4.1.7 Operating Conditions

In addition to the dimensional data described above, information about certain conditions at which the engine simulation is operated at are required. Examples of these might include duct wall and gas temperatures at the modelled operating speeds of the engine. This information allows the simulation model to more quickly reach steady state conditions. The closer the initial operating conditions are to actual, the better the simulation will be able to quickly and accurately reach its final results. The operating conditions required include the inlet and exhaust wall temperature, operating speed, piston, cylinder and head temperatures, ambient conditions and combustion information. If this information is not known, suggestions of typical values are provided by WAVE.

4.2 Design of Model

Before an engine model can be analysed by WAVE, it must first be created by the WAVE preprocessor called WAVEBUILD. WAVEBUILD is essentially a canvas onto which all of the model components are placed. These components, or building blocks, represent the various ducts and volumes of the engine as well as the other various engine components such as the combustion chambers and valves. WAVEBUILD accepts the input of the operating conditions and various required data for each of these building blocks. The intent of the following sections is to describe the model created for this research to be analysed by WAVE.

The modelling process began with the creation of the unmodified model of the engine used in this study. By using the term 'unmodified', it is meant that the engine is the original, or base engine, constructed and analysed prior to the implementation of any manifold bridging technique. The engine modelled is a Toyota 4A-GE used in North America in the high performance MR2 Mark I (1985 - 1989) and Corolla GTS (1988 - 1991) applications. The engine configuration is a 16 valve, inline 4 cylinder with a displacement of 1587 cc and a compression ratio of 10:1 [26]. This engine was used to provide the reference performance information needed to evaluate the results of the implementation of the proposed attenuating techniques.

It should be noted that the creation of a model, such as the one presented in this study, is a long and arduous process if meaningful results are expected. As a complete model was unavailable for this particular engine, it was necessary to disassemble the entire engine and physically measure all required parameters. The fundamental dimensional and engine data required by Wave to create the model of the Toyota engine has been provided in Appendix A. Wave outputs of the actual modelled parameters used are provided in Appendix B.

The intake system was the first to be disassembled. The length of all ducts and volumes were measured including the determination of any bend angles. It should be noted that the intake manifold for this engine is of a unique configuration because the manifold connection consists of two runners per cylinder.

For the cylinder head, the size of the intake and exhaust valves were verified as were the valve lift dimensions. Initial assumptions of temperature, pressure and flow coefficients were also established. These assumptions were later verified by running performance tests of the fired engine and comparing these modelled results to the known engine specifications. This lengthy, iterative process required the modification of many of the assumed values until a satisfactory correlation was achieved.

As with the case with the intake manifold, the exhaust manifold was also disassembled and measured. Of particular importance was the determination of the various volumes that make up the junctions where each of the ducts joined one another. Again, the accurate determination of the various angles and orientation of each of the ducts was undertaken with care in order to achieve good numerical results.

Examination of Figure 4.1 shows the completed unmodified engine model of the engine used in this study. In order to understand the representation of the building blocks comprising the model, a discussion of each of the component blocks is relevant. i.e. the intake ducting and manifold, the cylinder head and the exhaust manifold. A discussion of the optimisation of the bridge design is also presented.

4.2.1 Inlet Ducting

A schematic of the front end of the air induction system along with the corresponding WAVE components is shown in Figure 4.2. Here the inlet snorkel, which is open to the ambient conditions, is attached to the airbox where the air filter is housed. The airbox is modelled as two cylindrical volumes joined at the air filter element. This is represented by the hatched line in the upper figure. The air filter is modelled as a 'massless', or zero length duct, with a perforated obstruction. Exiting the airbox is the zip tube which is simply a duct running to the throttle body. The throttle in this case is modelled by two ducts joined by a junction which represents the effective area once the effects of all restrictions have been taken into account. The diameter of the throttle is variable and can be set to represent different engine loading conditions.

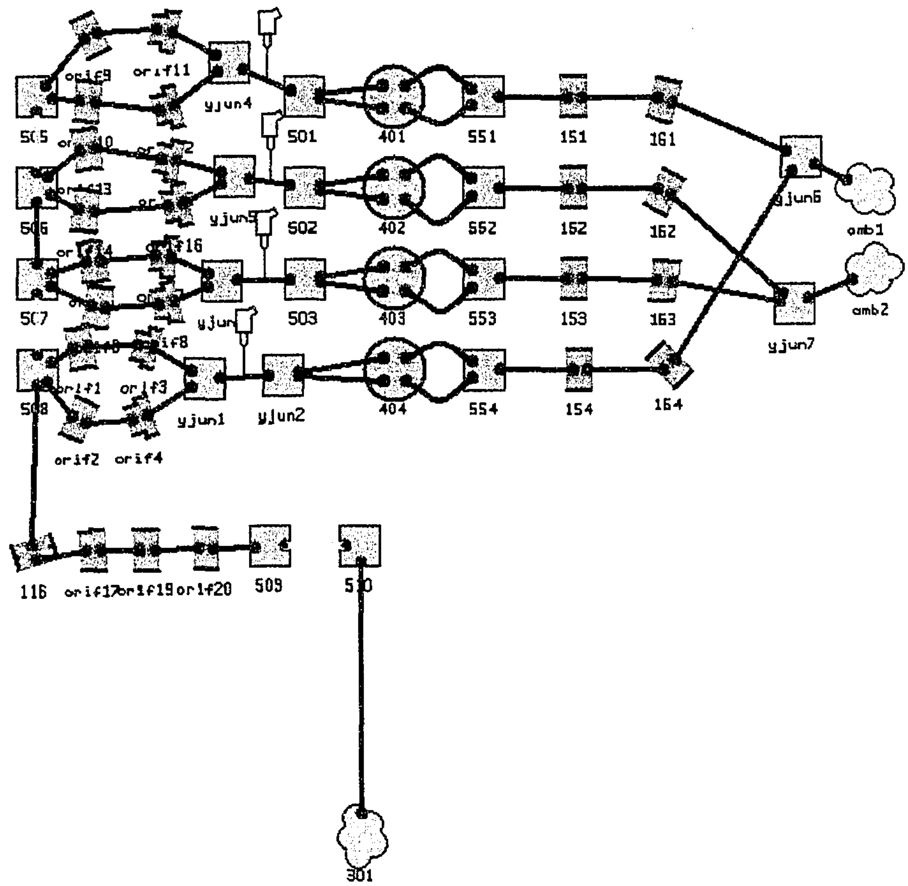

Figure 4.1: Screen shot of the Unmodified Engine Model from WAVEBUILD Showing the Layout of the Building Blocks for the Modelled Components

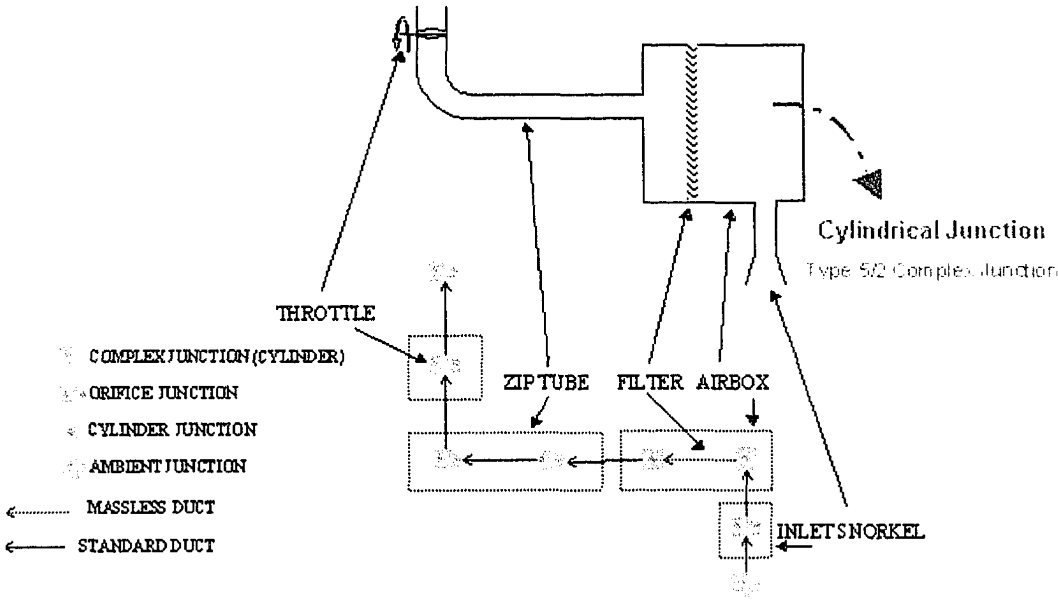

Figure 4.2: Schematic of the Front End of the Intake Subsystem along with the WAVEBUILD Building Blocks Used to Model These Components [40]

4.2.2 Intake Manifold

Figure 4.3 is a representation of the modelled unmodified intake manifold. The manifold consists of a plenum with four runners of dimensions as illustrated. The inlet to the plenum is the throttle body discussed previously. The runners are modelled by three individual ducts in series so as to accurately represent the changes in cross sectional area and any bends. The manifold mounted injectors (not shown) were placed in the final section of the modelled duct. These injectors continuously feed fuel for a spark ignited model based on the air flow at a specified fuel/air ratio.

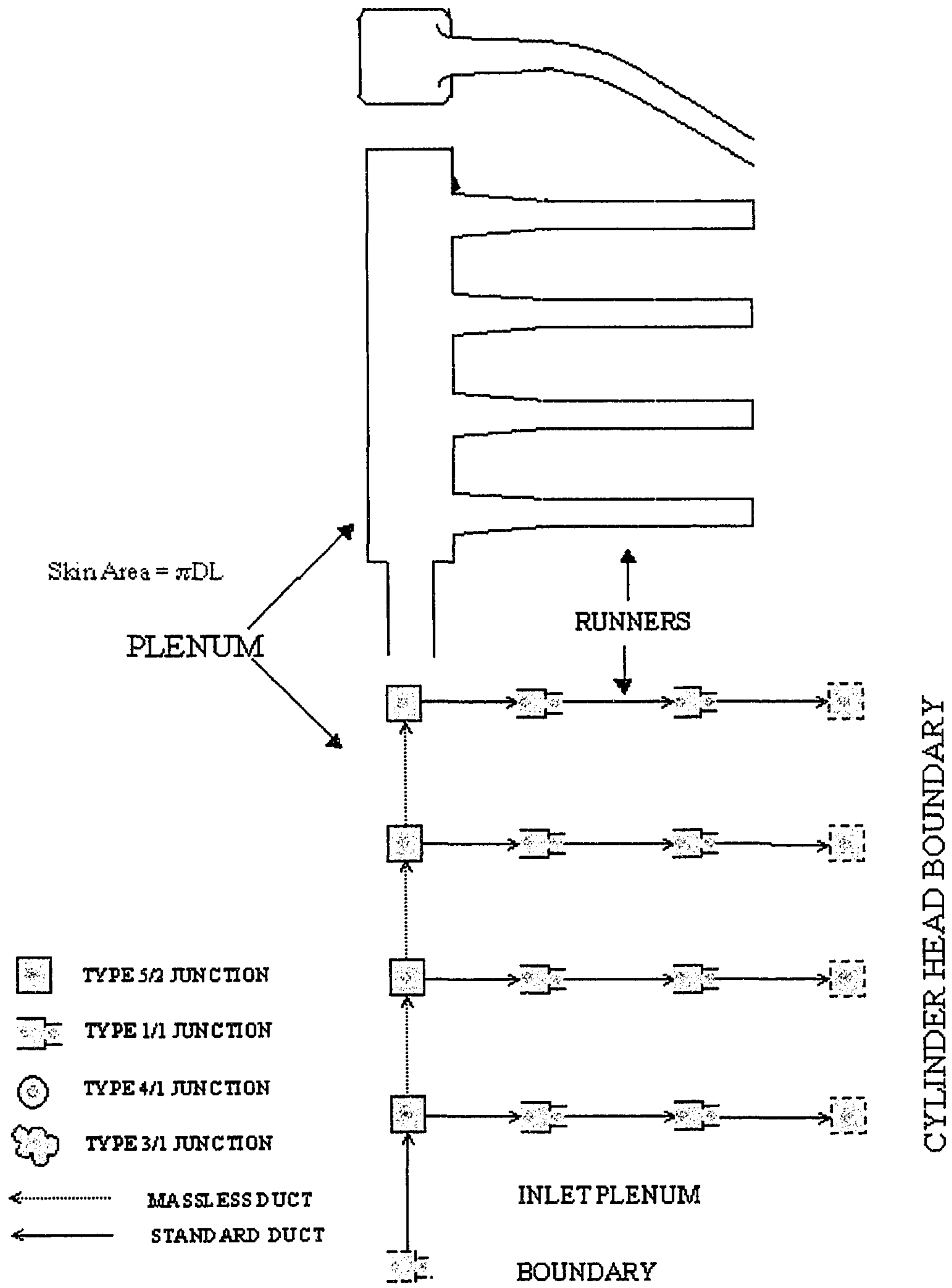

Figure 4.3: Schematic of an Intake Manifold along with the Required WAVEBUILD Building Blocks Used to Model Each of the Components [40]

4.2.3 Cylinder Head

The next subsection of the model is the cylinder head as represented in Figure 4.4. As previously stated, the engine is a 16 valve, four cylinder engine with four valves per cylinder. The diameter of each intake valve is 28 mm with a maximum lift of 8.3 mm. The exhaust valves have a diameter of 23.5 mm with a lift 8.0 mm. All losses related to the ports are taken into account through the specification of a flow coefficient for the intake as well as the exhaust. Figure 4.5 shows an output of the valve lift profile of the intake valves.

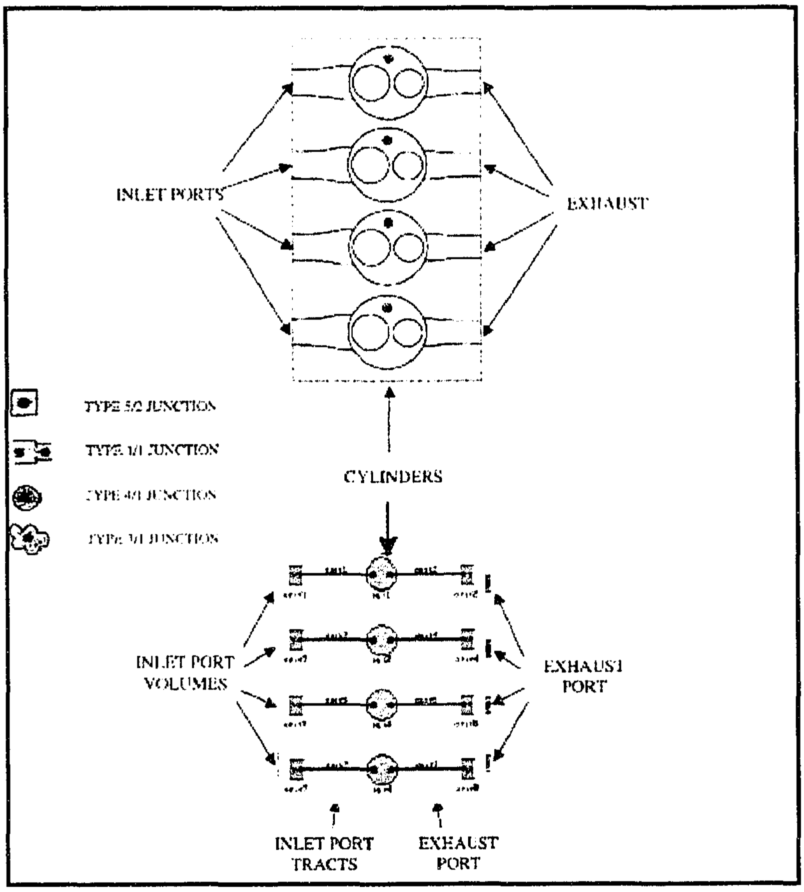

Figure 4.4: Schematic of an Engine Cylinder Head along with the WAVEBUILD Building Blocks used to Model these Components [42]

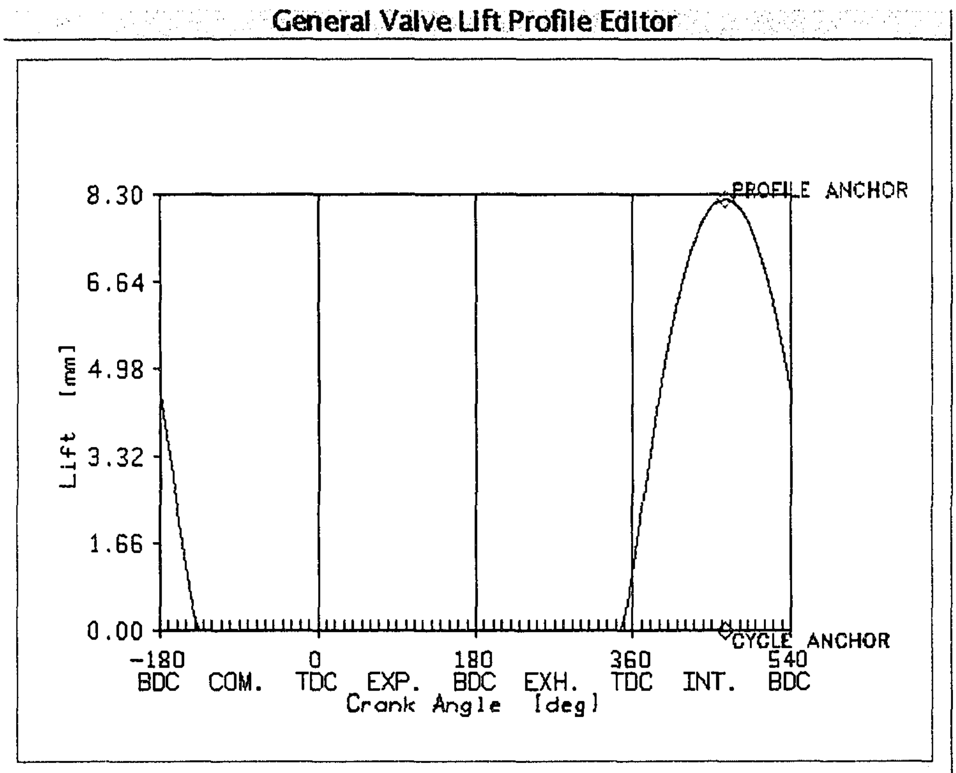

Figure 4.5: Intake Valve Lift Profile Showing Valve Lift Distance versus Crank Angle for the Intake Valve Used for this Study

4.2.4 Exhaust Manifold

The exhaust manifold for this engine is a four-to-two configuration. In other words, there are four exhaust runners which join to become two runners, subsequently meeting to become a single outlet further downstream of the modelled portion of the exhaust. A schematic of this configuration along with the WAVEBUILD input diagram is shown in Figure 4.6. Care must be taken to ensure that the angles and dimensions of the ducts be carefully represented in the model input parameters as they play an essential role in determining the dynamic behaviour of the exhaust system.

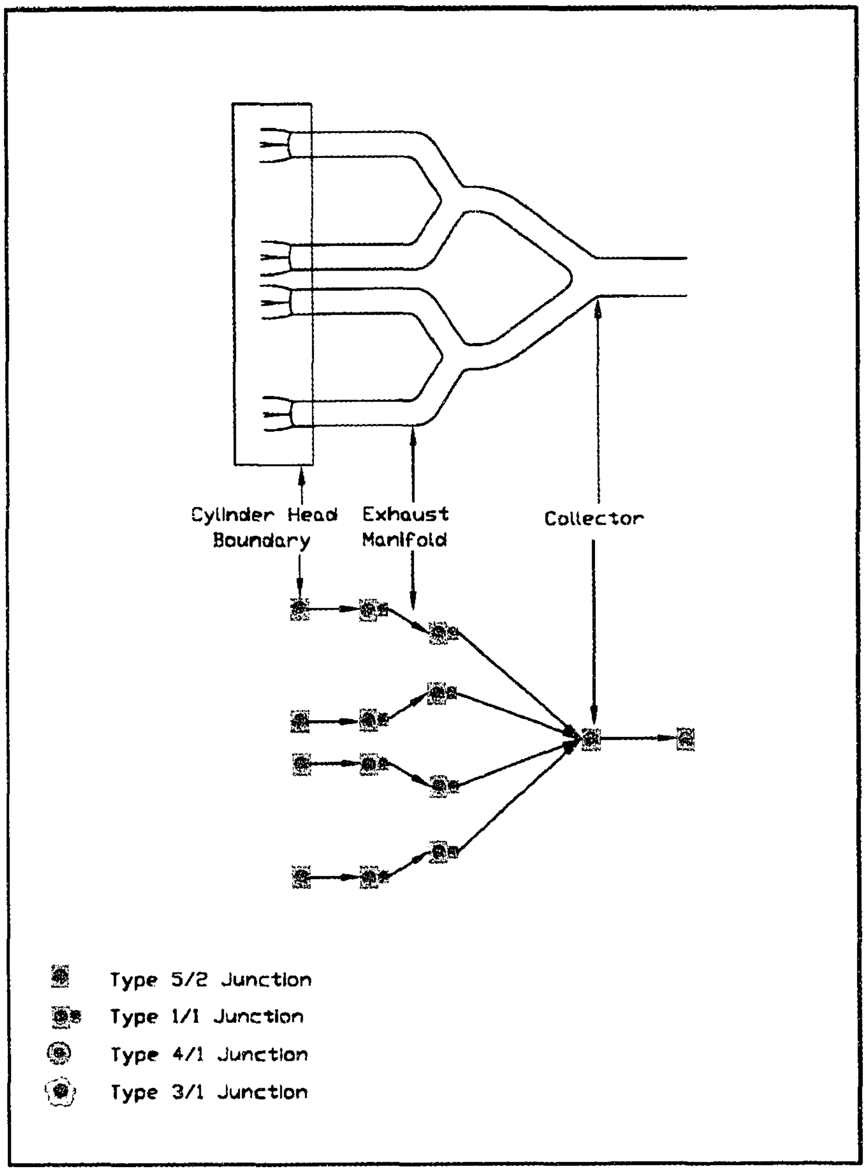

Figure 4.6: Schematic of a Four into One Exhaust Manifold System along with the Required WAVEBUILD Building Blocks used to Model each of the Components[40]

4.2.5 Optimization of Bridge Design

Once a working model of the unmodified engine was successfully created, the task of design and optimisation of the bridge configurations was undertaken. This included the determination of the exact layout of the bridging ducts as well as their individual lengths, diameters, and connection locations on each of the two manifolds.

Several bridge configurations were initially considered. The first bridge considered consisted of four ducts connecting intake and exhaust runners which were 180 degrees out of phase from each other with respect to the firing order of the engine. This model was created based on the principle that it would permit acoustic energy propagating through an exhaust runner, while that exhaust valve was open, to be transferred to a corresponding intake runner which would also have an open intake valve. The second configuration consisted of four ducts, each connected between one of the four exhaust manifold runners and one of the corresponding intake manifold runners. That is, an individual bridge duct connected to cylinder number one exhaust runner was connected also to cylinder number one intake runner. The third option consisted of a single bridge linked from the exhaust manifold plenum to the intake manifold plenum.

The next step was to dimensionally optimise each of the bridge configurations to determine the best option. This was accomplished using an iterative process involving WAVE. Each of the four bridge lengths were varied independently in increments of 25 mm until an optimised attenuation of induction noise was achieved for each of the four design options. The only constraint given in this process was that the lengths of each of the bridges had to be long enough to reach from the exhaust manifold to the corresponding intake manifold so that the construction of the bridge design was feasible. At the same time, an upper limit on length was imposed so as not to produce a bridge so long as to be impractical for implementation. Next, the diameters of each of the bridge ducts had to be optimised. Restrictions on the diameter were imposed to limit the maximum internal diameter. That limitation was set as the smaller of the two manifold diameters. In this case, the intake manifold diameter provided the limiting dimension of 26 mm. Subsequently, the predicted sound pressure levels at the intake openings were compared. A flow chart which illustrates this process is given as Figure 4.7. It was determined that the second configuration produced the greatest attenuation of intake noise using the predicted unweighted sound pressure as the deciding criteria. The optimized dimensions for the chosen design are given in Table 4.1.

Table 4.1: Dimension of the Manifold Bridge Used for the Numerical and Experimental Comparisons with the Noise Output of the Unmodified Toyota Engine

Bridge Number	Length (mm)	Diameter (mm)
1	975	26
2	1675	26
3	975	26
4	1275	26

4.3 Discussion of Modelling Outputs

This section describes the modelling output descriptors used to compare the acoustical performance of the modified engine to the original unmodified engine. The acoustical descriptors used to compare the experimental results to those obtained from the numerical modelling results are also discussed.

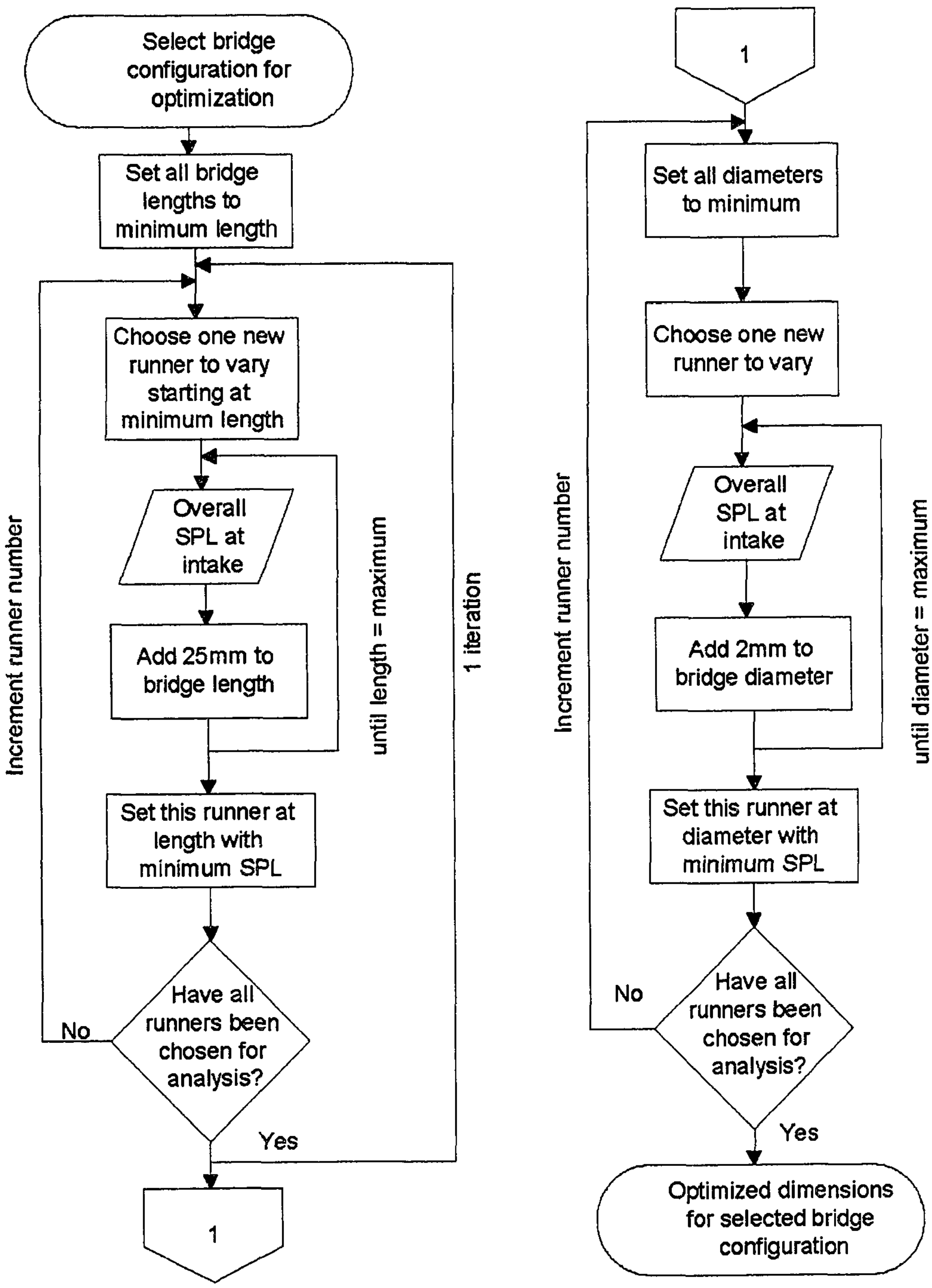

Figure 4.7: Flowchart which Describes the Optimization Process Used to Determine the Manifold Bridge Dimension for Best Acoustic Performance

4.3.1 Conventional Acoustical Analysis Techniques

The goal of validating the feasibility of using a manifold bridge to improve the acoustical performance of an automotive intake system brings with it the expectation of a realized change of the acoustical performance. Therefore, the acoustic parameters are the primary focus in determining success. These fundamental acoustic parameters are the sound pressure (Pa) at various locations in the ducts and the sound pressure level, with units of decibel (dB) at a specified location in the ambient environment. The sound pressure levels will be either unweighted (dB) or A-weighted (dBA). As described by Wilson, the use of an A-weighted sound level "takes the typical human response into account when all the audible frequency components of a noise sample are to be described by a single number." [54]

To compare the modified and unmodified modelled engines, as well as to optimize the bridge dimensions, duct pressure data versus engine crank angle was collected in the intake duct upstream of the airbox. When the data of the modified and unmodified modelled engines are compared, this information is indicative of the realized attenuation due to the implementation of the manifold bridge. An example of a duct pressure measurement at this location for the unmodified engine intake is illustrated in Figure 4.8. Shown here is the acoustic pressure amplitude versus the crank angle for one complete combustion cycle, or a crank rotation of 720 degrees.

Sound pressure level data, collected in the ambient at a distance of 100 mm from the induction inlet, was also used to compare the acoustical properties of the modified and unmodified modelled and experimental engines [13]. An example of a modelled sound pressure level of the unmodified engine is shown in Figure 4.9 as determined through the use of an acoustic post processor program dBSonic. Information regarding the functional capabilities of dBSonic will be presented in greater detail in a following section. The three-dimensional spectrogram shown represents the spectral output and is intended to illustrate the sound pressure amplitude versus acoustic frequency versus time characteristics of the unmodified engine. A similar representation of this output is shown in Figure 4.10 which is a waterfall representation of the same acoustic analysis. These outputs are used for transient runs of the models. For steady state cases of both the analytical and experimental results two dimensional spectral graphs of the sound pressure amplitude versus acoustic frequency will be presented.

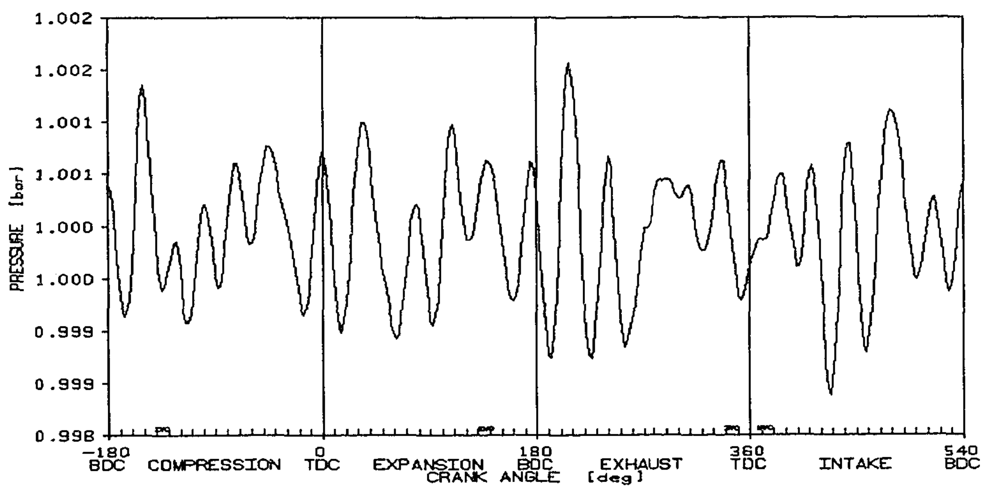

Figure 4.8: Example Duct Acoustic Pressure Versus Crank Angle Graph for Inside the Intake Manifold for One Complete Combustion Cycle using WAVE

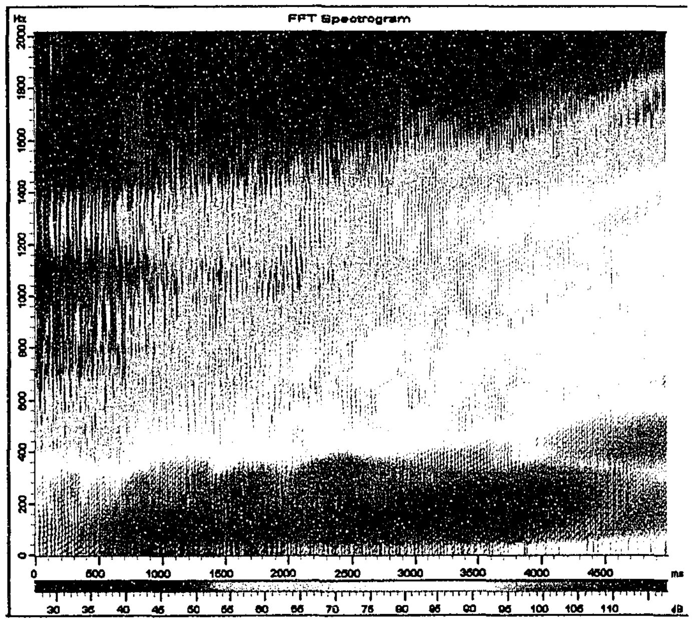

Figure 4.9: Modelled Sound Pressure Level (colour) vs Frequency (y-axis) vs Time (x-axis) Predicted 100 mm from the Intake Opening for the Unmodified Engine

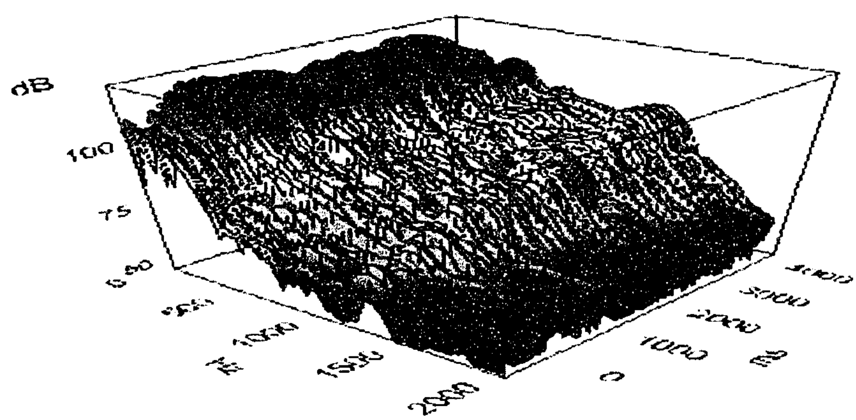

Figure 4.10: Modelled Acoustic Waterfall of Sound Pressure Level vs Frequency vs Time Predicted 100 mm from the Intake Opening for the Unmodified Engine

4.3.2 Psychoacoustic Analysis Techniques

In addition to the traditional acoustical measurements discussed above, several psychoacoustic metrics were also employed to assist in the characterization of the effectiveness of the manifold bridge. This type of analysis, often referred to as 'sound quality', is the quantification of a qualitative assessment of the resulting acoustic output of a source. This technique serves to illustrate the relationship that exists between the physical and perceptual attributes of sound. Using psychoacoustic metrics, the complicated relationships that exist between the physical and perceptual quantities can be visualized. The metrics that were used for this research include loudness, sharpness, fluctuation strength and roughness. In order to clarify for the reader the purpose of each of these metrics, a functional description of each has been included.

4.3.2.1 Loudness

Zwicker Loudness is a standardized metric that describes the human perception of loudness instead of simply a reported sound pressure level. According to Zwicker, this value takes into account the temporal processing of sounds as well as audiological masking effects [57]. "Loudness comparisons can lead to more precise results than magnitude estimations. For this reason, the loudness level was created to characterize the loudness sensation of any sound." [57]. It is often thought that the perceived loudness will directly depend on the physical quantity of sound pressure, resulting in the equal loudness contours, as long as the sound pressure remains equal. This is usually incorrect. Due to the temporal and spectral makeup of the sound, the loudness may differ from the equal sound pressure levels by a factor of as much as 1:4. This can be illustrated by the fact that broad band signals are perceived to be louder than narrow band signals that have the same sound pressure level [12].

The loudness level can be measured for any sound, but it is most easily illustrated using pure tones. The unit of loudness is the sone instead of decibel. Figure 4.11 illustrates the equal loudness contours for pure tones in a free field environment. Using a pure tone at 1000 Hz as a reference, the perceived loudness at all other frequencies were established through experimental jury tests. The loudness of the 1000 Hz tone with a sound pressure level of 40 dB was arbitrarily chosen as the reference signal and corresponds to a loudness of 40 phons. It should be noted that loudness is usually identified using sones where 40 phons is equal to 1 sone. A sound source which is perceived to be twice as loud as a 1 sone signal will have a corresponding loudness of 2 sones. The relationship between the phon and sone is given as:

$$S = 2^{(P-40)/10} \qquad (4.1)$$

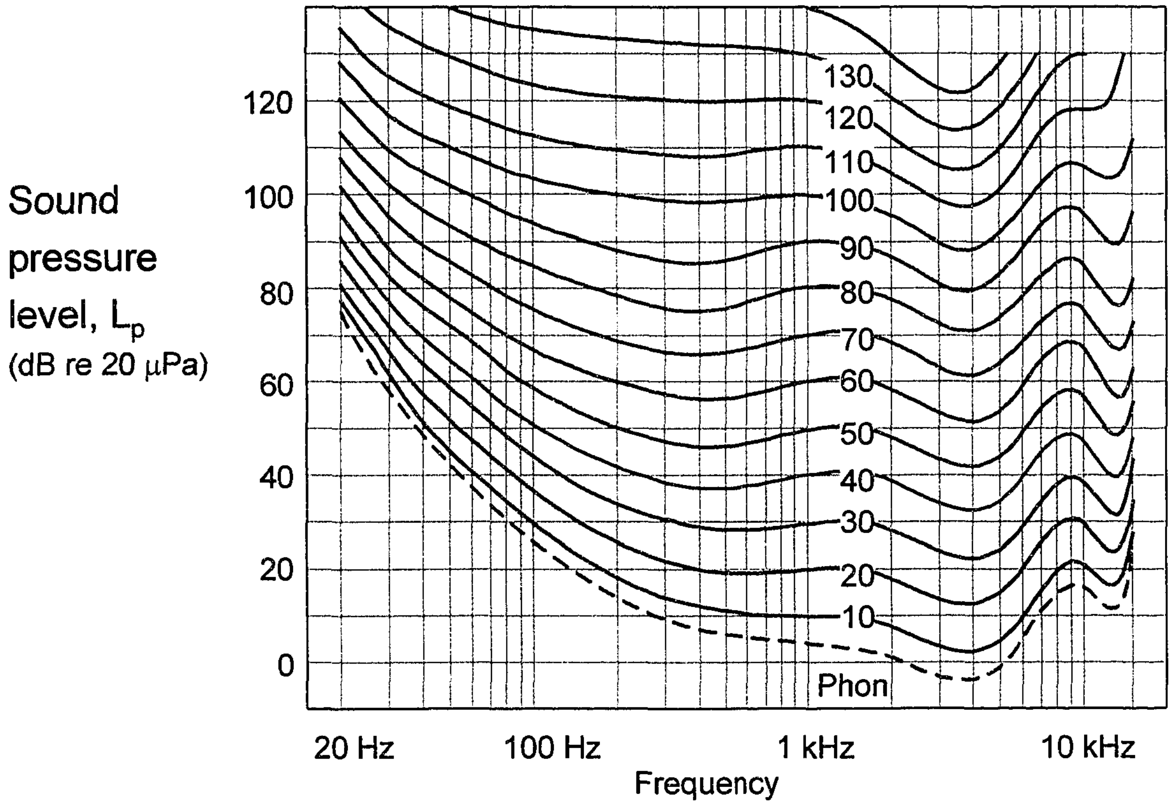

Figure 4.11: Equal Loudness Contours for Pure Tones in a Free Field Environment Relating Loudness and Sound Pressure Level and Frequency [23]

It should also be noted that loudness is usually expressed across non-conventional bandwidths called critical bandwidths instead of a fraction of the octave. A special scale is used to describe the critical band rate which is expressed by the unit "Bark" which has a range from 0 to 24. Table 4.2 shows the 24 accepted Bark bands with their centre, start and stop frequencies. Also shown is the relationship between the 24 Bark bands and the equivalent 1/3 octave bands.

Table 4.2: 24 Bark bands and the Equivalent 1/3 Octave Bands with Start, Stop and Centre Frequency and Bandwidth [23]

Bark Scale Frequencies

Bark Band #	Center Freq.	Bandwidth	Start	Stop	Equiv. 1/3 Octave Bands
1	50	100	0	100	1.25 - 100
2	150	100	100	200	100 - 200
3	250	100	200	300	200 - 315
4	350	100	300	400	315 - 400
5	450	110	395	505	400 - 500
6	570	120	510	630	500 - 630
7	700	140	630	770	630 - 800
8	840	150	765	915	800
9	1000	160	920	1080	1000
10	1170	190	1075	1265	1250
11	1370	210	1265	1475	1250
12	1600	240	1480	1720	1600
13	1850	280	1710	1990	2000
14	2150	320	1990	2310	2000
15	2500	380	2310	2690	2500
16	2900	450	2675	3125	3150
17	3400	550	3125	3675	3150
18	4000	700	3650	4350	4000
19	4800	900	4350	5250	5000
20	5800	1100	5250	6350	6300
21	7000	1300	6350	7650	6300
22	8500	1800	7600	9400	8000
23	10500	2500	9250	11750	10k
24	13500	3500	11750	15250	12.5k

$$\Delta f = 25 + 75 * [1 + 1.4 * (f_r / 1000)^2]^{0.69}$$

4.3.2.2 Sharpness

Sharpness describes the high frequency annoyance of noise by applying a weighting factor to the higher frequency band content. This overall measurement is useful for such sounds as broadband sources, wind or rushing air noise and gear meshing sounds. In an automobile engine, a high frequency component of intake noise is created by the intake air travelling across the valve seat at a high velocity. For this reason, it is assumed that sharpness is an appropriate metric for the evaluation of the merits of the manifold bridge.

air travelling across the valve seat at a high velocity. For this reason, it is assumed that sharpness is an appropriate metric for the evaluation of the merits of the manifold bridge.

The unit used to describe sharpness is the acum which is the Latin word for sharp. The calculation of sharpness is based on the loudness level in each of the frequency bands where more weight is given to the higher frequency bands. As explained by Zwicker, "The reference sound producing 1 acum is a narrow band noise, one critical band wide, at a centre frequency of 1 kHz having a level of 60 dB." [57]

4.3.2.3 Fluctuation Strength and Roughness

Fluctuation strength and roughness are both metrics used to describe the annoyance of modulating sounds depending on the frequency of the modulation. These are important because when two frequencies interfere with each other and cause an audible modulation, a very unpleasant sensation to the human ear results. Figure 4.12 illustrates the concept of modulation through the application of two individual pure tones. The first tone, or the top graph, is a 10 Hz sine wave where the second graph is an illustration of a 12 Hz tone. If both of these tones were to be played simultaneously, a modulation with a frequency of 2 Hz would appear as is shown on the bottom graph. In other words, rather than noticing the individual tones, the human ear would instead focus on the 2 Hz modulation frequency. Examples of modulating sources include beating sounds, air raid sirens, helicopters and fan blades.

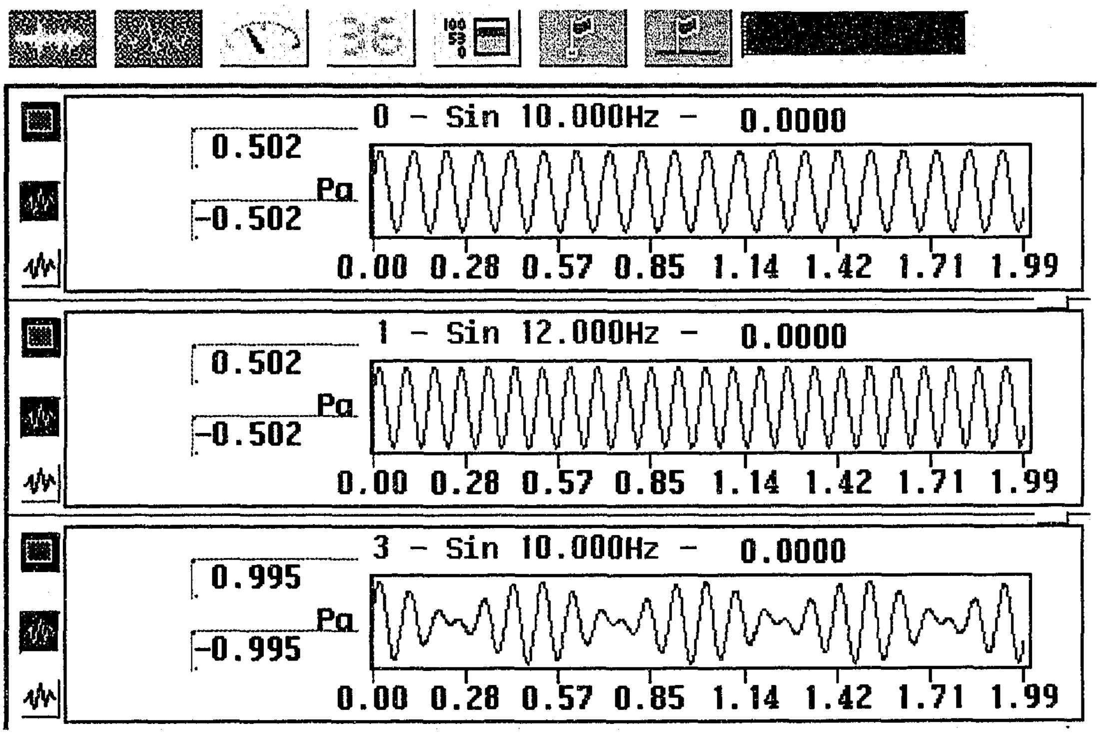

Figure 4.12: Illustration of the Creation of a 2 Hz Modulated Signal from two Pure Tones of 10 Hz and 12 Hz Respectively [19]

The fluctuation strength focuses on sounds which modulate at frequencies between 0.5 Hz and 20 Hz, with 4 Hz being the most annoying fluctuation to the human ear. When the modulation frequency is less than 20 Hz the sound functions are perceived to change in sound volume over time. Alternatively described, they appear to repeatedly fade in and out. Typically these fluctuation signals appear louder and are much more annoying than steady state signals of the same RMS amplitude.

The unit of amplitude for fluctuation strength is the vacil. The reference of 1 vacil is produced by a 1 kHz tone at 60 dB with a 100 percent amplitude modulation of 4 Hz. This can occur within an automotive intake system due to the low frequency modulations resulting from the geometry of the airbox and associated intake ducting.

The roughness metric is used to describe the situation where the modulation frequency is between 20 and 150 Hz. Within this frequency range of modulation, the sensation is a stationary but rough tone which is rather unpleasant. In automotive applications, this sensation is often associated with engine noise where fractional orders cause the modulation effects. Roughness increases with the degree of modulation and is less sensitive to the base frequency. The unit to describe roughness is called the asper where 1 asper is a representation of a 70 Hz modulated 1 kHz tone with a sound pressure level of 60 dB.

The underlying criteria used to determine the amplitude of these modulating metrics are not straightforward. An important element in the calculation of the modulation metrics is the temporal variations of the signal amplitude which results in the effect of masking. The quantitative algorithms to calculate these metrics involve the calculation of the partial or specific metric first in each critical band based on the modulation frequency, depth and masking effects which are also dependant on the loudness and integrating these to obtain the total modulation.

It should be noted that for high modulation frequencies above 300 Hz, three separate tones will be audible. When such a situation exists, the listener would be able to hear the two individual tones as well as the modulating tone, all at the same time. The ability to distinguish the three separate tones is considered to be less annoying.

V. EXPERIMENTAL DETAILS

When performing any experimental measurements, the data collected must be both meaningful and repeatable and also remain in conformance with any physical and theoretical restrictions imposed by the measurement systems. Also, a thorough understanding of the experimental procedure and equipment used in the verification process of the numerical results is most important. The purpose of the numerical modelling was to establish a dimensionally optimized bridge design from several different configurations as were discussed in the previous chapter. Subsequently, a comparison of the predicted intake noise attenuation of the chosen numerically optimized bridge was made to experimental measurements of the same configuration and design. A later experimental study included the other bridge designs. [52] Here, the conclusions derived from the numerical modelling study are that the bridge used in this study was the most effective was verified. The following sections will provide an overview of the equipment and instrumentation selected, the design and preparation of the experiment and a description of the tests done on the system.

5.1 Equipment and Instrumentation

The equipment and instrumentation used to facilitate the experimental procedure can be classified into three separate areas being:

1. The engine to which the manifold bridge was attached and on which it was experimentally tested.

2. The engine dynamometer and controlled acoustical measurement environment with which the experiments were conducted.

3. Equipment, instrumentation and software used for acquiring and analysing the experimental data.

5.1.1 Test Engine

The primary focus of the experimental portion of this research was to verify the numerically determined acoustic results obtained from the Ricardo WAVE simulations. In order to accomplish this, a physical representation of both the engine used in the modelling process as well as the manifold bridge was required. The engine used was a 16 valve inline 4 cylinder Toyota 4A-GE used in North America in the MR2 Mark I (1985 - 1989) and Corolla GTS (1988 -1991) applications. The geometrical and performance specifications of the Toyota 4A-GE engine are given below in Table 5.1.

Table 5.1: Technical Specifications of Toyota 4A-GE Engine [26]

Model	4A-GE
Type	DOHC inline-4
Bore x Stroke	3.19 x 3.03 in / 81 x 77 mm
Displacement	96.8 cu in / 1587cc
Compression Ratio	10.0:1
BHP @ RPM	124 @ 6500 (pre '88 is 122 @ 6600)
Torque @ RPM	110 lb-ft @ 5200 (pre '88 is 105 @ 5000)
Fuel Injection	MAP sensor based Bosch L-Jetronic

5.1.2 Test Equipment and Environment

When performing any simulation tests, the replication of real world operating parameters is very important. This is particularly true for acoustical tests since the results are very dependant on the environment from which they are acquired. Special attention must, therefore, be given to the design of vehicle and engine test dynamometers and acoustic chambers. The following sections describe and consider some of the important considerations that should be given in the use of such facilities with a specific focus on the facilities used in this study.

5.1.2.1 Anechoic Test Environment

Anechoic rooms are designed to approximate free field conditions where the effects of any obstacles or boundaries are negligible [54]. Ideally, all of the generated incident acoustic energy is absorbed by the interior surfaces of the room. This provides a measurement environment free from reflected sound. To achieve this, the room is lined with sound absorbing material on all surfaces such that shown in Figure 5.1. In this type of environment, the inverse square law relating measurement distance and sound pressure is expected to exist. The sound power level (dB) emitted by an ideal, spherically radiating source will decrease by six decibels for each doubling of distance between the source and receiver.

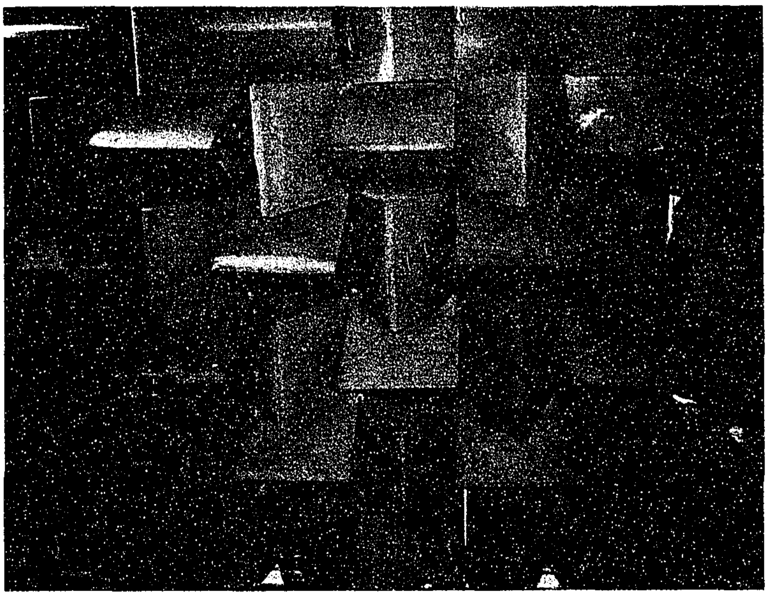

Figure 5.1: Sound Absorbing Material, or Wedges, Placed on the Wall of an Anechoic Environment.

The engine was located in a semi-anechoic room for the work presented herein. A semi-anechoic chamber is constructed in a manner similar to that of the anechoic room. The exception being the presence of a concrete floor which is acoustically reflective. The ambient noise in this room falls within an A-weighted sound pressure level range of 18 to 20 dBA which is ideal for the measurement of noise sources greater than 30 decibels. A photograph of the test engine attached to the dynamometer and mounted on the engine stand located inside the semi-anechoic room is provided in Figure 5.2.

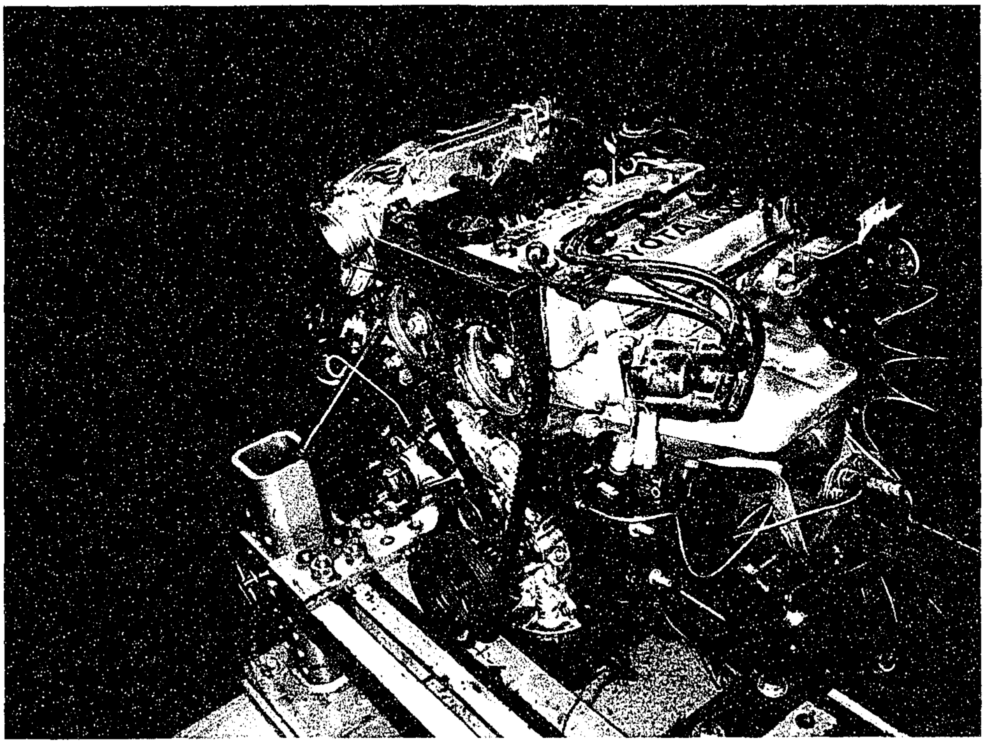

Figure 5.2: Toyota 4A-GE Test Engine Installed on the Dynamometer Test Sled located inside the Semi-Anechoic Test Environment

5.1.2.2 Dynamometer

An engine dynamometer is commonly used to measure the shaft output power of an engine by measuring the shaft speed and load created by the reaction torque at the trunnion bearings of the load cell. Some dynamometers, such as the one used in this study, also have the ability to motor an engine without combustion.

The model number 7290 167 dynamometer used in this study was manufactured by ASEA. The Simoreg, model 6R424 [47] dynamometer controller/converter was manufactured by Siemens. This setup is a direct current (DC) dynamometer which is schematically illustrated in Figure 5.3. As described by Randall, this type of dynamometer, "consists essentially of a trunnion mounted DC motor generator. Control is almost universally by means of a thyristor based AC/DC converter. DC dynamometers are robust, easily controlled, and capable of motoring and starting as well of absorbing power. Disadvantages of this design include limited maximum speed and high inertia" [38]. The current setup within the facilities used for this study is limited to only motored tests; therefore, all experiments were performed under these conditions. A photograph of the dynamometer and controller used for this study is shown in Figure 5.4. It can be seen that the output shaft of the dynamometer passes through the wall of the semi-anechoic room where it is connected to the test motor.

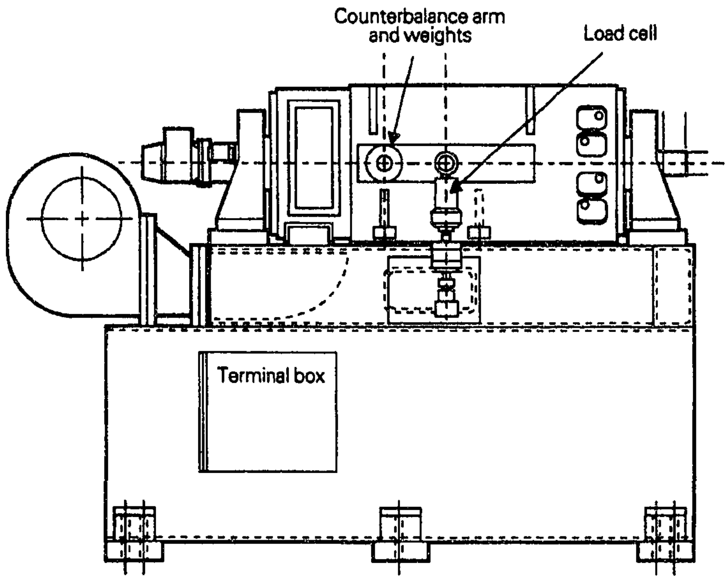

Figure 5.3: Schematic of a Typical D.C. Electrical Dynamometer Illustrating the Load Cell, Counterbalance Arm and Weights [38]

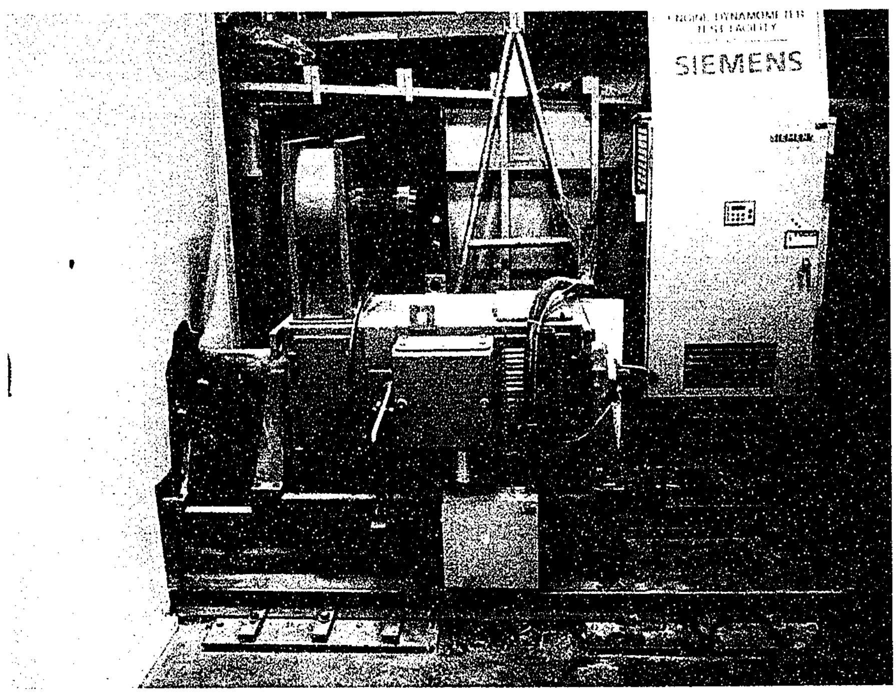

Figure 5.4: Photograph of the D.C. Electrical Dynamometer and Controller Used for this Study Located Outside the Semi-Anechoic Room

5.1.3 Data Acquisition and Analysis Software

Figure 5.5 illustrates the data acquisition hardware employed to record the induction noise data produced by the motored Toyota engine. A GRAS 40AF ½" free field condenser microphone connected to a GRAS 1B7 pin lemo pre-amplifier and 3 metre extension cable were used to acquire the noise data at the intake opening. The microphone was connected to a 01dB Orchestra eight channel dynamic signal analyser. The Orchestra was connected though a firewire interface to a personal computer (PC) located outside the semi-anechoic room. This setup enables simultaneous multi-channel real time analysis of acoustic signals while recording to the PC hard disk. The advantage of this is that it permits the monitoring of the overall and the $1/n^{th}$ octave acoustic information for data quality while the raw data is stored for future postprocessing.

Figure 5.5: Orchestra 8 Channel Data Acquisition Hardware with Microphone and Computer used to Record the Induction Noise

The real time acquisition and post processing software used was also created by 01dB and is called dBFA32. This software enables the direct to disk recording of the acoustical signal measured for the post processing activities presented further in this dissertation. This software is capable of performing traditional acoustical analysis such as overall sound levels, frequency analysis of steady state signals (FFT) and waterfall graphs of transient signals. In addition to this, dBFA32 was also used to post process the noise data to obtain the psychoacoustic quantities used as part of this study. A typical 'real time' screen shot of a measurement signal being collected by dBFA32 is shown in Figure 5.6. A second post processor, dBSonic, was also used to produce the psychoacoustic outputs which are presented in Chapter 7. This powerful program enables the measurement and analysis of audible differences in acoustics signals that until recent years could not be quantified. This postprocessor program has the ability to display the psychoacoustic results as single valued metric results, such as overall loudness, or as sophisticated spectra enabling the output of time varying and transient signals. A typical screen shot of a measurement signal that has been processed by dBSonic is illustrated in Figure 5.7. Additional information including technical descriptions for the acquisition hardware and software in the form of manufacturer literature is given in the appendix.

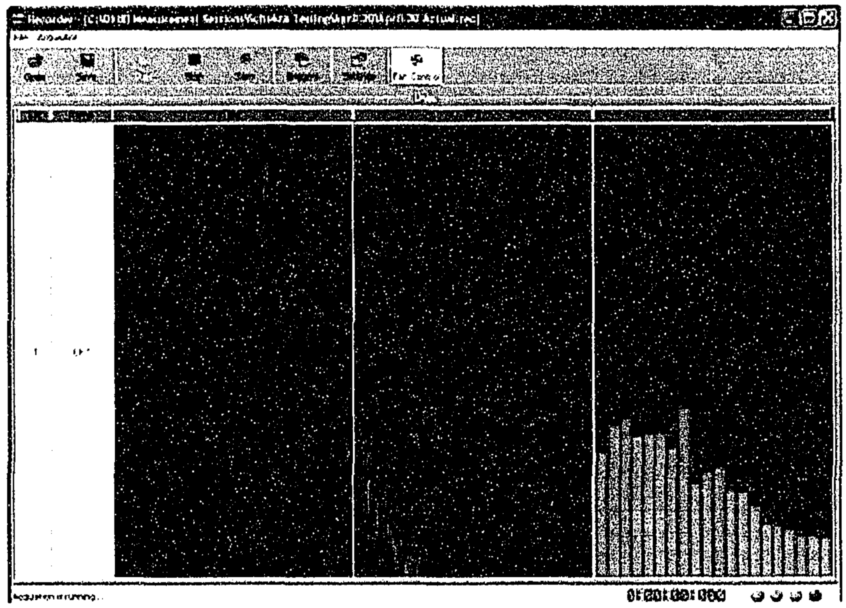

Figure 5.6: Screen Shot of dBFA32 Acquisition Software Collecting Noise Measurement Data and Displaying Time FFT and 1/3 Octave Real Time Results

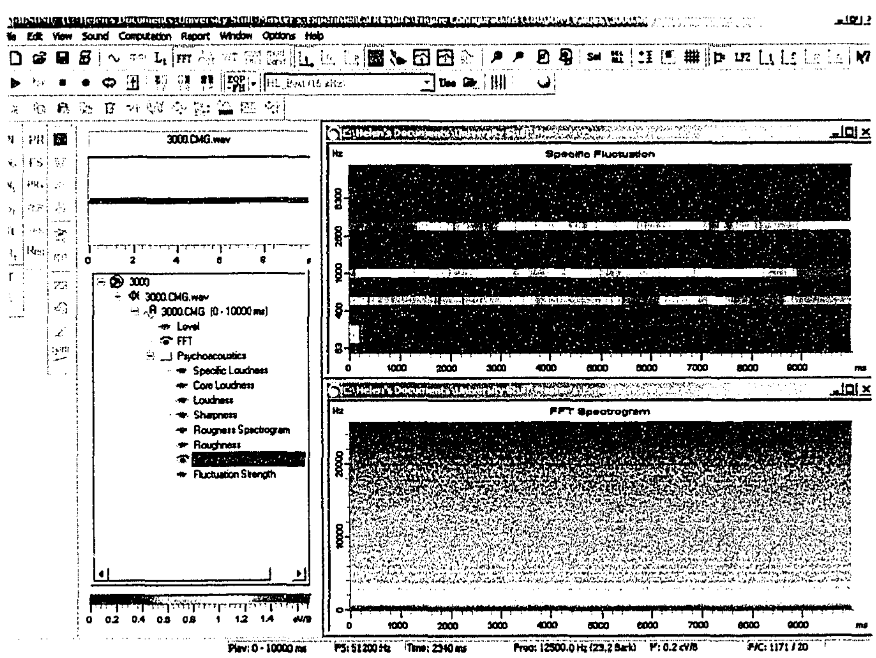

Figure 5.7: Screen Shot of the dBSonic Post processing Software Collecting Displaying Psychoacoustic Results

5.2 Experimental Design and Preparation

The steps taken to modify the physical Toyota engine and prepare it for the installation of the manifold bridge, as well as the physical construction of the bridge are outlined in the following section. Also, provided below is a description of the preparation of the dynamometer in order to facilitate the mounting of the engine as well as the steps taken for the installation of the engine.

5.2.1 Construction of the Manifold Bridge

Before the manifold bridge could be constructed, the exact parameters specifying the length, diameter and impingement location on each of the two manifolds had to be determined. A description of this process, along with the optimized bridge dimensions was described in Chapter 4. Using this information, the bridge was constructed and installed on the engine. The material used for the bridging duct was polyvinyl chloride. This material was chosen for its low cost, availability and ease of manipulation into various shapes. The following is a step by step procedure outlining the methodology used for the creation of the manifold bridge:

1. Determine the ideal duct diameter using the analytical model. This dimension is restricted by the physical limitations imposed by the smaller inside diameter of either the intake or exhaust manifold.

2. Determine the ideal bridge length using the WAVE model. This dimension also had restrictions imposed on it since it must be at least long enough to reach from the exhaust to the intake manifold, yet not be so long as to be unrealistic.

3. Modify the intake and exhaust manifold at the locations specified by the analytical model. Figure 5.8 is a photograph of the modified intake manifold. It should be noted that the manifold has two intake runners per cylinder with a vacuum controlled butterfly valve which would open when performance conditions dictated. For this study, the vacuum diaphragm was modified to

permit the valve to remain open, thus effectively allowing the two runners per cylinder to act as one.

4. Permanently attach the fittings to the manifolds using a polyurethane hot melt adhesive. This permitted the bridging ducts to be attached and removed to facilitate the experimental testing of several configurations as described in elsewhere [52]. Figure 5.9 is a photograph of the modified exhaust manifold.

5. Cut the ducting material to length and manipulate it to fit between the two manifolds. The manipulation of the conduit was achieved by softening the material with a heat gun and forming it to the desired shape. Figure 5.10 is a photograph of the engine with the manifold installed.

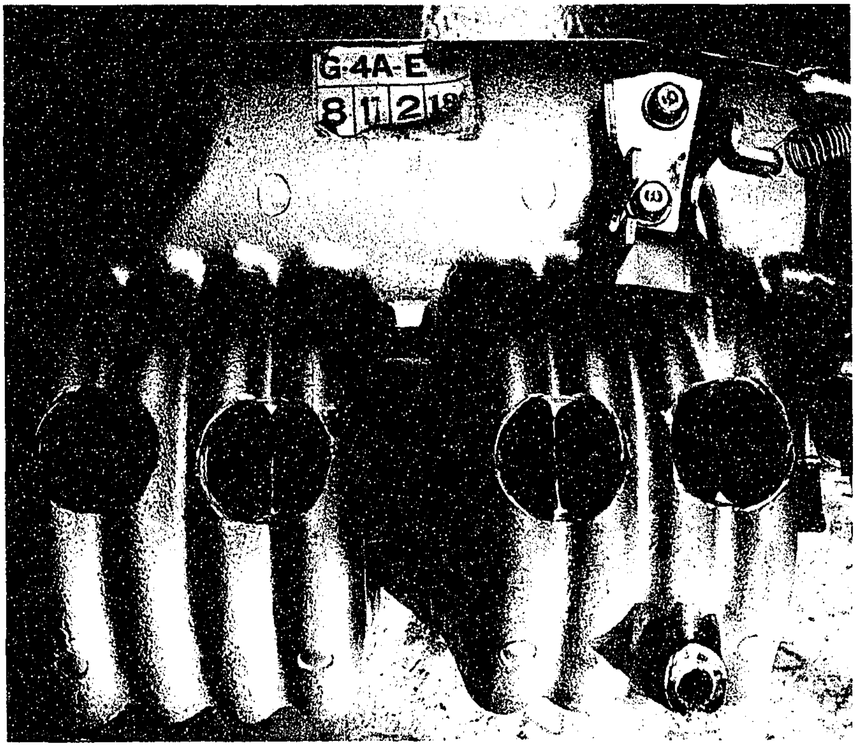

Figure 5.8: Modified Toyota Intake Manifold shown with Holes Drilled to Accommodate the manifold bridge.

Figure 5.9: Modified Toyota Exhaust Manifold showing the Manifold Bridge Fittings

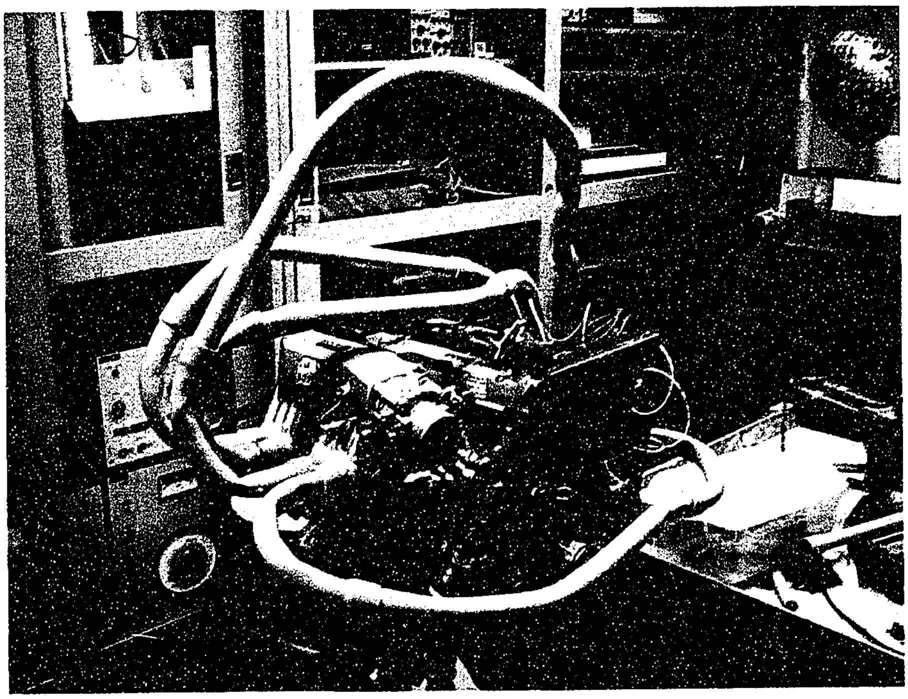

Figure 5.10: Modified Toyota Engine with a Typical Manifold Bridge Installed

5.2.2 Installation of the Engine

The dynamometer and Toyota engine needed to be prepared before any acoustical measurements of both the unmodified and bridged engines could be performed. Since this engine had never been installed on this dynamometer, special attention to the mounting procedure was required. The following outlines the steps taken to install the Toyota engine on the test bed of the semi-anechoic enclosure:

1. Design, manufacture and install spacers to fit between the existing engine mounting locations on the dynamometer test bed and the factory engine mounts on the Toyota engine. This was required to bring the centreline of the output shaft of the engine to the centreline of the dynamometer drive shaft.

2. Design, manufacture and install engine rear mounting plate. The mounting plate which is attached to the rear of the engine block behind the flywheel is subsequently bolted to the mating plate which is integral to the test bed. This fixture, which supports the rear of the engine on the test bed, is illustrated in Figure 5.11.

3. Connect the engine to the dynamometer drive shaft through a universal coupler.

4. Attach cold water supply and drain to the engine to act as an open cooling system.

5. Install a temperature sensor in the oil pan and connect to a digital readout to monitor the oil temperature of the engine to ensure the prevention of overheating of the engine.

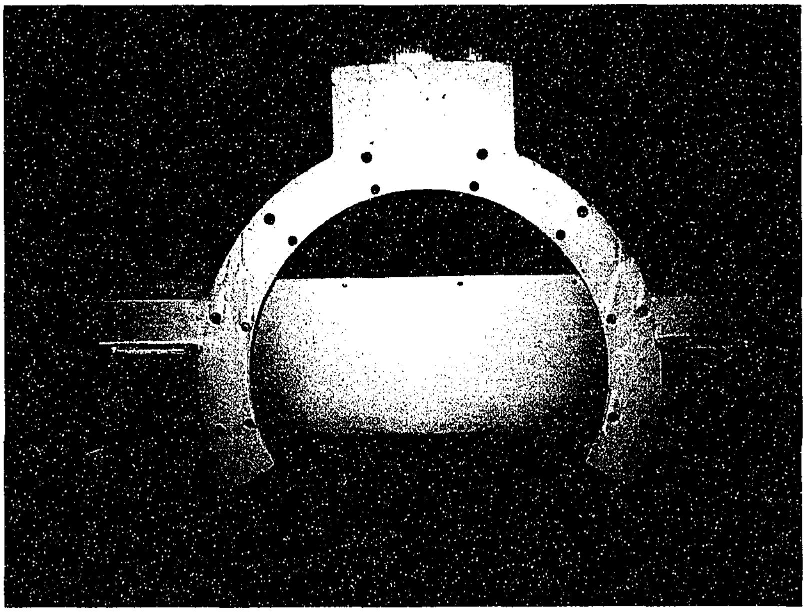

Figure 5.11: Typical Engine Rear Mounting Plate Used to Mount the Engine on the Dynamometer Test Sled

5.3 Testing Procedure

The following outlines the steps taken to acquire and analyse the induction noise data from the motored Toyota Engine:

1. Install the unmodified engine on the dynamometer complete with temperature and tachometer sensors and cooling supply.

2. Mount the microphone at a position of 0.1 metres from the air intake opening of the engine induction system as illustrated in Figure 5.12. Connect the microphone cable to the data acquisition system located outside the anechoic room at the operator's position.

3. Operate the engine at the first steady operational speed of 1000 rpm and acquire and store the acoustical data.

4. Increase the operating speed of the engine by increments of 500 rpm and repeat step 3 eight times.

5. Install the manifold bridge on the engine and repeat steps 3 and 4.

6. Post process the acquired acoustic data to determine 1/12 octave and overall sound pressure levels as well as the specified sound quality metrics.

7. Compare the processed results of the experimental measurements of the unmodified engine to those of the bridged engine. Similarly, quantitatively compare the results of the acquired experimental data to the results determined from the analytical Ricardo WAVE Model.

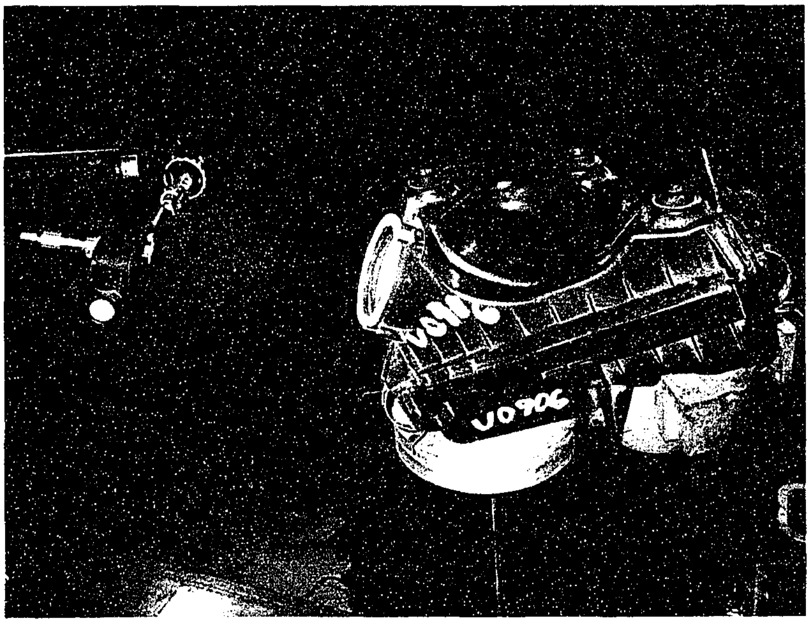

Figure 5.12: Microphone Acquiring induction Noise Data at a Distance of 100 mm from the Intake Opening of the engine.

VI. REVIEW OF DATA ACQUISITION AND ANALYSIS OF DATA

Two data types pertaining to the measured noise output were used for the quantification of any realized attenuation and to determine the effectiveness of the manifold bridge. These same data types, time domain information and frequency domain information, were also employed for the sound quality analysis since the information used to calculate the psychoacoustic metrics was synthesised from the collected raw acoustical information. In this chapter, the fundamental concepts pertaining to the collection and analysis of these two data types will be explored. The analysis techniques performed on both the numerical and experimental results were fundamentally the same. Given this, the discussions in the following sections pertain to both.

6.1 Data Collection

Before the acoustical results of either the numerical or experimental models could be analysed, the noise data had to first be collected and stored. The numerical data is created, stored and post processed in the digital domain. The experimental measurements, however, are measured as analogue signals which are then digitized and stored for future postprocessing. Figure 6.1 illustrates the process of acquiring an analogue acoustic signal and the subsequent steps to output a processed digital signal. Special attention must be given to the conversion process from the analogue to digital format. Specifically, careful consideration must be given to the rate of data sampling. Care must also be given to ensure a proper calibration of the measurement system used for the experimental portion of this work. As was the case for the experimental measurements, much of the numerical results from WAVE were post processed using the dBFA and dBSonic analysis software. This required that the digital output file from WAVE undergo equalization techniques to ensure meaningful results. Each of these is discussed in greater detail in the following sections.

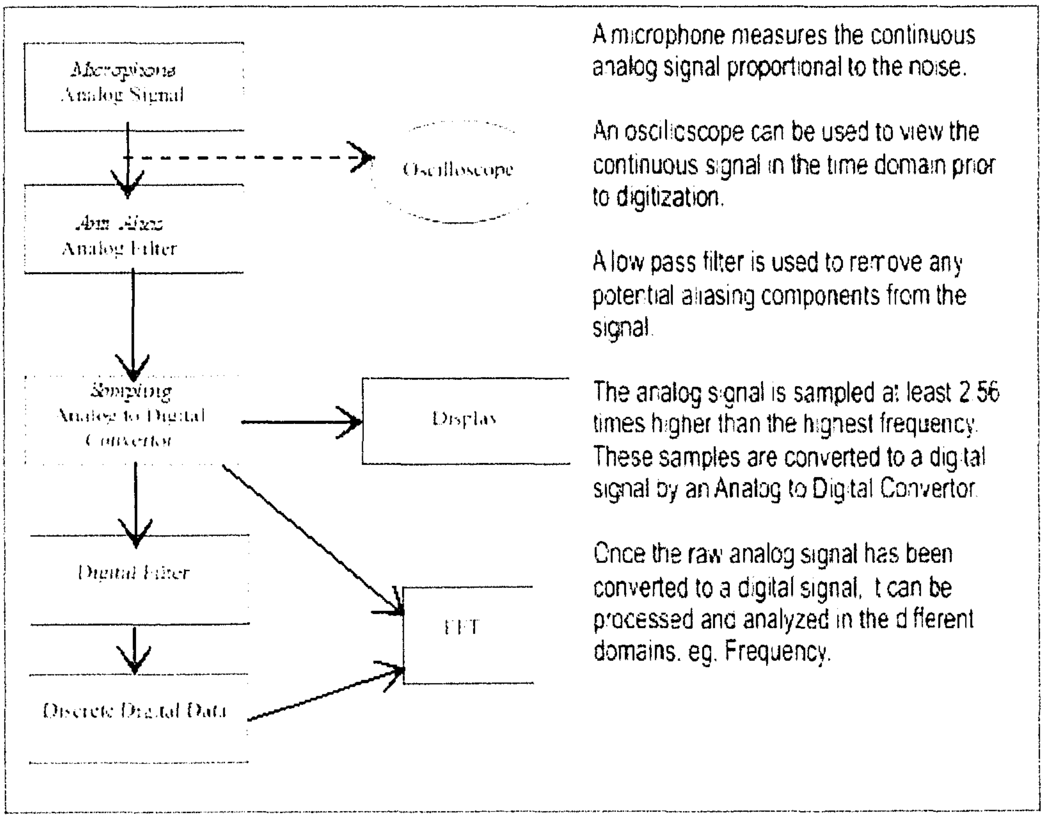

Figure 6.1: Flow Chart of the Process Required for the Acquisition, Digitization and Display of a Measured Analog Signal

6.1.1 Sampling

In order for the analogue voltage supplied by the microphone to be post processed, it must first be digitized. To do this, the continuous analog wave must be represented by a number of discrete equally spaced points of width Δt. This is shown in Figure 6.2.

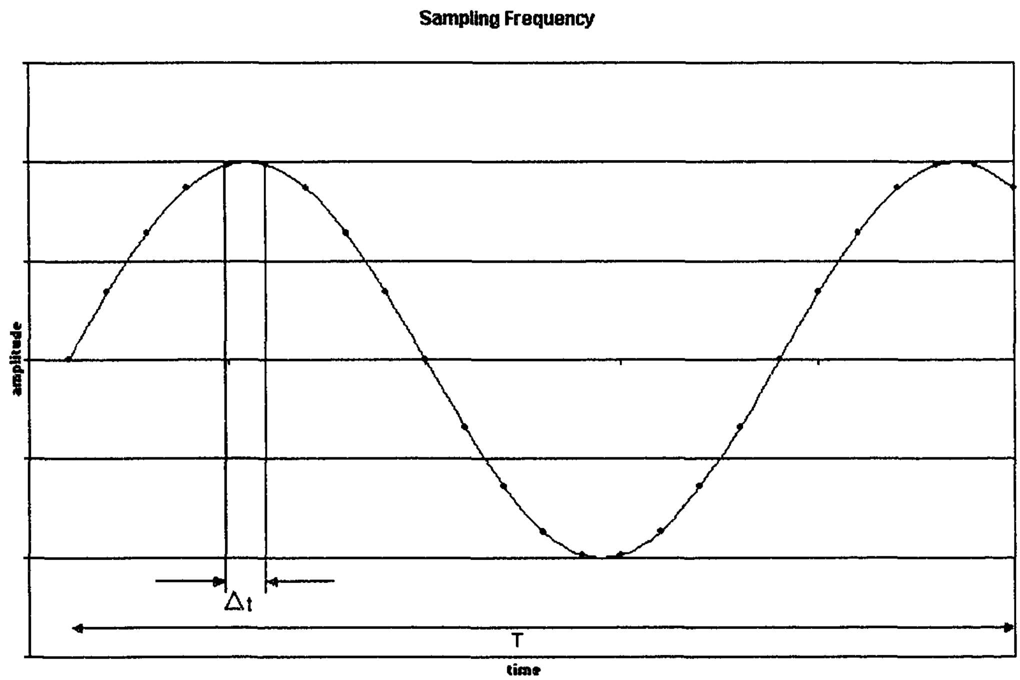

Figure 6.2: The Process of the Digitization of an Analog Signal by Discrete Sampling with an Illustrative Sampling Width of Δt

Randall described that the width of the sampling interval must be appropriately chosen since if it is too small, the time signal will be represented by more points than are needed, thus resulting in the unnecessary processing of extraneous data. "If too large a sampling interval is used, the high frequency components; that is, the frequencies above half the sampling frequency are misinterpreted as lower frequencies. This phenomenon is referred to as aliasing and must be avoided when digitizing continuous signals. A common example of aliasing is illustrated by the backward movement, or negative frequency, of wagon wheels in western movies because of the sampling involved in the filming." [32][38] To eliminate the problems associated with aliasing, the digitizing sampling rate should be at least 2.56

times the highest frequency of the data that is being collected. This is know as the Nyquist theorem and is used for the determination of sampling rate. [39]

To further avoid the effects of aliasing, an anti-alias low pass filter can be implemented prior to the digitizing operation. The function of this filter is to limit the input frequency by allowing only lower frequency signals to pass through and blocking higher frequency signals. While this does not prevent aliasing of the entire acquired signal, these filters do lessen the likelihood of the presence of an aliased component in the resulting signal.

6.1.2 Calibration and Equalization

Although the capabilities exist within WAVE, much of the post processing of the numerical WAVE model was completed by the dBFA and dBSonic software. This processing choice was taken not only to ensure a direct quantitative comparison between the modelled and experimental results but also to permit sound quality analysis of the WAVE outputs. In order to accomplish this, a reference, or calibrated signal of known frequency and amplitude was generated by WAVE. This digital signal was then imported into dBFA, the post processing software, where the amplitude of the calibration signal was evaluated for comparison. Any required corrections were completed through the use of the equalization capabilities of the dBFA program and a reference signal of 1000 Hz at 94.0 dB. All data processed by the dBSonic program was imported from the dBFA program and did not require additional equalization.

6.2 Time Domain Signal

As was indicated at the beginning of this chapter, the raw input signals were processed into two data types for eventual analysis of the manifold bridge. This section will describe the first data type, that being the time domain signal which is a representation of a given data type versus time. This discussion will include a description of the classification of the signal as well as an explanation of the analysis technique called time domain averaging (TDA).

6.2.1 Classification of the Signal

Randall recommended that prior to the determination of the analysis technique to be carried out on a time domain signal, the type, or classification of the data grouping must be established. [38] "For a stationary signal, that is, a signal whose average properties do not vary with time, it must be established whether the signal is deterministic or random. For a deterministic signal, a given instantaneous value is easy to predict at all points in time. In this case, the signal can be described by some explicit mathematical function. Random signals on the other hand, cannot be described by an explicit mathematical function. Stationary random signals can only be described by their statistical properties such as the mean values, variances etc." [32] For this study, the noise and pressure outputs are deterministic. In fact, it was said by Tjong that typical noise, vibration and cylinder pressure data of a properly running engine are usually deterministic in nature [50].

6.2.2 Time Domain Averaging

One might expect a repetitive waveform to be identical from one cycle to the next but, in reality, this is usually not the case for measured data. Extraneous background noise is often present in the resulting signal which adds to the variability of the resulting output. In fact, most stationary signals can be thought of as consisting of three fundamental components, these being the periodic, semi-periodic and the noise components [27]. To extract the periodic signal from the 'noisy' waveform, the technique of time domain averaging (TDA) is employed. This is accomplished by averaging the results of several time traces. This tool is often used for fault detection of a consistent, non-transient irregularity of a periodic signal [50].

For this study, time domain averaging is not necessary for the numerical outputs since these signals do not contain the spurious components that a measured signal does. This is due to the fact that these are modelled results and do not change once the model has reached convergence. The experimental results presented, however, have undergone a time domain averaging. By motoring the engine, combustion noise is absent and that results in a very steady periodic signal. Unfortunately, extraneous noise will still exist and time domain averaging can be employed to minimize its presence in the data to be processed.

6.3 Frequency Domain Signal

The second data type used for analysis of the attenuation of the manifold bridge comes from the frequency domain. This analysis technique is used to decompose a periodic signal into its various harmonic components. The mathematical basis of frequency analysis is the Fourier Transform which can take different forms. While a computational method known as the Discrete Fourier Transform (DFT) can fulfill the task of calculating the frequency domain of a signal, a more efficient algorithm has become more widely used. The Fast Fourier Transform (FFT) has become a standard tool in areas such as bearing fault detection, misalignment of mechanical systems, preventive maintenance and, as in this study, noise quantification. Figure 6.3 presents an illustration of a typical measured induction noise signal in the frequency domain of the unmodified Toyota engine used in this study.

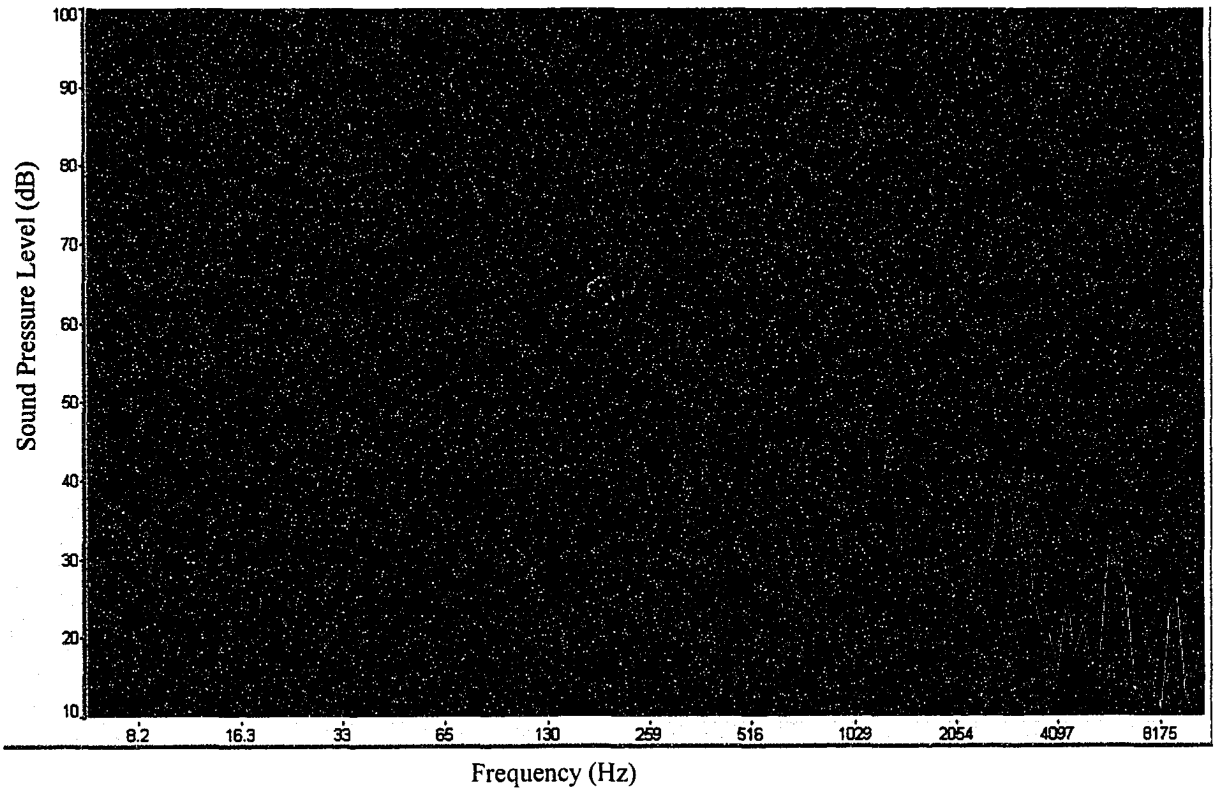

Figure 6.3: Typical Screen Shot of a Frequency Domain Output of Measured Induction Noise of the Toyota Engine Using dBFA Acquisition Software

The Fast Fourier Transform (FFT) method, according to Randall, has the advantage over the Discrete Fourier Transform in that it greatly speeds up the calculation of the DFT and allows easier avoidance of some of the pitfalls including aliasing as already discussed [38]. "Once a time signal has undergone an FFT process, the signal is represented by a vector in which each value represents the magnitude of the signal's amplitude at that frequency and covers the range of frequency values given for the vectors. This is usually illustrated in graphical form. For a detailed technical explanation the reader is encouraged to consult with the references" [32] [38].

6.3.1 FFT Analysis of the Manifold Bridge

For this study, both steady state and transient cases will undergo an FFT analysis. For the steady condition cases, where the engine is operated at a constant speed, a $1/12^{th}$ octave analysis of both the numerical and experimental induction noise was performed. Figure 6.4 presents an example of an FFT analysis output of the unmodified experimental engine using the postprocessor dBFA.

While an FFT analysis cannot be applied, in general, to a transient case where the engine is swept up though a speed range, Ricardo WAVE does have the capability to trigger the timing of its analysis and produce FFT's for discrete instances in time using another postprocessor called WNOISE. The result is displayed as either a three-dimensional waterfall graph or a colour plot. These transient analysis cases using WNOISE are presented in the results chapter. Figure 6.5 presents an example of a waterfall output of the unmodified engine where the three axes represent the frequency in hertz, noise amplitude in dB verses the time in milliseconds as shown. The time information can be translated to the rpm of the engine if desired. Figure 6.6 presents an example of a colour map output of the unmodified engine where in this case the third axis is represented by colour.

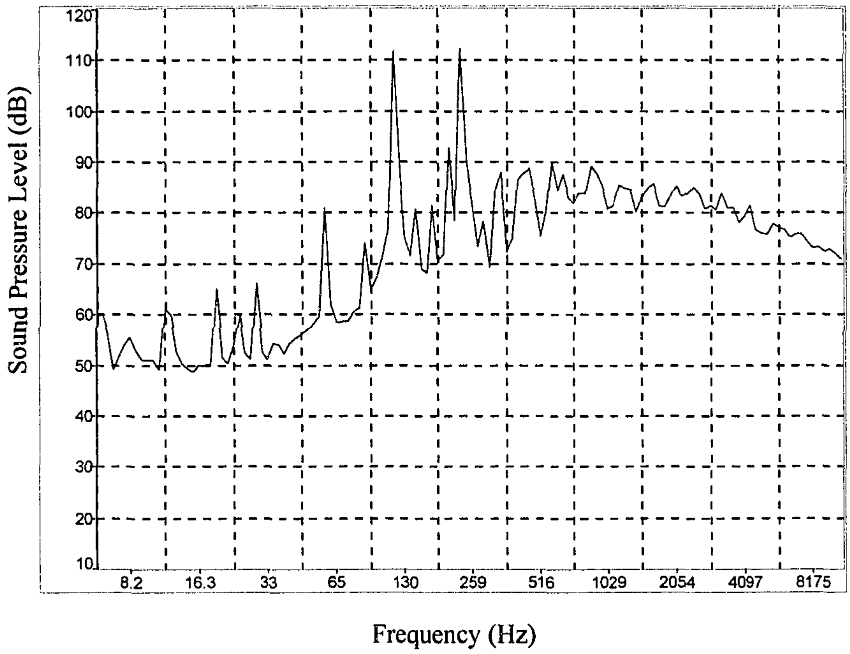

Figure 6.4: Illustrative Example FFT Output of Experimental Unmodified Engine Results using the dBFA Postprocessor. The X-Axis is Frequency (Hz) and the Y-Axis Represents SPL (dB).

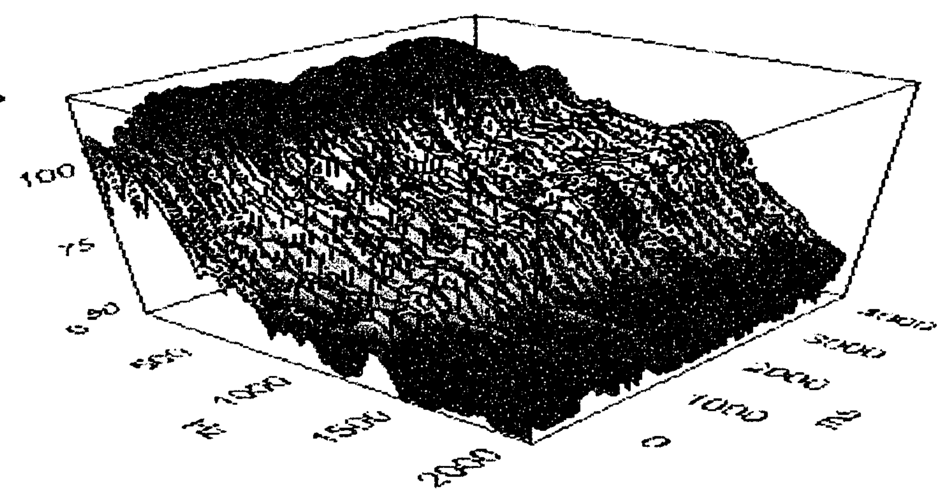

Figure 6.5: Waterfall Plot produced by WAVE of a Modelled Transient Measurement of Induction Noise of the Toyota Engine Showing Sound Pressure Level versus Frequency versus Time

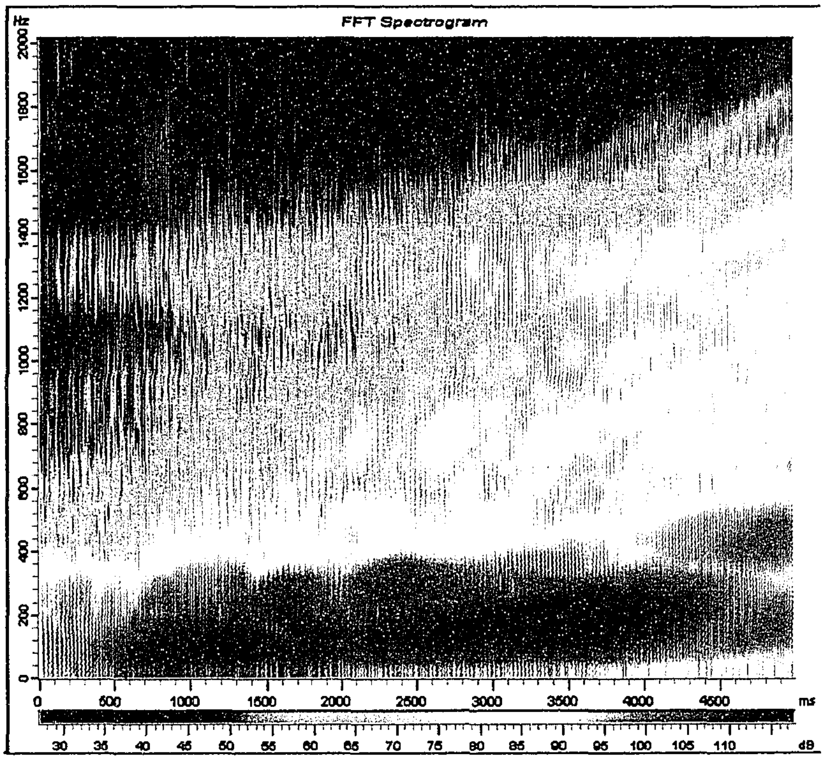

Figure 6.6: Colour Map of a Modelled Transient Measurement of Induction Noise of the Toyota Engine Showing Sound Pressure Level versus Frequency versus Time

6.3.2 FFT and Sound Quality

A special case that warrants discussion is the practical relevance of frequency analysis and the application of sound quality metrics. Given the temporal and spectral makeup of sound, many of the psychoacoustic metrics in existence today cannot be determined in the absence of knowledge of the frequency makeup of the source. For this study, the specific sound quality metrics which are frequency dependant are loudness and sharpness.

The overall loudness of a source is synonymous to a reported total sound pressure level (SPL) derived from a frequency spectrum. Here, the amplitude of loudness is measured over the frequency range in bark bands, as opposed to n^{th} octave bands, and summed to a total loudness level, as opposed to a total SPL. To accomplish this, the analyser must have the capability to translate the time domain signal in a modified frequency, or more appropriately, bark domain. The post processing software used in this study, has this capability. The preceding description represents a simplified summary of the analytical process required to calculate loudness since the algorithm employed must also take into consideration the temporal and masking effects of the sound.

The sound quality metric pertaining to sharpness also has obvious dependance on the frequency content of the noise signal. This is due to the fact that sharpness is fundamentally a measure of the high frequency annoyance of the source. The value for sharpness is derived from the application of a weighting factor to the higher frequency band content of the signal. Like loudness, the sharpness is determined by first dissecting the time domain signal into the bark domain prior to the application of the weighting factors. This is accomplished through the implementation of a Fourier Transform process [57].

VII. DISCUSSION OF RESULTS

This chapter presents the results comparing the various intake noise parameters of the unmodified Toyota engine to the engine modified with the addition of the manifold bridge. The results of the numerical Ricardo WAVE analysis of the modelled engines, with and without the manifold bridge, are first compared to evaluate the effectiveness of the bridging technique. For this discussion, the operation of the engine included the case of steady state at the various engine speeds as well as under transient condition. This is followed by a comparison of the results collected from the experimental measurements of the actual engine motored by the dynamometer, also with and without the implementation of the bridge. This analysis is limited to the case of steady state operation. Finally, the direct relationship between the numerical and experimental results will be presented.

7.1 Numerical Results

The acoustical output of the induction noise, measured 100 mm in front of the intake opening, was evaluated using the Ricardo WAVE model for the cases with and without the manifold bridge. Since all experimental results to be presented later were determined by motoring the engine, the modelled measurements were determined using the same procedure. That is to say that the Ricardo WAVE model was processed under the conditions of a motored engine instead of the usual case of a fired engine. This permits a direct comparison between the model and the experiment.

This section will be presented in four parts. First, a comparison of the averaged results for each steady state engine speed will be presented. This will be followed by a comparison of the unmodified and bridged engines using the results of a Fast Fourier Transform (FFT) and 1/3 octave analysis. Due to space constraints, this will be presented for the engine speed of 3500 rpm only. The reader is directed to Appendix D where a presentation of data for all other engine speeds has been provided. The results of several analyses as functions of time will then be presented for a 10-second sample at 3500 rpm. Finally, a comparison of a transient run from 1000 to 6500 rpm of the unmodified and bridged engine will be illustrated using waterfall and colour map presentations.

7.1.1 Averaged Results for Modelled Steady State Engine Operation

Figure 7.1 presents an illustration of the predicted intake noise for both the original and modified engines. The unweighted sound pressure levels (SPL) were determined for engine speeds from 1000 to 6500 revolutions per minute (rpm) in increments of 500 rpm. It should be understood that these were evaluated at steady speed conditions rather than during a transient speed sweep. By examining the results presented in Figure 7.1, an attenuation is observed as a result of the implementation of the manifold bridge that is represented by the green line covering engine speeds from 1500 to 6000 rpm. This attenuation ranges from 0.1 dB at 5500 rpm to 2.7 dB at 2000 rpm. While these predicted levels of attenuation may not appear significant, the effect of the manifold bridge would be most perceptible at engine speeds in the vicinity of 2000 rpm.

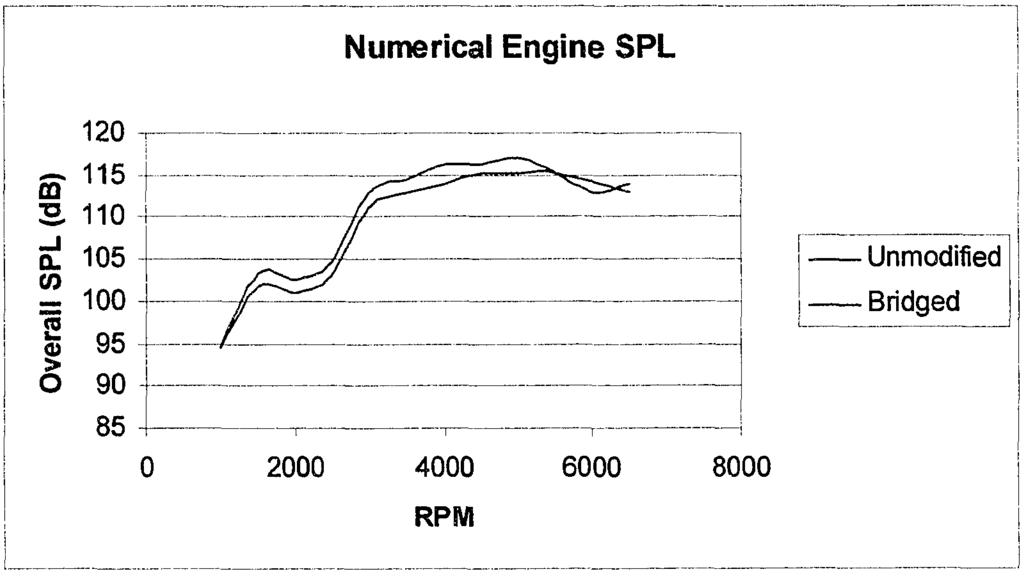

Figure 7.1: Predicted Intake Noise of Numerical Unmodified and Bridged Engines

Figure 7.2 presents the predicted A-weighted intake noise of the two variations of the numerical models. It can be seen that except for engine speeds above 3000 rpm, the numerical bridged model predicts noise levels which exceed the unmodified engine. As will be discussed in much greater detail in a subsequent section, this is due to a greater energy content appearing at high frequencies in the bridged model when compared to the original engine at the same, lower engine speeds.

Similar results are realized when comparing the loudness results of the two numerical models as is presented in Figure 7.3. This is understandably so since both the A-weighting curve and loudness curve follow similar contours and are both designed to compensate for the human perception of sound amplitude at various frequencies. However, even though the predicted loudness of the bridged model is higher than the unmodified engine at engine speeds under 3000 rpm, the differences are very minimal.

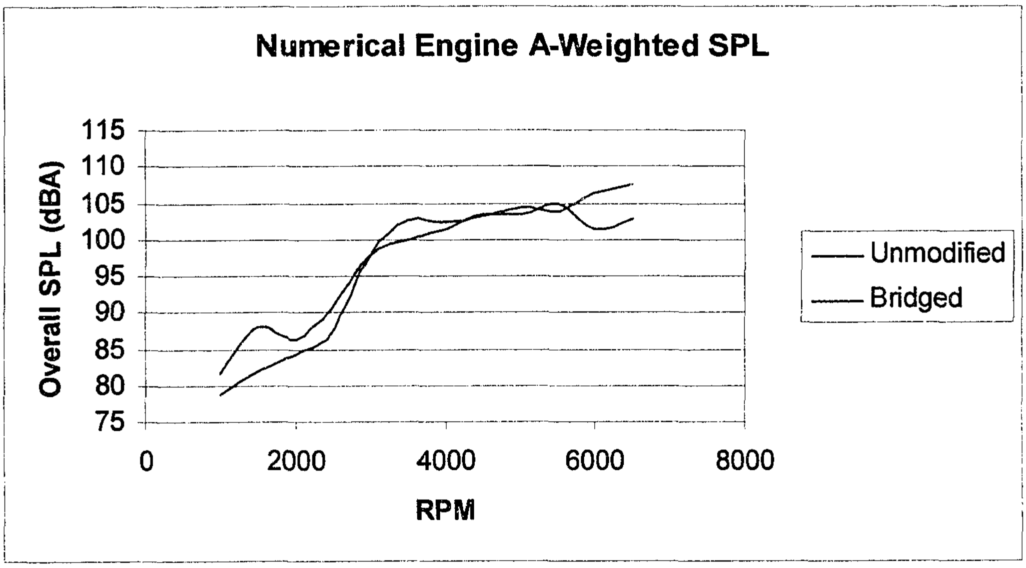

Figure 7.2: Predicted A-Weighted Intake Noise of Numerical Unmodified and Bridged Engines

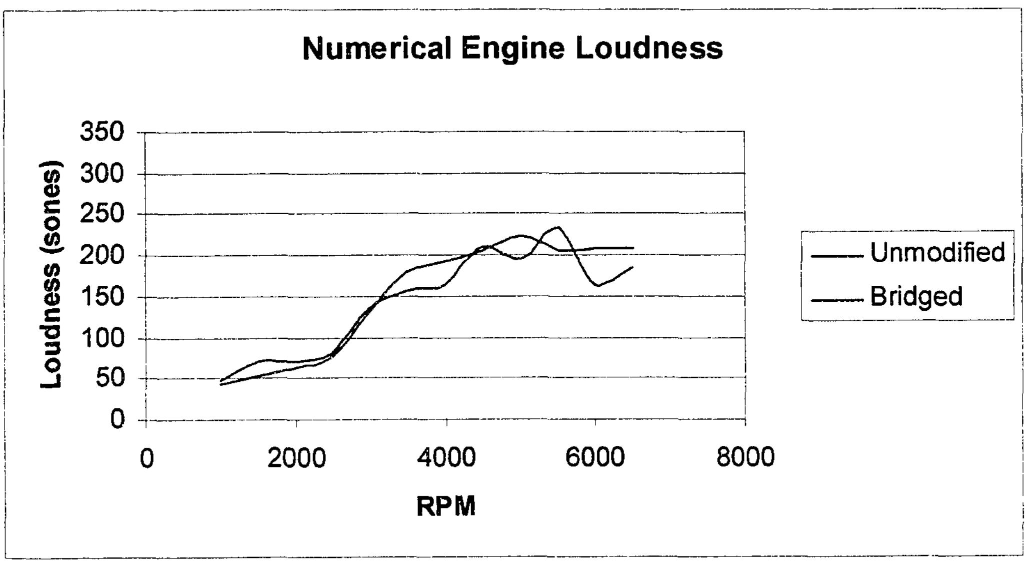

Figure 7.3: Predicted Loudness of Intake Noise of Numerical Unmodified and Bridged Engines

Figure 7.4 presents a comparison of the predicted sharpness of both the unmodified and bridged numerically modelled engines. While the information in this figure suggests that the bridged engine has a higher degree of sharpness associated with its induction noise, the amount of sharpness for both models, as well as the difference between the two models is very low. This suggests that both models exhibit very little high frequency content, with the bridged model producing marginally more than the unmodified engine.

Figure 7.5 presents a comparison of the predicted fluctuation strength of both the unmodified and bridged numerical modelled engines. The bridged model predicted improved fluctuation strength values for mid and high engine speeds. The reason for the increased fluctuation strength for engine speeds less than 2200 rpm and between approximately 3200 and 4300 rpm is the existence of some low frequency harmonics. These are not evident in the unmodified engine which can be seen in the FFT and 1/3 octave plots which will be presented later. An interesting observation is that while the sound pressure amplitudes in these low frequency ranges for the bridged model are lower than those observed in the unmodified model, they result in a higher realized fluctuation strength due to the harmonic peaks. To illustrate this point, FFT outputs of the two numerical models at 1000 rpm are presented in Figure 7.6 where a diminished low frequency content with the modulation causing spikes can be observed.

As in the case of the fluctuation strength, the bridge model prediction suggests an increased roughness as is presented in Figure 7.7. The exception to this is between the engine speeds of approximately 1800 to 2700 rpm. Here, the addition of the bridge contributed to modulation in the 20 to 300 Hz range for the numerical model.

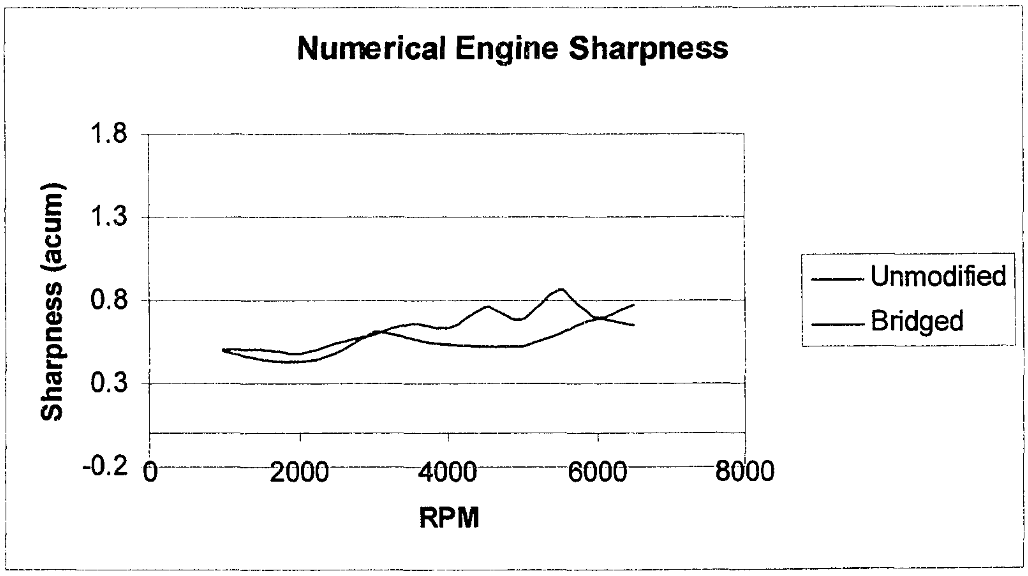

Figure 7.4: Predicted Sharpness of Intake Noise of Numerically Modelled Unmodified and Bridged Engines

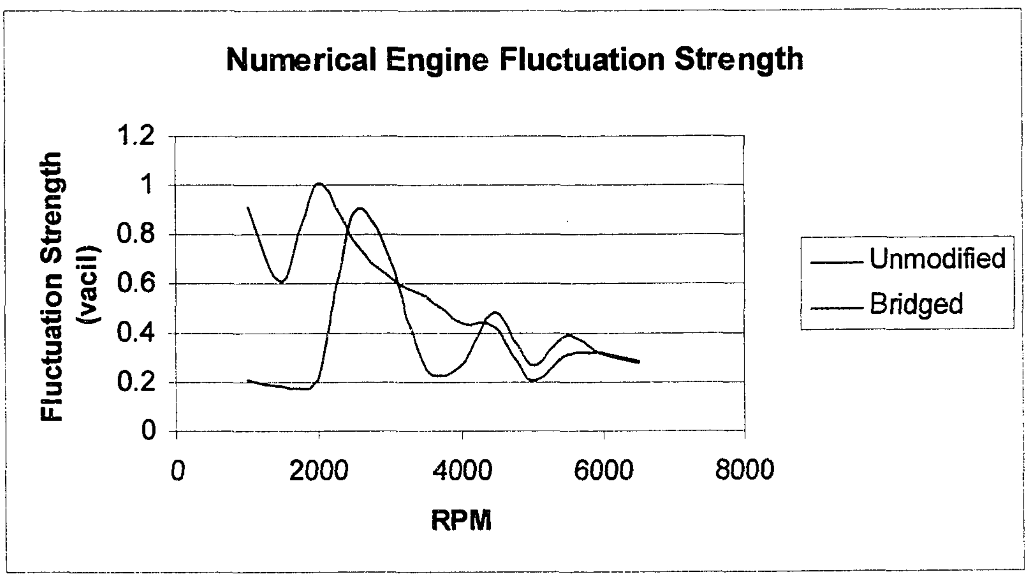

Figure 7.5: Predicted Fluctuation Strength of Intake Noise of Numerical Unmodified and Bridged Engines

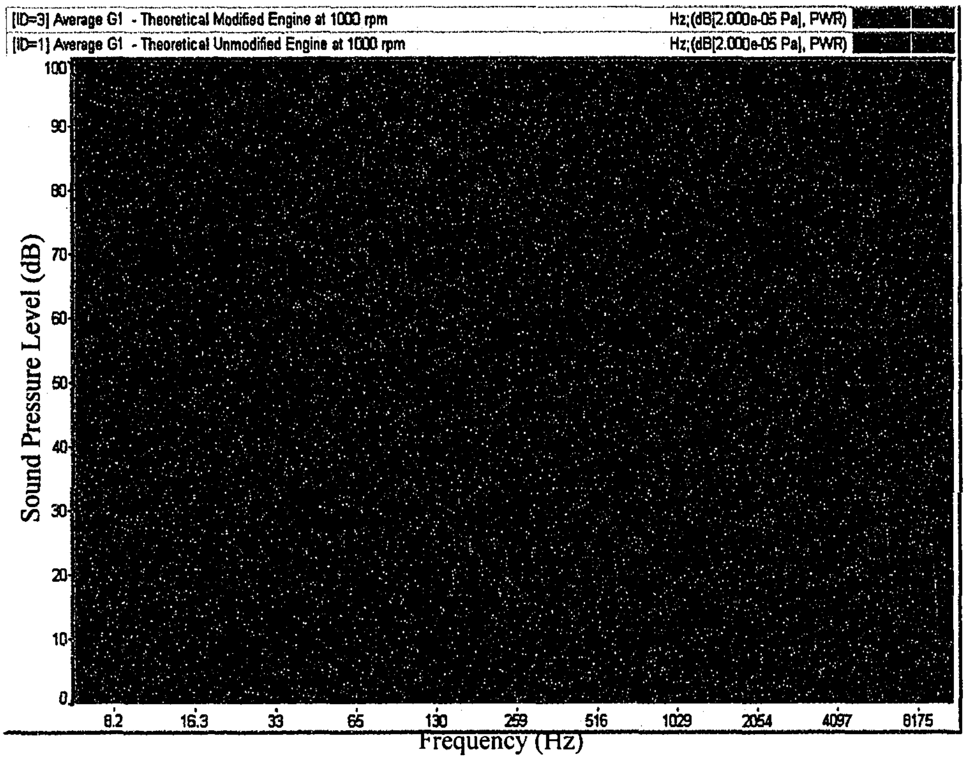

Figure 7.6: FFT of Numerical Intake Noise of Unmodified and Bridged Engines at 1000 rpm. Shown is SPL (dB) versus Frequency (Hz).

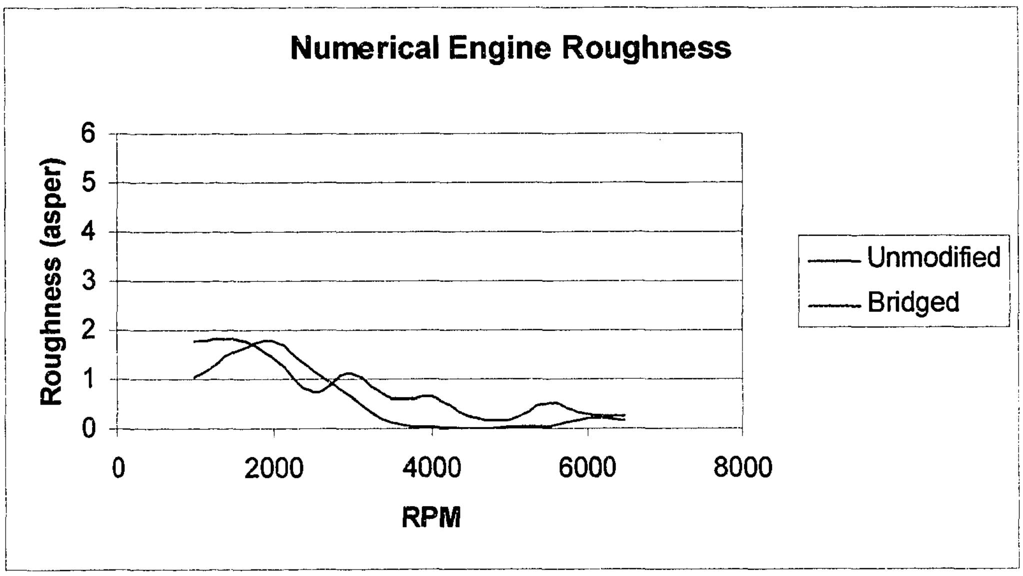

Figure 7.7: Predicted Roughness of Intake Noise of Numerical Unmodified and Bridged Engines

7.1.2 FFT and 1/3 Octave Analysis of Modelled Engine

In order to further add to the thoroughness of the data collection and analysis, FFT and 1/3 octave analyses were conducted for each of the steady state operations of the numerical engine. Only those for the engine speed of 3500 rpm are presented in this section. The reader is directed to Appendix D for the results for all other engine speeds.

Figures 7.8 and 7.9 present the FFT output results of the numerically modelled, unmodified and bridged engine models respectively. It can be seen that for the most part, the amplitudes of the fundamental and subsequent harmonics are lower for the frequencies with the highest energy peaks. This results in a lowering of the overall realized sound pressure level (SPL). It should also be noted that the lowering of the sound pressure level has also produced a detrimental effect on the fluctuation and roughness of the resulting acoustic output. Since the attenuated peaks, particularly at 115 and 230 Hz, are now at similar amplitudes to adjacent peaks, this has resulted in added modulation to the resulting signal. This added modulation is the cause of the increase in fluctuation strength and roughness.

Figures 7.10 and 7.11 present the 1/3 octave analysis of the numerical unmodified and bridged engine models respectively at 3500 rpm. These graphs also show the realized attenuation of the two fundamentals, or primary and subsequent harmonic operating frequencies. Also shown is the decrease of low frequency energy. These outcomes illustrate the benefits of the bridge. They do not convey the same information that the FFT outputs do with respect to the increase in modulation. In fact, the 1/3 octave outputs suggest, if anything, a smoother and more evenly distributed curve. Because of this, such octave analysis techniques are useful for the determination of overall distributed levels but not for more specific sound quality analysis, such as were conducted during this study.

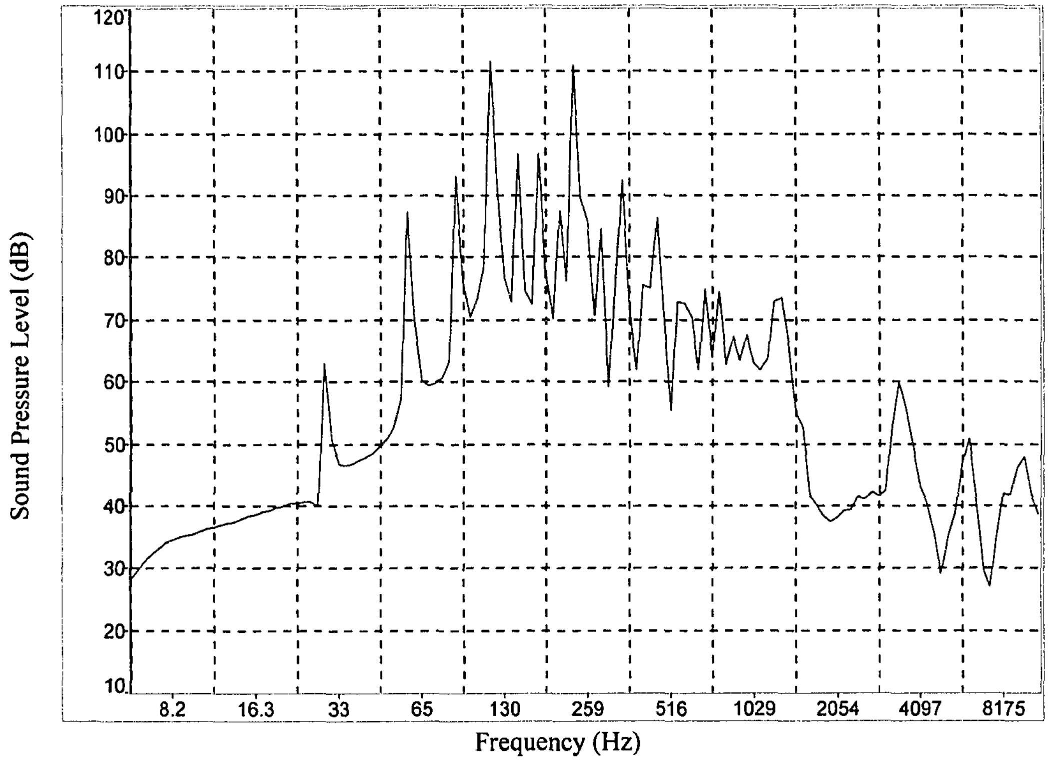

Figure 7.8: FFT of Numerical Unmodified Engine at 3500 rpm

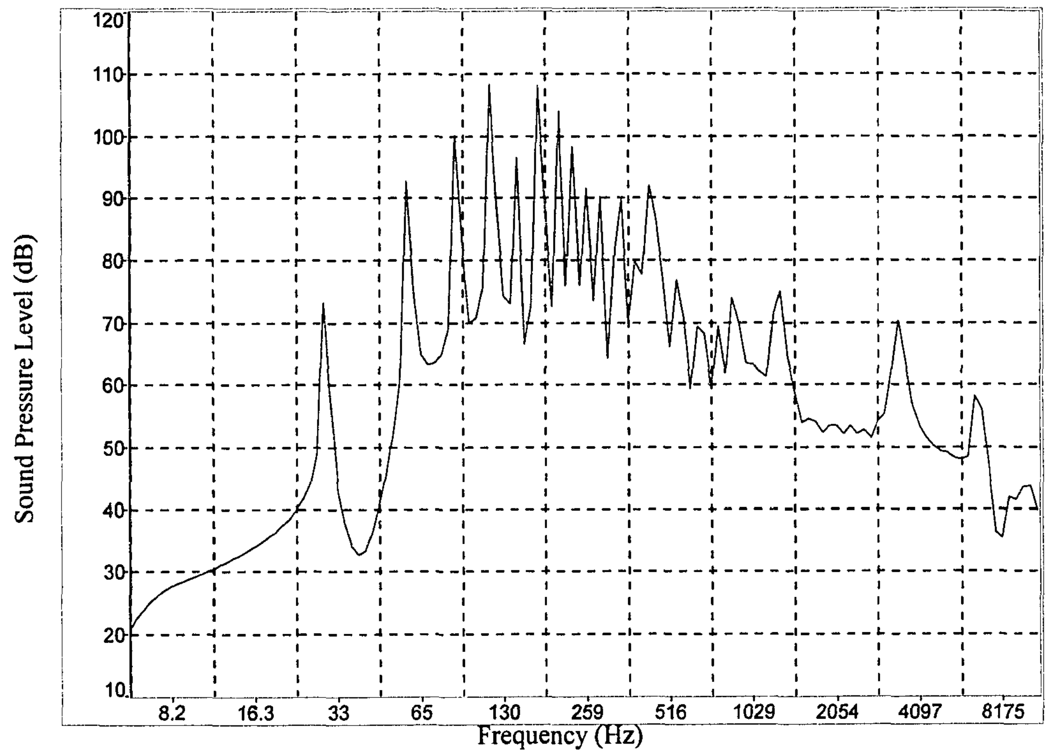

Figure 7.9: FFT of Numerical Bridged Engine at 3500 rpm

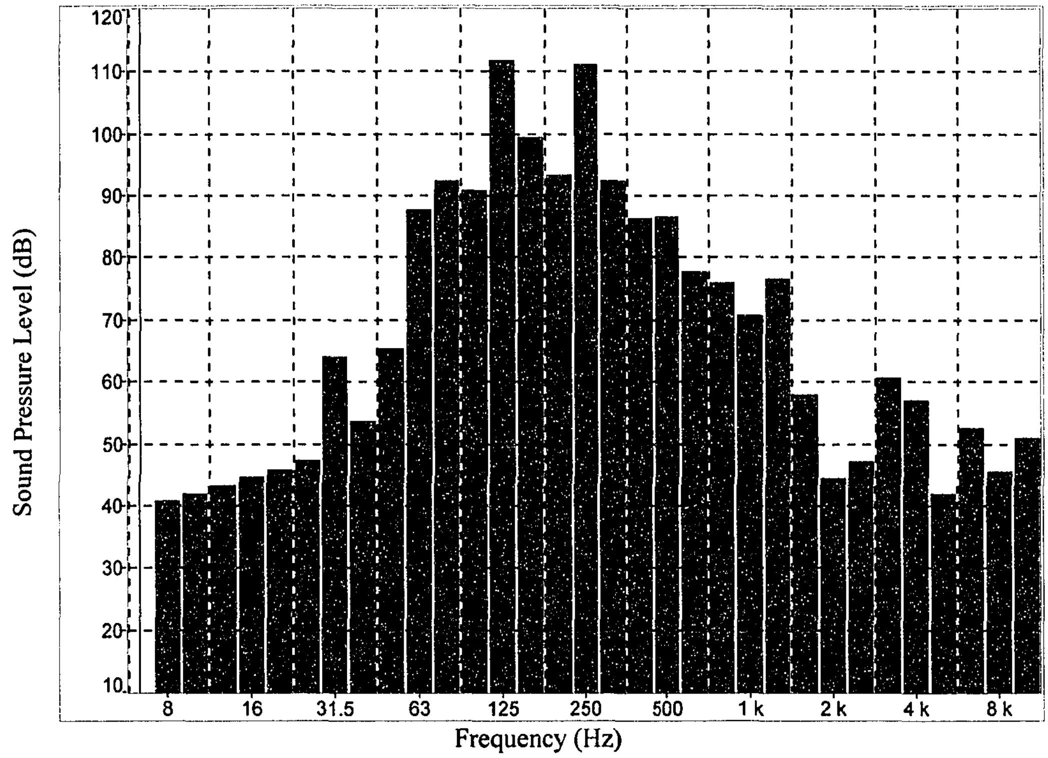

Figure 7.10: 1/3 Octave of Numerical Unmodified Engine at 3500 rpm

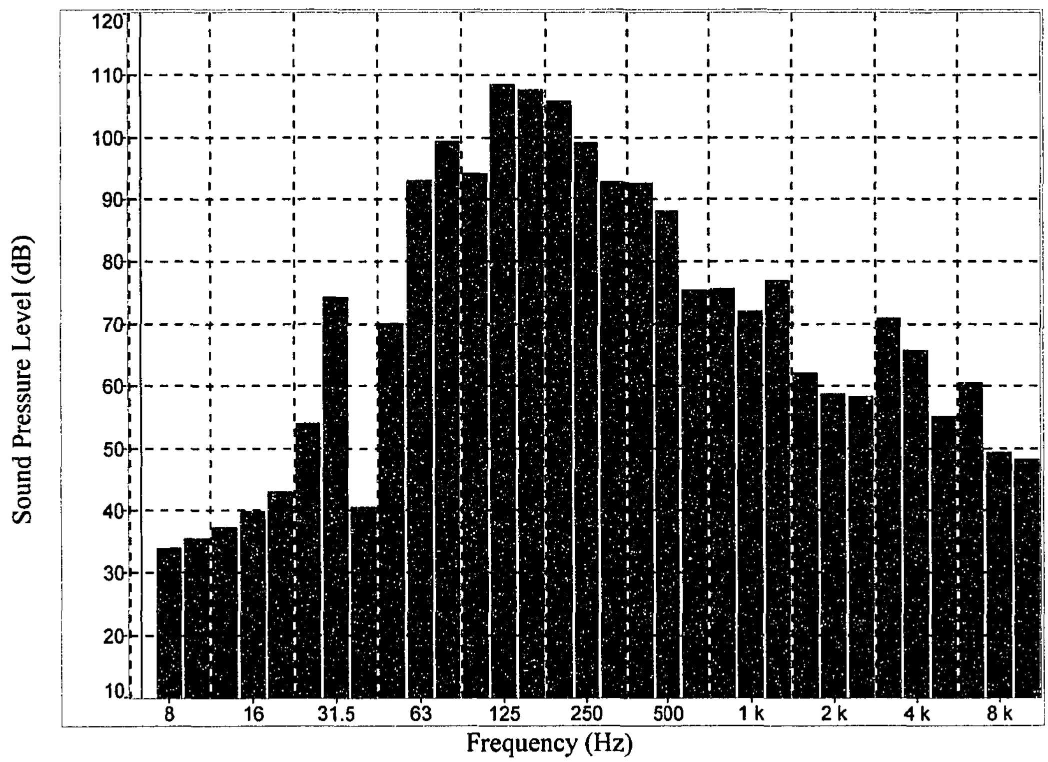

Figure 7.11: 1/3 Octave of Numerical Bridged Engine at 3500 rpm

7.1.3 Time Function Results for Modelled Steady State Engine Operation

Presented in this section are several analysis outputs given as a function of time as opposed to simply averaged values as presented earlier. The advantage of performing this analysis is that if a presumably steady signal were to vary over time, such analyses would make this obvious.

Figures 7.12 and 7.13 present the time functions of the unmodified and bridged engines for the analytical results. The influence on the time signal due to the introduction of the bridging device is evident in these two figures. Some attenuation in amplitude in the time signal is apparent, suggesting a quieter engine. The time period for each repetitive cycle of the bridged engine is double to that produced by the original engine. The existence of this suggests a potential increase in the subjective descriptors such as the roughness and fluctuation strength.

Figures 7.14 and 7.15 present the sound pressure level versus time values of the unmodified and bridged engines respectively. The point that should be noted here is that the assumed steady state signal is confirmed to remain steady for the recorded time period illustrated in the figures. Also, examinations of the levels produced by this analysis software on the time history closely follow the averaged levels reported in section 7.1.1 as determined using the dBFA analysis software. The mean value of the level versus time output is reported here to be 114.8 dB which is within 0.1 dB of the previously reported value presented in Figure 7.1. In fact, it was found that all mean values determined from the time functions with dBSonic differed from the averaged results by 0.1 dB. This is likely due to the initial delay in the time averaging response of the analyser which is illustrated by the steeply sloped curve at the beginning of each of the time function curves.

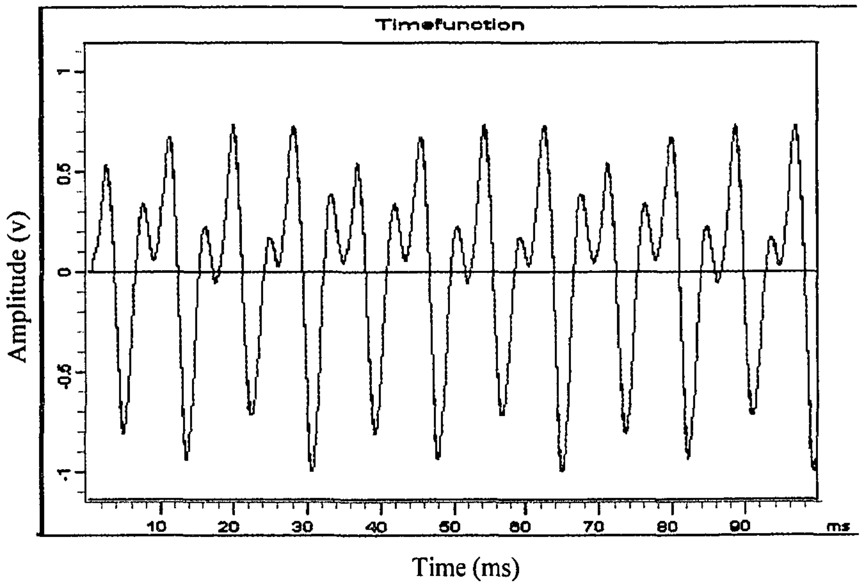

Figure 7.12: Time Function of Numerical Unmodified Engine at 3500 rpm

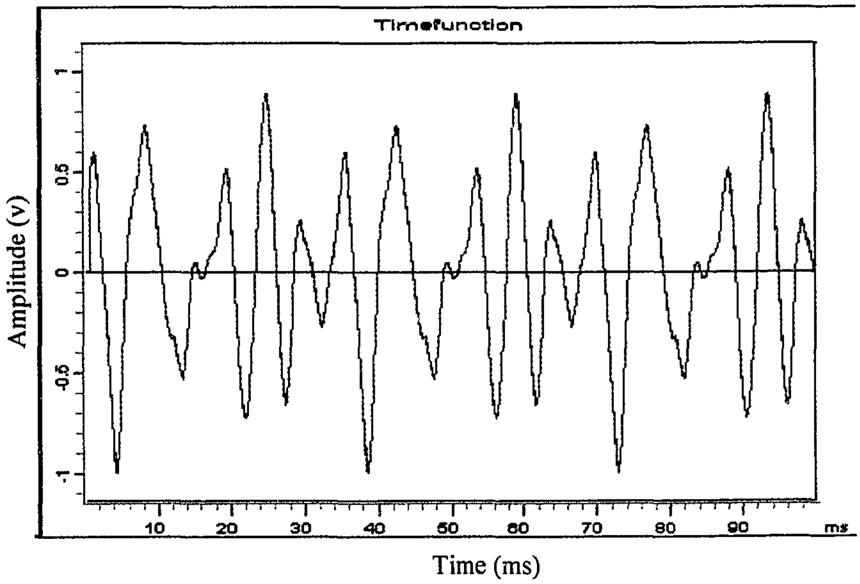

Figure 7.13: Time Function of Numerical Bridged Engine at 3500 rpm

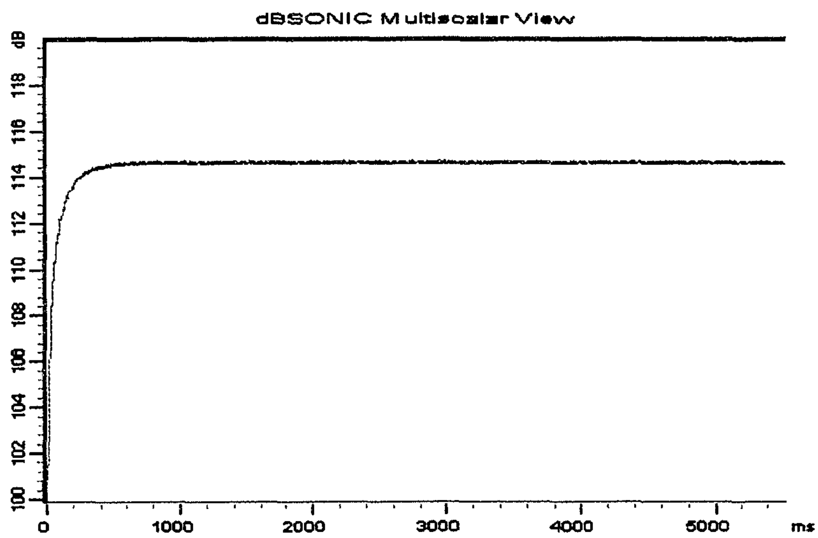

Figure 7.14: Level vs Time of Numerical Unmodified Engine at 3500 rpm

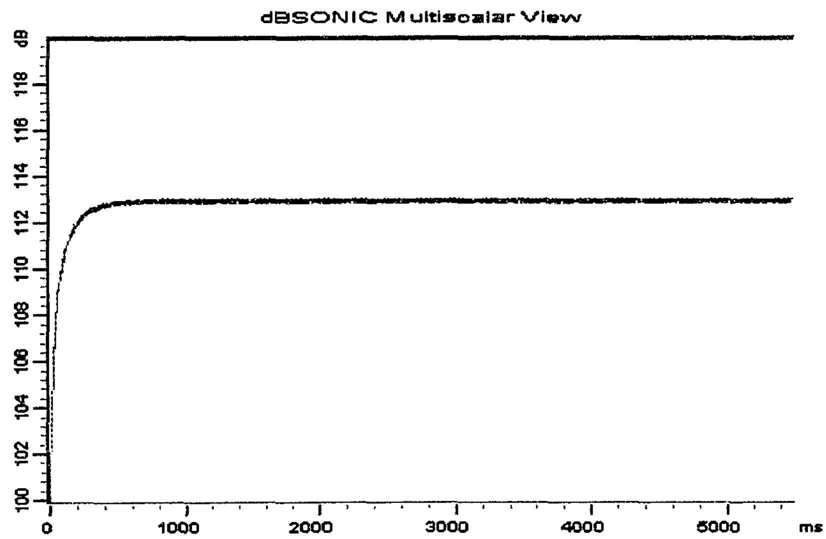

Figure 7.15: Level vs Time of Numerical Bridged Engine at 3500 rpm

Figures 7.16 and 7.17 present illustrations of the FFT spectrograms of the unmodified and bridged engines respectively. Similarly, Figures 7.18 and 7.19 present the third octave spectrograms of the unmodified and bridged engines. Both of these graph types illustrate three-dimensional outputs of frequency versus time with colour representing the third dimension, the amplitude of the measured noise. Both the FFT and third octave outputs illustrate the same concept with the FFT having a better resolution. At the lower frequencies, the FFT spectrogram shows less intensity of the red colour for the bridged engine, particularly at frequencies below 400 Hz. Lower amplitudes of noise are also present at bands centred around 750 Hz and 1100 Hz. These reinforce the realized overall attenuation given by the manifold bridge. Similar results are evident on review of the third octave spectrograms. The attenuation due to the bridge is most evident centred around the 250 Hz third octave band.

Figures 7.20 and 7.21 present illustrations of the loudness versus time values of the unmodified and bridged engines respectively. Examination of the loudness levels produced on the time history show its close fit to the averaged levels reported in section 7.1.1. Further, the advantages of the bridged engine are also apparent.

Figures 7.22 and 7.23 present illustrations of the roughness spectrogram of the unmodified and bridged engines respectively. Similarly, Figures 7.24 and 7.25 provide an illustration of the fluctuation strength spectrogram of the unmodified and bridged engines. For the engine speed of 3500 rpm, the frequency of the realized roughness is found to be centred around 800 Hz for the unmodified engine and approximately 300 Hz for the bridged engine. While it may not appear so in the spectrogram, the overall roughness is greater for the bridged engine. The fluctuation strength of the original engine is extremely low as presented in Figure 7.24.

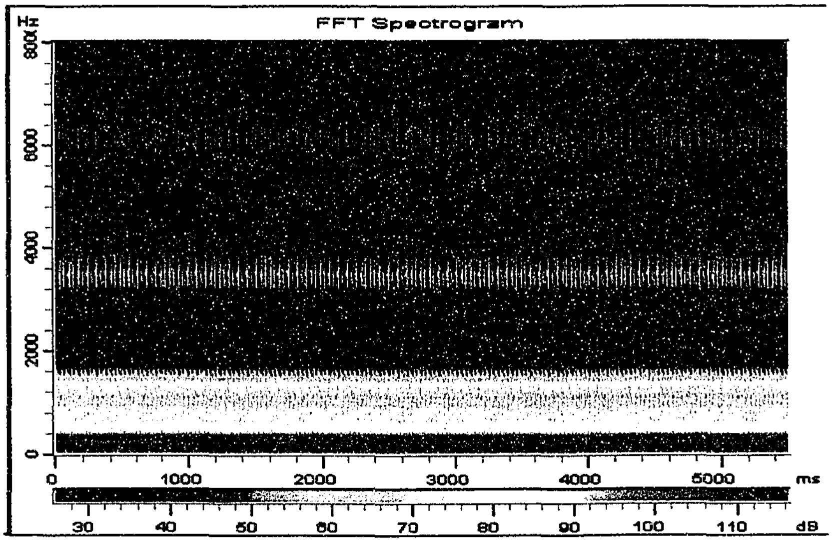

Figure 7.16: FFT Spectrogram of Numerical Unmodified Engine at 3500 rpm

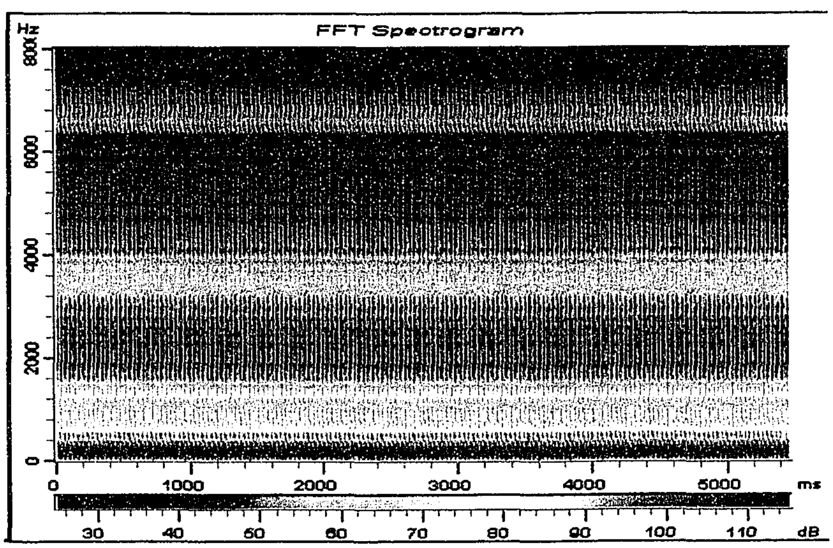

Figure 7.17: FFT Spectrogram of Numerical Bridged Engine at 3500 rpm

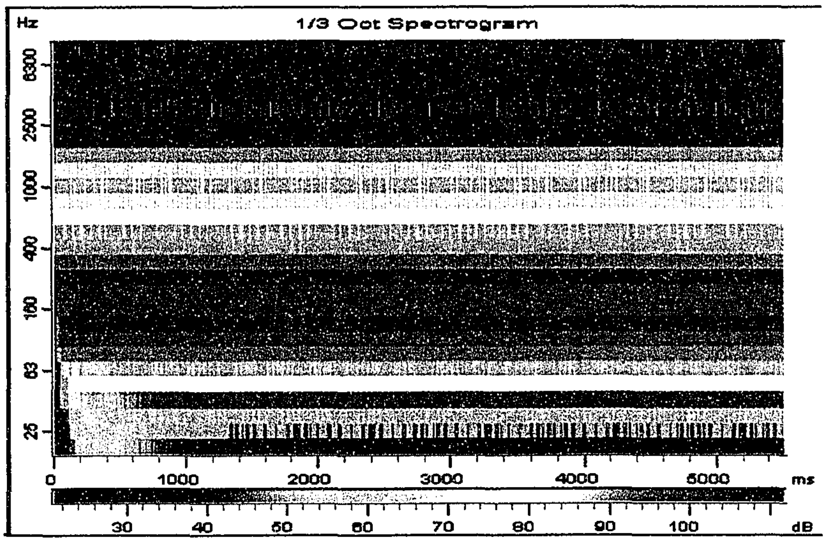

Figure 7.18: Third Octave Spectrogram of Numerical Unmodified Engine at 3500 rpm

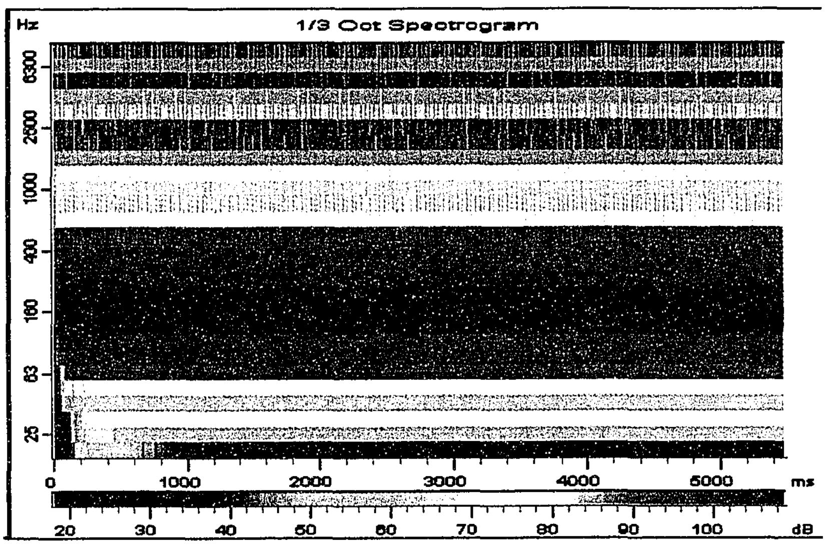

Figure 7.19: Third Octave Spectrogram of Numerical Bridged Engine at 3500 rpm

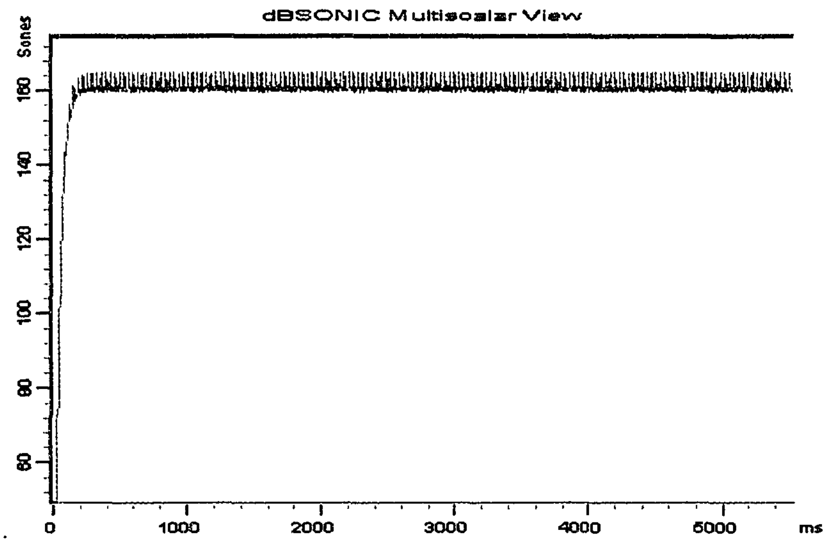

Figure 7.20: Loudness vs Time of Numerical Unmodified Engine at 3500 rpm

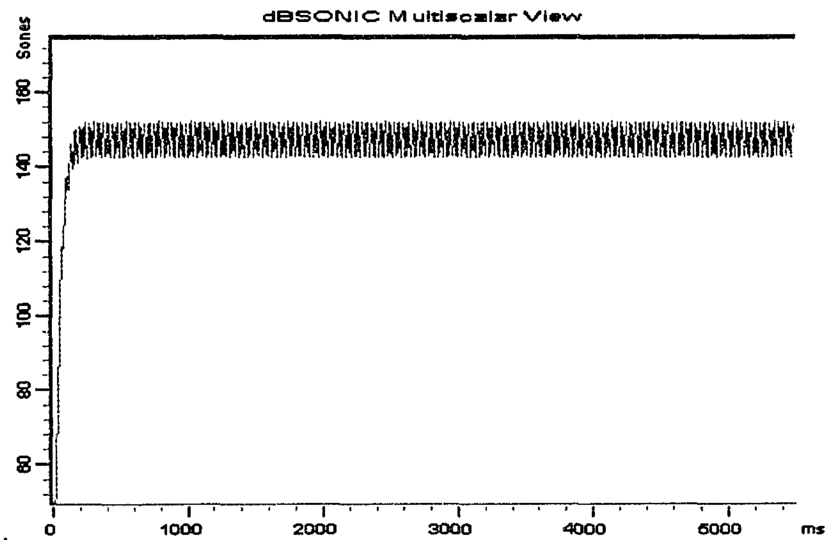

Figure 7.21: Loudness vs Time of Numerical Bridged Engine at 3500 rpm

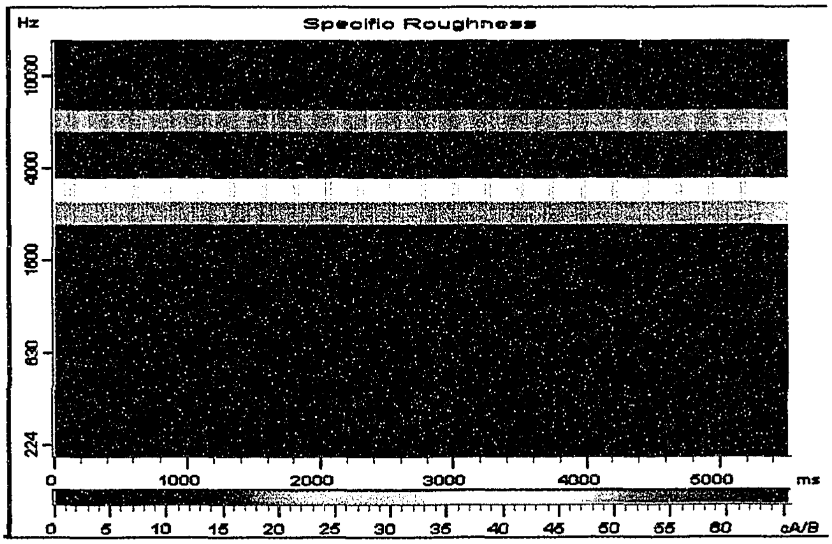

Figure 7.22: Roughness Spectrogram of Numerical Unmodified Engine at 3500 rpm

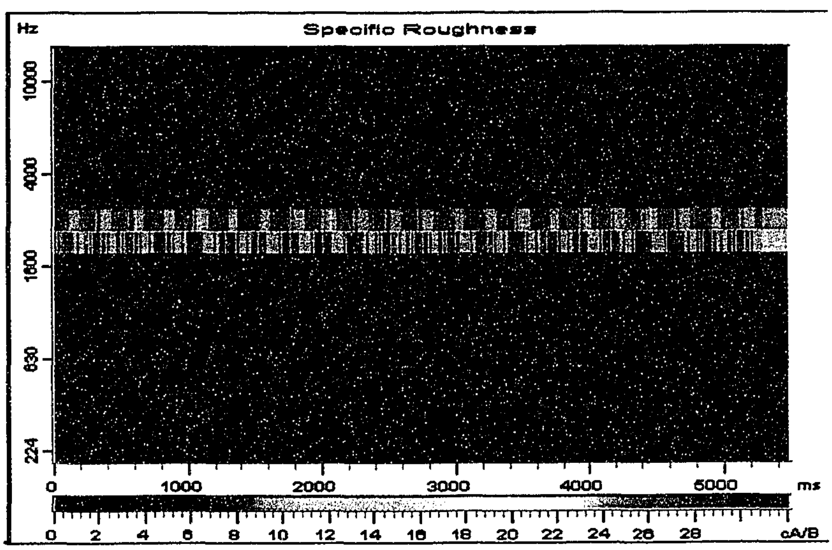

Figure 7.23: Roughness Spectrogram of Numerical Bridged Engine at 3500 rpm

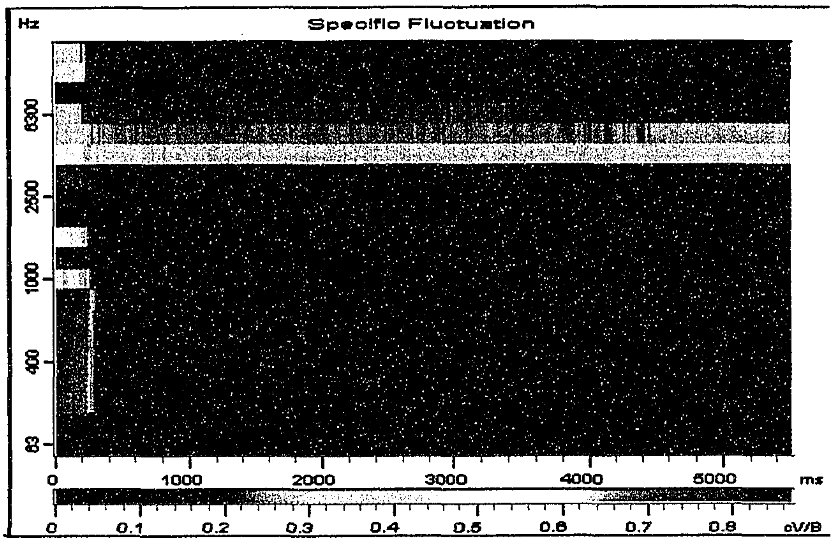

Figure 7.24: Fluctuation Strength Spectrogram of Numerical Unmodified Engine at 3500 rpm

Examination of Figure 7.25 shows a much higher fluctuation strength centred mostly about 300 Hz. The manifold bridge is not advantageous with respect to these particular metrics.

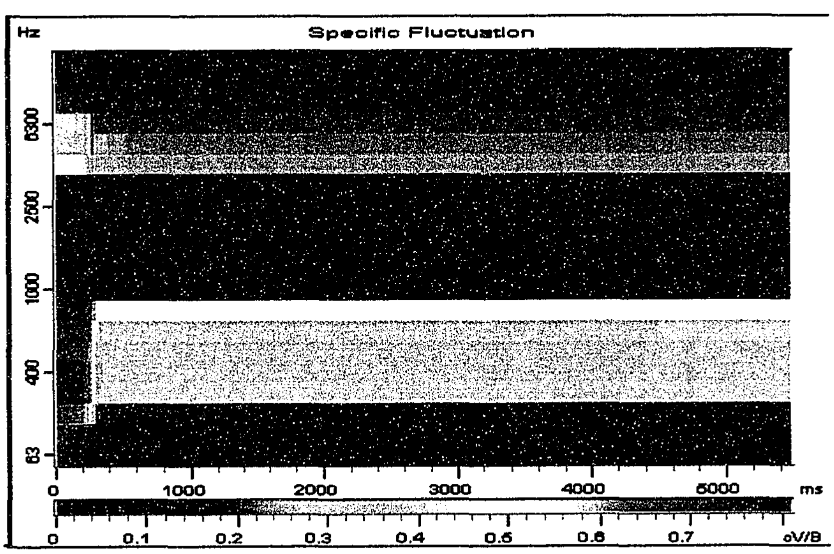

Figure 7.25: Fluctuation Strength Spectrogram of Numerical Bridged Engine at 3500 rpm

7.1.4 Results for Modelled Transient Engine Operation

Provided here is a comparison of a transient run from 1000 to 6500 rpm of the modelled unmodified and bridged engines. The duration of the linear transient run is five seconds which means that the engine speed increases 1100 rpm for each one second time step.

Figures 7.26 and 7.27 present the time signals of the two engines which clearly illustrate the advantages of the bridged engine over the unmodified engine for all engine speeds up to approximately 5600 rpm, or 4.2 seconds. This is also shown in the level versus time graphs presented in Figures 7.28 and 7.29.

Figures 7.30 and 7.31 present the combined waterfall-FFT spectrograms of the unmodified modelled engines with respect to time. Figures 7.32 and 7.33 present the data in the form of colour maps but are with respect to engine speed (rpm). Examination of the unmodified engine results indicate a predicted, greater amount of low frequency content below 375 Hz for most of the operating range of the engine when compared to the bridged engine. As in the time output cases discussed in the previous paragraph, the exception occurs within the final second of the run where the bridge engine is louder. This is particularly evident in the combined waterfall-FFT spectrograms by the existence of the dark red shading.

The amplitude of the loudness illustrated in the loudness versus time graph for the transient unmodified engine presented in Figure 7.34 is greater than the case of the bridged engine as presented in Figure 7.35. This is particularity evident around 1000 rpm as well as at approximately 4500 to 5000 rpm.

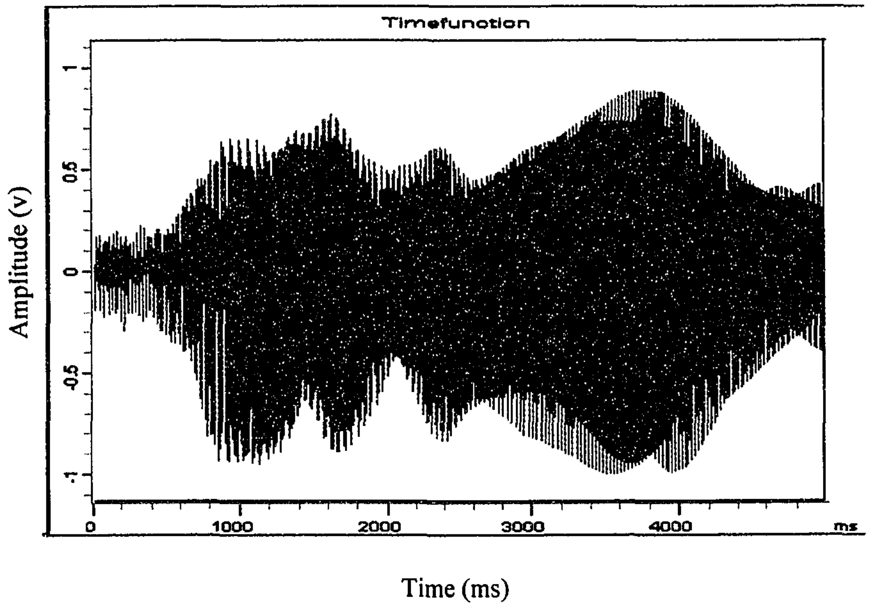

Figure 7.26: Time Function of Transient Numerical Unmodified Engine

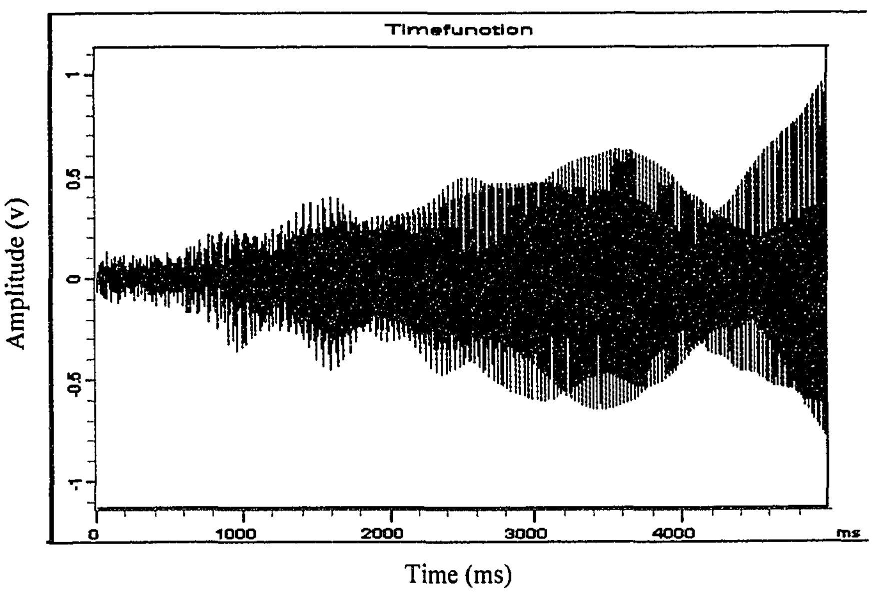

Figure 7.27: Time Function of Transient Numerical Bridged Engine

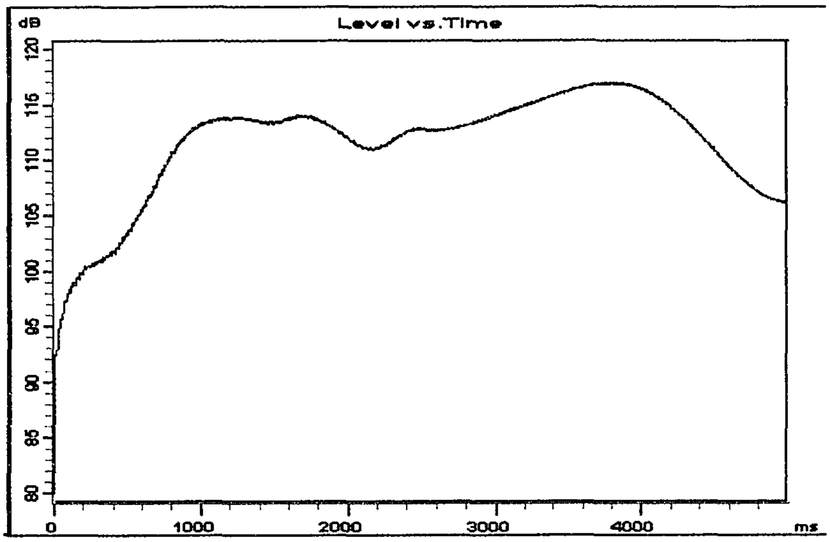

Figure 7.28: Level vs Time of Transient Numerical Unmodified Engine

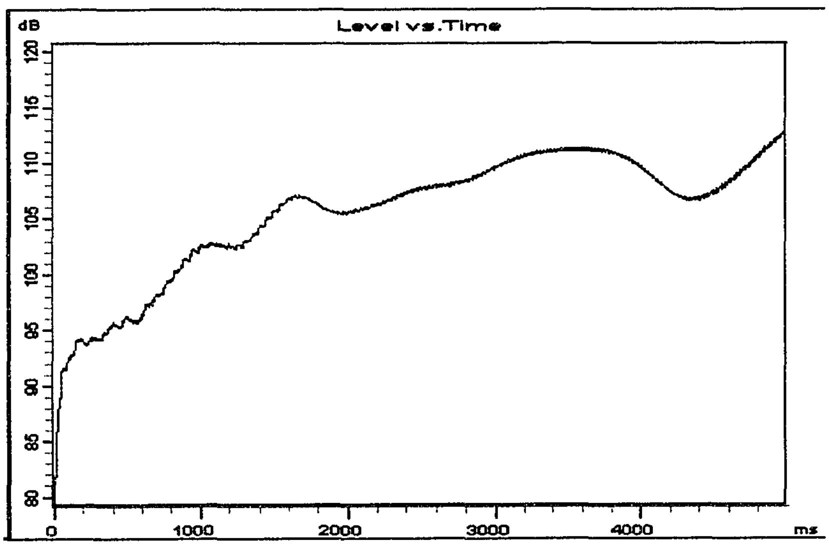

Figure 7.29: Level vs Time of Transient Numerical Bridged Engine

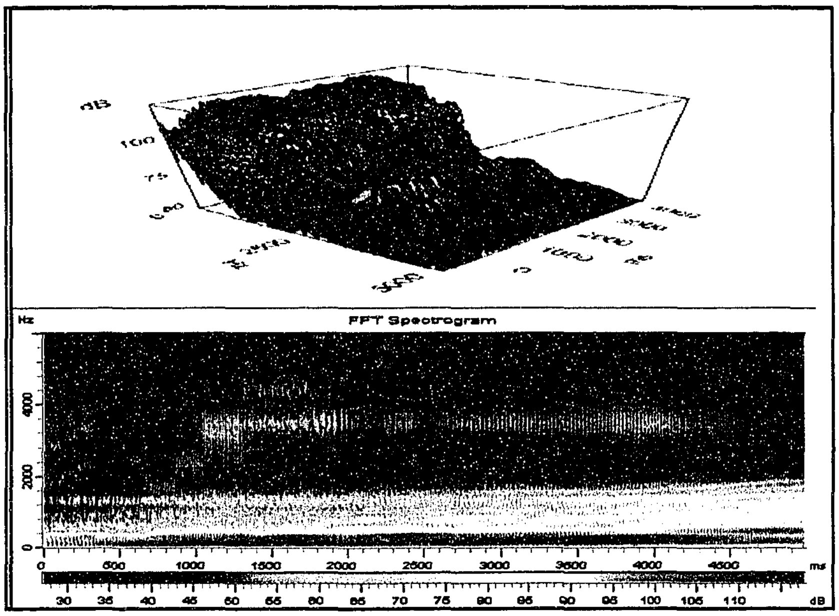

Figure 7.30: Waterfall and FFT Spectrogram of Transient Numerical Unmodified Engine

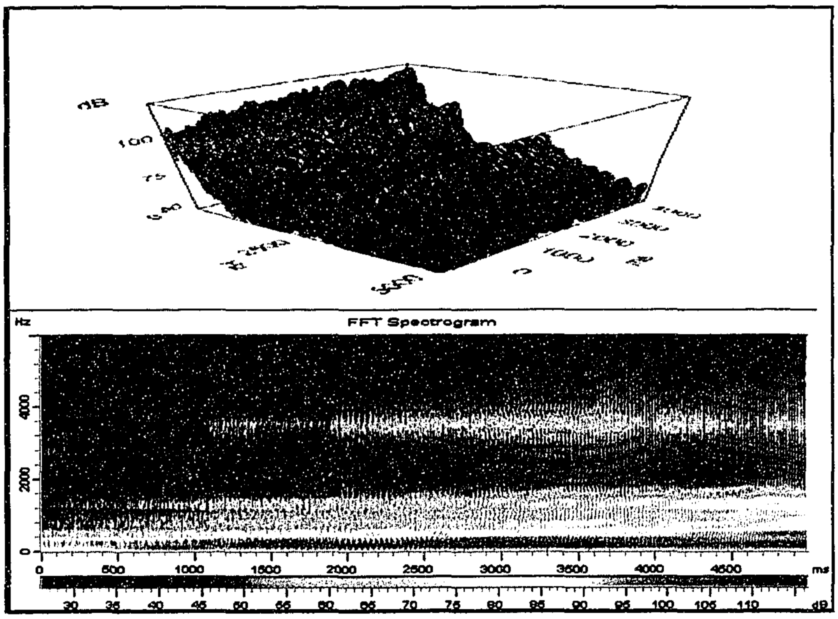

Figure 7.31: Waterfall and FFT Spectrogram of Transient Numerical Bridged Engine

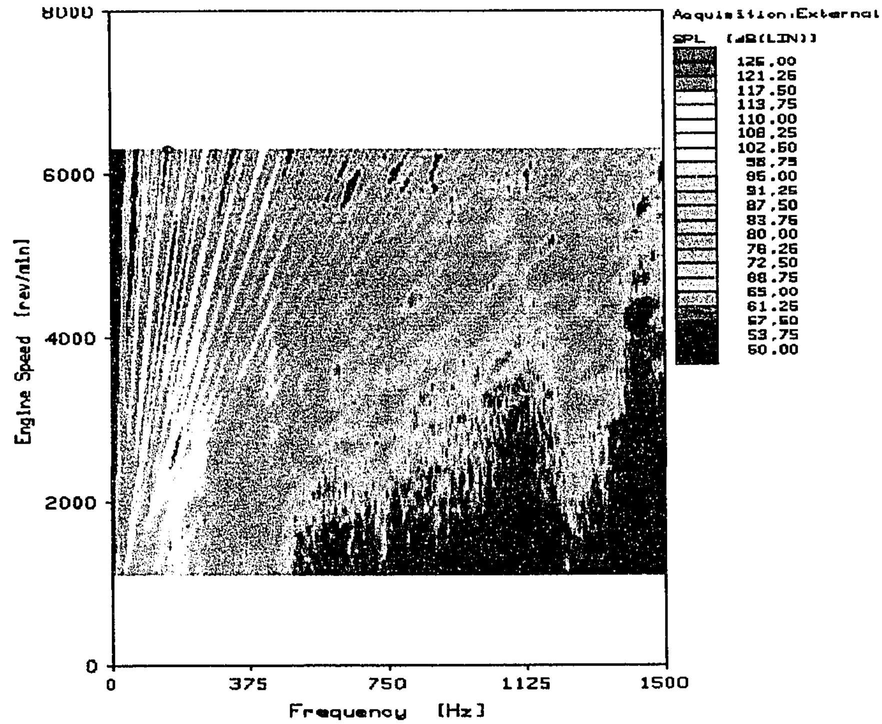

Figure 7.32 Colour Map of Transient Numerical Unmodified Engine with respect to rpm

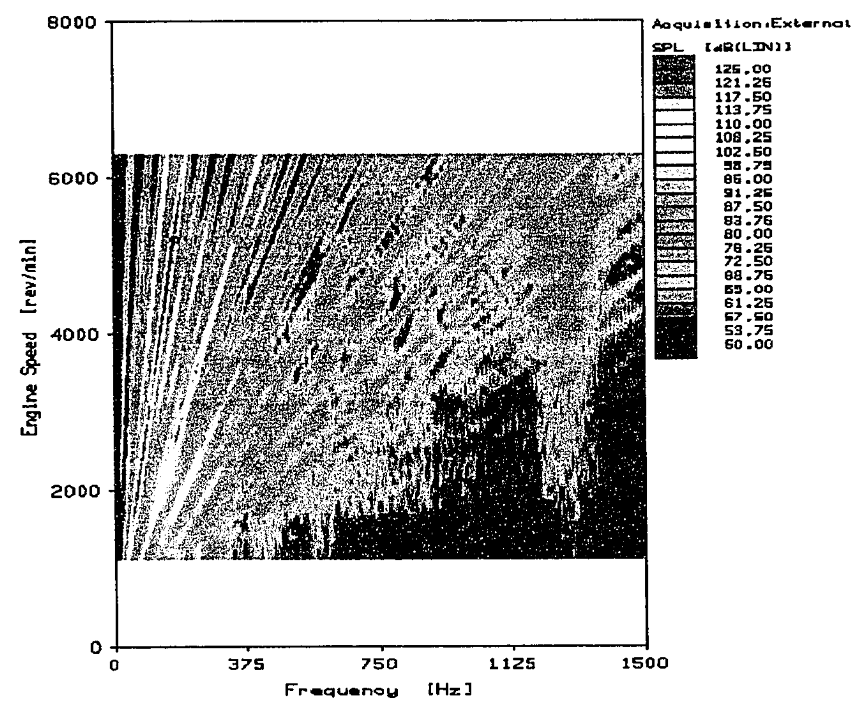

Figure 7.33 Colour Map of Transient Numerical Modified Engine with respect to rpm

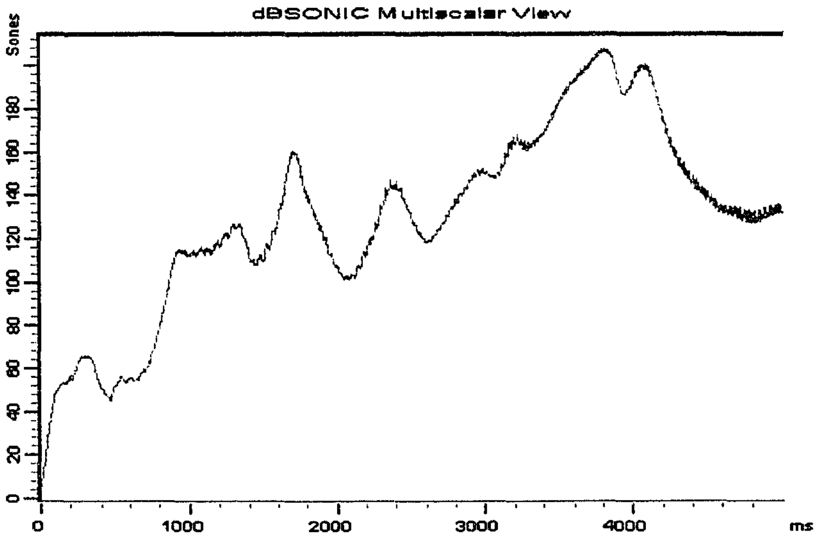

Figure 7.34: Loudness vs Time of Transient Numerical Unmodified Engine

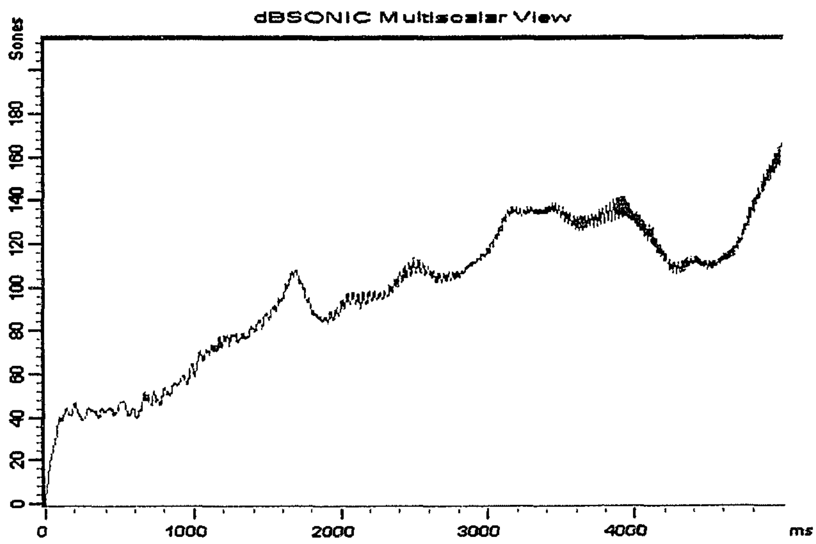

Figure 7.35: Loudness vs Time of Transient Numerical Bridged Engine

Figures 7.36 and 7.37 present the roughness spectrogram of the transient runs for the unmodified and bridged engines respectively. The interesting result here is that the roughness for the bridged engine is better than that calculated for the unmodified case. This is evident at approximately 4600 rpm. This is counter to the results obtained from the steady state analysis presented earlier. A further indication of this difference is observed in the roughness versus time graphs presented in Figures 7.38 and 7.39 for the two engine models.

Figures 7.40 and 7.41 present the fluctuation strength spectrograms for the two models. A higher fluctuation strength is evident at slower engine speeds for the case of the unmodified engine. Alternatively, the bridged engine exhibits greater fluctuation at higher engine speeds. Here, the implementation of the bridge produced both desirable and undesirable outcomes with respect to this metric.

7.2 Experimental Results

As in the case of the modelled results, the acoustical output of the experimentally measured induction noise was recorded 100 mm in front of the intake opening with the engine motored by the dynamometer. As with the WAVE model, these measurements were conducted with and without the manifold bridge.

This section will present the material similar to that presented in the previous section with the exception of the transient case. Due to limitations of the dynamometer, a transient run and subsequent analysis on the actual engine was not feasible. The steady state engine runs were also restricted to a top engine speed of 5000 rpm for safety reasons. As before, some of the more detailed results will be presented for the 3500 rpm range. All other data are available in Appendix D.

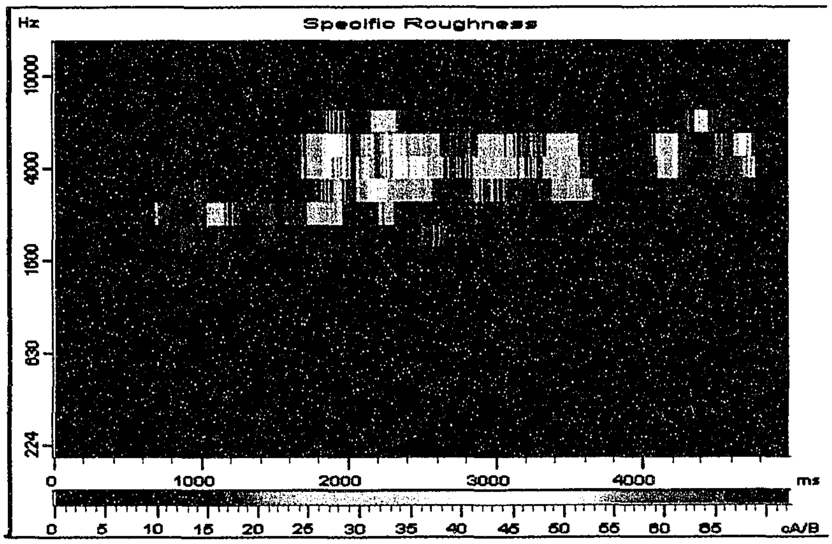

Figure 7.36: Roughness Spectrogram of Transient Numerical Unmodified Engine

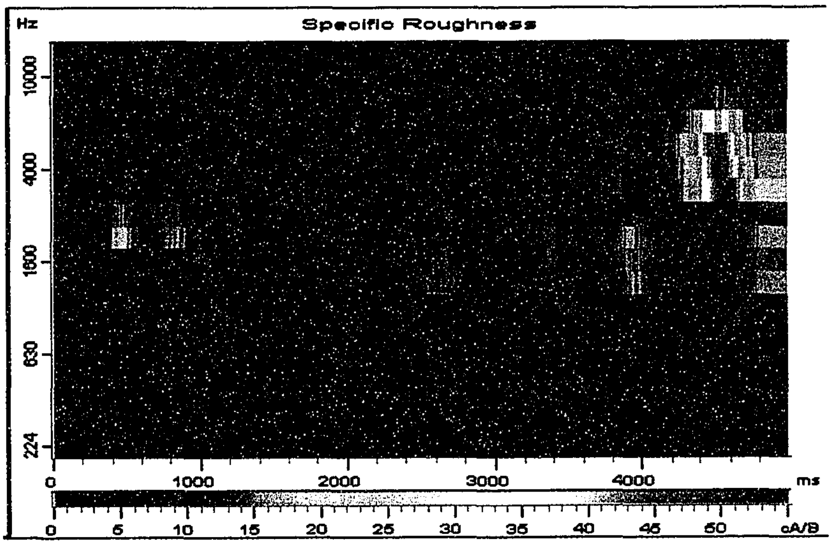

Figure 7.37: Roughness Spectrogram of Transient Numerical Bridged Engine

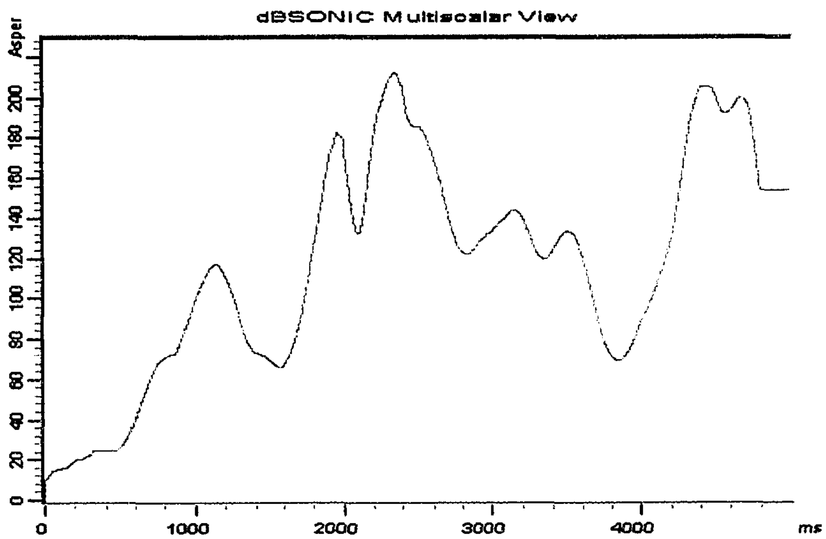

Figure 7.38: Roughness vs Time of Transient Numerical Unmodified Engine

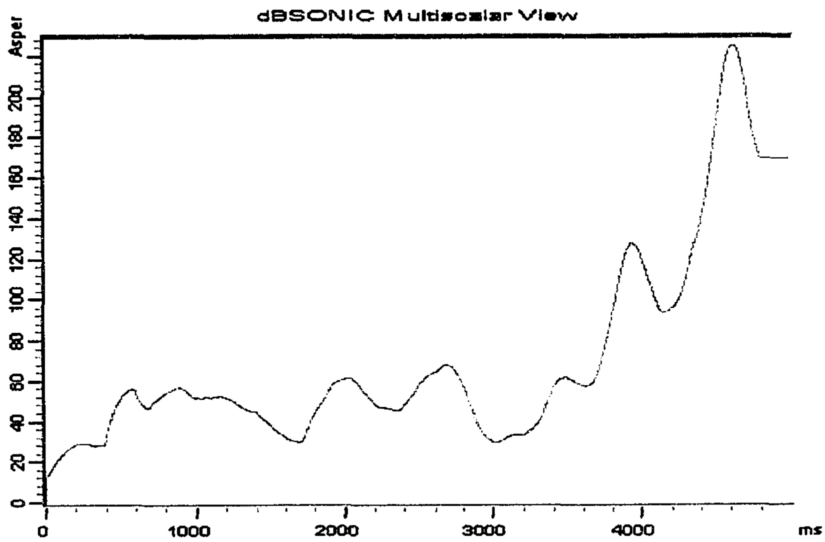

Figure 7.39: Roughness vs Time of Transient Numerical Bridged Engine

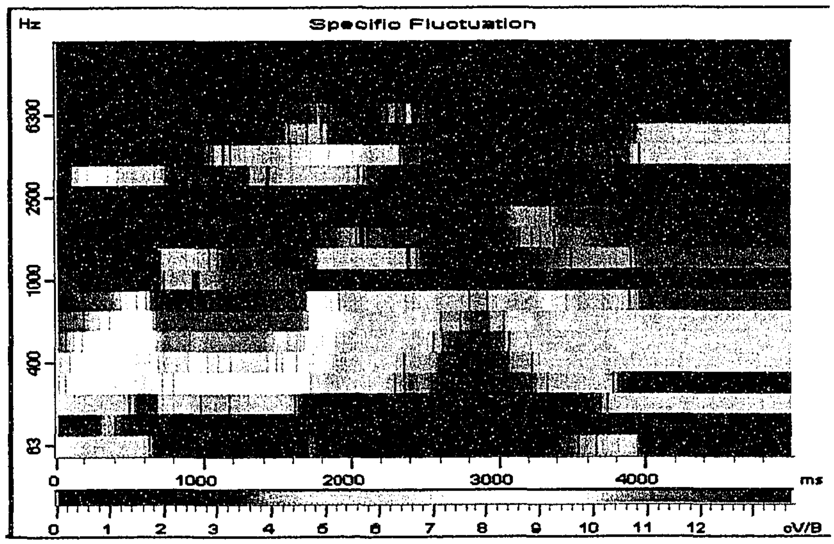

Figure 7.40: Fluctuation Strength Spectrogram of Transient Numerical Unmodified Engine

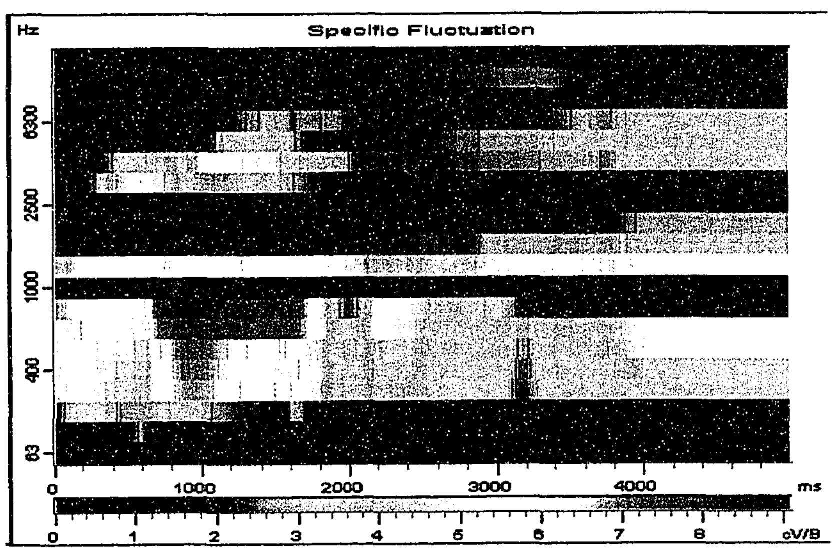

Figure 7.41: Fluctuation Strength Spectrogram of Transient Numerical Bridged Engine

7.2.1 Averaged Results for Experimental Steady State Engine Operation

Figure 7.42 presents the comparison of the measured intake noise for both the unmodified and bridged engine. These unweighted sound pressure levels (SPL) were measured for steady state engine speeds from 1000 to 5000 revolutions per minute (rpm) in increments of 500 rpm. It can be seen through examination of Figure 7.42 that an obvious attenuation is realized through the implementation of the manifold bridge for the entire engine range from 1000 to 5000 rpm. This attenuation ranges from 2.2 dB at 5000 rpm to 5.7 dB at 3000 rpm. These measured attenuation levels are much greater than those reported in the previous section for the numerical modelling results.

Figure 7.43 presents the experimentally measured A-weighted intake noise for the original and modified engines. Again, it can be seen that attenuation with the implementation of the manifold bridge is realized for all operating speeds of the engine. The maximum A-weighted attenuation of 7.1 dBA was achieved at the engine speed of 3500 rpm. The lowest A-weighted attenuation of 2.2 dBA was realized at 5000 rpm. Again, these attenuation levels are much higher than those predicted by the numerical model.

In comparing the experimentally determined loudness results shown in Figure 7.44, similar tendencies of the graphs are evident when compared to the A-weighted sound pressure results. This is used not only to re-enforce the validity of the A-weighted data, but also the effectiveness of the manifold bridging technique.

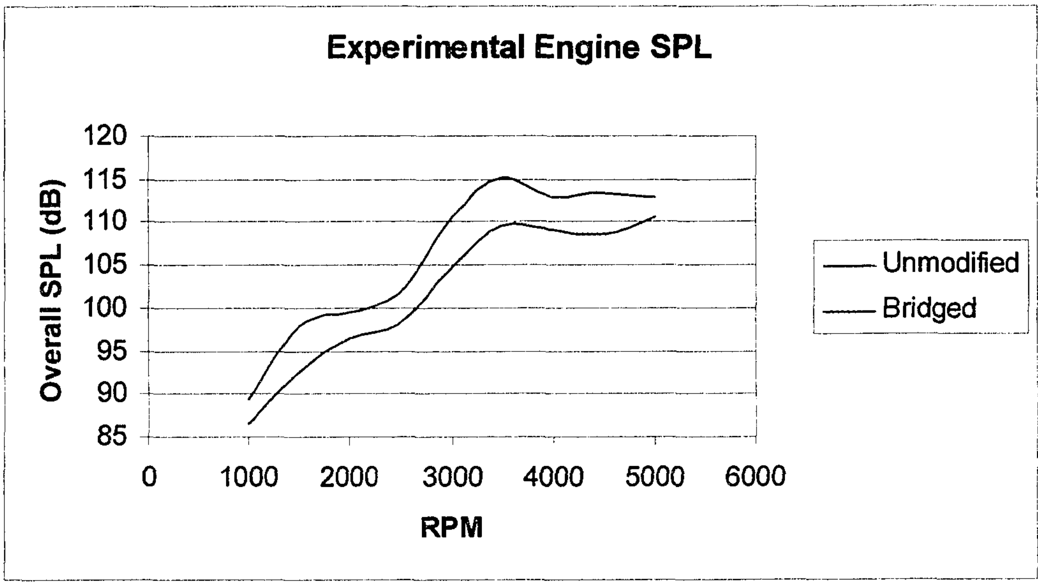

Figure 7.42: Measured Intake Noise of Experimental Unmodified and Bridged Engines

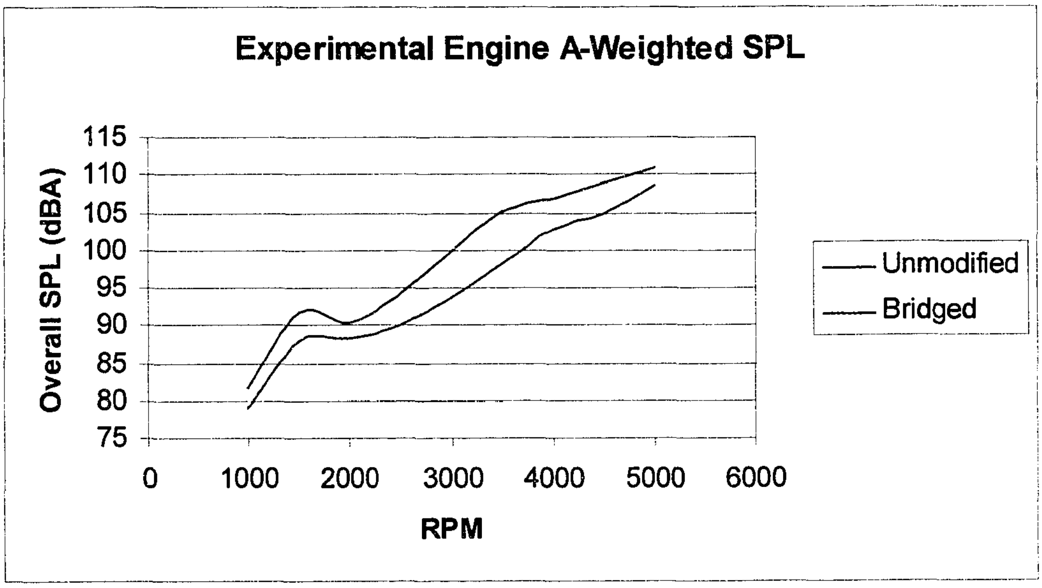

Figure 7.43: Measured Intake Noise of Experimental Unmodified and Bridged Engines

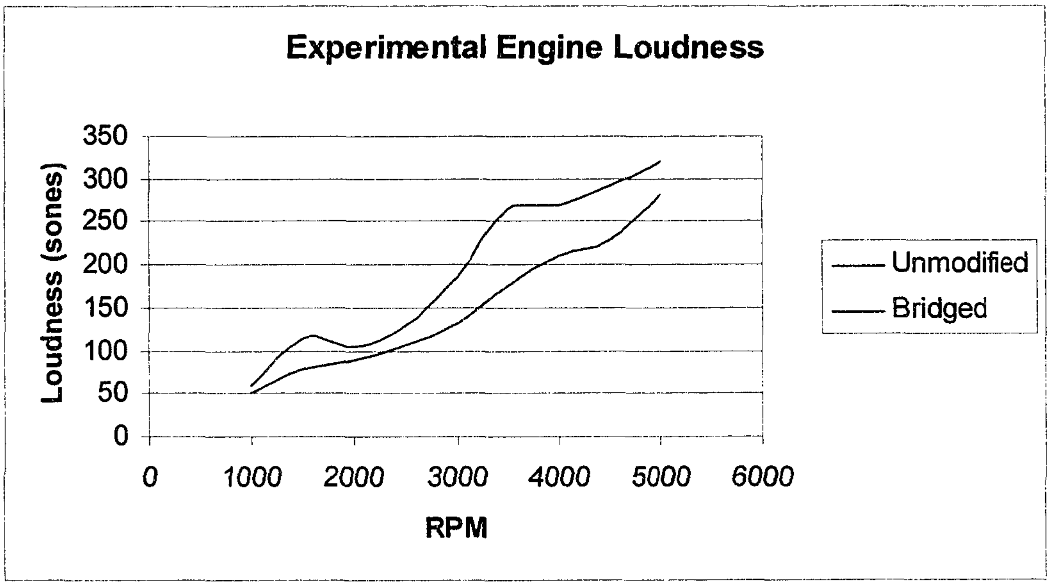

Figure 7.44: Measured Intake Noise of Experimental Unmodified and Bridged Engines

Figure 7.45 is a comparison of the calculated sharpness of both the experimental unmodified and bridged engines. The experimental results indicate that the manifold bridged engine has higher sharpness values for engine speeds from approximately 1800 rpm to about 4300 rpm. This is due to a slight increase in high frequency content for the bridged engine at these operating speeds. In spite of this, the amount of sharpness is still low for both engine results. That is to say, the results from both experimental engines exhibit very little high frequency content, with the bridged engine producing a bit more than the unmodified engine within the mid speed range.

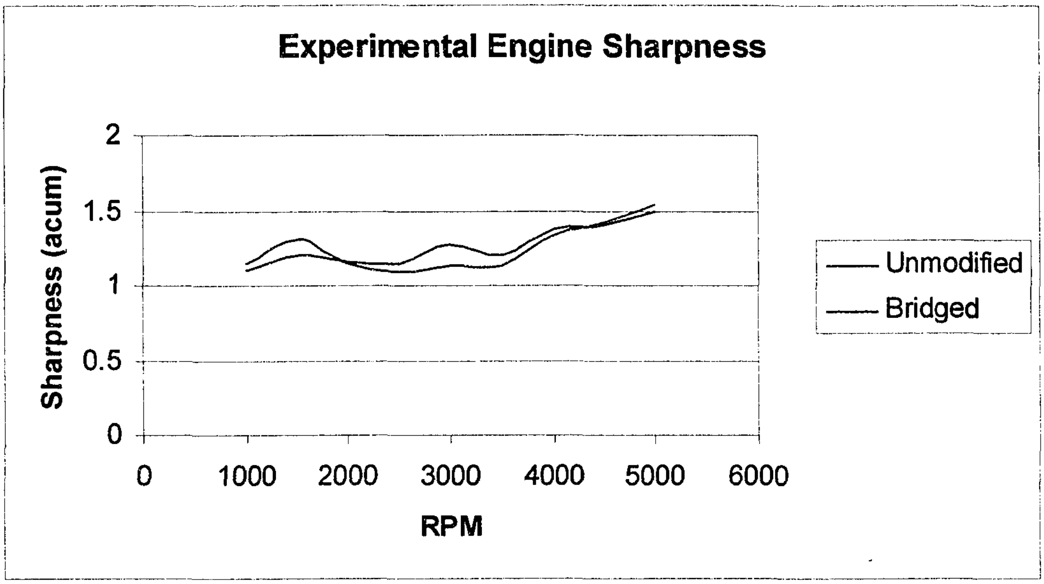

Figure 7.45: Measured Intake Noise of Experimental Unmodified and Bridged Engines

Figure 7.46 presents the fluctuation strength of both the unmodified and bridged experimental engines. The bridged engine exhibited improved fluctuation strength values for low engine speeds up to approximately 2500 rpm. The fluctuation strength increases as a result of bridging for higher engine speeds, particularly around 3500 rpm.

As can be seen in Figure 7.47, the bridged engine exhibited an increased roughness for all engine speeds less than 4200 rpm. This is especially evident at around 3500 rpm. The addition of the bridge contributed to modulation in the 20 to 300 Hz range for the experimentally bridged engine.

7.2.2 FFT and 1/3 Octave Analysis of Experimental Engine

As in the case of the numerical model, FFT and 1/3 octave analyses were conducted for each of the steady state operation of the unmodified and bridged experimental engine. Only those for the engine speed of 3500 rpm are presented in this section. The reader is referred to the appendix for the results for all other engine speeds.

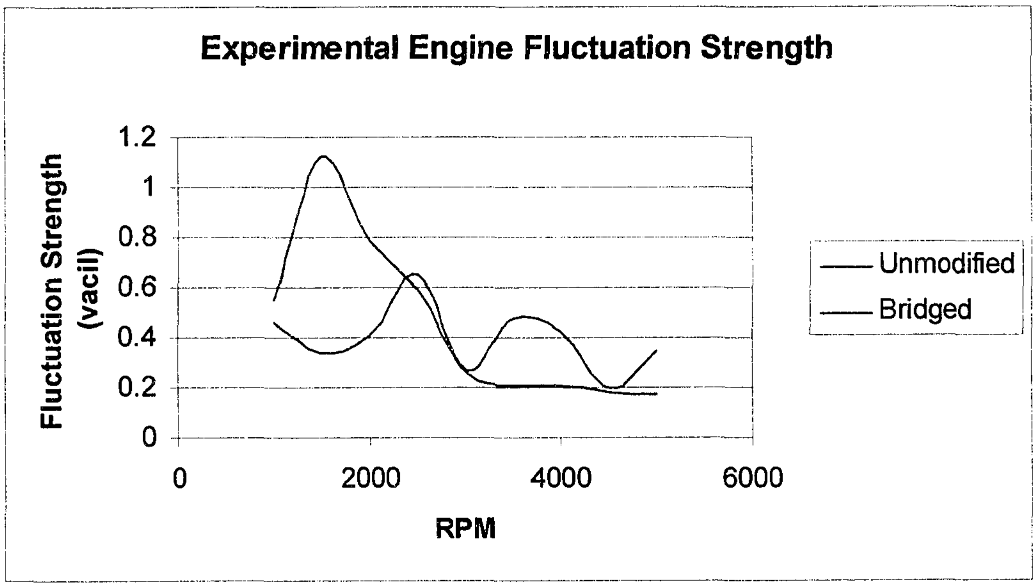

Figure 7.46: Measured Intake Noise of Experimental Unmodified and Bridged Engines

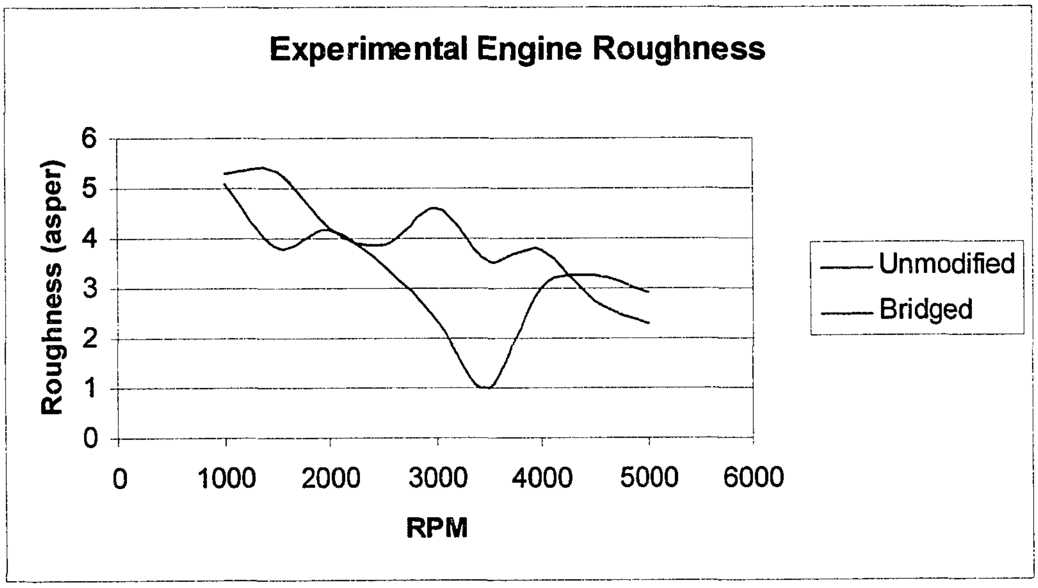

Figure 7.47: Measured Intake Noise of Experimental Unmodified and Bridged Engines

Figures 7.48 and 7.49 present the FFT outputs of the numerical unmodified and bridged engine models respectively. It can be seen that, for the most part, the amplitudes of the fundamental and subsequent harmonics are lower for the highest energy peaks. This results in a lowering of the overall realized sound pressure level. This has also resulted, however, in introducing a detrimental effect on the fluctuation and roughness of the resulting acoustic output. Since the attenuated peaks, particularly at 115 and 230 Hz, are now at similar amplitudes to adjacent peaks, this has resulted in added modulation to the resulting signal. This added modulation is the cause of the increase in fluctuation strength and roughness. Since the attenuated peaks, particularly at 115 and 230 Hz, are now at similar amplitudes to adjacent peaks, this has resulted in added modulation to the resulting signal. This added modulation is the cause of the increase in fluctuation strength and roughness.

Figures 7.50 and 7.51 present the 1/3 octave analyses of the numerical unmodified and bridged engine models respectively, at 3500 rpm. These graphical data also show the realized attenuation of the first two fundamentals as well as the lowering of low frequency energy. They, however, do not convey the same information that the FFT outputs do with respect to the increase in modulation. In fact, the 1/3 octave outputs suggest, if anything, a smoother and more evenly distributed curve. It is because of this, that such octave analysis techniques are useful for the determination of overall distributed levels but not for more specific sound quality analysis such as were conducted here.

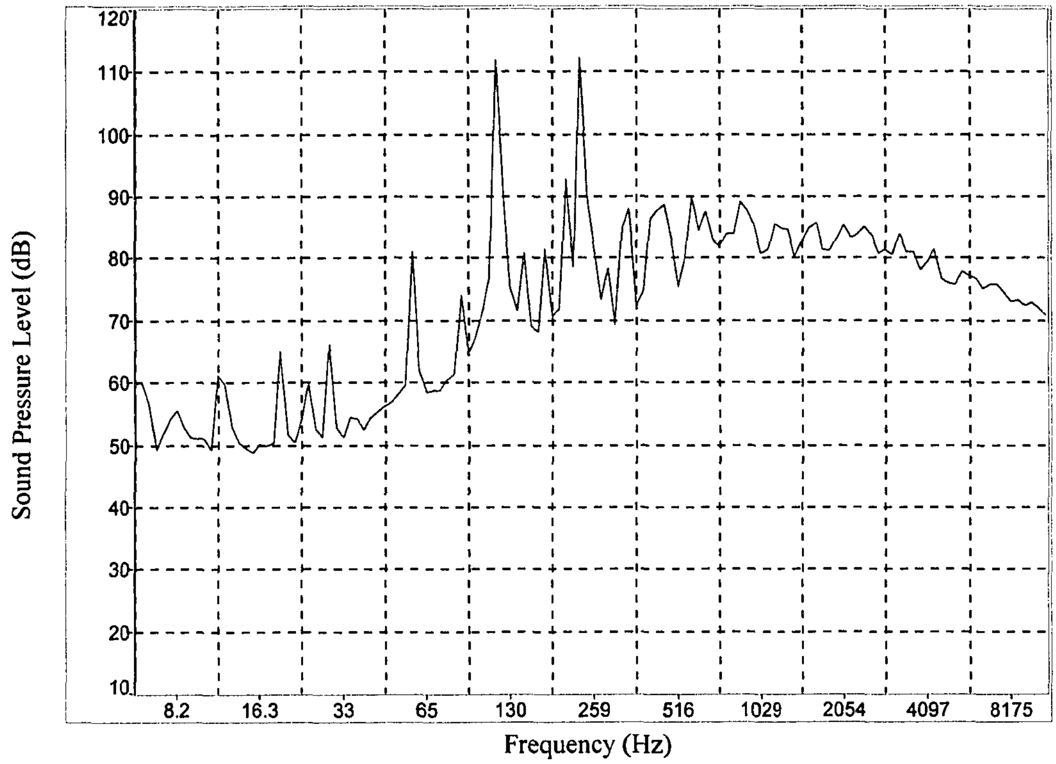

Figure 7.48: FFT of Experimental Unmodified Engine at 3500 rpm

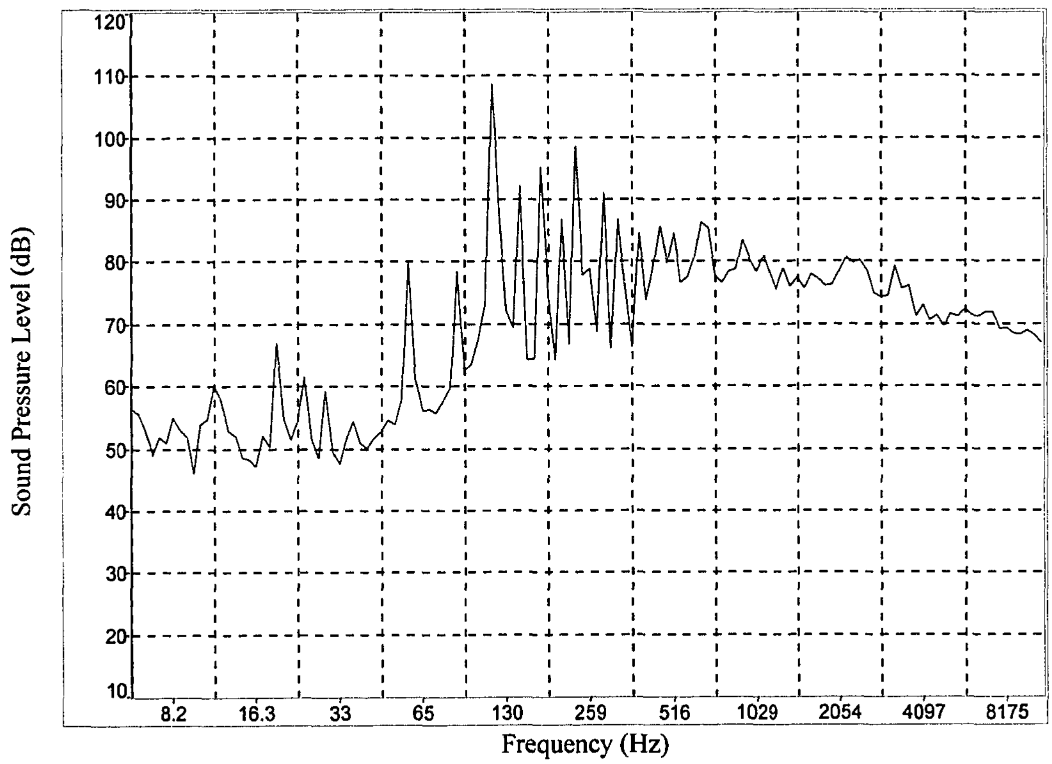

Figure 7.49: FFT of Experimental Bridged Engine at 3500 rpm

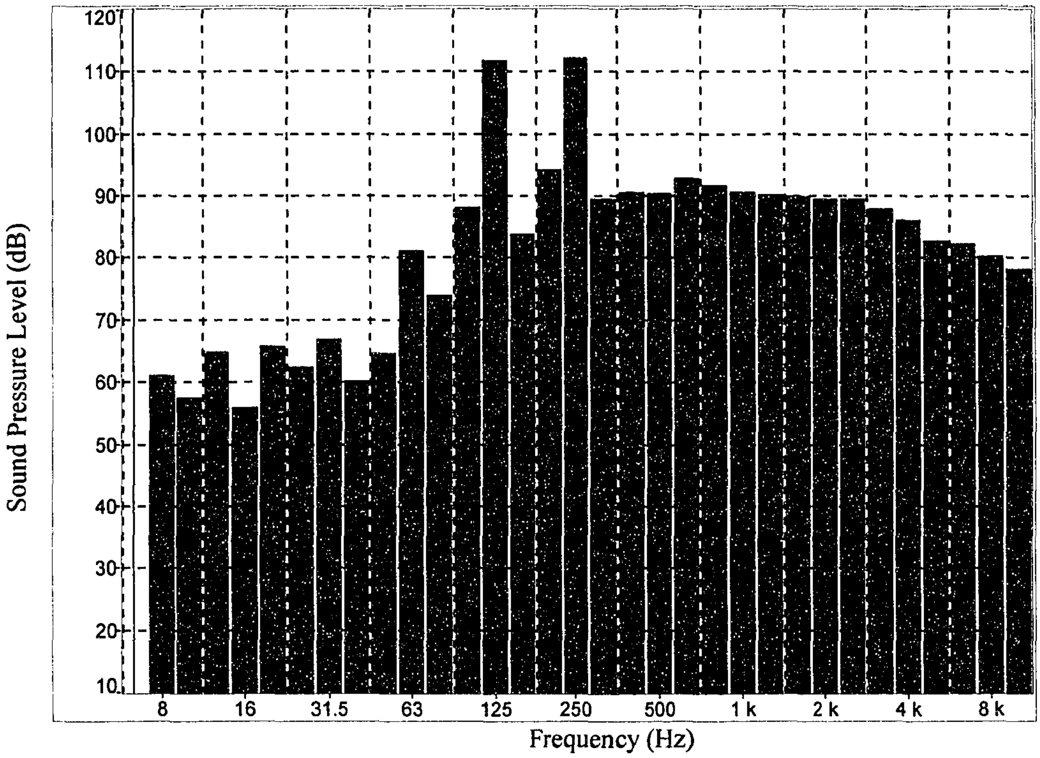

Figure 7.50: 1/3 Octaves of Experimental Unmodified Engine at 3500 rpm

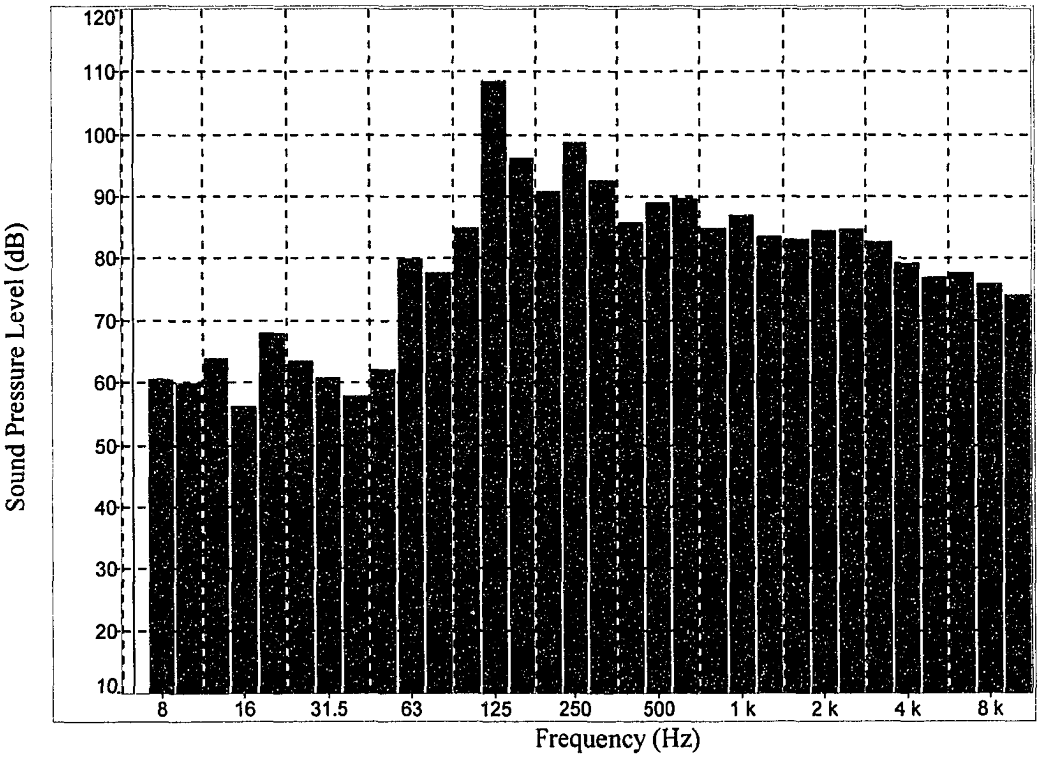

Figure 7.51: 1/3 Octaves of Experimental Bridged Engine at 3500 rpm

7.2.3 Time Function Results for Experimental Steady State Engine Operation

Presented are several time function analysis outputs of the experimental measurements taken of the Toyota engine with and without the manifold bridge. As in section 7.1.3, such an analysis yields insight with respect to the presumably steady results over time.

Presented in Figures 7.52 and 7.53 are the time functions of the experimental results for the unmodified and bridged engines respectively. The attenuation in amplitude of the time signal is apparent. Thus, reinforcing the results discussed in section 7.2.1 stating that the manifold bridge resulted in a quieter engine.

Figures 7.54 and 7.55 present the experimental level versus time results for the unmodified and bridged engines respectively. The steady attenuated values associated with the bridged engine when compared to the unmodified engine results reveal obvious differences over the entire analysis period. Again, examination of the levels produced on the time history closely follow the averaged levels reported in section 7.1.1.

The experimental FFT spectrograms of the unmodified and bridged engines are presented in Figures 7.56 and 7.57 respectively. Also, presented in Figures 7.58 and 7.59 are the third octave spectrograms. The majority of the reduced acoustic energy for the bridged engine is found in the low frequency region where the degree of solid red is not as prominent. This is more evident through examination of the third octave spectrograms. For the unmodified engine, very loud bands are evident at the 125 and 250 Hz third octave bands whereas for the bridged case, the dark band at 250 Hz is not evident, thus illustrating the positive effect of the manifold bridge.

The loudness versus time values of the unmodified and bridged engines are presented in Figure 7.60 and 7.61 respectively. Here, the advantages of the bridged engine are apparent with a much reduced loudness level over the entire time period.

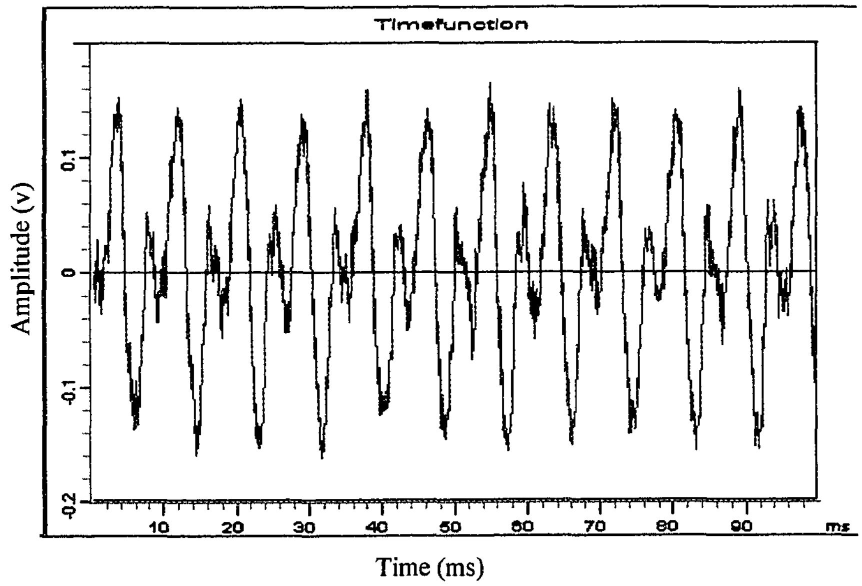

Figure 7.52: Time Function of Experimental Unmodified Engine at 3500 rpm

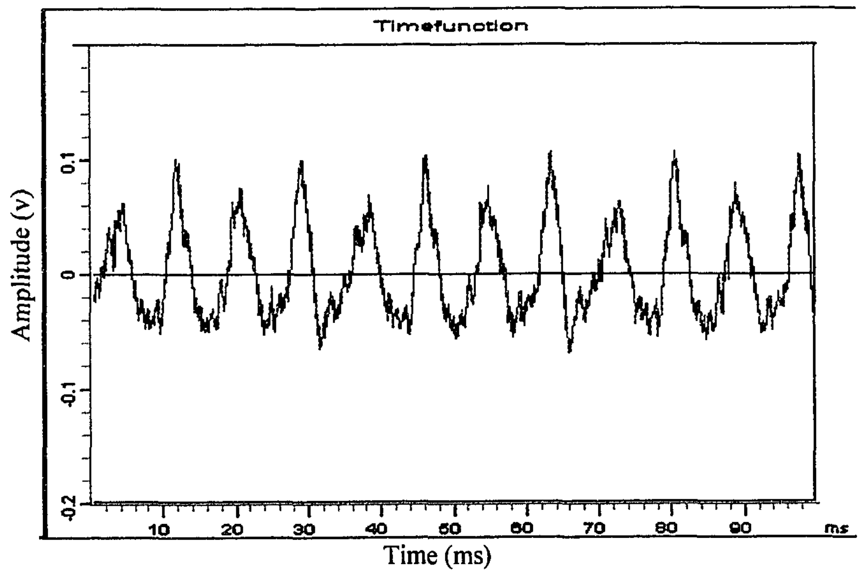

Figure 7.53: Time Function of Experimental Bridged Engine at 3500 rpm

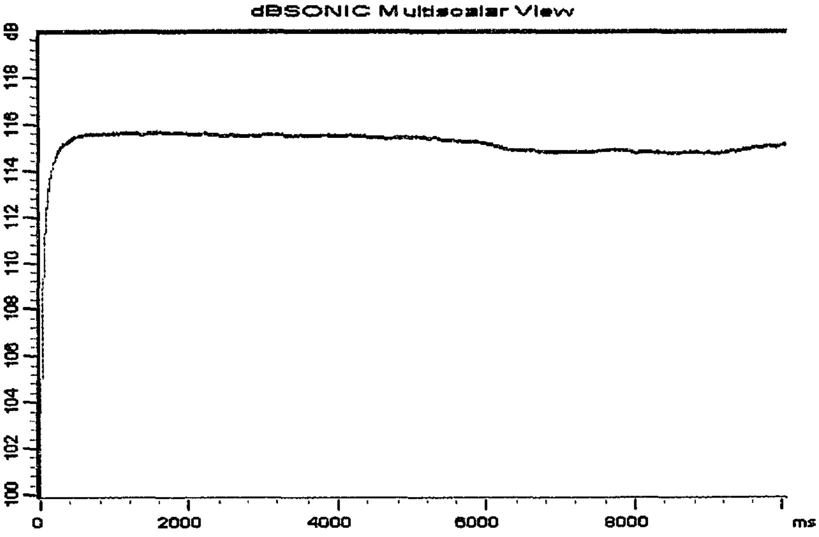

Figure 7.54: Level vs Time of Experimental Unmodified Engine at 3500 rpm

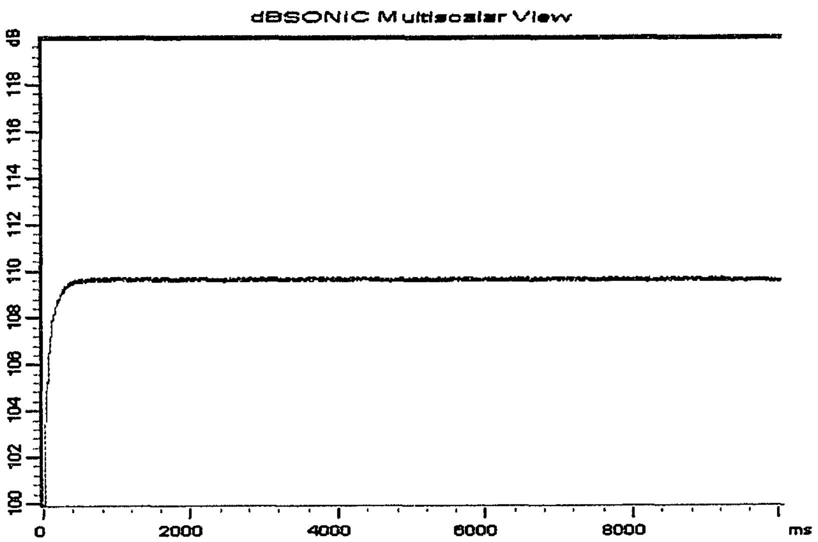

Figure 7.55: Level vs Time of Experimental Bridged Engine at 3500 rpm

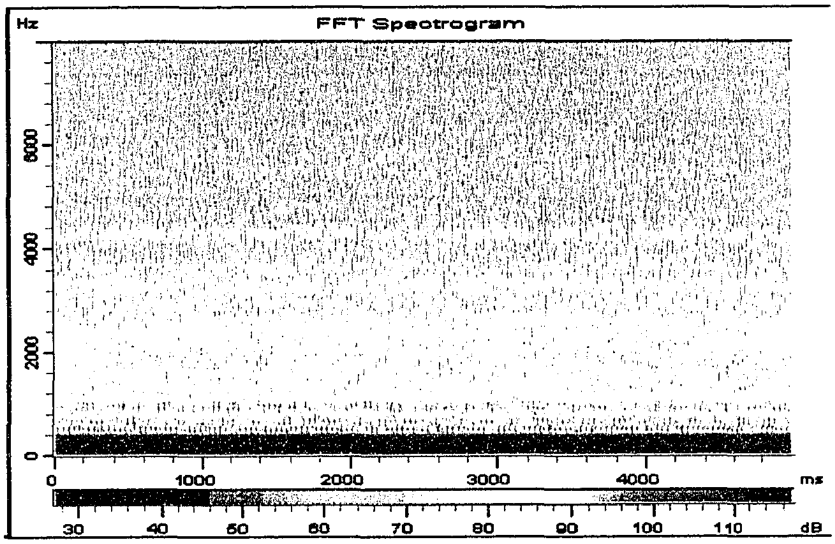

Figure 7.56: FFT Spectrogram of Experimental Unmodified Engine at 3500 rpm

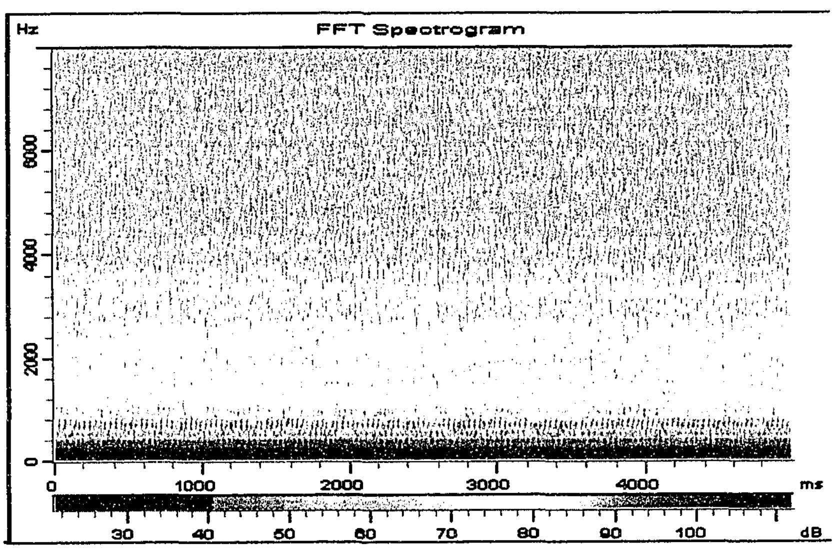

Figure 7.57: FFT Spectrogram of Experimental Bridged Engine at 3500 rpm

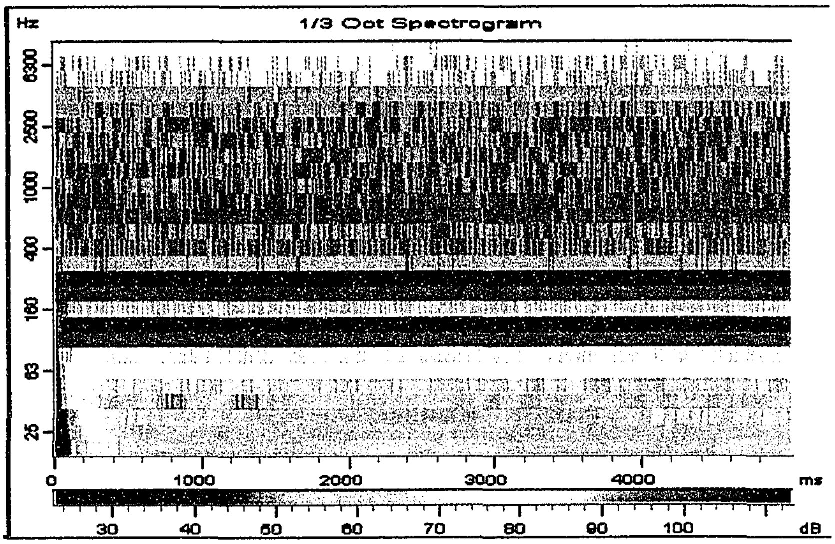

Figure 7.58: Third Octave Spectrogram of Experimental Unmodified Engine at 3500 rpm

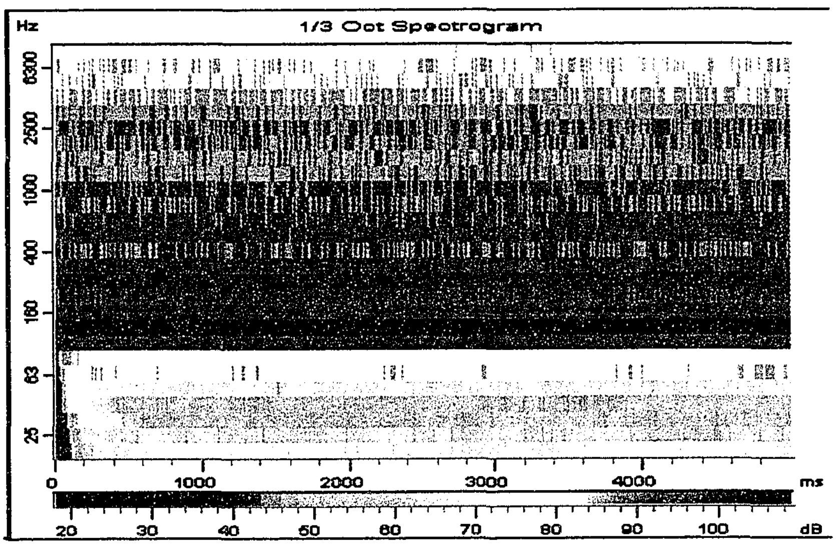

Figure 7.59: Third Octave Spectrogram of Experimental Bridged Engine at 3500 rpm

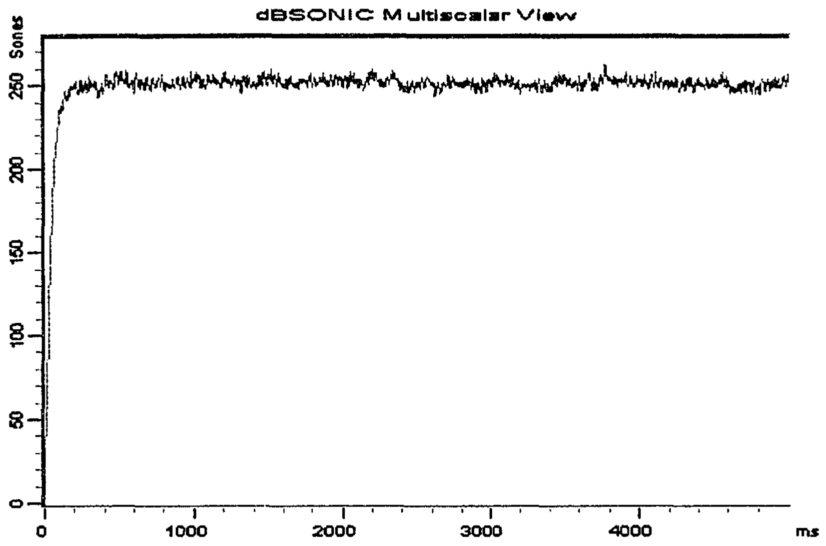

Figure 7.60: Loudness vs Time of Experimental Unmodified Engine at 3500 rpm

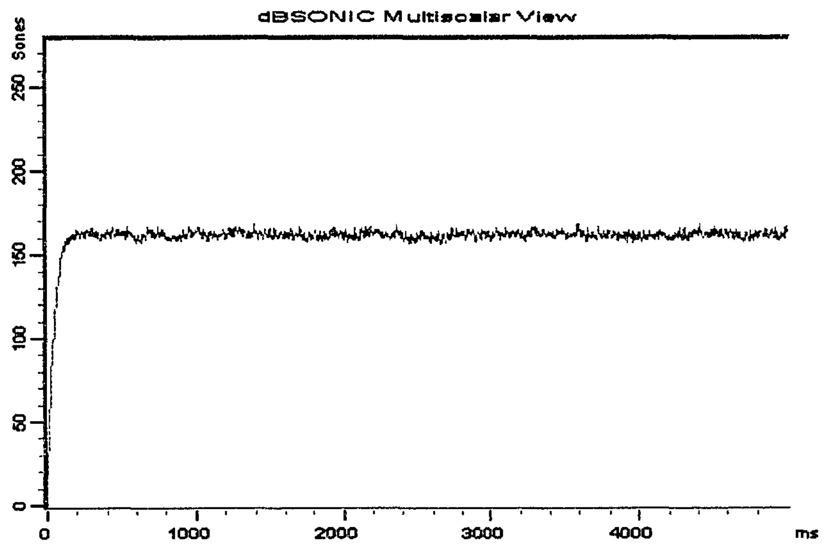

Figure 7.61: Loudness vs Time of Experimental Bridged Engine at 3500 rpm

Figures 7.62 and 7.63 present the roughness spectrograms of the experimental unmodified and bridged engines respectively. Similarly, Figures 7.64 and 7.65 present the fluctuation strength spectrogram of the same. In both cases, there is an obvious increase in both the roughness and fluctuation strength for the bridge engine.

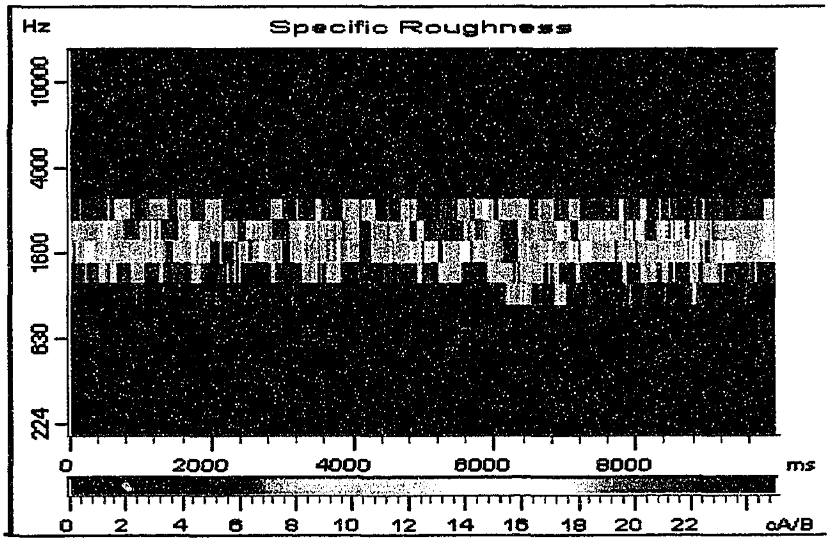

Figure 7.62: Roughness Spectrogram of Experimental Unmodified Engine at 3500 rpm

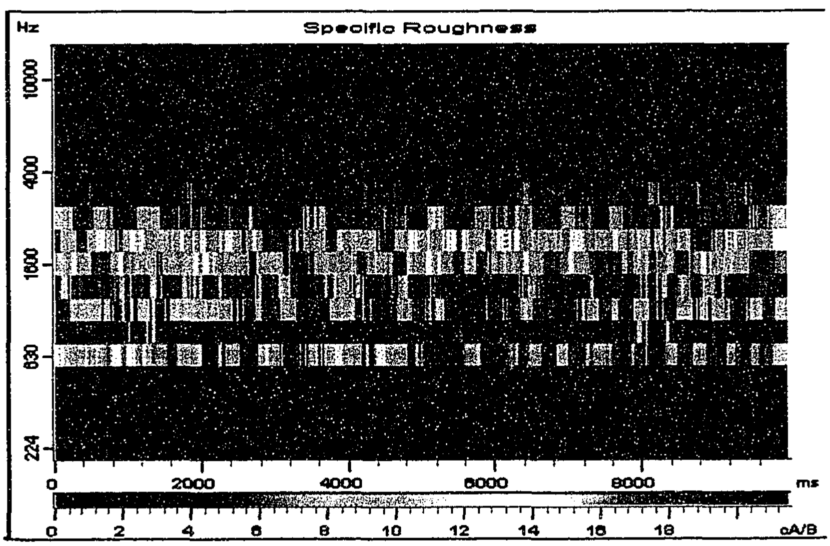

Figure 7.63: Roughness Spectrogram of Experimental Bridged Engine at 3500 rpm

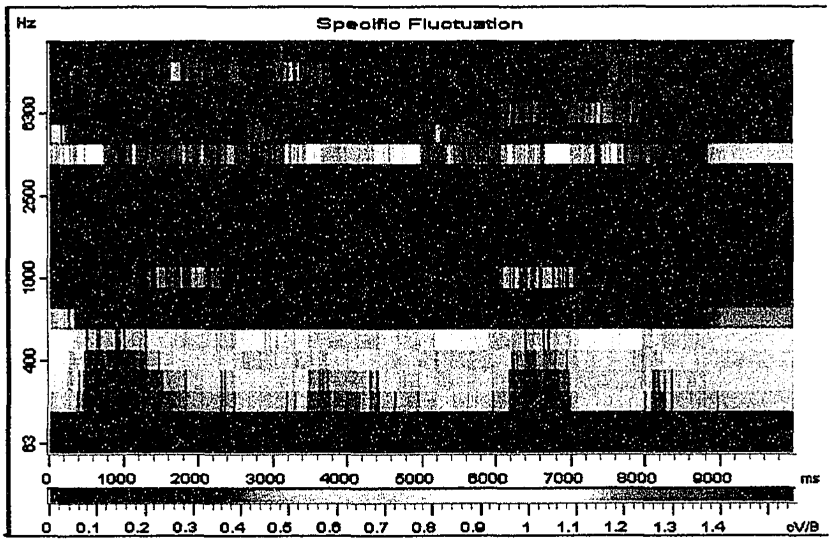

Figure 7.64: Fluctuation Strength Spectrogram of Unmodified Engine at 3500 rpm

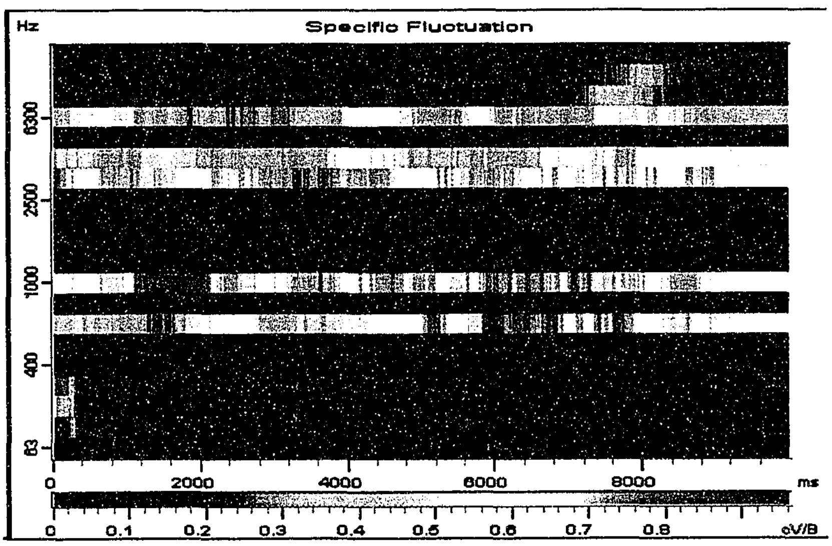

Figure 7.65: Fluctuation Strength Spectrogram of Bridged Engine at 3500 rpm

7.3 Comparison of Numerical and Experimental Results

This section will look at the direct relationship between the numerical and experimental results. To simplify things, the discussion is restricted to comparing the averaged results determined from the steady state operation of the engines as were individually examined in Sections 7.1.1 and 7.2.1.

Figure 7.66 represents the predicted unweighted sound pressure levels (SPL) of the intake noise for all four engine cases. It is noted that while both the modelled and experimental cases exhibited overall noise attenuation with the implementation of the manifold bridge, the experimental results showed a greater difference. That is, the addition of the bridging device resulted in greater attenuation with the experimental measurements.

Figure 7.67 presents the predicted A-weighted intake noise of the four engines. Good attenuation with the manifold bridge is demonstrated by the experimental results. The numerical results, however, do not fair as well. It can be seen that these modified and unmodified results cross each other several times throughout the operating speeds tested. This is similarly noted in the loudness diagram shown in Figure 7.68. This is due to a higher frequency content in the modelled results which did not materialize in the experimental measurements. It is suspected that the analytical model is failing to accurately predict results at the higher engine speeds.

Figure 7.69 presents the sharpness results of the four engine models which is a measure of the high frequency content of the noise. Again, the modelled and experimental results differ. As in the case of the A-weighted results, the numerical model is not accurately predicting the high frequency portion of the results.

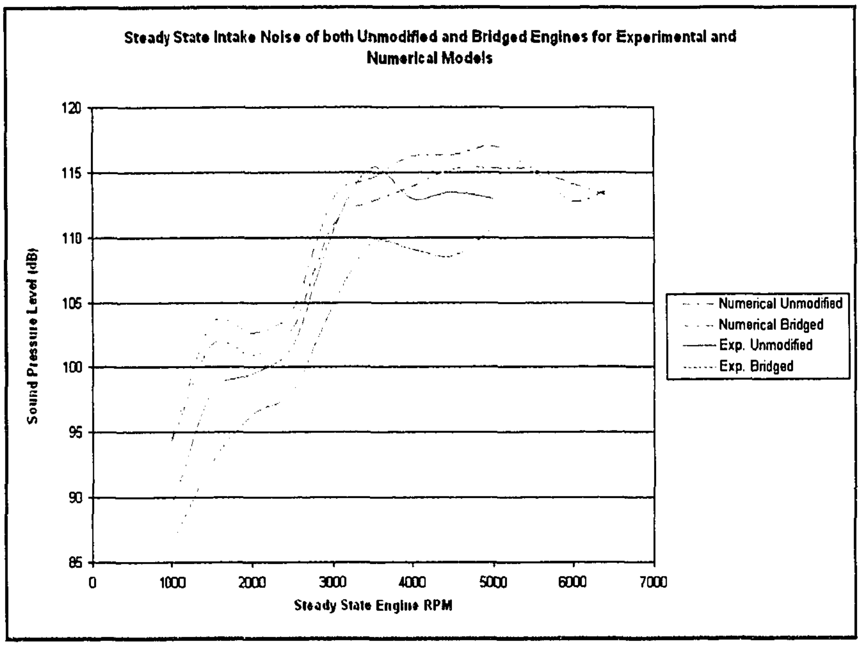

Figure 7.66: Predicted Intake Noise of Experimental and Numerical Unmodified and Bridged Engines

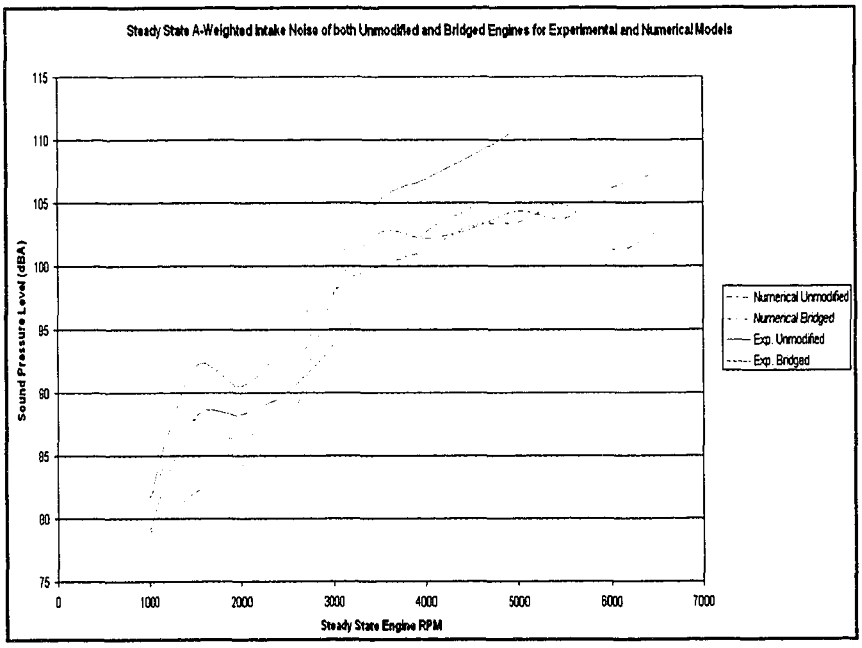

Figure 7.67:Predicted A-Weighted Intake Noise of Experimental and Numerical Unmodified and Bridged Engines

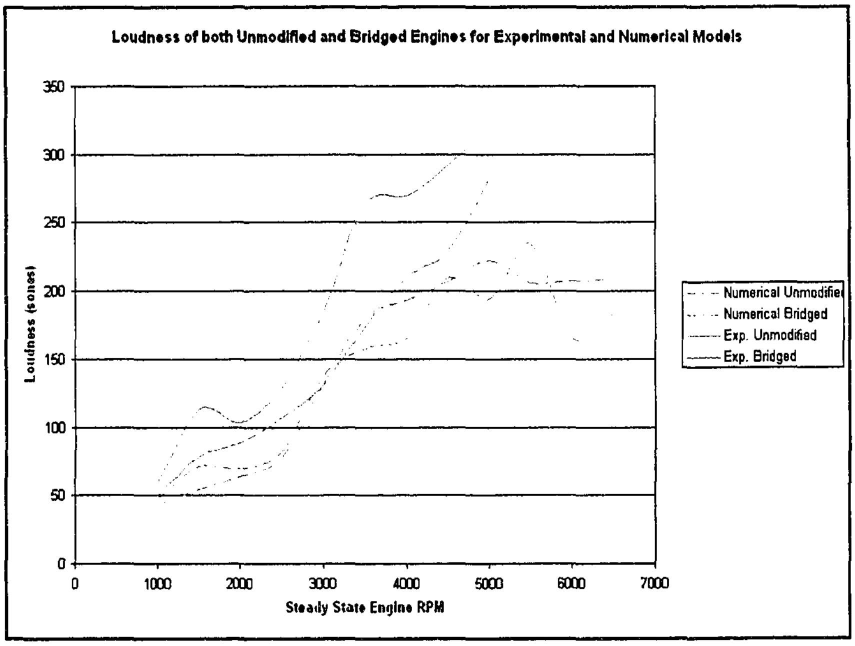

Figure 7.68: Predicted Loudness of Experimental and Numerical Unmodified and Bridged Engines

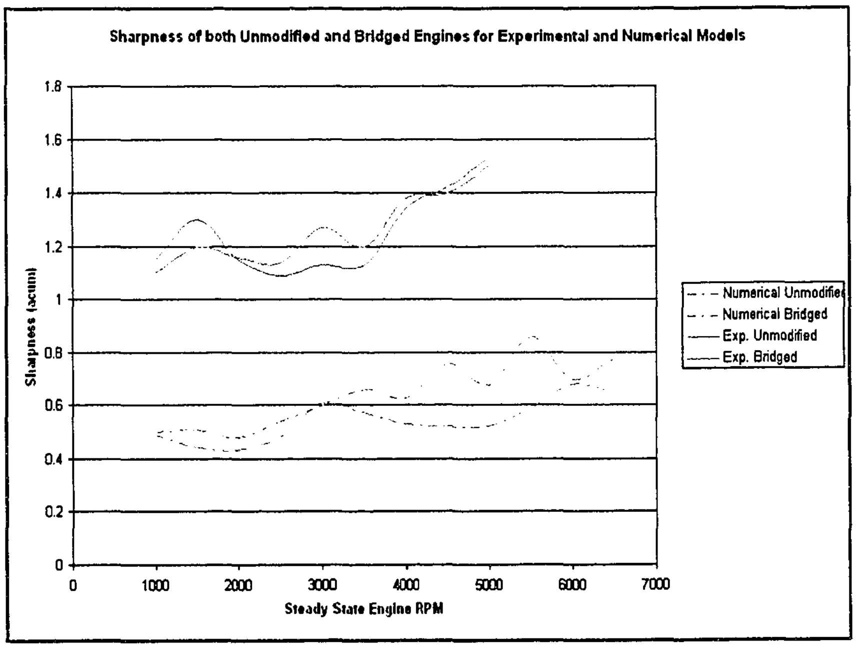

Figure 7.69: Predicted Sharpness of Experimental and Numerical Unmodified and Bridged Engines

Figure 7.70 presents the roughness results of the four configurations. The resulting pattern of the experimental and numerical results are for the most part similar, only with a greater dynamic range given to the experimental results. This gives some validity back to the analytical model given the additional high frequency content in the experimental results which can result in realized modulation.

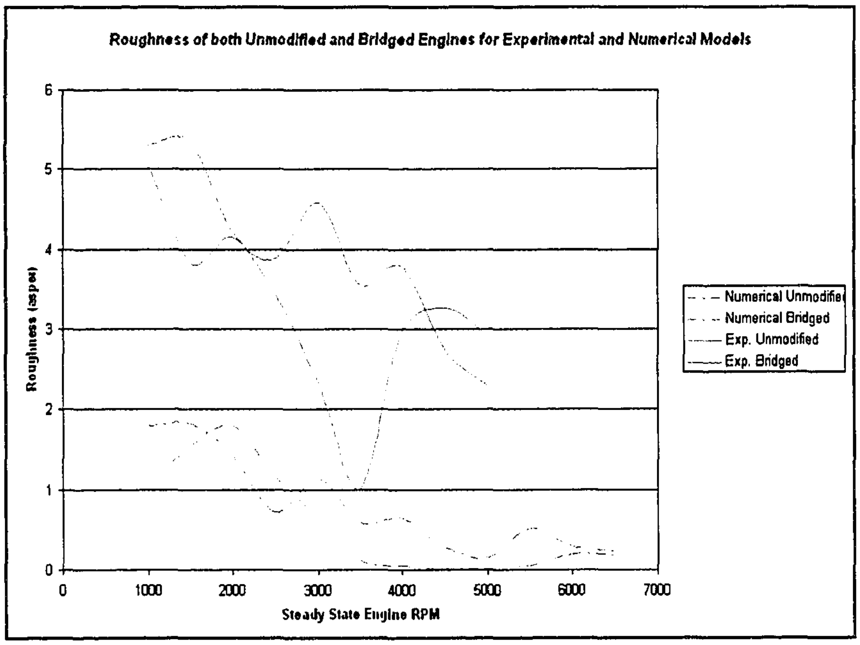

Figure 7.70: Predicted Roughness of Experimental and Numerical Unmodified and Bridged Engines

Figure 7.71 presents the fluctuation strength results of the four engines. Again the resulting pattern of the experimental and numerical results are for the most part similar, however, this time a slight phase shift is present between the experimental and numerical results, with the experimental curve features occurring at lower rpm than the numerical. In this circumstance, the modulation in the 20 to 300 Hz range causing the fluctuation signal is occurring first at lower engine speeds with the actual engine when compared to the analytical model.

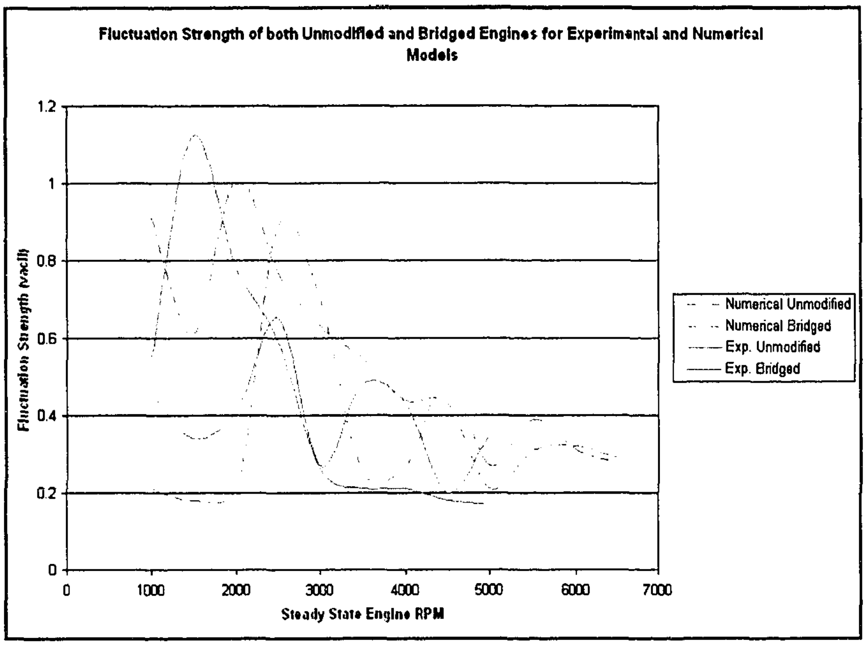

Figure 7.71: Predicted Fluctuation Strength of Experimental and Numerical Unmodified and Bridged Engines

7.4 Discussion of Error in WAVE Model

Presented in this section is a discussion of the potential reasons for the differing results achieved from the WAVE model when compared to the experimental measurements. As presented in the previous sections, the experimental results demonstrated a consistent overall acoustic improvement with the implementation of the manifold bridge when installed on the motored engine. The modelled predictions did not exhibit this same degree of consistency due much to the evident lack of high frequency content in the acoustic signal that is apparent in the experimental results. The proceeding paragraphs discuss some of the potential reasons for this.

As discussed in a previous chapter, WAVE uses a 1-dimensional approach in the solving for the acoustic propagation. This approach follows the assumption that all propagation is along the length of the duct and is constrained in the other dimensions. This approach is a valid one where the aspect ratio of duct length to duct diameter is very large. There are circumstances in the modelled geometry where this aspect ratio is not large. The connecting runner volumes contained within the exhaust manifold as well as the volume representing the intake filter housing are examples of these. It is due to the breakdown of this 1-dimensional assumption at these critical locations that may have contributed to the realized differences in acoustic prediction.

As part of the calculation procedure used by WAVE, the momentum equation for each of the model ducts and components is solved. However, this is not possible in the combustion chamber as this requires the implementation of a much more involved computational fluid dynamic (CFD) solution. As such, WAVE uses one of several available correlation models instead. The Weibe function is an example of such which is used for a spark ignited fired engine. A similar correlation model is also used for the motored case as was applied in this investigation. While this correlation model may provide good predictions for some performance criteria, it may not provide adequate results for an acoustic analysis.

Several flow coefficients are available in WAVEBUILD model which can be adjusted to calibrate a model. These include the friction coefficient to account for major losses, the pressure coefficient to account for minor losses, such as those found in a bending duct as well as the discharge coefficient. If not chosen correctly, the predicted flow results may not accurately represent the actual engine. For this investigation, some assumptions and correction factors were applied where applicable. In some other circumstances, default values were used. This could potentially have resulted in some of the error realized in the predicted noise emissions of the numerical investigation.

The engine motored on the dynamometer behaves much like a powerful air pump resulting in gas flow emissions from both the intake and exhaust of the engine. As a result, flow noise is generated at the intake opening which is evident by the high frequency noise found in the FFT results of the experimental measurements as discussed in sections 7.2 and 7.3. While WAVE does not have the ability to predict the flow variations due to the turbulent portion of this flow, the user does have the option of applying a correlation equation to simulate this flow noise. This equation developed by Green and Smith was presented in section 4.1.4. Use of this correlation equation directs the WAVE post-processor, WNOISE, to add a simulated white noise velocity source to the predicted steady flow velocity used in the noise radiation model. Extreme care must be taken in the application of this equation in that an appropriately chosen noise generation efficiency factor must also be applied. This efficiency factor is usually determined through experience derived from experimental testing. An inappropriate factor will not provide meaningful acoustic results. Given this, application of this feature was not employed in this investigation which more than likely accounts for some of the differences realized between the numerical and experimental results.

VIII. CONCLUSIONS AND RECOMMENDATIONS

8.1 Conclusions

Upon reviewing the results of this study, as well as recalling the stated objectives at the end of the introductory chapter of this report, the following is a presentation of conclusions that have been reached.

1) The purpose of this study was to determine the feasibility of using a nontraditional noise technique using the exhaust noise of an internal combustion engine to attenuate the engine's induction noise. Using a numerical modelling technique, it was found that attenuation of the intake noise of the motored engine was feasible.

2) The results of the numerical model were verified with measurements of an actual engine motored by a dynamometer using a dimensionally optimized manifold bridge determined through the use of the Ricardo WAVE software.

3) A reduction in the overall noise level was realized through implementation of the manifold bridge for both steady state and transient engine operations using traditional analysis methods. Using psychoacoustic metrics, however, implementation of the manifold bridge had both positive and negative impacts on the results.

4) While the overall linear sound pressure level (SPL) during both the modelled and experimental portions of this study decreased as a result of the bridge, the A-weighted SPL decreased only in the experimental results. The numerical A-weighted results increased with the manifold bridge at higher engine speeds.

5) Psychoacoustic metrics played an instrumental role in the evaluation process of the manifold bridge. It was found, as expected, that the loudness results over the operating

range of the engine closely followed that of the A-weighting curve, including the anomalies associated with the numerical results. Sharpness was found to not vary significantly between the modified and unmodified engines for both numerical and experimental results. Both roughness and fluctuation strength increased with the implementation of the manifold bridge for steady state engine operation according to the numerical and experimental results. Roughness was found to decrease during transient engine runs.

6) While the general conclusions derived through the numerical modelling technique follow those of the experimental results, some inconsistencies associated with the higher frequency components of the noise data, particularly at higher engine speeds, warrant caution. It is unknown at this point whether these are an artifact of the algorithm employed or the design of the analytical model itself. In any case, care must be taken in the physical model design to fully account for all thermo-fluid losses to ensure accurate results. Despite this, the inclusion of the numerical investigative part of the experimental study provided both valuable insight for discussion as well as comparative data to validate the measured acoustic results.

8.2 Contributions

The following is a summary of the major contributions to the state of the art that can be attributed to this work. It should also be noted that contributions by the author have been made to the literature through the following references [34] [35].

1) A physical bridging device between the exhaust and intake manifolds of an engine has not been used in the past for the control of induction noise. In this study, this unique and nontraditional attenuation technique for the control of automotive induction noise was developed and demonstrated to produce promising results under the specific conditions investigated.

2) While many sound quality metrics have been developed for, and are used by the automotive industry, their application has been for the most part applied to structure borne and aerodynamic noise. Here the application of some of these metrics was applied to the analysis of automotive induction noise. The value of using these psychoacoustic analysis techniques in parallel with more traditional techniques for the evaluation and development of automotive engine components, as how they relate to noise issues, was illustrated. Furthermore, valuable information of the applicability of these sound quality metrics for this specific application was realized and discussed.

3) Numerical modelling techniques have the advantage of being fairly inexpensive and fast for the analysis of new designs compared to the experimentation of a prototype. Through evaluation of the analytical technique used in this study by direct comparison with the experimental results, potential short comings of using numerical results alone for the evaluation of induction noise have been demonstrated.

4) A review of the published literature has shown that this specific study has not been pursued by others thus far. Given that intake noise is a recognized problem associated with both the design and operation of automobile engines, this innovative approach has contributed to engineering by not only showing some success in its implementation, but it has also opened new potential avenues of investigation. Examples of these potential strategies of investigation are given in the recommendations section below.

5) It has been generally accepted that both the amount of noise generated by the operation of the automobile as well as the perceived quality of that noise is important to the end user. The purpose of this study served to satisfy both of these demands. In doing so, the intent of this work is to contribute to the body of Engineering knowledge in a way which has not been previously pursued. Thus, it also meets the demands of the scientific community through traditional noise analysis as well as to account for the human factor through a psychoacoutic approach.

8.3 Recommendations

The creation and testing of the manifold bridge for the purpose of the attenuation of induction noise has demonstrated promise. There are, however, some areas where additional work can be undertaken to further this study before it can be declared commercially viable.

1) Both the numerical and experimental studies of the manifold bridge were for a motored engine. This is suitable for the inclusion of the propagating pressure pulses through the intake system resulting from the valve action of the engine. This study should, however, be expanded to include the effects of combustion. With this, the

ramifications on engine performance and exhaust gas recirculation (EGR) should be included.

2) It is recommended that the implementation of a diaphragmed bladder system be integrated in any future study. A diaphragm would serve to act as an isolation between the intake and exhaust gases. An actively controlled bladder would also provide additional control of the cancellation pulses introduced to the intake noise.

3) It is recommended that further refinements to the numerical model be implemented, if possible, or alternative numerical software be used for comparison.

4) While some of the sound quality metrics employed in this study proved to be both relevant as well as informative, others did not. It was found that due to a lack of high frequency contribution to the intake noise, the resulting measured sharpness values were insignificant, particularly in the numerical analysis. Two other metrics, roughness and fluctuation strength, did provide some meaningful measures of the data; however, these are indices of only low frequency content. With this, it is still felt that issues exist that are postulated to be effective within a frequency range beyond that of the implemented metrics. It is felt that a greater focus within the range of up to 1000 Hz is needed for an induction noise study. From this, it is recommended that the development of a new sound quality metric be investigated. This can be done through the filtering and subsequent jury testing of 1/3 octave and/or loudness signatures until a desirable sound signature is achieved. The implementation of these results could then be achieved through any number of control techniques including Helmholtz or quarter wave resonators.

5) This attenuation technique should be investigated using alternative engine types, sizes and configurations. Diesel engines have their own unique noise issues which may benefit from this technique. Also, six and eight cylinder configurations could be used in future studies.

REFERENCES

1. Bai, Mingsian, Cheng-Yuan Chang, and Chen Ray. "Passive and Active Control for Noises in Ducts: Experimental Investigations." *Journal of the Chinese Society of Mechanical Engineers* 16.2 (1995): 155-66.

2. Barron, Randall. *Industrial Noise Control and Acoustics*. New York: Marcel Dekker, Inc., 2003.

3. Beeson, Lisa, and George Schott. "Experience with Active Control of Exhaust Noise From a Large Frame Combustion Turbine." Paper presented at the International Gas Turbine & Aeroengine Congress & Exhibition. The American Society of Mechanical Engineers, 1997.

4. Bell, Lewis, and Douglas Bell. *Industrial Noise Control*. New York: Marcel Dekker, Inc., 1994.

5. Beranek, Leo. *Noise and Vibration Control*. Washington, DC: McGraw Hill, Inc., 1988.

6. Birdsong, Charles, and Radcliffe. "An Electronically Tunable Resonator for Noise Control." Paper presented at the SAE 2001 World Congress. Detroit, Michigan: Society of Automotive Engineers, March, 2001.

7. Boonen, Rene, and Paul Sas. "Development of an Active Exhaust Silencer for Internal Combustion Engines Using Feedback Control." Paper presented at the SAE 1999 World Congress. Detroit, Michigan: Society of Automotive Engineers, March, 1999.

8. Chaves, Rodrigo. "Active Noise Control Applied in Automotive Vehicles." Paper presented at the International Mobility Technology Conference & Exhibit. Sao Paulo, Brazil: Society of Automotive Engineers, 09/11, 1998.

9. Chiatti, G, and O Chiavola. "Engine Intake Noise Modelling by Using a Time/Frequency Approach." Paper presented at the SAE 2001 World Congress. Detroit, Michigan: Society of Automotive Engineers, March 2001, 2001.

10. Ciocci, Fabio, and Enrico Bradamante. "Intake System Analysis of the 550 Maranello Using the WAVE Code." 12/08 2002 <http://www.ricardo.com/pressrelease/ferrari-paper.pdf>.

11. Cofer, C.G., F. Bielert, and T. Kullman. "Durability, Acoustic Performance and Process Efficiencies of Absorbent Fibers for Muffler Filling." SAE Noise and Vibration Conference. Society of Automotive Engineers, 1999. 43-49.

12. Cortex Instruments. *Psychoacoustics - A Tool for Industrial Sound Design.* Cortex Instruments. Cortex Instruments.

13. Daly, Paul. Discussion of standard distance of microphone placement from intake opening. Siemens Windsor. August 1995.

14. Green, A.J, and P.N. Smith. "Gas Flow Noise and Pressure Loss in Heavy Vehicle Exhaust Systems." *IMechE.* Advances in the Control and Refinement of Vehicle Noise, 1988. 47-54.

15. Hansen, Colin. *Understanding Active Noise Cancellation.* Great Britain: Spon Press, 2001.

16. Hetherington, P., et al. "Simulating Odd Fire V-10 Exhaust Noise for Sound Quality Evaluation." Paper presented at the SAE 1999 World Congress. Detroit, Michigan: Society of Automotive Engineers, March, 1999.

17. Kido, K., H. Kanai, and M. Abe. "Active Reduction of Noise by Additional Noise Source and Its Limit." *Vibration, Acoustics, Stress and Reliability in Design* 111 (October 1989): 480-85.

18. Kostek, Theodore. "Combining Adaptive-Passive and Fully Active Noise Control in Ducts." *ASME Noise Control and Acoustics Division.* Vol. 24, 1997. 293-98.

19. LMS International. *Roughness and Fluctuation Strength.* LMS International <http://www.lmsna.com/faq/rough.html>.

20. Lu, Ming-Hung, and Ming Une Jen. "Intake/Exhaust Noise Reduction with Rig Test Optimization - Case Studies." Paper presented at the Noise & Vibration Conference & Exposition. Traverse City, Michigan: Society of Automotive Engineers, 17/05, 1999.

21. Lyon, Richard. *Designing for Product Sound Quality.* New York: Marcel Dekker, Inc., 2000.

22. Mangiante, G.A. "Active Sound Absorption." *Acoustical Society of America* 61.6 (June 1977): 1516-23.

23. Marroquin, Marc, Bruel & Kjaer. "Sound Quality Workshop." Bruel & Kjaer. 24/09. 2002.

24. McLean, Ian. "Active Control of Automotive Air Induction Noise Via Source Coupling." Paper presented at the SAE 2001 World Congress. Detroit, Michigan: Society of Automotive Engineers, March, 2001.

25. Mechel, F. *Formulas of Acoustics.* Heidelberg, Germany: Springer-Verlag, 2002.

26. *The Michael Canny Toyota MR2 Project.* <http://www.megaboost.co.uk/mr2/frames/>.

27. Miller, I., and J.E. Freund. *Probability and Statistics for Engineers.* Diss. Englewood Cliffs, NJ: Prentice-Hall Inc., 1985.

28. Munjal, M.L. *Acoustics of Ducts and Mufflers.* New York: John Wiley & Sons, 1987.

29. Nelson, P.A., and S.J. Elliott, Academic Press. *Active Control of Sound.* Ed. Academic Press. Great Britain: IBT Global, 1992. 9, 10.

30. Nelson, Paul, Butterworths. *Transportation Noise Reference Book.* Great Britain: University Press, Cambridge, 1987.

31. Nishio, Yoshitaka, Tokio Kohama, and Osamu Kuroda. "New Approach to Low-Noise Air Intake System Development." Paper presented at the SAE 1991 World Congress. Detroit, Michigan: Society of Automotive Engineers, March, 1991.

32. Novak, Colin. "Experimental Acoustic Model for Intake Manifold Testing." Thesis. Mechanical, Automotive and Materials Engineering, University of Windsor, 1996.

33. Novak, Colin, Helen Ule, and Robert Gaspar. "Comparative Investigation Between a Simplified Theoretical and a Complex Computer Simulation Muffler Model." *Transportation Noise.* CAA 2001. Toronto, Ontario: Canadian Acoustical Association, 03/10, 2001.

34. Novak, Colin, Helen Ule, and Robert Gaspar. "Preliminary Results of Intake Noise Cancellation Using a Manifold Bridging Technique." *Canadian Acoustical Association,* Vol. 32, No. 1, 2004. 21-29.

35. Novak, Colin, Helen Ule, and Robert Gaspar. "Use of Sound Quality Metrics for the Analysis of Automotive Intake Noise." *Transportation Noise.* CAA 2004. Ottawa, Ontario: Canadian Acoustical Association,(in print).

36. Plint, Michael, and Anthony Martyr. *Engine Testing Theory and Practice.* Society of Automotive Engineers, 1999.

37. Pricken, Franc. "Active Noise Cancellation in Future Air Intake Systems." *Powertrain Systems NVH.* SAE 2000 World Congress. Detroit, Michigan: Society of Automotive Engineers, 06/03, 2000.

38. Randall, R., and B. Tech. *Frequency Analysis.* Denmark: Bruel & Kjaer, 1987.

39. Rejskind, G. *The World of High Fidelity.* Diss. Longueuil, Quebec: Broadcast Canada, 1994.

40. Ricardo, Inc. "Rshelp.Htm." Compact Disc. Inc. Ricardo. *Ricardo WAVE Knowledge Center Tutorial*, 2002.

41. *WAVE Basic User Manual.* Ricardo Software. Burr Ridge, IL, 2001.

42. *WAVE V3.5 Tutorial Example.* Ricardo Software. Ricardo, Inc., 2001.

43. Sacks, Mal, and Steve Hackney. "Performance of Acoustic Components for Engine Induction Systems." Paper presented at the SAE 1988 World Congress. Detroit, Michigan: Society of Automotive Engineers, 29/02, 1988.

44. Scheuren, Joachim, Ulrich Widmann, and Jens Winkler. "Active Noise Control and Sound Quality Design in Motor Vehicles." Paper presented at the Noise and Vibration Conference & Exposition. Traverse City, Michigan: Society of Automotive Engineers, 17/05, 1999.

45. Selamet, A., et al. "Acoustic Attenuation Performance of Perforated Absorbing Silencers." Paper presented at the SAE 2001 World Congress. Detroit, Michigan: Society of Automotive Engineers, March, 2001.

46. Selamet, A., N.S. Dickey, and P.M. Radavich, Novak. "Theoretical, Computational and Experimental Investigation of Helmholtz Resonators: One-Dimensional Versus Multi-Dimensional Approach." Paper presented at the SAE 1994 World Congress. Detroit, Michigan: Society of Automotive Engineers, 28/02, 1994.

47. Siemens Energy & Automation. *SIMOREG 6RA24 Instructions*. Siemens Energy & Automation, Inc. 'Tundra' Alpharetta, GA: Siemens Energy & Automation, 1994.

48. Siemens. "Active Noise Control Presentation to Ford Hybrid Vehicle." Ford Motor Company Headquarters Dearborn, Michigan. Siemens Automotive. 14/07. 2000.

49. Snyder, Scott. *Active Noise Control Primer.* New York: Springer-Verlag, 2000.

50. Tjong, Jimi Sauw-Yoeng. "Engine Dynamic Signal Monitoring and Diagnostics." Diss. Mechanical, Automotive and Materials Engineering, University of Windsor, 1992.

51. Ule, Helen, Colin Novak, Tony Spadafora, Ramani Ramakrishnan and Robert Gaspar. "Comparison of Experimental and Modeled Insertion Loss of a Complex Multi-Chambered Muffler with Temperature and Flow Effects." *Transportation Noise*. CAA 2004. Ottawa, Ontario: Canadian Acoustical Association, (in print).

52. Ule, Helen. "Experimental Measurement of Active Control of Intake Noise." Thesis. Mechanical, Automotive and Materials Engineering, University of Windsor, 2004.

53. Ver, I.L. "Prediction Scheme for the Self-Generated Noise of Silencers." Inter-Noise '72, 1972. 294-98.

54. Wilson, Charles. *Noise Control*. New York: Harper & Row, 1989.

55. Winterbone, Desmond, and Richard Pearson, SAE, Inc. *Design Techniques for Engine Manifolds*. United Kingdom: J W Arrowsmith Limited, 2001. 268.

56. Wirtz, Robert. "Application of WAVE in Motorcycle Prototyping." 12/08 2002 <http://www.ricardo.com/pressrelease/ducati-paper.pdf>.

57. Zwicker, E, and H. Fastl. *Psychoacoustics Facts and Models*. Heidelberg, Germany: Springer-Verlag, 1999.

APPENDIX

APPENDIX A

A. Required Input Data for Ricardo WAVE Simulation

Required Data for WAVE Engine Simulation

RICARDO SOFTWARE

General Instructions

WAVE is a detailed multi-cylinder reciprocating engine simulation code. Its various sub-models require a number of input parameters related to combustion chamber geometry, valve flow, manifold configuration, etc. The data list below contains items which are either necessary or very helpful to successfully construct and validate a WAVE engine model.

Suggested units are provided where appropriate. Other units may be used, but these should be indicated clearly when supplied.

Finally, in order to validate the model with a high degree of precision, it is important to have as much engine test data as possible. Data sheets for this information are provided in Sections F, G and H. Test data can be provided as ASCII text files (preferred) or print-outs from data acquisition systems.

A. Power Cylinder

- Bore 81 [mm]
- Stroke 77 [mm]
- Connecting rod length, center to center 135 [mm]
- Piston pin offset (positive toward major thrust side) 0.1 [mm]
- TDC combustion chamber volume ________ [m^3]
- TDC combustion chamber surface area ________ [m^2]
- Compression ratio 10
- Number of cylinders 4
- Firing order 1 3 4 2
- Firing interval ________ [°CA]
- Two or four stroke 4
- Two-strokes: scavenging curve
- Heat transfer area of combustion chamber: piston and head surfaces [expressed as multiple of bore area] 1.1
- Clearance height between top of piston and top of cylinder ________ [mm]

B. Intake and Exhaust Geometry

- Intake piping and manifold geometry
- Exhaust piping and manifold geometry
- EGR circuit geometry

Note: Geometry data can be supplied as drawings, CAD models or hardware.

C. Valve/Port Data

Duplicate this information for each intake and exhaust valve.

Poppet Valves

• Profile of lift vs. crank (or cam) angle - ASCII text file preferred		
• Valve/cam timing events	____	
• Dynamic valve data (e.g. valve event phase shift vs. engine rpm)		
• Tappet type (hydraulic/fixed)	____	
• Valve lash (hot)	0.1	[mm]
• Rocker arm ratio (if cam lift is prescribed)	____	
• Inner seat diameter (D)	28	[mm]
• Maximum valve lift	8.3	[mm]
• Valve flow data: flow coefficient* vs. L/D - ASCII text file preferred		

* Forward and reverse

Piston Ported

• Number of ports of the same type	N/A	
• Port geometry and precise location (drawing)		
• Profile of geometrical area (as an alternative to lift profile)		
• Port flow data: flow coefficient		

Reed Valves

• Effective mass	N/A	[g]
• Effective spring constants	N/A	[N/m]
• Effective damping constants	N/A	[Nsec/m]
• Maximum lift to stop	N/A	[mm]
• Spring pre-load distance	N/A	[mm]
• Pressure force area below reed	N/A	[mm^2]
• Profile of geometrical open area vs. lift		
• Profile of flow coefficient vs. lift		

EGR Valves

• Max lift to stop	N/A	[mm]
• Cross-sectional area at maximum lift	N/A	[cm^2]
• Profile of pressure loss vs. Flow		
• Profile of flow coefficient vs. lift		

D. Turbocharger

• Compressor map showing operating points (map)		
• Compressor reference temperature	N/A	[K]
• Compressor reference pressure	N/A	[bar]
• Compressor gas Cp	N/A	[J/kgK]
• Specify total/total or total/static or static/static pressure ratio	N/A	
• Compressor speed: connected to turbine no.	N/A	
geared to crankshaft: supply gear ratio	N/A	
fixed speed	N/A	[rev/min]
• Compressor inlet diameter	N/A	[cm]
• Compressor exit diameter	N/A	[cm]
• Turbine map showing operating points	N/A	(map)
• Turbine reference temperature	N/A	[K]
• Turbine reference pressure	N/A	[bar]
• Turbine gas Cp	N/A	[J/kgK]
• Turbine speed: connected to compressor no.	N/A	
geared to crankshaft: supply gear ratio	N/A	
fixed speed	N/A	[rev/min]
• Turbine inlet diameter	N/A	[cm]
• Turbine exit diameter	N/A	[cm]
• Mechanical efficiency	N/A	[%]
• Moment of inertia of all rotating parts	N/A	[kgm^2]
• Wastegate (if equipped)		
• Variable geometry turbine (if equipped): provide maps at different settings		

E. Aftercooler

Supply for as many operating points as possible

• Cooler design (e.g. shell and tube)		
• Hot side passage geometry and number of passages	N/A	
• Cold side passage geometry and number of passages	N/A	
• Mass flow	N/A	[kg/hr]
• Effectiveness	N/A	[%]
• Pressure at outlet	N/A	[bar]
• Temperature at outlet	N/A	[K]
• Pressure drop across aftercooler	N/A	[bar]
• Temperature drop across aftercooler	N/A	[K]
• Coolant temperature	N/A	[K]

F. **Fuel and Operating Data: SI Engines**

General

• Fuel type	m	
• Lower heating value of fuel	m	[MJ/kg]
• Type of fuel system (i.e. MPI, carbureted)		
• Location of fuel injection points (drawing)		
• Ambient pressure	1	[bar]
• Ambient temperature	300	[K]

Specify for **each** operating condition

• Engine speed	V	[rev/min]
• Fuel rate	m	[kg/hr]
• Air/fuel ratio (specify overall or trapped)	m	
• Ignition timing	5.	[°BTDC]
• Combustion rate vs. crank angle		
• Average intake manifold pressure (and location)	V	[bar]
• Dynamic intake manifold/runner pressure (if available)	V	[bar]
• Average exhaust manifold pressure (and location)	V	[bar]
• Dynamic exhaust manifold pressure (if available)	V	[bar]
• Exhaust system back pressure (and location)	N/A	[bar]
• Trapped air data (2-stroke only): mass fresh air trapped + mass fresh air in mass fresh air trapped + total mass trapped mass fresh air in + theoretical mass in		
• Volumetric efficiency		[%]
• Trapped residual fraction	m	[%]

Note: m = motored v = varied

G. Fuel and Operating Data: CI Engines

General

- Fuel type N/A
- Lower heating value of fuel N/A [MJ/kg]
- Cetane number or octane number N/A
- Ambient pressure N/A [bar]
- Ambient temperature N/A [K]

Specify for each operating condition

- Engine speed N/A [rev/min]
- Fuel rate N/A [kg/hr]
- Duration of fuel injection N/A [°CA]
- Needle lift (start of injection) N/A [°BTDC]
- Profile of instantaneous injection rate vs. crank angle over injection period for a given cylinder (arbitrary units, WAVE will scale to be consistent with total fuel rate)
- Ignition delay N/A [°CA]
- Combustion rate vs. crank angle
- Average intake manifold pressure (and location) N/A [bar]
- Dynamic intake manifold pressure (if available) N/A [bar]
- Average exhaust manifold pressure (and location) N/A [bar]
- Dynamic exhaust manifold pressure (if available) N/A [bar]
- Exhaust system back pressure (and location) N/A [bar]
- Trapped air data (2-stroke only):
  mass fresh air trapped + mass fresh air in
  mass fresh air trapped + total mass trapped
  mass fresh air in + theoretical mass in

APPENDIX B

B. WAVE Output of Modelled Parameters for Unmodified and Modified Engine

EXHIBIT B1 - Output of Modelled Parameters for Unmodified Engine

```
RICARDO SOFTWARE — WAVE SIMULATION CODE — VERSION 5.1

BAS:CONSTANTS   =====================================================
ncyc            =       12
speed           =       1000
pamb            =       1.013
tamb            =       298
thb50           =       9
bdur            =       28
tpis            =       500
thead           =       550
tcyl            =       540
thrt            =       45
fard            =       0.08
BAS:GENERAL     PARAMET ==============================================
(ncyc)          0.6     1       simm    auto    !       TIMT/NCY CFL,DDEG UNITS
N               n       Y       0.01    !       RESTART DUMPCKF SKIPINIT,  AUTOCONVERGE
INDOLENE        !       FUELFILE
BAS:OUTPUT      &       PLOTTING =============================================
0               0       0       0       0       0       0       0       0       0       !       IOUT1   THROUGI-IOUT10
N               -30     120     -360    !       ZOOM,TZOOM(1,2),INCPL
postscript      draft   !       PFORMAT FONTNAME
all             NULL    CASE    !       SUMMARY\SUMFREQ
N               N       Y       N       !       ANIMATE, SOUNDTRACE
case            25      !       WARNFRE MAX_WARNINGS
BAS:TIME        PLOTS   ==============================================
titles          V5.1 Build 4
L:              0.5
P:              201     auto    auto
J:              401
P:              202     auto    auto
J:              401
P:              201     auto    auto
D:              761
P:              110     auto    auto
J:              401
P:              201     auto    auto
D:              734
P:              201     auto    auto
D:              739
BAS:TITLE       ======================================================
Motored         Manifold Unmodified Engine (speed) rpm
DUC:BENDS       ======================================================
734             0       !       LEX,ARC
761             35      !       LEX,ARC
762             45      !       LEX,ARC
763             45      !       LEX,ARC
764             35      !       LEX,ARC
duct2           110
duct7           110
duct11          110
duct15          110
duct20          110
duct26          110
duct29          110
duct35          110
duct36          0
duct38          0
duct42          0
duct46          30
DUC:DUCT        DATA    ==============================================
1               1       !       CFRICG  CHTRG
```

LEX	KJL	KJR	DL	DR	SDUCT	DX	TWALD	PDI	TDI	CFR	CHT	CP	CDL	CDR
731	506	505	75	75	0	0	0	0	0	1	1	0	aut	aut
732	507	508	75	75	25	36	300	1	300	1	1	0	aut	aut
733	508	507	75	75	0	0	0	0	0	1	1	0	aut	aut
734	116	506	60	60	50	36	300	1	300	1	1	0	aut	aut
737	509	orif20	65	65	100	36	300	1	300	1	1	0	aut	aut
739	301	510	65	65	15	36	300	1	300	1	1	0	aut	aut
751	551	151	33	33	90	44	850	1	900	1	1	0	aut	aut
752	552	152	33	33	130	44	850	1	900	1	1	0	aut	aut
753	553	153	33	33	150	44	850	1	900	1	1	0	aut	aut
754	554	154	33	33	130	44	850	1	900	1	1	0	aut	aut
761	151	161	33	33	60	44	850	1	900	1	1	0	aut	aut
762	152	162	33	33	60	44	850	1	900	1	1	0	aut	aut
763	153	163	33	33	60	44	850	1	900	1	1	0	aut	aut
764	154	164	33	33	60	44	850	1	900	1	1	0	aut	aut
7038	510	509	2.26	2.26	0	0	0	0	0	1	1	0	aut	aut
7501	401	551	23	15	50	50	470	1	470	0	1	0	aut	aut
7502	402	552	23	15	50	50	470	1	470	0	1	0	aut	aut
7503	403	553	23	15	50	50	470	1	470	0	1	0	aut	aut
7504	404	554	23	15	50	50	470	1	470	0	1	0	aut	aut
7511	401	551	23	15	50	50	470	1	470	0	1	0	aut	aut
7512	402	552	23	15	50	50	470	1	470	0	1	0	aut	aut
7513	403	553	23	15	50	50	470	1	470	0	1	0	aut	aut
7514	404	554	23	15	50	50	470	1	470	0	1	0	aut	aut
duct1	508	orif2	21	21	100	36	300	1	300	1	1	0	auto	auto
duct2	orif2	orif4	21	21	100	36	320	1	300	1	1	0	auto	auto
duct3	orif4	yjun1	30	30	175	36	340	1	320	1	1	0	auto	auto
duct4	yjun1	yjun2	45	45	10	36	370	1	320	1	1	0	auto	auto
duct5	yjun2	404	28	27	50	36	370	1	340	1	1	0	auto	auto
duct6	508	orif1	21	21	100	36	300	1	300	1	1	0	auto	auto
duct7	orif1	orif3	21	21	100	36	320	1	300	1	1	0	auto	auto
duct8	orif3	yjun1	30	30	175	36	340	1	320	1	1	0	auto	auto
duct9	yjun2	404	28	27	50	36	370	1	340	1	1	0	auto	auto
duct10	507	orif5	21	21	100	36	300	1	300	1	1	0	auto	auto
duct11	orif5	orif7	21	21	100	36	320	1	300	1	1	0	auto	auto
duct12	orif7	yjun3	30	30	175	36	340	1	320	1	1	0	auto	auto
duct13	yjun3	503	45	45	10	36	370	1	320	1	1	0	auto	auto
duct14	507	orif6	21	21	100	36	300	1	300	1	1	0	auto	auto
duct15	orif6	orif8	21	21	100	36	320	1	300	1	1	0	auto	auto
duct16	orif8	yjun3	30	30	175	36	340	1	320	1	1	0	auto	auto
duct17	503	403	28	27	50	36	370	1	340	1	1	0	auto	auto
duct18	503	403	28	27	50	36	370	1	340	1	1	0	auto	auto
duct19	505	orif9	21	21	100	36	300	1	300	1	1	0	auto	auto
duct20	orif9	orif11	21	21	100	36	320	1	300	1	1	0	auto	auto
duct21	orif11	yjun4	30	30	175	36	340	1	320	1	1	0	auto	auto
duct22	yjun4	501	45	45	10	36	370	1	320	1	1	0	auto	auto
duct23	501	401	28	27	50	36	370	1	340	1	1	0	auto	auto
duct24	501	401	28	27	50	36	370	1	340	1	1	0	auto	auto
duct25	505	orif10	21	21	100	36	300	1	300	1	1	0	auto	auto
duct26	orif10	orif12	21	21	100	36	320	1	300	1	1	0	auto	auto
duct27	orif12	yjun4	30	30	175	36	340	1	320	1	1	0	auto	auto

duct28	506	orif13	21	21	100	36	300	1	300	1	1	0	auto	auto
duct29	orif13	orif15	21	21	100	36	320	1	300	1	1	0	auto	auto
duct30	orif16	yjun5	30	30	175	36	340	1	320	1	1	0	auto	auto
duct31	yjun5	502	45	45	10	36	370	1	320	1	1	0	auto	auto
duct32	502	402	28	27	50	36	370	1	340	1	1	0	auto	auto
duct33	502	402	28	27	50	36	370	1	340	1	1	0	auto	auto
duct34	506	orif14	21	21	100	36	300	1	300	1	1	0	auto	auto
duct35	orif14	orif16	21	21	100	36	300	1	300	1	1	0	auto	auto
duct36	orif16	yjun5	30	30	175	36	340	1	320	1	1	0	auto	auto
duct37	161	yjun6	33	33	80	44	850	1	850	1	1	0	auto	auto
duct38	yjun6	amb1	39	39	60	44	800	1	800	1	1	0	auto	auto
duct40	162	yjun7	33	33	100	44	850	1	850	1	1	0	auto	auto
duct41	163	yjun7	33	33	100	44	850	1	850	1	1	0	auto	auto
duct42	yjun7	amb2	39	39	60	44	800	1	800	1	1	0	auto	auto
duct43	164	yjun6	33	33	150	44	850	1	850	1	1	0	auto	auto
duct44	orif17	116	60	60	50	36	300	1	300	1	1	0	auto	auto
duct46	orif20	orif19	65	65	50	36	300	1	300	1	1	0	auto	auto
duct47	orif19	orif17	65	65	100	36	300	1	300	1	1	0	auto	auto
ENG:GEOMETRY	========													
4	4	MOT	!	NCYL,ISTRK,ETYPE										
81	77	135	0.1	1	BORE,STROKE,CRL,PINOFF									
10	!	CR												
1	3	4	2	!	Timing:	IFIRE(1,NCYL)								
0	180	180	180	!	TDC	(1,NCYL)								
0.5	0.006	630	0.2	!	Friction:	ACF,BCF,CCF,QCF								
0	0	0	!	Output	:	IOUT1E,IOUT2E,IOUT3E								
ENG:HEAT	TRANSFE ========													
original														
1	1	0	!	CENHTO,CENHTC										
(tple)	(thead)	(tcyl)	(thead)	(thead)	!	TWCYLP,TWCYLH,TWCYLS								
1.05	1.1	1.5	!	AHTCYLP,AHTCYLH,SCLCYL										
ENG:OPERATING	PARAMET ========													
(speed)	(pamb)	(tamb)	!	RPM,PAMBE,TAMBE										
ENG:SI_WIEBE_COMB	========													
(thb50)	(bdur)	2	1	!	THB50,BDUR,WEXP,BURNFRAC									
ENG:VALVES	========													
NC,KEXC, (LEXD,IED,NVD--Repeated for each valve/duct)														
4	401	duct23	!	#1	duct24	!	#1	7501	•	#2	7511	•	#2	
3	402	duct32	!	#1	duct33	!	#1	7502	•	#2	7512	•	#2	
2	403	duct17	!	#1	duct18	!	#1	7503	•	#2	7513	•	#2	
1	404	duct9	!	#1	duct5	!	#1	7504	•	#2	7514	•	#2	
FFT:FFT	========													
titles														
32	J:	301	J:	510										
R	86	S:	auto	auto										
INJ:TYPE	========													
1														
prop														
300	0.2	auto	0	0.2	40	auto								
0	0.1	0	0	0.9										
INJ:VOLUME	========													
1	1	duct22	0	0										
0	(fard)	0												
————	!(separator)													
2	1	duct31	0	0										
0	(fard)	0												
————	!(separator)													
3	1	duct13	0	0										
0	(fard)	0												
————	!(separator)													
4	1	duct4	0	0										
0	(fard)	0												
JUN:JUNCTION	DATA	========												
KEX	KT1/KT2	AUX1	AUX2	AUX3	AUX4	AUX5								
116	1	1	(thrt)											
151	1	1	AUT											
152	1	1	AUT											
153	1	1	AUT											
154	1	1	AUT											
161	1	1	AUT											
162	1	1	AUT											
163	1	1	AUT											
164	1	1	AUT											
301	3	1	AUT	1	300	AUT	0	FIXED						
401	4	1	SINGLEZONE											
402	4	1	SINGLEZONE											
403	4	1	SINGLEZONE											
404	4	1	SINGLEZONE											
501	5	2												
502	5	2												
503	5	2												
505	5	2												
506	5	2												
507	5	2												
508	6	2												
509	5	2												
510	5	2												
551	5	2												
552	5	2												
553	6	2												
554	5	2												
amb1	3	1	AUTO	1	300	AUTO	0	FLOATING						
amb2	3	1	AUTO	1	300	AUTO	0	FLOATING						
orif1	1	1	auto											
orif2	1	1	auto											
orif3	1	1	auto											
orif4	1	1	auto											
orif5	1	1	auto											
orif6	1	1	auto											
orif7	1	1	auto											
orif8	1	1	auto											
orif9	1	1	auto											
orif10	1	1	auto											
orif11	1	1	auto											
orif12	1	1	auto											
orif13	1	1	auto											
orif14	1	1	auto											
orif15	1	1	auto											
orif16	1	1	auto											
orif17	1	1	auto											
orif19	1	1	auto											
orif20	1	1	auto											
yjun1	5	2												
yjun2	5	2												
yjun3	5	2												

```
yjun4            5      2
yjun5            5      2
yjun6            5      2
yjun7            5      2
JUN:YJUNCTION    DATA   ====================================================================
501              45     370    1      320    23656     2120      1    1    1      TP2: DIA5   TWL5   PK5   TK5   VOL5   AHT CFR5   CHT5
 LEX  VDIR1 VDIR2 VDIR3 DIA  CDK DELX DIAB THICK COUNT
duct24           20     90     -70    AUT    AUT       15        45   0    1
duct22           180    -90    90     AUT    AUT       15        45   0    1
duct23           -20    90     -110   AUT    AUT       15        45   0    1
---------------- lseparator
502              45     370    1      320    23656     2120      1    1    1      TP2: DIA5   TWL5   PK5   TK5   VOL5   AHT CFR5   CHT5
 LEX  VDIR1 VDIR2 VDIR3 DIA  CDK DELX DIAB THICK COUNT
duct32           -20    90     -110   AUT    AUT       15        45   0    1
duct31           180    -90    90     AUT    AUT       15        45   0    1
duct33           20     90     -70    AUT    AUT       15        45   0    1
---------------- lseparator
503              45     370    1      320    23656     2120      1    1    1      TP2: DIA5   TWL5   PK5   TK5   VOL5   AHT CFR5   CHT5
 LEX  VDIR1 VDIR2 VDIR3 DIA  CDK DELX DIAB THICK COUNT
duct13           180    -90    90     AUT    AUT       15        45   0    1
duct17           -20    90     -110   AUT    AUT       15        45   0    1
duct18           20     90     -70    AUTO   AUTO      15        45   0    1
---------------- lseparator
505              75     310    1      300    220693.2  16190.83  1    1    1      TP2: DIA5   TWL5   PK5   TK5   VOL5   AHT CFR5   CHT5
 LEX  VDIR1 VDIR2 VDIR3 DIA  CDK DELX DIAB THICK COUNT
duct19           45     135    90     AUT    AUT       75        75   0    1
731              90     90     0      AUT    AUT       50        75   0    1
duct25           45     135    90     AUTO   AUTO      75        75   0    1
---------------- lseparator
506              75     310    1      300    220693.2  11780.97  1    1    1      TP2: DIA5   TWL5   PK5   TK5   VOL5   AHT CFR5   CHT5
 LEX  VDIR1 VDIR2 VDIR3 DIA  CDK DELX DIAB THICK COUNT
duct28           45     135    90     AUT    AUT       75        75   0    1
731              90     90     -180   AUT    AUT       50        75   0    1
732              90     90     0      AUT    AUT       50        75   0    1
duct34           45     135    90     AUTO   AUTO      75        75   0    1
---------------- lseparator
507              75     310    1      300    220693.2  11780.97  1    1    1      TP2: DIA5   TWL5   PK5   TK5   VOL5   AHT CFR5   CHT5
 LEX  VDIR1 VDIR2 VDIR3 DIA  CDK DELX DIAB THICK COUNT
duct10           45     135    90     AUT    AUT       75        75   0    1
732              90     90     -180   AUT    AUT       50        75   0    1
733              90     90     0      AUT    AUT       50        75   0    1
duct14           45     135    90     AUTO   AUTO      75        75   0    1
---------------- lseparator
508              75     310    1      300    220693.2  11780.97  1    1    1      TP2: DIA5   TWL5   PK5   TK5   VOL5   AHT CFR5   CHT5
 LEX  VDIR1 VDIR2 VDIR3 DIA  CDK DELX DIAB THICK COUNT
duct1            45     135    90     AUT    AUT       75        75   0    1
733              90     90     -180   AUT    AUT       50        75   0    1
734              90     90     0      AUT    AUT       50        75   0    1
duct6            45     135    90     AUTO   AUTO      75        75   0    1
---------------- lseparator
509              152.2  300    1      300    1660000   72774.5   1    1    1      TP2: DIA5   TWL5   PK5   TK5   VOL5   AHT CFR5   CHT5
 LEX  VDIR1 VDIR2 VDIR3 DIA  CDK DELX DIAB THICK COUNT
737              150    240    90     AUT    AUT       120       140  0    1
7036             -90    0      90     AUT    AUT       50        2.26 4    7853
---------------- lseparator
510              152.2  300    1      300    2868000   72774.5   1    1    1      TP2: DIA5   TWL5   PK5   TK5   VOL5   AHT CFR5   CHT5
 LEX  VDIR1 VDIR2 VDIR3 DIA  CDK DELX DIAB THICK COUNT
739              -45    45     90     AUT    AUT       240       140  0    1
7036             90     180    90     AUT    AUT       80        2.26 4    7853
---------------- lseparator
551              35     450    1      450    14431.69  1649.3    1    1    1      TP2: DIA5   TWL5   PK5   TK5   VOL5   AHT CFR5   CHT5
 LEX  VDIR1 VDIR2 VDIR3 DIA  CDK DELX DIAB THICK COUNT
751              15     90     -75    AUT    AUT       15        35   0    1
7501             165    -90    -75    AUT    AUT       15        35   0    1
7511             195    90     105    AUT    AUT       15        35   0    1
---------------- lseparator
552              35     450    1      450    14431.69  1649.3    1    1    1      TP2: DIA5   TWL5   PK5   TK5   VOL5   AHT CFR5   CHT5
 LEX  VDIR1 VDIR2 VDIR3 DIA  CDK DELX DIAB THICK COUNT
752              0      90     90     AUT    AUT       15        35   0    1
7502             165    -90    -75    AUT    AUT       15        35   0    1
7512             195    90     105    AUT    AUT       15        35   0    1
---------------- lseparator
553              35     450    1      450    14431.69  1649.3    1    1    1      TP2: DIA5   TWL5   PK5   TK5   VOL5   AHT CFR5   CHT5
 LEX  VDIR1 VDIR2 VDIR3 DIA  CDK DELX DIAB THICK COUNT
753              0      90     90     AUT    AUT       15        35   0    1
7503             165    -90    -75    AUT    AUT       15        35   0    1
7513             195    90     105    AUT    AUT       15        35   0    1
---------------- lseparator
554              35     450    1      450    14431.69  1649.3    1    1    1      TP2: DIA5   TWL5   PK5   TK5   VOL5   AHT CFR5   CHT5
 LEX  VDIR1 VDIR2 VDIR3 DIA  CDK DELX DIAB THICK COUNT
754              -15    90     -105   AUT    AUT       15        35   0    1
7504             165    -90    -75    AUT    AUT       15        35   0    1
7514             195    90     105    AUT    AUT       15        35   0    1
---------------- lseparator
yjun1            45     370    1      320    31806.57  2827.4    1    1
 LEX  VDIR1 VDIR2 VDIR3 DIA  CDK DELX DIAB THICK COUNT
duct3            165    -90    75     AUTO   AUTO      20        30   0    1
duct4            0      90     90     AUTO   AUTO      20        45   0    1
duct8            195    90     105    AUTO   AUTO      20        30   0    1
---------------- lseparator
yjun2            45     370    1      320    23656     2120      1    1
 LEX  VDIR1 VDIR2 VDIR3 DIA  CDK DELX DIAB THICK COUNT
duct4            180    -90    90     AUTO   AUTO      15        45   0    1
duct5            20     90     -70    AUTO   AUTO      15        45   0    1
duct9            -20    90     -110   AUTO   AUTO      15        45   0    1
---------------- lseparator
yjun3            45     370    1      320    31806.57  2827.4    1    1
 LEX  VDIR1 VDIR2 VDIR3 DIA  CDK DELX DIAB THICK COUNT
duct12           195    90     105    AUTO   AUTO      20        30   0    1
duct13           0      90     90     AUTO   AUTO      20        45   0    1
duct16           165    -90    75     AUTO   AUTO      20        30   0    1
---------------- lseparator
yjun4            45     370    1      320    31806.57  2827.4    1    1
 LEX  VDIR1 VDIR2 VDIR3 DIA  CDK DELX DIAB THICK COUNT
duct21           195    90     105    AUTO   AUTO      20        30   0    1
duct22           0      90     90     AUTO   AUTO      20        45   0    1
duct27           165    -90    75     AUTO   AUTO      20        30   0    1
---------------- lseparator
yjun5            45     370    1      320    31806.57  2827.4    1    1
 LEX  VDIR1 VDIR2 VDIR3 DIA  CDK DELX DIAB THICK COUNT
duct30           195    90     105    AUTO   AUTO      20        30   0    1
duct31           0      90     90     AUTO   AUTO      20        45   0    1
duct36           165    -90    75     AUTO   AUTO      20        30   0    1
---------------- lseparator
yjun6            33     660    1      660    42765     5184      1    1
```

```
 LEX  VDIR1 VDIR2 VDIR3 DIA  CDK DELX DIAB THICK COUNT
duct37          120      90      -30     AUTO    AUTO    50      33      0       1
duct38          90       180     90      AUTO    AUTO    50      33      0       1
duct43          -135     90      -135    AUTO    AUTO    50      33      0       1
--------------- !separator
yjun7           33       850     1       850     42766   5184    1       1
 LEX  VDIR1 VDIR2 VDIR3 DIA  CDK DELX DIAB THICK COUNT
duct41          90       15      75      AUTO    AUTO    50      33      0       1
duct42          90       180     90      AUTO    AUTO    50      33      0       1
duct40          90       -15     105     AUTO    AUTO    50      33      0       1
VAL:VALVES      ================================================================
#1              GENL     28      465     0.1     !NV,VFLAG,DVALVE,THCYCLE,VLASH
POLY            FAST             !CAMCR,THVALV,HSCALE,VSCALE,ROCKER
8.3             250
VLI2:
0               0.032    0.065   0.097   0.129   0.161   0.194   0.226   0.258   0.29    0.34   #
CDF2:
0               0.086    0.176   0.259   0.339   0.41    0.451   0.479   0.496   0.496   0.497  #
CDR2:
0               0.086    0.176   0.259   0.339   0.41    0.451   0.479   0.496   0.496   0.497  #
--------------- !(separator)
#2              GENL     23.5    255     0.15    !NV,VFLAG,DVALVE,THCYCLE,VLASH
POLY            FAST             !CAMCR,THVALV,HSCALE,VSCALE,ROCKER
8               250
VLI2:
0               0.038    0.075   0.113   0.151   0.189   0.226   0.264   0.302   0.34    0.366  #
CDF2:
0               0.108    0.235   0.39    0.508   0.562   0.581   0.587   0.59    0.59    0.59   #
CDR2:
0               0.108    0.235   0.39    0.508   0.562   0.581   0.587   0.59    0.59    0.59   #
END:RUN         ================================================================

BAS:CONSTANTS
$case     =  1.,        $subcase  =  0.,         $Mulcase  =  1.0,  $prefix  =  1000.,     $date  =  26-Feb-2004, $version  =  5.1
$path     =  ./1000.wvm $file     =  1000.wvm,   $dir      =  ./,   $pi      =  3.1415927  NCYC   =  12.,         SPEED     =  1000
PAMB      =  1.013,     TAMB      =  298.,       TH850     =  9.,   BOUR     =  28.,       TPIS   =  500.,        THEAD     =  550.,   TCYL  =  540
THRT      =  48.,       FARD      =  0.08
BAS:GENERAL
!***            'SKIPINIT' SET      TO      'N'     FOR     FIRST   CASE
!***            reading  active.tags found  in      /usr/Ricardo/wave/5.1/config
!***            Loading  property  data:    INDOLENE /usr/Ricardo/wave/5.1/propty/indolene.fue
INDOLENE
BAS:TITLE
Motored         Transient Unmodified Engine  1000   rpm
36043           0.401956
BAS:OUTPUT
DUC:DUCT
DUC:BENDS
DUCT            ANGLE    Cp
761             35       0.063
762             45       0.108
763             45       0.108
764             35       0.063
duct2           110      0.189
duct7           110      0.189
duct11          110      0.189
duct15          110      0.189
duct20          110      0.189
duct25          110      0.189
duct29          110      0.189
duct35          110      0.189
duct46          30       0.066
JUN:JUNCTION
JUN:YJUNCTION
ENG:GEOMETRY

FIRING          SEQUENC  FIRING  TDC,    AND     FIRING  INTERVALS
1               3        4       2
0               180      360     540
180             180      180     180

!***            THIS     IS      A       MOTORIN RUN
ENG:HEAT
ENG:OPERATING
FFT:FFT
!***            REQUEST  PLOT    ID'S    AND     TITLES:
PLOT            #        185FFT: SOUND   PRESSUR LEVEL   VS.     FREQUENCY
LOCATIONS:      FFT#     301     FFT#    510
VAL:VALVES
!***            VALVE    #1:     TVO     =       346.4066, TVC   =       564.5946 FLOW   COEF   BASED  ON     SEAT  AREA
!***            NV       =       1       AEFFMAX =       305.9   (mm2)   DVALVE(M =      28     (mm)   CDMAX  =     0.42404
!***            VALVE    #2:     TVO     =       136.7137, TVC   =       373.2863 FLOW   COEF   BASED  ON     SEAT  AREA
!***            NV       =       2       AEFFMAX =       258.4   (mm2)   DVALVE(M =      23.5   (mm)   CDMAX  =     0.44238
ENG:VALVES
ENG:SI_WIEBE_COMB
INJ:TYPE
INJ:VOLUME
BAS:TIME
!***            REQUEST  PLOT    ID'S    AND     TITLES:
PLOT            #        2201PRESSURE
LOCATIONS:      JUNC:    401
PLOT            #        3202TEMPERATURE
LOCATIONS:      JUNC:    401
PLOT            #        4201PRESSURE
LOCATIONS:      DUCT:    761
PLOT            #        5110LOG-ICYCLE  P-V     PLOT
LOCATIONS:      JUNC:    401
PLOT            #        8201PRESSURE
LOCATIONS:      DUCT:    734
PLOT            #        7201PRESSURE
LOCATIONS:      DUCT:    739
END

!***            BEGINNIN 720     DEGREE  CYCLIC  WAVE    SIMULATION

TOTAL           DUCTS    :       68      TOTAL   JUNCTION:       55
TOTAL           VOLUMES  148     TOTAL   BOUNDAR 216
REG.            VOLUMES  145     INT.    BOUNDAR 80      DUCT/JUN BOUNDAR 136    AUX     VOLUM 3

TITLE:          Motored  Transient Unmodified Engine  1000   rpm
NC              ICYC     ISTEP   AIR-KG/H VOLEF  TEXH    PHI     IMEP    PMEP    IHP     ISFC    PCYL    TCYL    FTR
```

ENG:	1	0	1	0	0	470	0	0	0	0	0	1.001	340.1	0			
ENG	VOLEF(TC=		0	PHI(1)	=	0											
ENG:	3	1	1384	0	0	470	0	0	0	0	0	1.084	368.9	0			
ENG:	4	1	2759	0	0	470	0	0	0	0	0	1.083	369.8	0			
ENG:	2	1	4138	0	0	470	0	0	0	0	0	1.081	377.4	0			
ENG:	1	1	5515	11.08	0.787	370.8	0	-0.111	-0.029	-0.05	0	1.081	372.3	0			
ENG	VOLEF(TC=		0.1989	PHI(1)	=	0											
ENG:	3	2	6886	11.22	0.799	382.9	0	-0.134	-0.026	-0.06	0	1.082	368.3	0			
ENG:	4	2	8258	11.28	0.804	386.5	0	-0.142	-0.031	-0.06	0	1.084	368.2	0			
ENG:	2	2	9628	11.23	0.8	380.5	0	-0.143	-0.025	-0.06	0	1.083	369.1	0			
ENG:	1	2	10997	11.25	0.801	386.4	0	-0.144	-0.03	-0.06	0	1.082	368.7	0			
ENG	VOLEF(TC=		0.801	PHI(1)	=	0											
I***	AUTO-COICONDITIOMET																
ENG:	3	3	12366	11.25	0.801	384.8	0	-0.136	-0.026	-0.06	0	1.082	367.4	0			
ENG:	4	3	13736	11.27	0.803	385	0	-0.14	-0.03	-0.06	0	1.084	368.3	0			
ENG:	2	3	15108	11.23	0.8	385.3	0	-0.137	-0.026	-0.06	0	1.083	368.3	0			
ENG:	1	3	16475	11.27	0.803	385.6	0	-0.141	-0.03	-0.06	0	1.082	367.9	0			
ENG	VOLEF(TC=		0.8017	PHI(1)	=	0											
I***	AUTO-COI	Uvariance =	1.791	Pvariance	=		0.00061										
ENG:	3	4	17845	11.25	0.801	384.2	0	-0.136	-0.026	-0.06	0	1.082	367.5	0			
ENG:	4	4	19215	11.28	0.802	385.1	0	-0.141	-0.03	-0.06	0	1.084	368.6	0			
ENG:	2	4	20584	11.23	0.8	384.7	0	-0.136	-0.026	-0.06	0	1.083	368.2	0			
ENG:	1	4	21953	11.27	0.803	385	0	-0.14	-0.031	-0.06	0	1.082	367.9	0			
ENG	VOLEF(TC=		0.8015	PHI(1)	=	0											
I***	AUTO-COI	Uvariance =	7.294	Pvariance	=		0.000326										
I***	FAST	FOURIER	TRANSFO –		#	OF	HARMONI =		32								
I***	FFT	COMPLETE															
TIME	STEP	OUTPUT:	TOTAL	STEPS	IN	LAST	CYCLE	=	5478								
LIMITING	ELEMENT %		STEPS	(DOES	NOT	HAVE	TO	ADD	TO	100)							
DUCT:	duct4	25.6	DUCT:	duct13	24.4	DUCT:	duct22	27.9	DUCT:	duct31	22						
TITLE:	Motored	Transient	Unmodifiec Engine		1000	rpm											
F	I	N	A	L	O	U	T	P	U	T	O	F	D	U	C	T	S
Duct	Junction	TWALL	TAV	PAV	PMAX	PMIN	UMAX	UMIN	MACH	FLOW	A	CDout	CDin	HTKW			
K	K	BAR	BAR	BAR	M/S	M/S	NUMBER	KG/S	CM2	KW							
731	508	0	0	0	0	0	6.1	-2.6	0.0175	0.0031	44.17865	1	1	0			
732	507	300	300.6	0.999	1.012	0.962	7.6	-3.6	0.0219	0.0063	44.17865	1	1	0			
506	300	300.6	0.999	1.012	0.962	7.5	-3.6	0.0216	0.00625	44.179	1	1					
733	508	0	0	0	0	0	8.5	-3.4	0.0245	0.0094	44.17865	1	1	0			
03-Jan-02	0:00:00	300	300	0.999	1.01	0.985	23.4	-1.2	0.0674	0.0125	18.09558	0.81	0.81	0			
608	300	300	0.999	1.01	0.985	12	-0.6	0.0346	0.0125	28.274	1	0.63					
737	509	300	300	1	1.003	0.995	13.7	-0.9	0.0395	0.0125	33.18308	1	0.81	0			
orif20	300	300	1	1.004	0.993	11	-0.7	0.0316	0.0125	33.183	1	1					
739	301	300	300	1	1.001	0.998	14.6	-2.5	0.0421	0.0125	33.18308	1	0.8	0			
510	300	300	1	1.001	0.998	11.7	-3.1	0.0337	0.0125	33.183	1	0.81					
751	561	850	421.3	1.002	1.021	0.962	28.4	-10.7	0.0714	0.0031	8.55299	1	0.96	-0.127			
151	850	440.8	1.002	1.018	0.984	28.8	-11.4	0.07	0.00313	8.553	1	1					
752	562	850	420.3	1	1.026	0.978	29.5	-11.4	0.0744	0.0031	8.55299	1	0.96	-0.182			
152	850	456.3	1	1.022	0.981	30.9	-12	0.0742	0.00312	8.553	1	1					
753	553	850	423.6	1	1.026	0.977	29.5	-11.5	0.0744	0.0031	8.55299	1	0.96	-0.207			
153	850	464.4	1	1.021	0.981	31.4	-11.6	0.0747	0.00312	8.553	1	1					
754	554	850	421	1.002	1.026	0.98	28.9	-10.6	0.0727	0.0031	8.55299	1	0.96	-0.182			
154	850	457	1.002	1.022	0.983	30	-11.6	0.0721	0.00313	8.553	1	1					
761	151	850	463.1	1.001	1.016	0.985	28.6	-11.4	0.07	0.0031	8.55299	1	1	-0.079			
161	850	463.1	1.001	1.015	0.986	29.7	-11.7	0.071	0.00313	8.553	1	1					
762	152	850	478	1	1.019	0.983	30.9	-12	0.0742	0.0031	8.55299	1	1	-0.077			
162	850	478	1	1.019	0.983	32	-12.4	0.0749	0.00312	8.553	1	1					
763	153	850	485.7	1	1.018	0.983	31.4	-11.8	0.0747	0.0031	8.55299	1	1	-0.076			
163	850	485.7	1	1.018	0.983	32.5	-12.2	0.0754	0.00312	8.553	1	1					
764	154	850	478.6	1.002	1.02	0.984	30	-11.6	0.0721	0.0031	8.55299	1	1	-0.077			
164	850	478.6	1.002	1.02	0.984	31	-12.1	0.0727	0.00313	8.553	1	1					
7038	510	0	0	0	0	0	1.2	-0.2	0.0034	0.0125	0.04012	1	1	0			
7501	401	470	396.5	1.003	1.027	0.976	220.6	-53.3	0.5765	0.0016	2.56441	1	1	-0.009			
561	470	396.5	1.003	1.027	0.976	64.8	-31.6	0.1636	0.00157	1.7672	1	0.81					
7502	402	470	396	1.002	1.03	0.973	196.3	-62.8	0.5136	0.0016	0	1	1	-0.009			
562	470	396	1.002	1.03	0.973	67.2	-33.6	0.1699	0.00156	1.7672	1	0.81					
7503	403	470	396.6	1.002	1.03	0.974	184.5	-58.3	0.4623	0.0016	0	1	1	-0.009			
553	470	396.6	1.002	1.03	0.974	67.3	-34.2	0.1698	0.00156	1.7672	1	0.81					
7504	404	470	396.8	1.003	1.032	0.975	217.6	-43.9	0.5669	0.0016	0	1	1	-0.009			
554	470	396.8	1.003	1.032	0.975	65.9	-31.3	0.1662	0.00156	1.7672	1	0.81					
7511	401	470	396.6	1.003	1.027	0.976	220.6	-53.3	0.5765	0.0016	2.56441	1	1	-0.009			
561	470	396.6	1.003	1.027	0.976	64.8	-32	0.1636	0.00156	1.7672	1	0.81					
7512	402	470	396	1.002	1.03	0.973	196.3	-62.8	0.5135	0.0016	0	1	1	-0.009			
552	470	396	1.002	1.03	0.973	67.2	-33.8	0.1699	0.00156	1.7872	1	0.81					
7513	403	470	396.6	1.002	1.03	0.974	184.5	-58.3	0.4623	0.0016	0	1	1	-0.009			
553	470	396.6	1.002	1.03	0.974	67.3	-34.2	0.1698	0.00156	1.7672	1	0.81					
7514	404	470	396.8	1.003	1.032	0.975	217.6	-43.9	0.5669	0.0016	0	1	1	-0.009			
554	470	396.8	1.003	1.032	0.975	65.9	-30.9	0.1662	0.00157	1.7672	1	0.81					
duct1	508	300	300.4	0.998	1.014	0.979	45.6	-18.1	0.1321	0.0016	3.46361	1	0.8	0			
orif2	300	301.5	0.996	1.021	0.974	36.3	-15.7	0.1044	0.00157	3.4636	1	1					
duct2	orif2	320	302.7	0.996	1.024	0.971	38.3	-18.7	0.1044	0.0016	3.46361	1	1	-0.005			
orif4	320	304.7	0.998	1.029	0.964	35.9	-17.6	0.1032	0.00157	3.4636	1	0.85					

duct3	orif4	340	306.2	0.998	1.031	0.962	36.9	-17.5	0.1032	0.0016	3.46361	0.85	1	-0.015
yjun1	340	312.6	0.998	1.034	0.959	16.5	-5.8	0.0466	0.00157	7.0686	1	1		
duct4	yjun1	370	315.5	0.998	1.035	0.958	14.6	-5	0.041	0.0031	15.90431	1	1	-0.002
yjun2	370	315.5	0.998	1.035	0.958	14.5	-4.9	0.0407	0.00313	15.904	1	1		
duct5	yjun2	370	322.2	0.998	1.035	0.958	22.4	-6.2	0.063	0.0016	6.15752	1	0.83	-0.006
404	370	322.2	0.998	1.035	0.958	38.6	-144.2	0.3605	0.00157	0.0013	1	1		
duct6	508	300	300.4	0.998	1.014	0.979	45.8	-16.1	0.1321	0.0016	3.46361	1	0.8	0
orif1	300	301.5	0.998	1.021	0.974	36.3	-15.7	0.1044	0.00157	3.4636	1	1		
duct7	orif1	320	302.7	0.998	1.024	0.971	36.3	-15.7	0.1044	0.0016	3.46361	1	1	-0.005
orif3	320	304.7	0.998	1.029	0.964	35.9	-17.5	0.1032	0.00157	3.4636	1	0.85		
duct8	orif3	340	306.2	0.998	1.031	0.962	36.9	-17.5	0.1032	0.0016	3.46361	0.85	1	-0.015
yjun1	340	312.6	0.998	1.034	0.959	16.5	-5.8	0.0466	0.00157	7.0686	1	1		
duct9	yjun2	370	322.2	0.998	1.035	0.958	22.4	-6.2	0.063	0.0016	6.15752	1	0.83	-0.006
404	370	322.2	0.998	1.035	0.958	38.6	-144.2	0.3605	0.00157	0.0013	1	1		
duct10	507	300	300.6	0.998	1.014	0.977	45	-15.9	0.1296	0.0016	3.46361	1	0.8	0
orif5	300	301.6	0.998	1.019	0.974	35.5	-15.6	0.1023	0.00156	3.4636	1	1		
duct11	orif5	320	302.7	0.998	1.022	0.972	35.5	-15.6	0.1023	0.0016	3.46361	1	1	-0.005
orif7	320	304.7	0.998	1.026	0.967	35.2	-17.7	0.1011	0.00156	3.4636	1	0.85		
duct12	orif7	340	306.2	0.998	1.026	0.965	35.2	-17.7	0.1011	0.0016	3.46361	0.85	1	-0.014
yjun3	340	312.6	0.998	1.031	0.962	16.3	-5.9	0.046	0.00156	7.0686	1	1		
duct13	yjun3	370	315.4	0.998	1.032	0.961	14.4	-5.1	0.0405	0.0031	15.90431	1	1	-0.002
503	370	315.4	0.998	1.032	0.961	14.3	-5	0.0403	0.00312	15.904	1	1		
duct14	507	300	300.6	0.998	1.014	0.977	4.50E+01	-15.9	0.1296	0.0016	3.46361	1	0.8	0
orif6	300	301.6	0.998	1.019	0.974	35.5	-15.6	0.1023	0.00156	3.4636	1	1		
duct15	orif6	320	302.7	0.998	1.022	0.972	35.5	-15.6	0.1023	0.0016	3.46361	1	1	-0.005
orif8	320	304.7	0.998	1.026	0.967	35.2	-17.7	0.1011	0.00156	3.4636	1	0.85		
duct16	orif8	340	306.2	9.98E-01	1.026	0.965	3.52E+01	-17.7	0.1011	0.0016	3.46361	0.85	1	-0.014
yjun3	340	312.6	0.998	1.031	0.962	16.3	-5.9	0.046	0.00156	7.0686	1	1		
duct17	503	370	322.3	0.998	1.033	0.961	22.2	-6.3	0.0623	0.0016	6.15752	1	0.83	-0.006
403	370	322.3	0.998	1.033	0.961	80.7	-143.4	0.3782	0.00156	0	1	1		
duct18	503	370	322.3	0.998	1.033	0.961	2.22E+01	-6.3	0.0623	0.0016	6.15752	1	0.83	-0.006
403	370	322.3	0.998	1.033	0.961	80.7	-143.4	0.3782	0.00156	0	1	1		
duct19	505	300	301.5	0.998	1.015	0.976	47.2	-16.3	0.1356	0.0016	3.46361	1	0.8	0.001
orif9	300	302.5	0.998	1.021	0.973	37.3	-15.9	0.1071	0.00156	3.4636	1	1		
duct20	orif9	320	303.7	9.98E-01	1.025	0.97	3.73E+01	-15.9	0.1071	0.0016	3.46361	1	1	-0.005
orif11	320	305.7	0.998	1.03	0.964	36.9	-17.7	0.1059	0.00156	3.4636	1	0.85		
duct21	orif11	340	307.1	0.998	1.032	0.962	36.9	-17.7	0.1059	0.0016	3.46361	0.85	1	-0.014
yjun4	340	313.3	0.998	1.035	0.958	16.8	-5.7	0.0474	0.00156	7.0686	1	1		
duct22	yjun4	370	316.1	9.98E-01	1.036	0.958	1.48E+01	-4.9	0.0417	0.0031	15.90431	1	1	-0.002
501	370	316.1	0.998	1.036	0.958	14.7	-4.9	0.0414	0.00313	15.904	1	1		
duct23	501	370	322.7	0.998	1.036	0.957	22.7	-6.1	0.0639	0.0016	6.15752	1	0.83	-0.006
401	370	322.7	0.998	1.036	0.957	37.3	-144.6	0.3815	0.00156	0	1	1		
duct24	501	370	322.7	0.998	1.036	0.957	22.7	-6.1	0.0639	0.0016	6.15752	1	0.83	-0.005
401	370	322.7	0.998	1.036	0.957	37.3	-144.6	0.3815	0.00156	0	1	1		
duct25	505	300	301.5	0.998	1.015	0.976	47.2	-16.3	0.1356	0.0016	3.46361	1	0.8	0.001
orif10	300	302.5	0.998	1.021	0.973	37.3	-15.9	0.1071	0.00156	3.4636	1	1		
duct26	orif10	320	303.7	0.998	1.025	0.97	37.3	-15.9	0.1071	0.0016	3.46361	1	1	-0.005
orif12	320	305.7	0.998	1.03	0.964	36.9	-17.7	0.1059	0.00156	3.4636	1	0.85		
duct27	orif12	340	307.1	0.998	1.032	0.962	36.9	-17.7	0.1059	0.0016	3.46361	0.85	1	-0.014
yjun4	340	313.3	0.998	1.035	0.958	16.8	-5.7	0.0474	0.00156	7.0686	1	1		
duct28	506	300	301.1	0.998	1.014	0.976	45.2	-16	0.1301	0.0016	3.46361	1	0.8	0.001
orif13	300	302	0.998	1.019	0.973	35.7	-15.7	0.1025	0.00156	3.4636	1	1		
duct29	orif13	320	303.2	0.998	1.021	0.971	35.7	-15.7	0.1025	0.0016	3.46361	1	1	-0.005
orif15	320	305.1	0.998	1.026	0.965	35.3	-17.7	0.1013	0.00156	3.4636	1	0.85		
duct30	orif15	340	306.7	0.998	1.028	0.963	35.3	-17.7	0.1013	0.0016	3.46361	0.85	1	-0.014
yjun5	340	312.7	0.998	1.031	0.96	16.3	-5.9	0.0461	0.00156	7.0686	1	1		
duct31	yjun5	370	314.5	0.998	1.032	0.96	14.4	-5.1	0.0405	0.0031	15.90431	1	1	-0.002
502	370	314.5	0.998	1.032	0.96	14.3	-5	0.0403	0.00312	15.904	1	1		
duct32	502	370	321.5	0.998	1.032	0.959	22.1	-6.4	0.0623	0.0016	6.15752	1	0.83	-0.006
402	370	321.5	0.998	1.032	0.959	59.7	-143.5	0.3788	0.00156	2.8553	1	1		
duct33	502	370	321.5	0.998	1.032	0.959	22.1	-6.4	0.0623	0.0016	6.15752	1	0.83	-0.006
402	370	321.5	0.998	1.032	0.959	59.7	-143.5	0.3788	0.00156	2.8553	1	1		
duct34	506	300	300.9	0.998	1.014	0.976	45.2	-15.9	0.1301	0.0016	3.46361	1	0.8	0
orif14	300	301	0.998	1.019	0.973	35.7	-15.5	0.1026	0.00156	3.4636	1	1		
duct35	orif14	300	301.2	0.998	1.021	0.971	35.7	-15.5	0.1026	0.0016	3.46361	1	1	0.001
orif16	300	302.2	0.998	1.026	0.965	35.1	-17.7	0.1011	0.00156	3.4636	1	0.85		
duct36	orif16	340	304.1	0.998	1.026	0.963	35.1	-17.7	0.1011	0.0016	3.46361	0.85	1	-0.015
yjun5	340	310.7	0.998	1.031	0.96	16.3	-5.9	0.0459	0.00156	7.0686	1	1		
duct37	161	850	476.7	1.001	1.012	0.989	29.7	-11.7	0.071	0.0031	8.55299	1	1	-0.101
yjun6	850	490.7	1.001	1.01	0.99	31	-12	0.0709	0.00313	8.553	1	1		
duct38	yjun6	800	524.6	1	1.003	0.996	34.6	-16.1	0.076	0.0063	8.55299	0.9	1	-0.086
amb1	800	524.6	1	1.003	0.996	25.3	-12.9	0.0536	0.00626	11.946	1	0.8		
duct40	162	850	494.2	1	1.015	0.986	32	-12.4	0.0749	0.0031	8.55299	1	1	-0.122
yjun7	850	509.9	1	1.011	0.989	33.6	-12.9	0.0746	0.00312	8.553	1	1		
duct41	163	850	501.5	1	1.015	0.986	32.5	-12.2	0.0754	0.0031	8.55299	1	1	-0.12
yjun7	850	516.5	1	1.012	0.99	34.1	-12.7	0.0753	0.00312	8.553	1	1		
duct42	yjun7	800	528.5	1	1.004	0.997	35.8	-14.2	0.0784	0.0062	8.55299	0.9	1	-0.084

amb2	800	528.5	1	1.004	0.997	26	-11.4	0.0556	0.00824	11.946	1	0.8		
duct43	164	860	494.9	1.001	1.017	0.986	31	-12.1	0.0727	0.0031	8.55299	1	1	-0.179
yjun6	850	525.2	1.001	1.011	0.99	33.1	-12.1	0.0722	0.00313	8.553	1	1		
duct44	orif17	300	299.9	0.999	1.009	0.987	13.1	-0.6	0.0378	0.0125	28.27434	1	0.95	0
116	300	299.9	0.999	1.009	0.987	23.4	-1.2	0.0674	0.0125	18.096	0.81	0.81		
duct46	orif20	300	300	1	1.005	0.992	11	-0.7	0.0316	0.0125	33.16306	1	1	0
orif19	300	300	1	1.005	0.992	10.8	-0.7	0.0312	0.0125	33.183	1	1		
duct47	orif19	300	300	1	1.006	0.99	10.8	-0.7	0.0312	0.0125	33.16306	1	1	0
orif17	300	300	1	1.006	0.986	13.1	-0.6	0.0378	0.0125	28.274	0.95	1		

FINAL OUTPUT OF JUNCTIONS

Junction	TWALL	TAV	PAV	PMAX	PMIN	HTKW
K	K	BAR	BAR	BAR	KW	
501	370	317.8	0.998	1.036	0.958	-0.002
502	370	316.3	0.998	1.032	0.96	-0.002
503	370	317.2	0.998	1.032	0.961	-0.002
505	310	301.6	0.999	1.013	0.981	-0.003
506	310	301.1	0.999	1.012	0.982	-0.002
507	310	300.6	0.999	1.012	0.983	-0.002
508	310	300.3	0.999	1.011	0.984	-0.002
509	300	300	1	1.002	0.996	0
510	300	300	1	1.002	0.997	0
551	450	401.2	1.002	1.022	0.98	-0.002
552	450	400.7	1.001	1.027	0.977	-0.002
553	450	401.4	1.001	1.028	0.978	-0.002
554	450	401.5	1.002	1.027	0.979	-0.002
yjun1	370	314.2	0.998	1.034	0.958	-0.004
yjun2	370	317.2	0.998	1.035	0.958	-0.002
yjun3	370	314.2	0.998	1.032	0.961	-0.004
yjun4	370	314.8	0.998	1.036	0.958	-0.004
yjun5	370	313.3	0.998	1.031	0.96	-0.004
yjun6	850	515.9	1.001	1.008	0.992	-0.068
yjun7	850	520.4	1	1.008	0.993	-0.067
TITLE:	Motored	Transient	Unmodified	Engine	1000	rpm

ENGINE SUMMARY

NC	MASS	IN	VOL EFF.	TRAP.RAT	IMEP	PMEP	IHP	TEXH	RES(%)	EGR(%	PHI	PMAX	HTR
KG/HR	BAR	BAR	K	BAR	KW								
1	11.27	0.803	1.08	-0.1402	-0.09289	385	0	0	0	22.2	-0.1652		
2	11.23	0.7999	1.084	-0.1357	-0.0864	384.7	0	0	0	22.2	-0.1644		
3	11.25	0.8009	1.084	-0.1357	-0.08648	384.2	0	0	0	22.19	-0.1661		
4	11.28	0.8023	1.081	-0.1406	-0.09285	385.1	0	0	0	22.22	-0.1644		

Breathing Quantities

AMB.VOL.EFF	(AIR	IN	/	AMB.	REF.)	=	0.802	TRAP.RAT	(FRESH	TR/	FRESH	IN	)	=	1.062	
DEL.EFF.	(FRESH	IN	/	PLEN.	REF.)	=	0.869	SCAV.RAT	(GAS	IN	/	GAS	TR.	)	=	0.9
CHARG.EFF.	(FRESH	TR/	PLEN.	REF.)	=	0.94	SCAV.EFF	(FRESH	TR/	GAS	TR.	)	=	1		
TOT.DEL.EFF	(GAS	IN	/	PLEN.	REF.)	=	0.869	RESID.FR	(RESID	TR/	GAS	TR.	)	=	0	
EGR	FR.	(RESID	IN	/	GAS	IN	)	=	0							
TITLE:	Motored	Transient	Unmodified	Engine	1000	rpm										

ENGINE GEOMETRY

I	DISPL/CY	(LIT.)	=	0.3958	I	NUMBER	OF	CYLINDEF=		4	I	I				
I	(IN3)	=	24.21	I	COMPRES	RATIO	=	10	I	EFFEC	CR	(VC-TDC)	=	9.023	I	
I	BORE	(MM)	=	81	I	BORE/STF=		1.062	I	I						
I	(IN)	=	3.189	I	CON.	ROD	LENGTH(I=		135	I	I					
I	STROKE	(MM)	=	77	I	WRIST	PIN	OFFSET(I=		0.1	I	I				
I	(IN)	=	3.031	I	CLEARAN	VOL.	(M3)	=	4.41E-06	I	ENGINE	TYPE	=	MOTORED	I	
I	INT.	VALVE	DIA.(MM)	=	28	I	EXH.	VALVE	DIA.(MM)	=	23.5	I	#1	EVO	=	137 I
I	MAX.	LIFT	(MM)	=	8.2	I	MAX.	LIFT	(MM)	=	7.85	I	#1	EVC	=	373 I
I	I	I	#1	IVO	=	345.4	I									
I	NO.	INTAKE	VALVES	=	2	I	NO.	EXHAUST	VALVES	=	2	I	#1	IVC	=	565 I

OPERATING CONDITIONS

I	RPM	=	1000	I	#1	INT.PORT	PR(BAR)	=	0.9983	I	#1	IGN	DELAY(CA)		=	0 I	
I	AMB.	PRESSUR	(BAR)	=	1.013	I	(IN.HG)	=	29.56	I	#1	COMB.	START(CA)		=	### I	
I	(IN.HG)	=	30	I	#1	INT.PORT	TEMP(K)	=	318.3	I	INJ.TIMIN	(ATDC)	=	1000000	I		
I	AMB.	TEMP.	(K)	=	298	I	(F)	=	113.2	I	MID.INJ.PI=		0	I			
I	(F)	=	76.73	I	#1	EXH.PORT	PR(BAR)	=	1.003	I	(PSI)	=	0	I			
I	FUEL	TYPE	(C:H:O)	C	=	7.3	I	(IN.HG)	=	29.71	I	INJ.DURA	(CA)	=	0	I	
I	H	=	13.9	I	I	FUEL	RATE	(KG/HR)	=	0	I						
I	O	=	0	I	PISTON	VEL.	(M/S)	=	2.567	I	(MULTI)	(LBM/HR)	=	0	I		
I	FUEL	LHV	(MJ/KG)	=	43.18	I	(FT/MIN)	=	505.2	I	#1	FUEL	/	SHOT	(KG)	= 0	I
I	(BTU/LBM=		18580	I	I	I											
I	(A/F)	STOICH	=	14.56	I	I	0.01	FUEL	PWR/CYL	(W)	=	0	I				
I	FUEL	MOLEC.	WEIGHT	=	0	I	I	I									

Predicted Performances:

I	INDIC.	POWER	(HP)	=	-0.2446	I	BRAKE	POWER	(HP)	=	-1.803	I	PMEP	(BAR)	=	-0 I		
I	IND.EFFIC	(%)	=	0	I	BRAKE	EFFICIEN=		0	I	(PSI)	=	-0.41	I				
I	IMEP(NET	(BAR)	=	-0.138	I	BMEP	(BAR)	=	-1.017	I	FMEP	(BAR)	=	0.8788	I			
I	(PSI)	=	-2.002	I	(PSI)	=	-14.75	I	(PSI)	=	12.75	I						
I	ISFC	(KG/KWH)=		0	I	BSFC	(KG/KWH)=		0	I	IMEP(GRC	(BAR)	=	-0.1097	I			
I	(LBM/BHP=		0	I	(LBM/BHP=		0	I	(PSI)	=	-1.591	I						
I	IND.	TORQUE	(N-M)	=	-1.743	I	BRAKE	TORQUE	(N-M)	=	-12.84	I	FRICT.	TORQUE	(N-M)	= 11.1	I	
I	(FT-LB)	=	-1.286	I	(FT-LB)	=	-9.471	I	PUMP.	TORQU	(N-M)	=	-0.36 I					
I	AUXILIAR	POWER	[hp]	=	0	I	I	#1	EXHAUST	TEMP	(K)	=	385 I					
I	AUXILIAR	POWER	[kW]	=	0	I	I	(F)	=	233.4 I								
I	IND.	ENERGY	BALANCE I		FRESH	AIR	IN	(KG/H)	=	45.02	I	#1	PMAX	(BAR)	=	22 I		
I	NET	PISTON	WORK	(%)	=	0	I	(WET)	(LBM/HR)=	99.26	I		(PSI) =		322	I		
I	AVAIL.EXI	(%)	=	9999	I	TRAPPINC	RATIO	=	1.062	I	#1	CA	AT	PMAX	=	-0 I		
I	DEBIT	INTK.ENTI=		9999	I	VOL.EFF.(=		0.8015	I	#1	MAX	DP/DTH	(BAR) =		0.5174	I		
I	H.	TRAN.(IN-=		0	I	#1	VOL.EFF.(=	0.8702	I		(PER	DEG)	(PSI) =		7.505	I		
I	BLOWBY	AT	RING1	(%)	=	9999	I	A/F	TRAPPED=		0	I	#1	CA	AT	MAX DP/DTH	=	-17 I
I	IMBALANC	(%)	=	9999	I	PHI	TRAPPED=		0	I	#1	MAX	AVG.G T(K)		=	837 I		
I	PUMPING	WORK	(%)	=	0	I	RESIDUAL	FRAC.	(%)	=	0	I	(F)	=	1047	I		
I	I	BRAKE	POWER	(KW)	=	-1.345	I	FRIC.	(%FUEL	ENER.)=	0	I						
I	I	I	H.TRAN.(I=		-0.6602	I												

ENGINE OUTEMISSIONS

NOx (PPM) = 0	HC EMISSION(PPMC1) = 0	CO EMISS (PPM) = 0
NOx AS NO2 (g/hr) = 0	(g/hr) = 0	(g/hr) = 0
(g/bkW-hr) = 0	(g/bkW-hr) = 0	(g/bkW-hr) = 0

TITLE: Motored Transient Unmodified Engine 1000 rpm

ENGINE CYLINDER BACKFLOW

CYL	BEFORE EVC AMOUNT(I	% OF TOTAL	AFTER EVC AMOUNT(I	% OF TOTAL
1	1.22E-09	0.000324	3.12E-05	8.311
2	1.02E-09	0.000273	3.07E-05	8.207
3	3.1E-10	8.26E-05	3.13E-05	8.336
4	6.21E-10	0.000165	3.04E-05	8.1

ENGINE INTAKE VALVE BACKFLOW

CYL	VAL	BEFORE EVC AMOUNT(I	% OF TOTAL	AFTER EVC AMOUN	% OF TOTAL	REV ANGLE
1	1	6.09E-10	0.000324	1.56E-05	8.311	539.7
1	1	6.09E-10	0.000324	1.56E-05	8.311	539.7
2	1	5.11E-10	0.000273	1.54E-05	8.207	541.4
2	1	5.11E-10	0.000273	1.54E-05	8.207	541.4
3	1	1.55E-10	8.26E-05	1.56E-05	8.336	540.6
3	1	1.55E-10	8.26E-05	1.56E-05	8.336	540.6
4	1	3.11E-10	0.000165	1.52E-05	8.1	540.3
4	1	3.11E-10	0.000165	1.52E-05	8.1	540.3

CYCLE AVERAGED ENGINE CYLINDER EXHAUST INDICTAED SPECIFIC EMISSIONS

CYL	NO (g/kW/hr)	(g/hp/hr)	NO2 (g/kW/hr)	(g/hp/hr)	CO (g/kW/hr)	(g/hp/h	HC (g/kW/hr)	(g/hp/hr)
1	•	•	•	•	•	•	•	•
2	•	•	•	•	•	•	•	•
3	•	•	•	•	•	•	•	•
4	•	•	•	•	•	•	•	•

CYCLE AVERAGED AMBIENT EMMISIONS

AMBIENT	NO (g/hr)	NO2 (g/hr)	CO (g/hr)	HC (g/hr)
301	0	0	0	0
amb1	0	0	0	0
amb2	0	0	0	0

EXHIBIT B2 - Output of Modelled Parameters for Modified Engine

```
RICARDO SOFTWARE — WAVE SIMULATION CODE — VERSION 5.1

BAS:CONSTANTS
ncyc            =       12
speed           =       1000
pamb            =       1.013
tamb            =       298
thb50           =       9
bdur            =       28
tpis            =       500
thead           =       550
tcyl            =       540
thrt            =       48
fard            =       0.08
BAS:GENERAL     PARAMET
{ncyc}          0.8     1       simm    auto    !       TIMT/NCY CFL,DDEC UNITS
N               n       Y       0.01    !       RESTART DUMPCKF SKIPINIT, AUTOCONVERGE
INDOLENE        !       FUELFILE
BAS:OUTPUT      &       PLOTTING
0               0       0       0       0       0       0       0       0       0       !       IOUT1   THROUGH IOUT10
N               -30     120     -360    !       ZOOM,TZOOM(1,2),INCPL
postscript      draft   !       PFORMAT FONTNAME
all             NULL    CASE    !       SUMMARY SUMFREQ
N               N       Y       N       !       ANIMATE, SOUNDTRACE
case            25      !       WARNFRE MAX_WARNINGS
BAS:TIME        PLOTS
titles          V5.1 Build 4
L:              0.5
P:              201     auto    auto
J:              401
P:              202     auto    auto
J:              401
P:              201     auto    auto
D:              761
P:              110     auto    auto
J:              401
P:              201     auto    auto
D:              734
P:              201     auto    auto
D:              739
BAS:TITLE
Motored         Manifold Bridge Engine {speed} rpm
DUC:BENDS
734             0       !       LEX,ARC
761             35      !       LEX,ARC
762             45      !       LEX,ARC
763             45      !       LEX,ARC
764             35      !       LEX,ARC
duct2           55
duct7           55
duct11          55
duct15          55
duct20          55
duct26          55
duct29          55
duct35          55
duct36          0
duct37          55
duct38          0
duct40          55
duct41          55
duct42          0
duct43          55
duct46          30
duct56          180
duct59          180
duct62          180
duct65          180
duct66          55
duct67          55
duct68          55
duct69          55
duct70          90
duct71          90
duct72          90
duct73          90
DUC:DUCT        DATA
1               1       !       CFRICG  CHTRG
```

LEX	KJL	KJR	DL	DR	SDUCT	DX	TWALD	PDI	TDI	CFR	CHT	CP	CDL	CDR
731	506	505	75	75	0	0	0	0	0	1	1	0	aut	aut
732	507	506	75	75	25	36	300	1	300	1	1	0	aut	aut
733	508	507	75	75	0	0	0	0	0	1	1	0	aut	aut
734	116	508	60	60	50	36	300	1	300	1	1	0	aut	aut
737	509	orif20	65	65	100	36	300	1	300	1	1	0	aut	aut
739	301	510	65	65	15	36	300	1	300	1	1	0	aut	aut
751	551	yjun12	33	33	70	44	850	1	900	1	1	0	aut	aut
752	552	yjun13	33	33	100	44	850	1	900	1	1	0	aut	aut
753	553	yjun14	33	33	100	44	850	1	900	1	1	0	aut	aut
754	554	yjun15	33	33	100	44	850	1	900	1	1	0	aut	aut
761	151	161	33	33	60	44	850	1	900	1	1	0	aut	aut
762	152	162	33	33	60	44	850	1	900	1	1	0	aut	aut
763	153	163	33	33	60	44	850	1	900	1	1	0	aut	aut
764	154	164	33	33	60	44	850	1	900	1	1	0	aut	aut
7038	510	509	2.26	2.26	0	0	0	0	0	1	1	0	aut	aut
7501	401	551	23	15	50	50	470	1	470	0	1	0	aut	aut
7502	402	552	23	15	50	50	470	1	470	0	1	0	aut	aut
7503	403	553	23	15	50	50	470	1	470	0	1	0	aut	aut
7504	404	554	23	15	50	50	470	1	470	0	1	0	aut	aut
7511	401	551	23	15	50	50	470	1	470	0	1	0	aut	aut
7512	402	552	23	15	50	50	470	1	470	0	1	0	aut	aut
7513	403	553	23	15	50	50	470	1	470	0	1	0	aut	aut
7514	404	554	23	15	50	50	470	1	470	0	1	0	aut	aut
duct1	506	orif2	21	21	100	36	300	1	300	1	1	0	auto	auto
duct2	orif2	yjun11	21	21	50	36	320	1	300	1	1	0	auto	auto
duct3	orif4	yjun1	30	30	175	36	340	1	320	1	1	0	auto	auto
duct4	yjun1	yjun2	45	45	10	36	370	1	320	1	1	0	auto	auto
duct5	yjun2	404	28	27	50	36	370	1	340	1	1	0	auto	auto
duct6	506	orif1	21	21	100	36	300	1	300	1	1	0	auto	auto
duct7	orif1	yjun11	21	21	50	36	320	1	300	1	1	0	auto	auto
duct8	orif3	yjun1	30	30	175	36	340	1	320	1	1	0	auto	auto
duct9	yjun2	404	28	27	50	36	370	1	340	1	1	0	auto	auto
duct10	507	orif5	21	21	100	36	300	1	300	1	1	0	auto	auto
duct11	orif5	yjun10	21	21	50	36	320	1	300	1	1	0	auto	auto

duct12	orif7	yjun3	30	30	175	36	340	1	320	1	1	0	auto	auto
duct13	yjun3	503	45	45	10	36	370	1	320	1	1	0	auto	auto
duct14	507	orif6	21	21	100	36	300	1	300	1	1	0	auto	auto
duct15	orif6	yjun10	21	21	50	36	320	1	300	1	1	0	auto	auto
duct16	orif8	yjun3	30	30	175	36	340	1	320	1	1	0	auto	auto
duct17	503	403	28	27	50	36	370	1	340	1	1	0	auto	auto
duct18	503	403	28	27	50	36	370	1	340	1	1	0	auto	auto
duct19	505	orif9	21	21	100	36	300	1	300	1	1	0	auto	auto
duct20	orif9	yjun8	21	21	50	36	320	1	300	1	1	0	auto	auto
duct21	orif11	yjun4	30	30	175	36	340	1	320	1	1	0	auto	auto
duct22	yjun4	501	45	45	10	36	370	1	320	1	1	0	auto	auto
duct23	501	401	28	27	50	36	370	1	340	1	1	0	auto	auto
duct24	501	401	28	27	50	36	370	1	340	1	1	0	auto	auto
duct25	505	orif10	21	21	100	36	300	1	300	1	1	0	auto	auto
duct26	orif10	yjun8	21	21	50	36	320	1	300	1	1	0	auto	auto
duct27	orif12	yjun4	30	30	175	36	340	1	320	1	1	0	auto	auto
duct28	508	orif13	21	21	100	36	300	1	300	1	1	0	auto	auto
duct29	orif13	yjun9	21	21	50	36	320	1	300	1	1	0	auto	auto
duct30	orif15	yjun5	30	30	175	36	340	1	320	1	1	0	auto	auto
duct31	yjun5	502	45	45	10	36	370	1	320	1	1	0	auto	auto
duct32	502	402	28	27	50	36	370	1	340	1	1	0	auto	auto
duct33	502	402	28	27	50	36	370	1	340	1	1	0	auto	auto
duct34	506	orif14	21	21	100	36	300	1	300	1	1	0	auto	auto
duct35	orif14	yjun9	21	21	50	36	300	1	300	1	1	0	auto	auto
duct36	orif16	yjun5	30	30	175	36	340	1	320	1	1	0	auto	auto
duct37	yjun8	orif11	21	21	50	36	320	1	300	1	1	0	auto	auto
duct38	yjun6	amb1	39	39	60	44	800	1	800	1	1	0	auto	auto
duct39	161	yjun6	33	33	80	44	850	1	850	1	1	0	auto	auto
duct40	yjun9	orif15	21	21	50	36	320	1	300	1	1	0	auto	auto
duct41	yjun10	orif7	21	21	50	36	320	1	300	1	1	0	auto	auto
duct42	yjun7	amb2	39	39	60	44	800	1	800	1	1	0	auto	auto
duct43	yjun11	orif3	21	21	50	36	320	1	300	1	1	0	auto	auto
duct44	orif17	116	60	60	50	36	300	1	300	1	1	0	auto	auto
duct45	yjun12	151	33	33	20	44	650	1	900	1	1	0	auto	auto
duct46	orif20	orif19	65	65	50	36	300	1	300	1	1	0	auto	auto
duct47	orif19	orif17	65	65	100	36	300	1	300	1	1	0	auto	auto
duct48	yjun13	152	33	33	30	44	850	1	900	1	1	0	auto	auto
duct49	164	yjun6	33	33	150	44	850	1	850	1	1	0	auto	auto
duct50	yjun14	153	33	33	50	44	850	1	900	1	1	0	auto	auto
duct51	yjun15	154	33	33	30	44	850	1	900	1	1	0	auto	auto
duct52	163	yjun7	33	33	100	44	850	1	850	1	1	0	auto	auto
duct53	yjun12	orif22	32	32	200	44	300	1	300	1	1	0	auto	auto
duct54	orif29	orif23	32	32	600	44	300	1	300	1	1	0	auto	auto
duct55	162	yjun7	33	33	100	44	850	1	850	1	1	0	auto	auto
duct56	orif23	yjun8	32	32	200	44	300	1	300	1	1	0	auto	auto
duct57	yjun13	orif18	32	32	200	44	300	1	300	1	1	0	auto	auto
duct58	orif28	orif21	32	32	500	44	300	1	300	1	1	0	auto	auto
duct59	orif21	yjun9	32	32	200	44	300	1	300	1	1	0	auto	auto
duct60	yjun14	orif24	32	32	200	44	300	1	300	1	1	0	auto	auto
duct61	orif31	orif25	32	32	1200	44	300	1	300	1	1	0	auto	auto
duct62	orif25	yjun10	32	32	200	44	300	1	300	1	1	0	auto	auto
duct63	yjun15	orif26	32	32	200	44	300	1	300	1	1	0	auto	auto
duct64	orif30	orif27	32	32	500	44	300	1	300	1	1	0	auto	auto
duct65	orif27	yjun11	32	32	200	44	300	1	300	1	1	0	auto	auto
duct66	yjun8	orif12	21	21	60	36	320	1	300	1	1	0	auto	auto
duct67	yjun9	orif16	21	21	50	36	300	1	300	1	1	0	auto	auto
duct68	yjun10	orif8	21	21	50	36	300	1	300	1	1	0	auto	auto
duct69	yjun11	orif4	21	21	50	36	300	1	300	1	1	0	auto	auto
duct70	orif28	orif18	32	32	75	44	300	1	300	1	1	0	auto	auto
duct71	orif29	orif22	32	32	75	44	300	1	300	1	1	0	auto	auto
duct72	orif30	orif26	32	32	75	44	300	1	300	1	1	0	auto	auto
duct73	orif31	orif24	32	32	75	44	300	1	300	1	1	0	auto	auto

```
ENG:GEOMETRY      ----------------------
4                 4       MOT     !       NCYL,ISTRK,ETYPE
81                77      135     0.1     !       BORE,STROKE,CRL,PINOFF
10                !       CR
1                 3       4       2       !       Timing:   IFIRE(1,NCYL)
0                 180     180     180     !       TDC       (1,NCYL)
0.5               0.006   630     0.2     !       Friction: ACF,BCF,CCF,QCF
0                 0       0       !       Output    :       IOUT1E,IOUT2E,IOUT3E
ENG:HEAT          TRANSFE ==========================================
original
1                 1       0       !       CENHTO,CENHTC
{tpis}            {thead} {tcyl}  {thead} {thead}   !       TWCYLP,TWCYLH,TWCYLS
1.05              1.1     1.5     !       AHTCYLP,AHTCYLH,SCLCYL
ENG:OPERATING     PARAMET ==========================================
{speed}           {pamb}  {tamb}  !       RPM,PAMBE,TAMBE
ENG:SI_WIEBE_COMB ----------------------
{thb50}           {bdur}  2       1       !       THB50,BDUR,WEXP,BURNFRAC
ENG:VALVES        ----------------------
NC,KEXC, (LEXD,IED,NVD--Repeated for each valve/duct)
4                 401     duct23  i       #1      duct24  i       #1      7501    e       #2      7511    e       #2
3                 402     duct32  i       #1      duct33  i       #1      7502    e       #2      7512    e       #2
2                 403     duct17  i       #1      duct18  i       #1      7503    e       #2      7513    e       #2
1                 404     duct9   i       #1      duct5   i       #1      7504    e       #2      7514    e       #2
FFT:FFT           ----------------------
ttitles
32                J:      301     J:      510
R                 85      S:      auto    auto
INJ:TYPE          ----------------------
1
prop
300               0.2     auto    0       0.2     40      auto
0                 0.1     0       0       0.9
INJ:VOLUME        ----------------------
1                 1       duct22  0       0
0                 {fard}  0
------------------!(separator)
2                 1       duct31  0       0
0                 {fard}  0
------------------!(separator)
3                 1       duct13  0       0
0                 {fard}  0
------------------!(separator)
4                 1       duct4   0       0
0                 {fard}  0
JUN:JUNCTION      DATA    ==========================================
KEX               KT1/KT2 AUX1    AUX2    AUX3    AUX4    AUX5
116               1       1       {thrt}
151               1       1       AUT
152               1       1       AUT
153               1       1       AUT
154               1       1       AUT
161               1       1       AUT
162               1       1       AUT
```

```
163              1     1     AUT
164              1     1     AUT
301              3     1     AUT       1     300   AUT    0     FIXED
401              4     1     SINGLEZONE
402              4     1     SINGLEZONE
403              4     1     SINGLEZONE
404              4     1     SINGLEZONE
501              5     2
502              5     2
503              5     2
505              5     2
506              5     2
507              5     2
508              5     2
509              5     2
510              5     2
551              5     2
552              5     2
553              5     2
554              5     2
amb1             3     1     AUTO      1     300   AUTO   0     FLOATING
amb2             3     1     AUTO      1     300   AUTO   0     FLOATING
orf1             1     1     auto
orf2             1     1     auto
orf3             1     1     auto
orf4             1     1     auto
orf5             1     1     auto
orf6             1     1     auto
orf7             1     1     auto
orf8             1     1     auto
orf9             1     1     auto
orf10            1     1     auto
orf11            1     1     auto
orf12            1     1     auto
orf13            1     1     auto
orf14            1     1     auto
orf15            1     1     auto
orf16            1     1     auto
orf17            1     1     auto
orf18            1     1     auto
orf19            1     1     auto
orf20            1     1     auto
orf21            1     1     auto
orf22            1     1     auto
orf23            1     1     auto
orf24            1     1     auto
orf25            1     1     auto
orf26            1     1     auto
orf27            1     1     auto
orf28            1     1     auto
orf29            1     1     auto
orf30            1     1     auto
orf31            1     1     auto
yjun1            5     2
yjun2            5     2
yjun3            5     2
yjun4            5     2
yjun5            5     2
yjun6            5     2
yjun7            5     2
yjun8            5     1
yjun9            5     1
yjun10           5     1
yjun11           5     1
yjun12           5     1
yjun13           5     1
yjun14           5     1
yjun15           5     1
JUN:YJUNCTION    DATA  ========================================================================
501              45    370   1      320   23656     2120      1     1      !      TP2: DIA5 TWL5 PK5 TK5 VOL5 AHT CFR5 CHT5
LEX              VDIR1 VDIR2 VDIR3  DIA   CDK       DELX      DIAB  THICK  COUNT
duct24           20    90    -70    AUT   AUT       15        45    0      1
duct22           180   -90   90     AUT   AUT       15        45    0      1
duct23           -20   90    -110   AUT   AUT       15        45    0      1
---------------- !separator
502              45    370   1      320   23656     2120      1     1      !      TP2: DIA5 TWL5 PK5 TK5 VOL5 AHT CFR5 CHT5
LEX              VDIR1 VDIR2 VDIR3  DIA   CDK       DELX      DIAB  THICK  COUNT
duct32           -20   90    -110   AUT   AUT       15        45    0      1
duct31           180   -90   90     AUT   AUT       15        45    0      1
duct33           20    90    -70    AUT   AUT       15        45    0      1
---------------- !separator
503              45    370   1      320   23656     2120      1     1      !      TP2: DIA5 TWL5 PK5 TK5 VOL5 AHT CFR5 CHT5
LEX              VDIR1 VDIR2 VDIR3  DIA   CDK       DELX      DIAB  THICK  COUNT
duct13           180   -90   90     AUT   AUT       15        45    0      1
duct17           -20   90    -110   AUT   AUT       15        45    0      1
duct18           20    90    -70    AUTO  AUTO      15        45    0      1
---------------- !separator
505              75    310   1      300   220893.2  16190.83  1     1      !      TP2: DIA5 TWL5 PK5 TK5 VOL5 AHT CFR5 CHT5
LEX              VDIR1 VDIR2 VDIR3  DIA   CDK       DELX      DIAB  THICK  COUNT
duct19           45    135   90     AUT   AUT       75        75    0      1
731              90    90    0      AUT   AUT       50        75    0      1
duct25           45    135   90     AUTO  AUTO      75        75    0      1
---------------- !separator
506              75    310   1      300   220893.2  11780.97  1     1      !      TP2: DIA5 TWL5 PK5 TK5 VOL5 AHT CFR5 CHT5
LEX              VDIR1 VDIR2 VDIR3  DIA   CDK       DELX      DIAB  THICK  COUNT
duct28           45    135   90     AUT   AUT       75        75    0      1
731              90    90    -180   AUT   AUT       50        75    0      1
732              90    90    0      AUT   AUT       50        75    0      1
duct34           45    135   90     AUTO  AUTO      75        75    0      1
---------------- !separator
507              75    310   1      300   220893.2  11780.97  1     1      !      TP2: DIA5 TWL5 PK5 TK5 VOL5 AHT CFR5 CHT5
LEX              VDIR1 VDIR2 VDIR3  DIA   CDK       DELX      DIAB  THICK  COUNT
duct10           45    135   90     AUT   AUT       75        75    0      1
732              90    90    -180   AUT   AUT       50        75    0      1
733              90    90    0      AUT   AUT       50        75    0      1
duct14           45    135   90     AUTO  AUTO      75        75    0      1
---------------- !separator
508              75    310   1      300   220893.2  11780.97  1     1      !      TP2: DIA5 TWL5 PK5 TK5 VOL5 AHT CFR5 CHT5
LEX              VDIR1 VDIR2 VDIR3  DIA   CDK       DELX      DIAB  THICK  COUNT
duct1            45    135   90     AUT   AUT       75        75    0      1
733              90    90    -180   AUT   AUT       50        75    0      1
734              90    90    0      AUT   AUT       50        75    0      1
duct6            45    135   90     AUTO  AUTO      75        75    0      1
---------------- !separator
509              182.2 300   1      300   1680000   72774.5   1     1      !      TP2: DIA5 TWL5 PK5 TK5 VOL5 AHT CFR5 CHT5
```

LEX	VDIR1	VDIR2	VDIR3	DIA	CDK	DELX	DIAB	THICK	COUNT									
737	150	240	90	AUT	AUT	120	140	0	1									
7038	-90	0	90	AUT	AUT	50	2.26	4	7853									
———	lseperator																	
510	152.2	300	1	300	2886000	72774.5	1	1	!	TP2:	DIA5	TWL5	PK5	TK5	VOL5	AHT CFR5	CHT5	
LEX	VDIR1	VDIR2	VDIR3	DIA	CDK	DELX	DIAB	THICK	COUNT									
739	-45	45	90	AUT	AUT	240	140	0	1									
7038	90	180	90	AUT	AUT	60	2.26	4	7853									
———	lseperator																	
561	35	450	1	450	14431.69	1649.3	1	1	!	TP2:	DIA5	TWL5	PK5	TK5	VOL5	AHT CFR5	CHT5	
LEX	VDIR1	VDIR2	VDIR3	DIA	CDK	DELX	DIAB	THICK	COUNT									
751	15	90	-75	AUT	AUT	15	35	0	1									
7501	165	-90	-75	AUT	AUT	15	35	0	1									
7511	195	90	105	AUT	AUT	15	35	0	1									
———	lseperator																	
562	35	450	1	450	14431.69	1649.3	1	1	!	TP2:	DIA5	TWL5	PK5	TK5	VOL5	AHT CFR5	CHT5	
LEX	VDIR1	VDIR2	VDIR3	DIA	CDK	DELX	DIAB	THICK	COUNT									
752	0	90	90	AUT	AUT	15	35	0	1									
7502	165	-90	-75	AUT	AUT	15	35	0	1									
7512	195	90	105	AUT	AUT	15	35	0	1									
———	lseperator																	
563	35	450	1	450	14431.69	1649.3	1	1	!	TP2:	DIA5	TWL5	PK5	TK5	VOL5	AHT CFR5	CHT5	
LEX	VDIR1	VDIR2	VDIR3	DIA	CDK	DELX	DIAB	THICK	COUNT									
753	0	90	90	AUT	AUT	15	35	0	1									
7503	165	-90	-75	AUT	AUT	15	35	0	1									
7513	195	90	105	AUT	AUT	15	35	0	1									
———	lseperator																	
564	35	450	1	450	14431.69	1649.3	1	1	!	TP2:	DIA5	TWL5	PK5	TK5	VOL5	AHT CFR5	CHT5	
LEX	VDIR1	VDIR2	VDIR3	DIA	CDK	DELX	DIAB	THICK	COUNT									
754	-15	90	-105	AUT	AUT	15	35	0	1									
7504	165	-90	-75	AUT	AUT	15	35	0	1									
7514	195	90	105	AUT	AUT	15	35	0	1									
———	lseperator																	
yjun1	45	370	1	320	31808.57	2827.4	1	1										
LEX	VDIR1	VDIR2	VDIR3	DIA	CDK	DELX	DIAB	THICK	COUNT									
duct3	165	-90	75	AUTO	AUTO	20	30	0	1									
duct4	0	90	90	AUTO	AUTO	20	45	0	1									
duct8	195	90	105	AUTO	AUTO	20	30	0	1									
———	lseperator																	
yjun2	45	370	1	320	23656	2120	1	1										
LEX	VDIR1	VDIR2	VDIR3	DIA	CDK	DELX	DIAB	THICK	COUNT									
duct4	160	-90	90	AUTO	AUTO	15	45	0	1									
duct5	20	90	-70	AUTO	AUTO	15	45	0	1									
duct9	-20	90	-110	AUTO	AUTO	15	45	0	1									
———	lseperator																	
yjun3	45	370	1	320	31808.57	2827.4	1	1										
LEX	VDIR1	VDIR2	VDIR3	DIA	CDK	DELX	DIAB	THICK	COUNT									
duct12	195	90	105	AUTO	AUTO	20	30	0	1									
duct13	0	90	90	AUTO	AUTO	20	45	0	1									
duct16	165	-90	75	AUTO	AUTO	20	30	0	1									
———	lseperator																	
yjun4	45	370	1	320	31808.57	2827.4	1	1										
LEX	VDIR1	VDIR2	VDIR3	DIA	CDK	DELX	DIAB	THICK	COUNT									
duct21	195	90	105	AUTO	AUTO	20	30	0	1									
duct22	0	90	90	AUTO	AUTO	20	45	0	1									
duct27	165	-90	75	AUTO	AUTO	20	30	0	1									
———	lseperator																	
yjun5	45	370	1	320	31808.57	2827.4	1	1										
LEX	VDIR1	VDIR2	VDIR3	DIA	CDK	DELX	DIAB	THICK	COUNT									
duct30	195	90	105	AUTO	AUTO	20	30	0	1									
duct31	0	90	90	AUTO	AUTO	20	45	0	1									
duct36	165	-90	75	AUTO	AUTO	20	30	0	1									
———	lseperator																	
yjun6	33	660	1	660	42765	5184	1	1										
LEX	VDIR1	VDIR2	VDIR3	DIA	CDK	DELX	DIAB	THICK	COUNT									
duct39	120	90	-30	AUTO	AUTO	50	33	0	1									
duct38	90	180	90	AUTO	AUTO	50	33	0	1									
duct49	-135	90	-135	AUTO	AUTO	50	33	0	1									
———	lseperator																	
yjun7	33	660	1	660	42765	5184	1	1										
LEX	VDIR1	VDIR2	VDIR3	DIA	CDK	DELX	DIAB	THICK	COUNT									
duct52	90	15	75	AUTO	AUTO	50	33	0	1									
duct42	90	180	90	AUTO	AUTO	50	33	0	1									
duct55	90	-15	105	AUTO	AUTO	50	33	0	1									
———	lseperator																	
yjun8	32	300	1	300	1	1												
LEX	VDIR1	VDIR2	VDIR3	DIA	CDK	DELX	DIAB	THICK	COUNT									
duct20	-90	0	90	AUTO	AUTO													
duct26	-90	0	90	AUTO	AUTO													
duct37	90	180	90	AUTO	AUTO													
duct56	180	90	90	AUTO	AUTO													
duct66	90	180	90	AUTO	AUTO													
———	lseperator																	
yjun9	32	300	1	300	1	1												
LEX	VDIR1	VDIR2	VDIR3	DIA	CDK	DELX	DIAB	THICK	COUNT									
duct35	-90	0	90	AUTO	AUTO													
duct29	-90	0	90	AUTO	AUTO													
duct40	90	180	90	AUTO	AUTO													
duct67	90	180	90	AUTO	AUTO													
duct59	-180	90	90	AUTO	AUTO													
———	lseperator																	
yjun10	32	300	1	300	1	1												
LEX	VDIR1	VDIR2	VDIR3	DIA	CDK	DELX	DIAB	THICK	COUNT									
duct15	-90	0	90	AUTO	AUTO													
duct11	-90	0	90	AUTO	AUTO													
duct62	180	90	90	AUTO	AUTO													
duct68	90	180	90	AUTO	AUTO													
duct41	90	180	90	AUTO	AUTO													
———	lseperator																	
yjun11	32	300	1	300	1	1												
LEX	VDIR1	VDIR2	VDIR3	DIA	CDK	DELX	DIAB	THICK	COUNT									
duct7	-90	0	90	AUTO	AUTO													
duct2	-90	0	90	AUTO	AUTO													
duct43	90	180	90	AUTO	AUTO													
duct69	90	180	90	AUTO	AUTO													
duct65	-180	90	90	AUTO	AUTO													
———	lseperator																	
yjun12	33	300	1	300	1	1												
LEX	VDIR1	VDIR2	VDIR3	DIA	CDK	DELX	DIAB	THICK	COUNT									
751	-180	90	90	AUTO	AUTO													
duct46	0	90	90	AUTO	AUTO													
duct53	-90	0	90	AUTO	AUTO													
———	lseperator																	
yjun13	33	300	1	300	1	1												
LEX	VDIR1	VDIR2	VDIR3	DIA	CDK	DELX	DIAB	THICK	COUNT									

```
752            180       90        90        AUTO      AUTO
duct46         0         90        90        AUTO      AUTO
duct57         -90       0         90        AUTO      AUTO
-------------- !separator
yjun14         33        300       1         300       1         1
LEX            VDIR1     VDIR2     VDIR3     DIA       CDK       DELX      DIAB      THICK     COUNT
753            180       90        90        AUTO      AUTO
duct60         0         90        90        AUTO      AUTO
duct60         -90       0         90        AUTO      AUTO
-------------- !separator
yjun15         33        300       1         300       1         1
LEX            VDIR1     VDIR2     VDIR3     DIA       CDK       DELX      DIAB      THICK     COUNT
754            180       90        90        AUTO      AUTO
duct63         -90       0         90        AUTO      AUTO
duct51         0         90        90        AUTO      AUTO
VAL:VALVES     ----------------------
#1             GENL      28        465       0.1       !NV,VFLAG,DVALVE,THCYCLE,VLASH
POLY           FAST                ICAMCR,THVALV,HSCALE,VSCALE,ROCKER
8.3            250
VLI2:
0              0.032     0.065     0.097     0.129     0.161     0.194     0.226     0.258     0.29      0.34      #
CDF2:
0              0.088     0.176     0.259     0.339     0.41      0.451     0.479     0.495     0.496     0.497     #
CDR2:
0              0.088     0.176     0.259     0.339     0.41      0.451     0.479     0.496     0.498     0.497     #
-------------- !(seperator)
#2             GENL      23.5      255       0.15      !NV,VFLAG,DVALVE,THCYCLE,VLASH
POLY           FAST                ICAMCR,THVALV,HSCALE,VSCALE,ROCKER
8              250
VLI2:
0              0.038     0.075     0.113     0.151     0.189     0.226     0.264     0.302     0.34      0.365     #
CDF2:
0              0.108     0.235     0.39      0.508     0.562     0.581     0.587     0.59      0.59      0.59      #
CDR2:
0              0.108     0.235     0.39      0.508     0.562     0.581     0.587     0.59      0.59      0.59      #
END:RUN        ----------------------


BAS:CONSTANTS
$case          =    1.,          $subcase   =    0.,          $fullcase  =    1.0,    $prefix  =    1000,       $date   =    26-Feb-2004,  $version  =  5.1
$path          =    ./1000.wvm   $file      =    1000.wvm,    $dir       =    ./,     $pi      =    3.1415927   NCYC    =    12,           SPEED     =  1000
PAMB           =    1.013,       TAMB       =    298,         TH650      =    9,      BDUR     =    28,         TP1S    =    500,          THEAD     =  550,     TCYL  =  540
THRT           =    48,          FARD       =    0.06
BAS:GENERAL
!***           'SKIPINIT' SET    TO         'N'       FOR       FIRST     CASE
!***           reading   active.tags found  in        /usr/Ricardo/wave/5.1/config
!***           Loading   property  data:    INDOLENE /usr/Ricardo/wave/5.1/propty/indolene.fue
INDOLENE
BAS:TITLE
Motored        Manifold  Bridge    Engine    1000      rpm
26-Feb-04      9:07:09
BAS:OUTPUT
DUC:DUCT
DUC:BENDS
DUCT           ANGLE     Cp
761            35        0.083
762            45        0.108
763            45        0.108
764            35        0.083
duct2          55        0.123
duct7          55        0.123
duct11         55        0.123
duct15         55        0.123
duct20         55        0.123
duct26         55        0.123
duct29         55        0.123
duct36         55        0.123
duct37         55        0.123
duct40         55        0.123
duct41         55        0.123
duct43         55        0.123
duct46         30        0.066
duct56         180       0.246
duct59         180       0.246
duct62         180       0.246
duct65         180       0.246
duct66         55        0.123
duct67         55        0.123
duct68         55        0.123
duct69         55        0.123
duct70         90        0.19
duct71         90        0.19
duct72         90        0.19
duct73         90        0.19
JUN:JUNCTION
JUN:YJUNCTION
ENG:GEOMETRY

FIRING SEQUENCE, FIRING TDC, AND FIRING INTERVALS
1              3         4         2
0              180       360       540
180            180       180       180

!***           THIS      IS        A         MOTORIN RUN
ENG:HEAT
ENG:OPERATING
FFT:FFT
!***           REQUESTED PLOT ID'S AND TITLES
PLOT           #         185FFT:   SOUND     PRESSUR LEVEL    VS.       FREQUENCY
LOCATIONS:     FFT#      301       FFT#      510
VAL:VALVES
!***           VALVE     #1:       TVO       =         345.4055,  TVC      =         584.5945  FLOW      COEF      BASED     ON        SEAT   AREA
!***           NV        =         1         AEFFMAX = 305.9      (mm2)    DVALVE(N =          28        (mm)      CDMAX     =      0.42404
!***           VALVE     #2:       TVO       =         138.7137,  TVC      =         373.2863  FLOW      COEF      BASED     ON        SEAT   AREA
!***           NV        =         2         AEFFMAX = 258.4      (mm2)    DVALVE(N =          23.5      (mm)      CDMAX     =      0.44238
ENG:VALVES
ENG:SI_WIEBE_COMB
INJ:TYPE
INJ:VOLUME
BAS:TIME
!***           REQUESTED PLOT ID'S AND TITLES
PLOT           #         2201PRESSURE
LOCATIONS:     JUNC:     401
PLOT           #         3202TEMPERATURE
LOCATIONS:     JUNC:     401
```

PLOT	#	4201PRESSURE		
LOCATIONS:	DUCT:	761		
PLOT	#	5110LOG-I CYCLE	P-V	PLOT
LOCATIONS:	JUNC:	401		
PLOT	#	6201PRESSURE		
LOCATIONS:	DUCT:	734		
PLOT	#	7201PRESSURE		
LOCATIONS:	DUCT:	739		
END				

I*** BEGINNING 720 DEGREE CYCLIC WAVE SIMULATION

TOTAL	DUCTS	:	98	TOTAL	JUNCTION:		75			
TOTAL	VOLUMES 256		TOTAL	BOUNDAF 352						
REG.	VOLUMES 253		INT.	BOUNDAF 160		DUCT/JUN	BOUNDAF 192		AUX.	VOLUM 3

TITLE:	Motored	Manifold	Bridge	Engine	1000	rpm								
NC	ICYC	ISTEP	AIR-KG/HF	VOLEF	TEXH	PHI	IMEP	PMEP	IHP	ISFC	PCYL	TCYL	FTR	
ENG:	1	0	1	0	0	470	0	0	0	0	0	1.001	340.1	0
ENG	VOLEF(TC	=	0	PHI(1)	=	0								
ENG:	3	1	1381	0	0	470	0	0	0	0	0	1.091	367.7	0
ENG:	4	1	2757	0	0	470	0	0	0	0	0	1.094	370.7	0
ENG:	2	1	4136	0	0	470	0	0	0	0	0	1.075	374.7	0
ENG:	1	1	5512	10.84	0.772	370.3	0	-0.11	-0.028	-0.05	0	1.079	372.7	0
ENG	VOLEF(TC	=	0.193	PHI(1)	=	0								
ENG:	3	2	6862	11.22	0.799	383.2	0	-0.135	-0.026	-0.06	0	1.081	367.8	0
ENG:	4	2	8253	11.06	0.788	385.8	0	-0.14	-0.028	-0.06	0	1.082	368.6	0
ENG:	2	2	9624	11.1	0.791	389.4	0	-0.14	-0.026	-0.06	0	1.083	369.7	0
ENG:	1	2	10992	11.08	0.786	388.4	0	-0.141	-0.028	-0.06	0	1.084	369.6	0
ENG	VOLEF(TC	=	0.7912	PHI(1)	=	0								
I***	AUTO-COI	Uvariance	=	3.15	Pvariance	=	1.18E-02							
ENG:	3	3	12360	11.2	0.798	384.6	0	-0.134	-0.026	-0.06	0	1.081	367.2	0
ENG:	4	3	13728	11.04	0.787	385.2	0	-0.137	-0.028	-0.06	0	1.081	368.4	0
ENG:	2	3	15098	11.16	0.796	385.7	0	-0.137	-0.026	-0.06	0	1.083	368.1	0
ENG:	1	3	16475	10.99	0.783	385.6	0	-0.138	-0.027	-0.06	0	1.083	371.2	0
ENG	VOLEF(TC	=	0.7906	PHI(1)	=	0								
I***	AUTO-COI	Uvariance	=	5.55E-02	Pvariance	=	3.58E-03							
ENG:	3	4	17849	11.22	0.799	384.2	0	-0.134	-0.026	-0.06	0	1.082	367.4	0
ENG:	4	4	19226	11.02	0.785	385.1	0	-0.137	-0.028	-0.06	0	1.081	369.6	0
ENG:	2	4	20608	11.16	0.796	384.6	0	-0.136	-0.026	-0.06	0	1.083	368.2	0
ENG:	1	4	22010	10.68	0.761	386.8	0	-0.139	-0.027	-0.06	0	1.083	380.7	0
ENG	VOLEF(TC	=	0.7849	PHI(1)	=	0								
I***	AUTO-COI	Uvariance	=	0.1539	Pvariance	=	2.19E-03							
ENG:	3	5	23400	11.21	0.798	384.3	0	-0.134	-0.026	-0.06	0	1.082	367.7	0
ENG:	4	5	24797	10.67	0.774	388	0	-0.138	-0.027	-0.06	0	1.082	374.7	0
ENG:	2	5	26198	11.14	0.794	384.6	0	-0.135	-0.026	-0.06	0	1.083	368.7	0
ENG:	1	5	27606	10.51	0.748	393.7	0	-0.147	-0.027	-0.06	0	1.083	386.5	0
ENG	VOLEF(TC	=	0.7765	PHI(1)	=	0								
I***	AUTO-COI	Uvariance	=	5.61E-02	Pvariance	=	2.21E-03							
ENG:	3	6	29003	11.15	0.794	384.5	0	-0.135	-0.026	-0.06	0	1.083	369.2	0
ENG:	4	6	30408	10.7	0.762	389.7	0	-0.141	-0.027	-0.06	0	1.082	380.5	0
ENG:	2	6	31811	11.13	0.792	385.1	0	-0.138	-0.028	-0.06	0	1.083	369.2	0
ENG:	1	6	33222	10.49	0.747	397.9	0	-0.151	-0.026	-0.07	0	1.083	387.7	0
ENG	VOLEF(TC	=	0.7738	PHI(1)	=	0								
I***	AUTO-COI	Uvariance	=	3.58E-02	Pvariance	=	1.73E-03							
ENG:	3	7	34620	11.06	0.787	385.5	0	-0.135	-0.026	-0.06	0	1.082	371.9	0
ENG:	4	7	36028	10.63	0.757	393.9	0	-0.146	-0.027	-0.06	0	1.082	383	0
ENG:	2	7	37432	11.12	0.792	385.4	0	-0.137	-0.028	-0.06	0	1.083	369.7	0
ENG:	1	7	38843	10.49	0.747	398.7	0	-0.152	-0.026	-0.07	0	1.084	387.9	0
ENG	VOLEF(TC	=	0.7706	PHI(1)	=	0								
I***	AUTO-COI	CONDITIO	MET											
ENG:	3	8	40243	10.97	0.782	387.5	0	-0.138	-0.026	-0.06	0	1.082	374.4	0
ENG:	4	8	41651	10.62	0.756	395.7	0	-0.147	-0.027	-0.07	0	1.081	383.7	0
ENG:	2	8	43056	11.1	0.791	385.7	0	-0.137	-0.026	-0.06	0	1.084	370.2	0
ENG:	1	8	44468	10.48	0.747	398.8	0	-0.152	-0.026	-0.07	0	1.084	388	0
ENG	VOLEF(TC	=	0.7687	PHI(1)	=	0								
I***	AUTO-COI	CONDITIO	MET											
ENG:	3	9	45670	10.93	0.779	389.3	0	-0.14	-0.026	-0.06	0	1.083	375.8	0
ENG:	4	9	47279	10.61	0.758	396.2	0	-0.149	-0.027	-0.07	0	1.082	384.2	0
ENG:	2	9	48683	11.07	0.789	386.1	0	-0.137	-0.026	-0.06	0	1.083	371	0
ENG:	1	9	50096	10.48	0.746	398.9	0	-0.152	-0.026	-0.07	0	1.084	388.2	0
ENG	VOLEF(TC	=	0.7673	PHI(1)	=	0								
I***	AUTO-COI	CONDITIO	MET											
I***	*FAST*	*FOURIER*	*TRANSFO*	–	#	*OF*	*HARMONI*	=	32					
I***	FFT	COMPLETE												

TIME	STEP	OUTPUT:	TOTAL	STEPS	IN	LAST	CYCLE	=	5628	
LIMITING	ELEMENT	%	STEPS	(DOES	NOT	HAVE	TO	ADD	TO	100)
DUCT:	duct4	64.3	DUCT:	duct22	25.4	DUCT:	duct31	10.3		

TITLE: Motored Manifold Bridge Engine 1000 rpm

FINAL OUTPUTS OF DUCTS

Duct K	Junction K	TWALL BAR	TAV BAR	PAV BAR	PMAX M/S	PMIN M/S	UMAX NUMBER	UMIN KG/S	MACH CM2	FLOW KW	A	CDout	CDin	HTKW
731	506	0	0	0	0	0	4.2	-2.5	0.0118	0.0004	44.17865	1	1	0
732	507	300	309.1	1	1.012	0.99	4.2	-2.9	0.0118	0.0021	44.17865	1	1	0.001
506	300	309.1	1	1.012	0.99	4.1	-2.9	0.0116	0.00209	44.179	1	1		
733	508	0	0	0	0	0	4.6	-3.4	0.0129	0.0036	44.17865	1	1	0
734	116	300	301.9	1	1.01	0.991	11.6	-5.5	0.0332	0.0041	18.09558	0.81	0.81	0
508	300	301.9	1	1.01	0.991	5.9	-3	0.0169	0.00414	28.274	1	0.88		
737	509	300	300	1	1.004	0.998	7.1	-3.3	0.0205	0.0041	33.18308	1	0.81	0
orif20	300	300	1	1.005	0.998	5.6	-3.1	0.0162	0.00414	33.183	1	1		
739	301	300	300	1	1.002	0.998	8.2	-4	0.0236	0.0041	33.18308	1	0.8	0
510	300	300	1	1.002	0.998	6.5	-4.9	0.0188	0.00414	33.183	1	0.81		
751	551	850	425.9	1	1.013	0.987	28.2	-8.8	0.0704	0.003	8.55299	1	0.98	-0.095
yjun12	850	441.7	1	1.012	0.988	36.5	-10.4	0.0894	0.00295	7.0686	0.94	1		
752	552	850	427	1	1.018	0.984	28	-9.1	0.0701	0.003	8.55299	1	0.98	-0.138
yjun13	850	447.9	1	1.016	0.985	36.9	-10.9	0.0899	0.00304	7.0686	0.94	1		

753	653	650	423.4	1	1.016	0.982	28.4	-10.2	0.0712	0.0031	8.55299	1	0.96	-0.139
yjun14	650	444.9	1	1.015	0.984	37.7	-13	0.0924	0.00306	7.0686	0.94	1		
754	554	650	436.1	1	1.017	0.983	28.3	-9.6	0.07	0.0029	8.55299	1	0.96	-0.132
yjun15	650	456	1	1.017	0.985	37.3	-11.8	0.0901	0.00291	7.0686	0.94	1		
761	151	650	491.5	1	1.011	0.991	23.8	-12.8	0.0571	0.0005	8.55299	1	1	-0.074
161	650	491.5	1	1.011	0.991	24.5	-12.7	0.0575	0.00047	8.553	1	1		
762	152	650	496.8	1	1.012	0.989	27.1	-9.5	0.0648	0.0017	8.55299	1	1	-0.07
162	650	496.8	1	1.012	0.989	28	-9.4	0.0656	0.00168	8.553	1	1		
763	153	650	504.5	1	1.01	0.99	27.2	-11.3	0.0646	0.0016	8.55299	1	1	-0.071
163	650	504.5	1	1.01	0.99	28.1	-11.3	0.0647	0.00161	8.553	1	1		
764	154	650	511.6	1	1.013	0.986	24	-11.4	0.0567	0.0005	8.55299	1	1	-0.067
164	650	511.6	1	1.013	0.986	24.8	-11.8	0.0571	0.0005	8.553	1	1		
7038	510	0	0	0	0	0	0.6	-0.4	0.0018	0.0041	0.04012	1	1	0
7501	401	470	405.7	1.002	1.018	0.984	157.5	-66	0.4053	0.0015	2.56441	1	1	-0.008
551	470	405.7	1.002	1.018	0.984	64.6	-26.3	0.1614	0.00148	1.7672	1	0.81		
7502	402	470	400.7	1.001	1.019	0.981	184.7	-67.3	0.4791	0.0015	0	1	1	-0.009
552	470	400.7	1.001	1.019	0.981	64.1	-27.2	0.1606	0.00152	1.7672	1	0.81		
7503	403	470	396.9	1.001	1.02	0.975	190.1	-74.7	0.4959	0.0015	0	1	1	-0.009
553	470	396.9	1.001	1.02	0.975	64.7	-30.2	0.1628	0.00154	1.7672	1	0.81		
7504	404	470	409.3	1.002	1.021	0.982	162.7	-64.3	0.4168	0.0015	0	1	1	-0.007
554	470	409.3	1.002	1.021	0.982	64.7	-28.6	0.1605	0.00145	1.7672	1	0.81		
7511	401	470	405.8	1.002	1.018	0.984	157.5	-66	0.4053	0.0015	2.56441	1	1	-0.008
551	470	405.8	1.002	1.018	0.984	64.8	-26.5	0.1614	0.00147	1.7672	1	0.81		
7512	402	470	400.7	1.001	1.019	0.981	184.7	-67.3	0.4791	0.0015	0	1	1	-0.009
552	470	400.7	1.001	1.019	0.981	64.1	-27.2	0.1606	0.00152	1.7672	1	0.81		
7513	403	470	396.9	1.001	1.02	0.975	190.1	-74.7	0.4959	0.0015	0	1	1	-0.009
553	470	396.9	1.001	1.02	0.975	64.7	-30.2	0.1628	0.00154	1.7672	1	0.81		
7514	404	470	409.2	1.002	1.021	0.982	162.7	-64.3	0.4168	0.0015	0	1	1	-0.006
554	470	409.2	1.002	1.021	0.982	64.7	-28.5	0.1605	0.00146	1.7672	1	0.81		
duct1	508	300	319	0.969	1.009	0.989	33.4	-14.4	0.0945	0.0003	3.46361	1	0.8	0.008
orif2	300	328.5	0.999	1.013	0.985	26.5	-14.4	0.0746	0.00025	3.4636	1	1		
duct2	orif2	320	334.3	0.999	1.016	0.983	26.5	-14.4	0.0746	0.0003	3.46361	1	1	0.003
yjun11	320	334.3	0.999	1.016	0.983	26.4	-16.7	0.0742	0.00025	3.4636	1	0.85		
duct3	orif4	340	333.7	0.999	1.021	0.975	34.2	-15.8	0.0934	0.0015	3.46361	0.85	1	-0.002
yjun1	340	337.8	0.999	1.022	0.972	15.9	-5.1	0.0432	0.00145	7.0686	1	1		
duct4	yjun1	370	339.8	0.999	1.022	0.972	14.1	-4.4	0.0382	0.0029	15.90431	1	1	-0.001
yjun2	370	339.8	0.999	1.022	0.972	14	-4.4	0.0381	0.00291	15.904	1	1		
duct5	yjun2	370	344	0.999	1.022	0.97	21.7	-5.6	0.0591	0.0015	6.15752	1	0.83	-0.003
404	370	344	0.999	1.022	0.97	47.9	-142.5	0.3659	0.00146	0.0014	1	1		
duct6	505	300	319	0.999	1.009	0.989	33.4	-14.4	0.0945	0.0003	3.46361	1	0.8	0.008
orif1	300	328.5	0.999	1.013	0.985	26.5	-14.4	0.0746	0.00025	3.4636	1	1		
duct7	orif1	320	334.3	0.999	1.016	0.983	26.5	-14.4	0.0746	0.0003	3.46361	1	1	0.003
yjun11	320	334.3	0.999	1.016	0.983	26.4	-16.7	0.0742	0.00025	3.4636	1	0.85		
duct8	orif3	340	334.8	0.999	1.021	0.975	34.3	-15.9	0.0936	0.0015	3.46361	0.85	1	-0.002
yjun1	340	338.5	0.999	1.022	0.972	15.9	-5.1	0.0433	0.00146	7.0686	1	1		
duct9	yjun2	370	344	0.999	1.022	0.97	21.7	-5.6	0.0591	0.0015	6.15752	1	0.83	-0.003
404	370	344	0.999	1.022	0.97	47.9	-142.5	0.3659	0.00146	0.0014	1	1		
duct10	507	300	308.3	0.999	1.011	0.985	36.1	-15.9	0.1023	0.0008	3.46361	1	0.8	0.002
orif5	300	308.6	0.999	1.011	0.984	28.5	-15.6	0.081	0.00078	3.4636	1	1		
duct11	orif5	320	309.5	0.999	1.012	0.983	28.5	-15.6	0.081	0.0008	3.46361	1	1	-0.001
yjun10	320	309.5	0.999	1.012	0.983	28.4	-17.9	0.0806	0.00078	3.4636	1	0.85		
duct12	orif7	340	311.7	0.999	1.018	0.975	33.1	-12.9	0.094	0.0015	3.46361	0.85	1	-0.012
yjun3	340	316.5	0.999	1.021	0.972	15.8	-4.6	0.0442	0.00154	7.0686	1	1		
duct13	yjun3	370	318.4	0.999	1.021	0.971	13.9	-4	0.039	0.0031	15.90431	1	1	-0.002
503	370	318.4	0.999	1.021	0.971	13.9	-3.9	0.0389	0.00307	15.904	1	1		
duct14	507	300	308.3	0.999	1.011	0.985	36.1	-15.9	0.1023	0.0008	3.46361	1	0.8	0.002
orif6	300	308.6	0.999	1.011	0.984	28.6	-15.6	0.081	0.00078	3.4636	1	1		
duct15	orif6	320	309.5	0.999	1.012	0.983	28.5	-15.6	0.081	0.0008	3.46361	1	1	-0.001
yjun10	320	309.5	0.999	1.012	0.983	28.4	-17.9	0.0806	0.00078	3.4636	1	0.85		
duct16	orif8	340	310.7	0.999	1.018	0.975	33	-12.9	0.0938	0.0015	3.46361	0.85	1	-0.012
yjun3	340	315.8	0.999	1.021	0.972	15.7	-4.6	0.0441	0.00153	7.0686	1	1		
duct17	503	370	324.8	0.999	1.021	0.97	21.5	-4.9	0.0602	0.0015	6.15752	1	0.83	-0.005
403	370	324.8	0.999	1.021	0.97	50	-133.4	0.3499	0.00154	0	1	1		
duct18	503	370	324.8	0.999	1.021	0.97	21.5	-4.9	0.0602	0.0015	6.15752	1	0.83	-0.005
403	370	324.8	0.999	1.021	0.97	50	-133.4	0.3499	0.00154	0	1	1		
duct19	505	300	319.8	0.999	1.012	0.987	32.3	-14.6	0.0906	0.0002	3.46361	1	0.8	0.007
orif9	300	325	0.999	1.011	0.984	25.5	-13.9	0.0716	0.00022	3.4636	1	1		
duct20	orif9	320	326.5	0.999	1.011	0.982	25.5	-13.9	0.0716	0.0002	3.46361	1	1	0.001
yjun8	320	326.5	0.999	1.011	0.982	25.5	-15.8	0.0715	0.00022	3.4636	1	0.85		
duct21	orif11	340	329.7	0.999	1.015	0.973	34.9	-12.7	0.096	0.0015	3.46361	0.85	1	-0.004
yjun4	340	333.3	0.999	1.018	0.969	16.4	-4	0.045	0.00147	7.0686	1	1		
duct22	yjun4	370	335.1	0.999	1.018	0.969	14.6	-3.6	0.0397	0.003	15.90431	1	1	-0.001
501	370	335.1	0.999	1.018	0.969	14.4	-3.6	0.0395	0.00295	15.904	1	1		
duct23	501	370	339.9	0.999	1.019	0.967	22.4	-4.6	0.0612	0.0015	6.15752	1	0.83	-0.003
401	370	339.9	0.999	1.019	0.967	36.8	-133.4	0.3438	0.00147	0	1	1		
duct24	501	370	339.9	0.999	1.019	0.967	22.4	-4.6	0.0612	0.0015	6.15752	1	0.83	-0.003

401	370	339.9	0.999	1.019	0.967	36.8	-133.4	0.3438	0.00147	0	1	1		
duct25	505	300	319.8	0.999	1.012	0.987	32.3	-14.6	0.0606	0.0002	3.46361	1	0.8	0.007
orif10	300	325	0.999	1.011	0.984	25.6	-13.9	0.0716	0.00022	3.4636	1	1		
duct26	orif10	320	328.5	0.999	1.011	0.982	25.5	-13.9	0.0716	0.0002	3.46361	1	1	0.001
yjun8	320	328.5	0.999	1.011	0.982	25.5	-15.8	0.0715	0.00022	3.4636	1	0.85		
duct27	orif12	340	329.7	0.999	1.015	0.973	34.9	-12.7	0.096	0.0015	3.46361	0.85	1	-0.004
yjun4	340	333.3	0.999	1.018	0.969	16.4	-4	0.045	0.00147	7.0686	1	1		
duct28	506	300	311.9	0.999	1.012	0.988	34.7	-11	0.098	0.0008	3.46361	1	0.8	0.004
orif13	300	314.1	0.999	1.011	0.987	27.3	-11.1	0.0773	0.00083	3.4636	1	1		
duct29	orif13	320	316.4	0.999	1.011	0.985	27.3	-11.1	0.0773	0.0008	3.46361	1	1	0
yjun9	320	316.4	0.999	1.011	0.985	27.1	-13.1	0.0766	0.00083	3.4636	1	0.85		
duct30	orif15	340	318.9	0.998	1.016	0.977	32.7	-14.7	0.0918	0.0015	3.46361	0.85	1	-0.009
yjun5	340	323	0.999	1.02	0.976	15.3	-5.1	0.0425	0.00152	7.0686	1	1		
duct31	yjun5	370	324.8	0.999	1.02	0.976	13.5	-4.4	0.0376	0.003	15.90431	1	1	-0.002
502	370	324.8	0.999	1.02	0.976	13.5	-4.3	0.0375	0.00303	15.904	1	1		
duct32	502	370	330.6	0.999	1.021	0.974	21	-5.5	0.0583	0.0015	6.15752	1	0.83	-0.004
402	370	330.6	0.999	1.021	0.974	49.4	-137.1	0.3676	0.00152	2.8553	1	1		
duct33	502	370	330.6	0.999	1.021	0.974	21	-5.5	0.0583	0.0015	6.15752	1	0.83	-0.004
402	370	330.6	0.999	1.021	0.974	49.4	-137.1	0.3676	0.00152	2.8553	1	1		
duct34	506	300	311.6	0.999	1.012	0.988	34.7	-10.9	0.0981	0.0008	3.46361	1	0.8	0.004
orif14	300	313.5	0.999	1.011	0.987	27.4	-11.1	0.0774	0.00083	3.4636	1	1		
duct35	orif14	300	315	0.999	1.011	0.985	27.4	-11.1	0.0774	0.0008	3.46361	1	1	0.002
yjun9	300	315	0.999	1.011	0.985	27.1	-13.1	0.0765	0.00083	3.4636	1	0.85		
duct36	orif16	340	317.9	0.999	1.016	0.977	32.6	-14.7	0.0916	0.0015	3.46361	0.85	1	-0.009
yjun5	340	322.2	0.999	1.02	0.976	15.2	-5.1	0.0424	0.00151	7.0686	1	1		
duct37	yjun8	320	329.4	0.999	1.014	0.973	40.9	-11	0.1128	0.0015	3.46361	1	0.85	0.001
orif11	320	329.4	0.999	1.014	0.973	34.9	-12.7	0.096	0.00147	3.4636	1	0.85		
duct38	yjun6	800	483.1	1	1.003	0.997	23.9	-21.4	0.0512	0.001	8.55299	0.9	1	-0.085
amb1	800	483.1	1	1.003	0.997	17.5	-16.9	0.042	0.00097	11.946	1	0.8		
duct39	161	850	499	1	1.009	0.992	24.5	-12.7	0.0675	0.0005	8.55299	1	1	-0.097
yjun6	850	502.6	1	1.008	0.992	25.3	-12.6	0.0568	0.00047	8.553	1	1		
duct40	yjun9	320	318.1	0.998	1.014	0.976	38.4	-12.7	0.1079	0.0015	3.46361	1	0.85	0
orif15	320	318.1	0.998	1.014	0.976	32.7	-14.7	0.0918	0.00152	3.4636	1	0.85		
duct41	yjun10	320	310.3	0.998	1.016	0.975	38.6	-11.3	0.1097	0.0015	3.46361	1	0.85	-0.001
orif7	320	310.3	0.998	1.016	0.975	33.1	-12.9	0.094	0.00153	3.4636	1	0.85		
duct42	yjun7	800	532.6	1	1.002	0.998	29.8	-19.4	0.0652	0.0033	8.55299	0.9	1	-0.075
amb2	800	532.6	1	1.002	0.998	21.7	-15.5	0.0461	0.00329	11.946	1	0.8		
duct43	yjun11	320	335	0.999	1.019	0.975	40.2	-13.8	0.1107	0.0015	3.46361	1	0.85	0.002
orif3	320	335	0.999	1.019	0.975	34.3	-15.9	0.0936	0.00146	3.4636	1	0.85		
duct44	orif17	300	300.4	1	1.009	0.992	6.5	-3.1	0.0186	0.0041	28.27434	1	0.95	0
116	300	300.4	1	1.009	0.992	11.6	-6.5	0.0332	0.00414	18.096	0.81	0.81		
duct45	yjun12	850	475	1	1.011	0.99	28.4	-16.6	0.0696	0.0005	7.06858	0.94	1	-0.027
151	850	475	1	1.011	0.99	23.8	-12.8	0.0571	0.00046	8.553	1	1		
duct46	orif20	300	300	1	1.006	0.995	5.6	-3.1	0.0162	0.0041	33.18308	1	1	0
orif19	300	300	1	1.006	0.995	5.5	-3	0.0159	0.00414	33.183	1	1		
duct47	orif19	300	300	1	1.007	0.994	5.5	-3	0.0159	0.0041	33.18308	1	1	0
orif17	300	300.1	1	1.008	0.993	6.5	-3.1	0.0186	0.00414	28.274	0.95	1		
duct48	yjun13	850	474.5	1	1.014	0.988	32.1	-12.4	0.0785	0.0017	7.06858	0.94	1	-0.039
152	850	474.5	1	1.014	0.988	27.1	-9.6	0.0648	0.00168	8.553	1	1		
duct49	164	850	523.1	1	1.01	0.99	24.8	-11.8	0.0571	0.0005	8.55299	1	1	-0.165
yjun6	850	527.6	1	1.007	0.992	26.4	-12	0.0561	0.00051	8.553	1	1		
duct50	yjun14	850	482	1	1.011	0.988	32	-14.7	0.0767	0.0016	7.06858	0.94	1	-0.064
153	850	482	1	1.011	0.988	27.2	-11.3	0.0646	0.00161	8.553	1	1		
duct51	yjun15	850	494	1	1.014	0.987	28.5	-14.5	0.0689	0.0005	7.06858	0.94	1	-0.037
154	850	494	1	1.014	0.987	24	-11.4	0.0567	0.0005	8.553	1	1		
duct52	163	850	520.8	1	1.008	0.992	28.1	-11.3	0.0647	0.0016	8.55299	1	1	-0.112
yjun7	850	532.7	1	1.008	0.993	29.2	-11.1	0.0634	0.00161	8.553	1	1		
duct53	yjun12	300	471.1	1	1.013	0.987	14.9	-4.6	0.0344	0.0025	7.06858	0.95	1	0.085
orif22	300	443.9	1	1.017	0.985	12	-3.2	0.0285	0.00249	8.0425	1	1		
duct54	orif29	300	427.7	1	1.018	0.984	11.5	-2.7	0.0271	0.0025	8.04248	1	1	0.185
orif23	300	359.1	1	1.014	0.98	9	-3.7	0.0239	0.0025	8.0425	1	1		
duct55	162	850	514.4	1	1.01	0.992	20	-9.4	0.0656	0.0017	8.55299	1	1	-0.11
yjun7	850	528.8	1	1.008	0.994	29.3	-9.4	0.0653	0.00168	8.553	1	1		
duct56	orif23	300	356.9	1	1.014	0.98	9	-3.7	0.0239	0.0025	8.04248	1	1	0.027
yjun8	300	347.8	1	1.014	0.981	11.7	-6.4	0.0314	0.0025	6.6467	0.94	1		
duct57	yjun13	300	459.6	0.999	1.015	0.985	11.4	-5.9	0.0268	0.0014	7.06858	0.95	1	0.086
orif18	300	420.1	0.999	1.017	0.982	9.1	-4.6	0.0222	0.00136	8.0425	1	1		
duct58	orif28	300	399.3	0.999	1.018	0.982	8.6	-4.2	0.0215	0.0014	8.04248	1	1	0.082
orif21	300	346.2	0.999	1.011	0.983	6.8	-5.3	0.0182	0.00137	8.0425	1	1		
duct59	orif21	300	343.5	0.999	1.011	0.983	6.8	-5.3	0.0182	0.0014	8.04248	1	1	0.018
yjun9	300	331.6	0.999	1.011	0.985	9	-7.8	0.0246	0.00137	6.6467	0.94	1		
duct60	yjun14	300	464.6	0.999	1.013	0.986	11.9	-3.3	0.0281	0.0015	7.06858	0.95	1	0.068
orif24	300	426	0.999	1.013	0.985	9.4	-2.8	0.0227	0.00148	8.0425	1	1		
duct61	orif31	300	405.6	0.999	1.015	0.983	9.2	-2.9	0.0226	0.0015	8.04248	1	1	0.139
orif25	300	317.8	0.999	1.02	0.982	5.9	-4.5	0.0165	0.00149	8.0425	1	1		
duct62	orif25	300	316.6	0.999	1.019	0.982	5.9	-4.5	0.0165	0.0015	8.04248	1	1	0.008
yjun10	300	311.3	0.999	1.014	0.983	7.8	-6.7	0.0221	0.00151	6.6467	0.94	1		

duct63	yjun15	300	483.6	1	1.016	0.986	12.8	-3.8	0.0295	0.0024	7.06858	0.96	1	0.091
orif28	300	454.7	1	1.019	0.983	10.1	-3.6	0.0236	0.00241	8.0425	1	1		
duct64	orif30	300	436.5	1	1.019	0.96	9.8	-3.5	0.0229	0.0024	8.04248	1	1	0.142
orif27	300	365.2	1	1.015	0.982	8	-3.1	0.0203	0.00241	8.0425	1	1		
duct65	orif27	300	382	1	1.016	0.982	8	-3.1	0.0203	0.0024	8.04248	1	1	0.04
yjun11	300	368.6	1	1.016	0.982	11.9	-6.5	0.0306	0.00241	6.6457	0.94	1		
duct66	yjun8	320	329.4	0.999	1.014	0.973	40.9	-11	0.1126	0.0015	3.46361	1	0.85	0.001
orif12	320	329.4	0.999	1.014	0.973	34.9	-12.7	0.096	0.00147	3.4636	1	0.85		
duct67	yjun9	300	316.8	0.998	1.014	0.976	38.3	-12.6	0.1076	0.0015	3.46361	1	0.85	0.003
orif16	300	316.8	0.998	1.014	0.976	32.6	-14.7	0.0916	0.00151	3.4636	1	0.85		
duct68	yjun10	300	309	0.998	1.016	0.975	38.6	-11.2	0.1096	0.0015	3.46361	1	0.85	0.001
orif8	300	309	0.998	1.016	0.975	33	-12.9	0.0938	0.00153	3.4636	1	0.85		
duct69	yjun11	300	333.6	0.999	1.019	0.975	40.2	-13.8	0.1106	0.0015	3.46361	1	0.85	0.005
orif4	300	333.6	0.999	1.019	0.975	34.2	-15.8	0.0934	0.00145	3.4636	1	0.85		
duct70	orif26	300	405.3	0.999	1.016	0.982	4.2	-8.6	0.0215	-0.001	8.04248	1	1	0.019
orif18	300	413.5	0.999	1.018	0.982	4.6	-9.1	0.0222	-0.00136	8.0425	1	1		
duct71	orif29	300	433.1	1	1.018	0.984	2.7	-11.5	0.0271	-0.002	8.04248	1	1	0.027
orif22	300	436.7	1	1.018	0.984	3.2	-12	0.0285	-0.00249	8.0425	1	1		
duct72	orif30	300	442.7	1	1.019	0.981	3.5	-9.8	0.0229	-0.002	8.04248	1	1	0.029
orif26	300	449	1	1.019	0.982	3.6	-10.1	0.0236	-0.00241	8.0425	1	1		
duct73	orif31	300	413	0.999	1.015	0.984	2.9	-9.2	0.0226	-0.001	8.04248	1	1	0.02
orif24	300	419.8	0.999	1.014	0.984	2.8	-9.4	0.0227	-0.00148	8.0425	1	1		

FINAL OUTPUT OF JUNCTIONS

Junction	TWALL	TAV	PAV	PMAX	PMIN	HTKW
K	K	BAR	BAR	BAR	KW	
501	370	336.2	0.999	1.019	0.968	-0.001
502	370	326.1	0.999	1.02	0.976	-0.002
503	370	319.9	0.999	1.021	0.971	-0.002
505	310	315.7	1	1.012	0.989	0.002
506	310	311.2	1	1.012	0.99	0
507	310	308.7	1	1.011	0.99	0
508	310	309.2	1	1.011	0.99	0
509	300	300	1	1.004	0.997	0
510	300	300	1	1.003	0.997	0
551	450	409.7	1.001	1.013	0.967	-0.001
552	450	405.1	1	1.016	0.984	-0.002
553	450	401.4	1	1.017	0.98	-0.002
554	450	413.6	1.001	1.017	0.983	-0.001
yjun1	370	339.2	0.999	1.022	0.972	-0.002
yjun2	370	340.6	0.999	1.022	0.972	-0.001
yjun3	370	317.4	0.999	1.021	0.971	-0.004
yjun4	370	334.4	0.999	1.018	0.969	-0.003
yjun5	370	323.9	0.999	1.02	0.975	-0.003
yjun6	850	504.8	1	1.008	0.994	-0.006
yjun7	850	533	1	1.005	0.995	-0.062
yjun8	300	334.2	1	1.013	0.981	0.003
yjun9	300	319.7	0.999	1.012	0.985	0.002
yjun10	300	309.8	0.999	1.014	0.983	0.001
yjun11	300	343.6	1	1.018	0.982	0.004
yjun12	300	460.4	1	1.012	0.989	0.02
yjun13	300	456.2	1	1.015	0.986	0.018
yjun14	300	456.8	1	1.013	0.986	0.019
yjun15	300	475.1	1	1.016	0.986	0.021

TITLE: Motored Manifold Bridge Engine 1000 rpm

ENGINE SUMMARY

NC	MASS	IN	VOL.EFF.	TRAP.RAT	IMEP	PMEP	IHP	TEXH	RES(%)	EGR(%	PHI	PMAX	HTR
KG/HR	BAR	BAR	K	BAR	KW								
1	10.48	0.7462	1.103	-0.1522	-0.09382	398.9	0	0	0	21.96	-0.1223		
2	11.07	0.7867	1.092	-0.1367	-0.08671	386.1	0	0	0	22.18	-0.1596		
3	10.93	0.7785	1.091	-0.1402	-0.08756	389.3	0	0	0	22.09	-0.1503		
4	10.61	0.7556	1.099	-0.149	-0.09281	398.2	0	0	0	21.98	-0.1311		

Breathing Quantities

AMB.VOL.EFF	(AIR	IN	/	AMB.	REF.)	=	0.767	TRAP.RAT	(FRESH	TR./	FRESH	IN	)	=	1.098	
DEL.EFF.	(FRESH	IN	/	PLEN.	REF.)	=	0.869	SCAV.RAT	(GAS	IN	/	GAS	TR.	)	=	0.9
CHARG.EFF.	(FRESH	TR./	PLEN.	REF.)	=	0.975	SCAV.EFF	(FRESH	TR./	GAS	TR.	)	=	1		
TOT.DEL.EFF	(GAS	IN	/	PLEN.	REF.)	=	0.889	RESID.FR	(RESID	TR./	GAS	TR.	)	=	0	
EGR	FR.	(RESID	IN	/	GAS	IN	)	=	0							

TITLE: Motored Manifold Bridge Engine 1000 rpm

ENGINE GEOMETRY

I	DISPL/CY	(LIT.)	=	0.3968	I	NUMBER	OF	CYLINDEF=		4	I	I				
I	(IN3)	=	24.21	I	COMPRES	RATIO	=	10	I	EFFEC	CR	(VC-TDC)	=	9.023	I	
I	BORE	(MM)	=	81	I	BORE/STF=		1.052	I	I						
I	(IN)	=	3.189	I	CON.	ROD	LENGTH(I=		135	I	I					
I	STROKE	(MM)	=	77	I	WRIST	PIN	OFFSET(I=		0.1	I	I				
I	(IN)	=	3.031	I	CLEARAN	VOL.	(M3)	=	4.41E-05	I	ENGINE	TYPE	=	MOTORED	I	
I	INT.	VALVE	DIA.(MM)	=	28	I	EXH.	VALVE	DIA.(MM)	=	23.5	I	#1	EVO	=	137 I
I	MAX.	LIFT	(MM)	=	8.2	I	MAX.	LIFT	(MM)	=	7.65	I	#1	EVC	=	373 I
I	I	I	#1	IVO	=	345.4	I									
I	NO.	INTAKE	VALVES	=	2	I	NO.	EXHAUST	VALVES	=	2	I	#1	IVC	=	585 I

OPERATING CONDITIONS

I	RPM	=	1000	I	#1	INT.PORT	PR(BAR)	=	0.9966	I	#1	IGN	DELAY(CA)		=	0 I
I	AMB.	PRESSUR	(BAR)	=	1.013	I	(IN.HG)	=	29.58	I	#1	COMB.	START(CA)		=	### I
I	(IN.HG)	=	30	I	#1	INT.PORT	TEMP(K)	=	340.6	I	INJ.TIMIN	(ATDC)	=	1.00E+06	I	
I	AMB.	TEMP.	(K)	=	298	I	(F)	=	153.4	I	MID.INJ.PI=		0	I		
I	(F)	=	76.73	I	#1	EXH.PORT	PR(BAR)	=	1.002	I	(PSI)	=	0	I		
I	FUEL	TYPE	(C:H:O)	C	=	7.3	I	(IN.HG)	=	29.66	I	INJ.DURA'	(CA)	=	0	I
I	H	=	13.9	I	I	FUEL	RATE	(KG/HR)	=	0	I					
I	O	=	0	I	PISTON	VEL.	(M/S)	=	2.567	I	(MULTI)	(LBM/HR)	=	0	I	

FUEL	LHV	(MJ/KG)	=	43.18	(FT/MIN)	=	505.2	#1	FUEL	/	SHOT	(KG)	=	0		
(BTU/LBM	=	1.86E+04														
(A/F)	STOICH	=	14.66	1%	FUEL	PWR/CYL	(W)	=	0							
FUEL	MOLEC.	WEIGHT	=	0												

Predicted Performances:

INDIC.	POWER	(HP)	=	-0.2563	BRAKE	POWER	(HP)	=	-1.813	PMEP	(BAR)	=	###					
IND.EFFIC(%)	=	0	BRAKE	EFFICIEN	=	0	(PSI)	=	-0.38									
IMEP(NET	(BAR)	=	-0.1445	BMEP	(BAR)	=	-1.022	FMEP	(BAR)	=	0.8778							
(PSI)	=	-2.098	(PSI)	=	-14.83	(PSI)	=	12.73										
ISFC	(KG/KWH)	=	0	BSFC	(KG/KWH)	=	0	IMEP(GRC	(BAR)	=	-0.1184							
(LBM/BHP	=	0	(LBM/BHP	=	0	(PSI)	=	-1.717~										
IND.	TORQUE	(N-M)	=	-1.825	BRAKE	TORQUE	(N-M)	=	-12.91	FRICT.	TORQUE	(N-M)	=	11.09				
(FT-LB)	=	-1.346	(FT-LB)	=	-9.523	PUMP.	TORQL	(N-M)	=	-0.33								
AUXILIAR	POWER	[hp]	=	0	#1	EXHAUST	TEMP	(K)	=	398.9								
AUXILIAR	POWER	[kW]	=	0	(F)	=	258.4											
IND.	ENERGY	BALANCE	FRESH	AIR	IN	(KG/H)	=	43.09	#1	PMAX	(BAR)	=	22					
NET	PISTON	WORK	(%)	=	0	(WET)	(LBM/HR)	=	95.02	(PSI)	=	318.6						
AVAIL.EXI	(%)	=	9999	TRAPPING	RATIO	=	1.098	#1	CA	AT	PMAX	=	-0					
DEBIT	INTK.ENTI	=	9999	VOL.EFF.(	=	0.7673	#1	MAX	DP/DTH	(BAR)	=	0.5082						
H.	TRAN.(IN-	=	0	#1	VOL.EFF.(	=	0.665	(PER	DEG)	(PSI)	=	7.371						
BLOWBY	AT	RING1	(%)	=	9999	A/F	TRAPPED	=	0	#1	CA	AT	MAX DP/DTH	=	-17			
IMBALANC	(%)	=	9999	PHI	TRAPPED	=	0	#1	MAX	AVG.GT(K)	=	872						
PUMPING	WORK	(%)	=	0	RESIDUAL	FRAC.	(%)	=	0	(F)	=	1110						
BRAKE	POWER	(KW)	=	-1.352	FRIC.	(%FUEL	ENER.)	=	0									
H.TRAN.(I	=	-0.5633																

ENGINE OUTEMISSIONS

NOx	(PPM)	=	0	HC	EMISSION	(PPMC1)	=	0	CO	EMISS	(PPM)	=	0	
NOx	AS	NO2	(g/hr)	=	0	(g/hr)	=	0	(g/hr)	=	0			
(g/bkW-hr)	=	0	(g/bkW-hr)	=	0	(g/bkW-hr)	=	0						

TITLE: Motored Manifold Bridge Engine 1000 rpm

ENGINE CYLINDER BACKFLOW

CYL	BEFORE	EVC AMOUNT(II	AFTER %	EVC OF	TOTAL	AMOUNT(II	%	OF	TOTAL
1		1.71E-08	4.90E-03		2.62E-05	7.487			
2		1.16E-09	3.15E-04		2.98E-05	8.061			
3		2.97E-10	8.14E-05		2.95E-05	8.102			
4		2.09E-07	5.91E-02		2.93E-05	8.288			

ENGINE INTAKE VALVE BACKFLOW

CYL	BEFORE VAL	EVC	AMOUNT(II	AFTER %	EVC OF	TOTAL	AMOUI	%	OF TOTAL	REV ANGLE
1	1		8.55E-09	4.90E-03		1.31E-05	7.487	535.7		
1	1		8.55E-09	4.90E-03		1.31E-05	7.487	535.7		
2	1		5.82E-10	3.15E-04		1.49E-05	8.061	539.6		
2	1		5.82E-10	3.15E-04		1.49E-05	8.061	539.6		
3	1		1.48E-10	8.14E-05		1.48E-05	8.102	530.5		
3	1		1.48E-10	8.14E-05		1.48E-05	8.102	530.5		
4	1		1.04E-07	5.91E-02		1.47E-05	8.288	538.2		
4	1		1.04E-07	5.91E-02		1.47E-05	8.288	538.2		

CYCLE AVERAGED ENGINE CYLINDER EXHAUST INDICTAED SPECIFIC EMISSIONS

	NO	NO2	CO	HC					
CYL	(g/kWhr)	(g/hp/hr)	(g/kWhr)	(g/hp/hr)	(g/kWhr)	(g/hp/h	(g/kWhr)	(g/hp/hr)	
1	•	•	•	•	•	•	•	•	
2	•	•	•	•	•	•	•	•	
3	•	•	•	•	•	•	•	•	
4	•	•	•	•	•	•	•	•	

CYCLE AVERAGED AMBIENT EMMISIONS

AMBIENT	NO (g/hr)	NO2 (g/hr)	CO (g/hr)	HC (g/hr)
301	0	0	0	0
amb1	0	0	0	0
amb2	0	0	0	0

APPENDIX C

C. Acquisition Hardware and Software Specifications

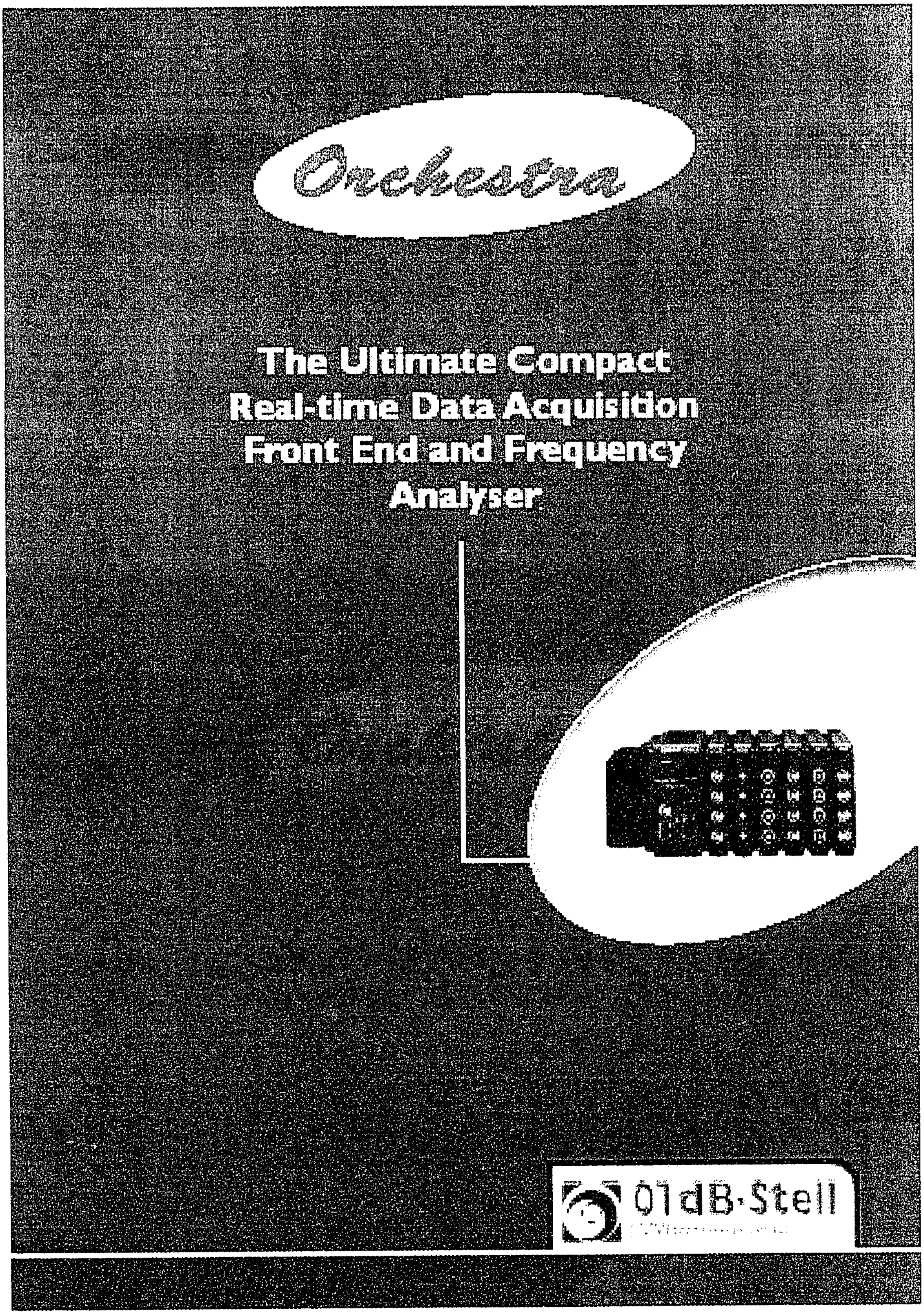
Orchestra
The Ultimate Compact
Real-time Data Acquisition
Front End and Frequency
Analyser
01dB-Stell

Orchestra is made up of one or several modular multichannel hardware units and of the dBFA software suite dedicated to real-time data recording and frequency analysis.

Orchestra is a configurable and modular system containing separate and independent modules. No main frame is needed and all modules can be mounted very easily.

Three kinds of modules can be mounted together:

- Interface module allowing connection to PC through Firewire interface (IEEE 1394)
- Input module for 4 transducers with conditioning and 24 bits A/D conversion
- Function module adding features like output module for signal out or generator

One interface unit can manage up to 24 channels (6 input modules). Independent frequency sampling can be used on each input module. Several different input modules are available for Direct voltage/ICP® transducers, Microphones, Charge accelerometers, Thermocouple, Strain gage, Tacho sensors,...

A main unique feature of Orchestra is to allow a Multi-channel real-time analysis while recording on a PC hard disk.

With the to Firewire interface capability, unrivalled feature is the network and distributed measurement performed with several Orchestra systems (two 24-channel Orchestra units constitute a measurement group). 192 channels can be measured and analysed at the same time with a maximum distance of 100 m between groups.

The dBFA software suite manages in real-time all data coming from Orchestra when it is used as a front end. The recording mode transforms Orchestra into a data acquisition front end and stores all signals on the PC hard disk while monitoring (Oscilloscope, Overall values, FFT, 1/3 octave) is performed to check data quality. The Analyser mode transforms Orchestra into a real-time frequency analyser dedicated to many industrial applications.

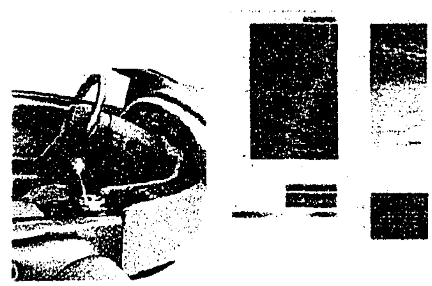

Expandability

- Any combination of 4-channel input modules and function modules can be used for one measuring group
- 4 to 24 channels (max. 6 modules) per measuring group
- 8 measuring groups can be connected together via Firewire interface

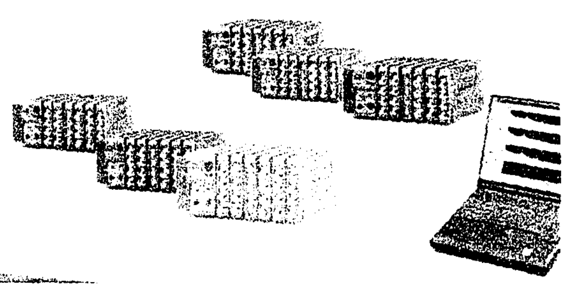

Orchestra

Measurement	Software	Hardware
Firewire transfer rate: max. 26 Mbps	Data recording / Throughput to disk	No main frame
32 channels real time up to 20 kHz bandwidth	Frequency Analysis (FFT / 1/n octave)	*Direct connection of sensors*
Networked and distributed measurement up to 192 channels by 8 units	Sound Intensity / Sound Power	Several module types
Up to 100 m between each measuring group	Structural Analysis	Easy mounting of mechanical modules
	Material Testing	Synchronous 24 bits ADC
	Psychoacoustics / Sound Quality	Multi-frequency sampling
	Rotating Machine Analysis	>100 dB dynamic range
	Predictive Maintenance	Multiple tacho inputs
		High-speed Firewire interface
		AC/DC and battery powered

Exemple of module combination for one measuring group

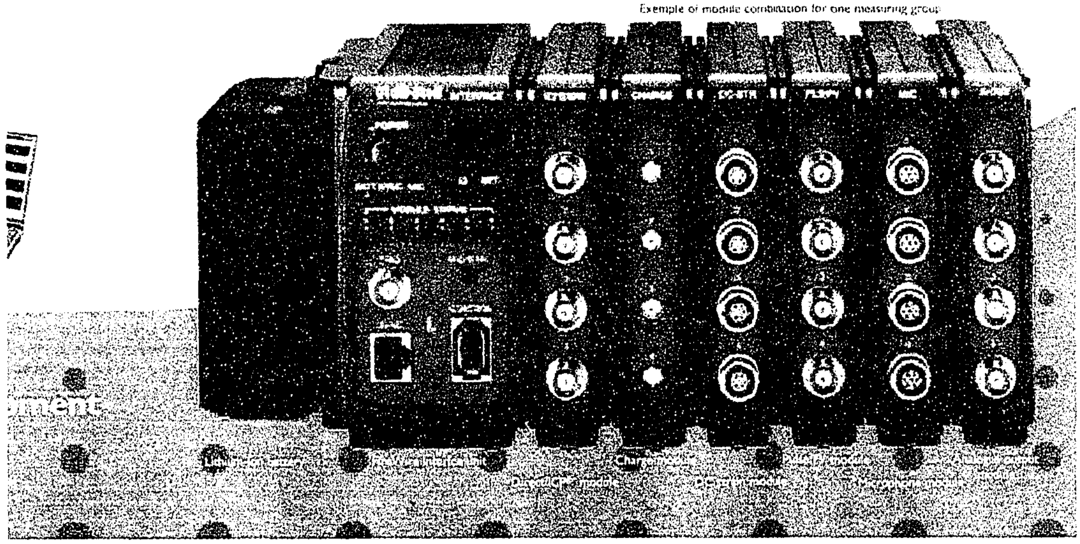

Technical specifications

General specifications:
- Input channels: 4 to 24 channels - 4 ch. per module - max. 6 modules can be connected
- Sampling frequencies: 3 types
  Type 1: From 25 Hz up 51200 Hz
  Type 2: From 8 Hz up to 65536 Hz
  Type 3: from 10 Hz up to 10 kHz
- Same frequency sampling type within the system
- Frequency sampling selectable per module
- Bandwidth: sampling frequency/2.56
- Transfer rate: 26.2144 Mbps
- ADC: 16 or 24 bits selectable
- Vibration resistance: MIL-STD-810C/E
- Measuring group: dimensions for 4ch. W88 x H110 x D200 mm and for 24 ch. W213 x H110 x D200 mm
- Weight: 4ch. 1.9 kg - 24ch. 4.8 kg
- Power supply: AC - 110 to 240 V; DC - 11 to 30 V; Battery Pack (Optional)
- Power consumption: 18 W @ DC 12 V; 44 W @ DC 12 V

Interface unit module specifications:
- PC interface: Firewire (IEEE 1394)
- Number of modules connectable: 6
- Triggers: Trigger channel - TTL level/edge; pre/post
- Fan control mode: on/off
- Input range: from ±0.1 to 20 Vpk
- Weighting filters: A, B, C

Direct/ICP® Input module specifications:
- Number of channels: 4 BNC connectors (Single ended) or 2 (differential)
- *Coupling*: AC/DC
- High-pass filter: 0.5 Hz, 20 Hz
- Low-pass filter: digital filter
- Input range: from ±0.1 to 20 Vpk
- Weighting filters: A, B, C

Microphone Input module specifications:
- Number of channels: 4 Lemo 7 pin connectors (Single ended)
- Preamp. power and polarisation: ±14 V and 0, 200 V
- High-pass filter: 0.5 Hz, 20 Hz
- Low-pass filter: digital filter
- Input range: ±7 m to 7 Vpk

Charge Input module specifications:
- Number of channels: 4 Microdot connectors (Single ended)
- Charge sensitivity: 0.1 to 100 pc/m/s²
- High-pass filter: 0.5 Hz (1st order RC)
- Low-pass filter: digital filter
- Input range: 1, 3.16, 10, 31.6, 100, 316, 1000, 3160, 10000 pC

DC strain Input module specifications:
- Number of channels: 4 Lemo 6 pin connectors (differential)
- Coupling: DC
- Bridge type and voltage: full bridge, DC 2.5, 5, 10 V
- Zero adjustment: automatic
- Low-pass filter: digital filter
- Input range: from ±0.2 to 10 mV/V

Thermocouple Input module specifications:
- Number of channels: 4 screw terminal connectors (differential)
- Thermocouple: J and K type
- Low-pass filter: digital filter
- Input range: J - from 50 to 1200°C; K - from 50 to 1300°C

Pulse/FV Input module specifications:
- *Number of channels*: 4 BNC connectors (Pulse) or 1 (FV)
- Input: Logic (TTL); Bipolar (AC)
- Digital input sampling frequency: from 2 to 32 MHz selectable. Accuracy: 25 ns
- Frequency measurement: from 1 to 500 kHz selectable
- Threshold: logic (from 0 to 4 V variable)

Analogue output module specifications:
- Number of channels: 4 BNC connectors (single ended)
- Output range: ±1.2 pk (fixed) or variable at 0.1 V step with ±5 Vpk max.

Function generator module specifications:
- Output 1ch (BNC connector)
- Peak level: 0dB (5 V), -10 dB, -20 dB
- Frequency range: DC ~ 20 kHz
- Offset range: ±5000 mV @ 10 mV step
- THD: -70 dB or less
- Signal generated: Pink noise, white noise, sine wave, sweep sine wave

01dB-Stell
MVI technologies group

Orchestra software main features:

dBFA software suite is a modular solution:
- From 1 to 192 channels depending on the hardware platform
- Versatile: acoustics, vibrations, etc.
- Direct-to-disk multichannel digital signal recording with a frequency range up to 20 kHz with audio playback
- Signal, overall values and FFT - 1/3 octave spectra monitoring of several channels during recording
- Manual or automatic measurement gain settings
- Advanced trigger functions (channel, positive or negative delay, and/or conditions, etc.)
- Overload indicators with storage
- Real-time narrow band FFT analysis (from 101 to 3201 lines) of autospectra, cross-spectra, transfer functions, coherence, etc., from 0 Hz to 20 kHz, with or without zoom factor (2 to 128); linear and exponential averaging, max. hold
- Broad band analysis by digital filtering (1/1 and 1/3 octave according to Class 1 - IEC 61260). Autospectra from 1 Hz to 20 kHz
- Narrow-band (2 FFT passes - autospectra, cross-spectra, coherence) and broad-band (1/1 and 1/3 octave - autospectra) analysis of sound pressure and sound intensity (active and reactive)
- Sound power determination according to ISO 9614 parts 1 and 2
- Tachometric acquisition and calculation
- Real-time and post-processing order analysis for rotating machinery; rotation run-ups and coast-downs
- Transient analysis on pulses, shocks, etc., with or without point *coordinate management.*
- Time frequency analysis (FFT, 1/n octave, Wigner-Ville, Wavelets, Capon, AR)

Benefits

- Acoustics and Vibration
- Process signals
- Multichannel front end
- Real-time frequency analyser
- Multi-frequency sampling
- Network capability
- Modular / expandable
- Transducer conditioning
- Many industrial applications

France
(Head Office)
200, chemin des Ormeaux
F - 69578 Limonest Cedex
Phone +33 4 72 52 48 00
Fax. +33 4 72 52 47 47

Italy
Phone +39 049 920 0966
Fax. +39 049 920 1239

USA
Phone +1 315 685 31 41
Fax. +1 315 685 31 94

Brazil
Phone +55 11 49 92 3600
Fax +55 11 44 27 5206

Asia Pacific
Phone +60 3 563 22 633
Fax. +60 3 563 18 633

Web: www.01db-stell.com
Mail: infogb@01db-stell.com

Rev. : 07.2002

The presented characteristics are subject to change without notice.

FREE FIELD MICROPHONES

A Free field microphone is designed to measure the sound pressure in the sound field, compensated for the influence of the presence of the microphone in the sound field. In effect, the microphone measures the sound pressure as it existed before the microphone was introduced into the sound field, i.e. free field conditions.

The Free field microphone should be pointed towards the sound source, at a 0° angle of incidence.

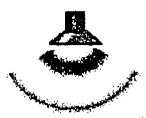

1/2" Free field, High sensitivity
Type 40AF
A general purpose microphone, covering the frequency range from 3.15 Hz to 20 kHz. Due to the high sensitivity, the microphone can measure sound pressure levels down to 15 dB(A).
The microphone is intended for type 0 and type 1 measurements according to IEC 60651 standard.

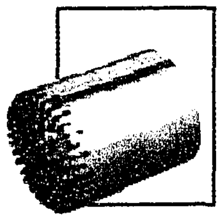

1/2" Free field, Prepolarized
Type 40AE
A general purpose microphone, similar to type 40AF, but as an electret condenser type and hence requires no external polarization voltage. They are typically used with ICP preamplifiers, type 1 sound level meters or for other less critical measurements.

1/2" Free field, Wide frequency
Type 40AC
A high precision microphone for laboratory work and as working standard microphone in calibration laboratories, covering the frequency range from 3.15 Hz to 40 kHz. The small size and lower sensitivity makes the microphone extremely rugged and stable.
The microphone can measure sound levels up to 160 dB.

1/4" Free field, High Level
Type 40BF
A 1/4" microphone for high level and high frequency measurements. The low sensitivity of the microphone makes it ideal for measuring very high sound pressure levels: up to 174 dB. The small size reduces disturbances in the sound field, resulting in a frequency range up to 100 kHz.

1/4" Prepolarized Free field, High Level
Type 40BE
A 1/4" Prepolarized microphone similar to Type 40BF, but requires no polarization voltage. The microphone is ideal for use with ICP preamplifiers, for very high level or high frequency applications.

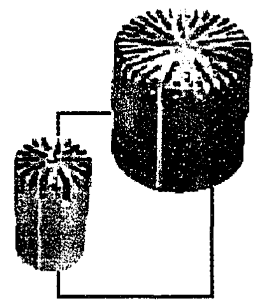

SPECIFICATIONS

Type	40AF	40AC	40AE	40BF	40BE	
Sensitivity	50	12.5	50	4	4	mV/Pa
Frequency range	3.15-20k	3.15-40k	6.3-20k	10-100k	10-100k	Hz
Dynamic range	15-146	27-160	15-146	40-174	40-168	dB re. 20μPa
Polarization voltage	200	200	0	200	0	V
Outside diameter (with protection grid)	13.2	13.2	13.2	6.9	6.9	
Length (with and without protection grid)	16.2 / 15.3	12.5 / 11.6	16.2 / 15.3	10.5 / 9.1	10.5 / 9.1	mm

1/2" PREAMPLIFIERS

These microphone preamplifiers are small rugged units optimized for acoustical measurements with condenser microphones.

The connections to the preamplifiers are most often made with a 7-pin Lemo series 1B plug. The connections (as shown below) are widely used, ensuring compatibility with a wide range of power supplies, analysers etc

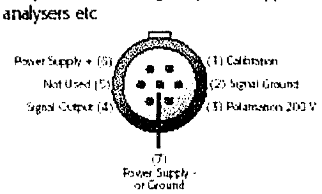

The preamplifiers are all compatible with measurement microphones as defined in *the international standard* IEC 1094 "Measurement Microphones, Part 4: Specifications for working standard microphones".

All the G.R.A.S. preamplifiers are based on a small ceramic substrate thickfilm precision amplifier with very high input impedance. The casings are made of stainless steel for maximum strength and durability with minimum sensitivity to vibration and microphonics.

1/2" Preamplifier
Type 26AK

The 26AK is a 1/2" preamplifier with integrated 7-pin Lemo connector. A 3 m cable AA0008 is available with 7 pin - 7 pin Lemo connectors. Other lengths are available on request.

1/2" Preamplifier
Type 26AJ

The 26AJ is a variant of the 26AK having a built-in SysCheck facility to allow easy system checks to be made.

1/2" Preamplifier
Type 26AH

The 26AH is a 1/2" preamplifier similar to 26AJ, but with integrated 3m cable terminating in a 7-pin LEMO connector.

1/2" Preamplifier
Type 26AM

The 26AM is a 1/2" preamplifier similar to 26AK, but with integrated 3m cable terminating in a 7-pin LEMO connector.

1/2" Preamplifier
Type 26AG

The 26AG is a 1/2" preamplifier with integrated 7-pin Lemo connector. The preamplifier has the necessary configuration to allow the insert voltage method to be used to determine the open-circuit sensitivity of microphones. A 3 m cable AA0008 is available with 7 pin - 7 pin Lemo connectors. Other lengths are available on request.

1/2" ICP* Preamplifier
Type 26CA

The 26CA is a 1/2" ICP preamplifier for connection to standard ICP* input channels. The 26CA has a standard BNC output connector and is intended for used with prepolarized microphones. The 26CA is delivered without a cable. The Built-in TEDS* chip enables it to be programmed as a complete unit together with a microphone.

** Transducer Electronic Data Sheet - as proposed by IEEE P1451.4*

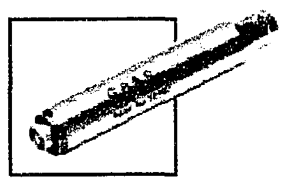

SPECIFICATIONS

26AH, 26AJ, 26AK, 26AM and 26AG
Frequency range: 2 Hz- 200 kHz (±0.2 dB)
Input impedance: 20 GΩ, 0.4 pF
Output: Impedance: 55 Ω (typical) Connector: 7-pin LEMO male
Power Supply: Single: 120 V 2.5 mA down to 28 V 0.7 mA
Dual: ± 60 V 2.5 mA down to ± 14 V 0.7 mA
Noise: (with dummy microphone)
A-weighted: <2.5 μV rms (typical: 1.8 μV rms)
Linear: (20 Hz - 20 kHz): < 6μV rms (typical: 3.5 μV rms)
Gain: - 0.15 dB (typical)
Temperature: Operation: -30°C +70°C Storage: -40°C +85°C
Dimensions: (ex. cable)
Diameter: 12.7 mm (1/2")
Length: 77.5 mm
Weight: 35 g

26CA
Frequency range: 2 Hz- 200 kHz (±0.2 dB)
Input impedance: 20 GΩ, 0.4 pF
Output: Impedance: 50 Ω Connector: coaxial BNC
Power Supply: 2 mA to 20 mA (typical 4 mA)
Noise: (with dummy microphone)
A-weighted: <2.5 μV rms (typical: 1.8 μV rms)
Linear: (20 Hz - 20 kHz): < 6μV rms (typical: 3.5 μV rms)
Gain: - 0.25 dB (typical)
Temperature: Operation: -30°C +70°C Storage: -40°C +85°C
Dimensions:
Diameter: 12.7 mm (1/2")
Length: 73 mm
Weight: 26 g

ICP® is a registered trademark of PCB Piezotronics dBFA32 is a practical and efficient software packages, which transforms your computer into a versatile sound and vibration frequency analyser and much more...

Completely modular in concept, dBFA32 can be configured according to specific user needs by choosing only the options required...

dBFA32 has been developed under the Windows® environment, which guarantees user-friendliness, high performance and total compatibility with office software, such as word processors and spreadsheets (to generate reports including graphs and tables), as well as other tools (e.g., MATLAB®) for further data analysis.

The applications of dBFA32 are:

- Mesurements and Controls
  - Overall levels
  - Frequency analysis of the signal
  - Frequency analysis of systems
  - Structure analysis
  - Sound power
  - Commissioning test
  - ...
- Sound and vibration comfort
  - Physiological effects of vibrations
  - Psychoacoustics - Sound Quality
  - Material tests
  - ...
- Error diagnosis
  - Sound intensity
  - Sound mapping
  - Machine order analysis
  - Study of transient phenomena
  - Time-frequency analysis
  - ...

There are a lot of application fields: Automotive, Aeronautic, Space, Railway, Mechanical, Materials, Household appliances, Electro-acoustics, Telecommunications, ...

dBFA32

Main functions

MEASURING WITH dBFA32:

- From 1 to 16 channels depending on the hardware platform (JAZZ, SYMPHONIE, HARMONIE, MELODIE).
- Versatile: acoustics, vibrations, etc.
- Direct-to-disk digital signal recording with a frequency range varying from 40* Hz up to 80* kHz with audio playback
- Signal and FFT spectrum monitoring of one of the channels during recording
- Manual or automatic measurement gain setting
- Advanced trigger functions (channel, positive or negative delay, and/or conditions, etc.)
- Overload indicators with storage
- Real-time narrow bands FFT analysis (from 101 to 3201* lines) of autospectra, cross-spectra, transfer functions, coherence, etc., from 0 Hz to 80 kHz, with or without zoom factor (2 to 128); linear and exponential averaging, max. hold
- Broad-band analysis by digital filtering (1/1 and 1/3 octave according to Class 1 - IEC 61260). Autospectra from 1 Hz to 20 kHz
- Narrow-band (2 FFT passes - autospectra, cross-spectra, coherence) and broad-band (1/1 and 1/3 octave - autospectra) analysis of sound pressure and sound intensity (active and reactive)
- Sound power determination according to ISO 9614 parts 1 and 2
- Tachometric acquisition and calculation
- Order analysis for rotating machinery; rotation run-ups and coast-downs
- Transient analysis on impulses, shocks, etc.
- Impulse response using the MLS method (SYMPHONIE)
- Signal generator* (sine, white and pink noise, loop, MLS as an option)

**depending on the acquisition front end used*

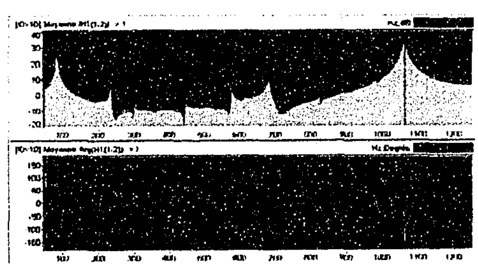

DATA PROCESSING WITH dBFA32

- Numerous formats for data importation (UFF58, .Wav, Teac, Sony, etc.)
- Download of data from 01dB-Stell sound level meters and stand-alone frequency analysers
- Numerous processing functions with analysis script
- Narrow-band and broad-band spectra and multispectra (down to 1/48th octave), narrow-band cross-spectra and frequency response functions
- Low-pass, high-pass, band-pass, band-cut and notch filtering
- Under-sampling, re-sampling, sound and ISO 2631 and ISO 5349 vibration weightings and windowing on audio data
- Frequency re-composition in broad bands and in Loudness/Bark bands, time re-composition, integration/derivation
- Cross-spectra, transfer functions (H1, H2, 1/H1 and 1/H2) and coherence. Bode, Nyquist, Nichols displays.
- Single and double cursors, harmonic and sideband cursors, peak searching cursors
- Arithmetics on signals and spectra: addition, subtraction and averaging
- Stationary psychoacoustics criteria (Loudness, Loudness 10%, Fluctuation Strength, Harshness, Tonality, Roughness, Unbiased Annoyance, Sensory Pleasantness, Articulation Index), Bark band spectra, specific loudness, time history of psychoacoustic criteria (loudness, harshness)
- Histograms, Echograms
- Order extraction, cycle defaults, order filter
- Time-Frequency Analysis (Wigner-Ville, Wavelets, Capon, AR), Denoising, Convolution
- ...

CUSTOMISING dBFA32

Regardless of the selected options, dBFA32 features a large number of management functions, offering user-friendliness and ease-of-use:

- Editing of IS physical units and references for all types of measured quantities and hardware sensitivity
- Transducer, calibrator and hardware databases with storage of measurement set-ups for later use
- Storage of numerous measurement and display set-ups
- Storage of user-defined analysis scripts
- Storage and display (including data sorting functions) of measurement results in campaign files
- Follow-up of each processing operation
- Batch data processing (signals, spectra, etc.)
- Data exchange with other applications
- DDE interface, user-defined remote controls, etc.
- Extensive help functions in HTML format for each module
- Cut, Copy, Paste commands for both graphs and data to be used in a word or spreadsheet processor

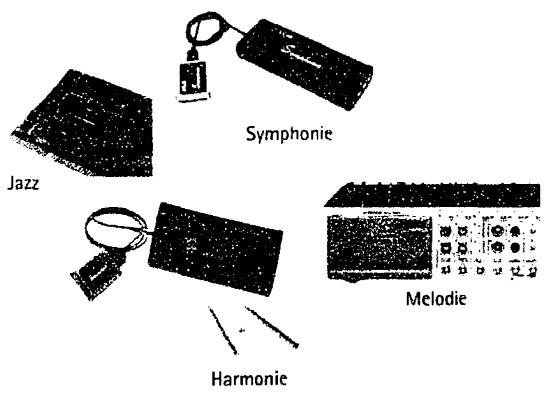

dBFA32

Software packages

Depending on your application, dBFA32 can be made up of several complementary modules.

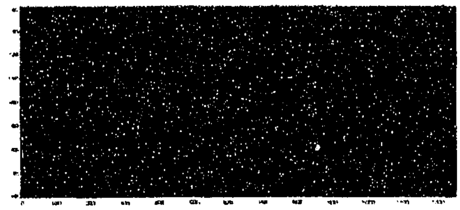

SUPER POST PROCESSING PACK (S3P)

This module allows for direct-to-disk recording on the PC hard disk and for the post processing of most of the standard sound and vibration application needs.

In dBFA32, digital recording of the signal can be performed on 16* channels maximum, and over a frequency range from 80* kHz down to several Hertz. Acquisition is made easier using advance triggering functions (thresholds, software or harware remote control, etc.).

- Signal recording with monitoring of one of the selected channels (signal + real-time FFT spectrum) and bar-graph display for all recorded channels

Furthermore, importing/exporting signals allows to:

- Import signal files: standard and 01dB WAVE, MPEG3, SONY PCSCAN II, TEAC GX1, nSoft Dac
- Export signal files: standard and 01dB WAVE, ASCII, MPEG3, UFF58

Processing is based on the use of a calculation server allowing the operator to carry out a series of operations (script) on the same piece or set of data, such as signals, spectra, etc.

- Signal processing (low-pass, high-pass, band-pass, band-cut, notch filters, under-sampling, re-sampling, gain optimisation, windowing)
- Signal analysis (FFT 3200 lines, autospectra with or without zoom, 1/1 and 1/3 octave autospectra, echogram, overall levels, weightings, histogram, etc.)
- System analysis (FFT, cross-spectra, frequency response functions: direct, inverse and cross, coherence)
- Average spectra and multispectra
- Importation of spectra (dBFA 16bits, UFF58)
- Exportation of spectra (ASCII, Matlab, UFF58)
- Operations on spectra (frequency and time recomposition, time history of overall level)
- Arithmetics on spectra, signals and overall levels (addition, subtraction, averaging)
- Single and double cursors, harmonic and sideband cursors, cursor for peak searching. Effects of FFT weighting windows
- Synchronisation of cursors on several signal and spectrum displays
- Energy calculation between cursors and on user-defined frequency range
- Simple and double integration / derivation of spectra
- 2D display of signals, autospectra, complex spectra (Re, Im, Modulus, Phase) and multispectra
- Superposition of spectra (up to 6 on the same display)
- Batch processing
- 1/N octave frequency analysis (N = 6, 12, 24, 48)
- Sonagram display for multispectra with time and frequency cross-section
- Bode, Nyquist, Nichols displays
- Lissajou calculation - Y(t)=f(X(t))
- Direct tachometric acquisition on SYMPHONIE and HARMONIE
- Conversion of tachometric signals (periodic tops) into speed profiles
- Operators for rotating machinery with variable rotation speed, designed for order extraction, order filtering and calculation of cycle defects
- Average and instantaneous cepstrum
- Dual-channel (shocks,...) transient analysis on threshold and MLS (SYMPHONIE only). Customisation of FFT time weighting windows. Calculations of autospectra, interspectra, frequency response functions and coherence. Manual and automated mode

MULTI-CHANNEL REAL TIME PACK (RTP)

This package includes the "S3P" configuration and can be used to perform real-time acquisition of narrow-band spectra using FFT analysis with various FFT windows (Rectangular, Hanning, Kaiser Bessel, Flat Top, etc.), with or without zoom factor (f1, f2). This module can also be used to perform real-time analysis of 1/1 and 1/3 octave spectra.

When performing multi-channel measurements, cross-spectra, transfer functions and coherence are also available. Data can be displayed either in polar form (modulus and phase) or complex form (real and imaginary parts).

- FFT analysis on 16* channels (1 to 3201* lines) up to 80* kHz
- 1/1 and 1/3 octave analysis on 16* channels from 1 Hz to 20 kHz with multispectrum rate down to 20 ms
- Real-time noise generator* (sine, pink and white noise, loop)

*depending on the front-end and PC used

dBFA32

Software packages (cont'd)

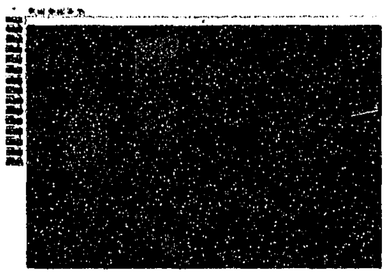

PSYCHOACOUSTICS PACK (PACP)

This module can be used independently from the others and offers:

- Signal recording, wave importation/exportation
- Specific loudness
- Psychoacoustics criteria (Loudness, Loudness 10%, Fluctuation strength, Harshness, Tonality, Roughness, Unbiased annoyance, Sensory pleasantness, Articulation index)
- Time history of psychoacoustics criteria (Loudness, Harshness)
- Bark band time history of overall loudness

ACOUSTIC INTENSITY PACK (AIP)

This module can be used on a stand-alone basis.

The characteristics of the intensity probe (space between microphones, etc.) are user-defined for intensimetry measurements.

The probe can be calibrated (levels and phase) using the specific software package dBSONDE32 and calibrator G51AB so that the system complies with IEC 1043.

- Signal recording, importation/exportation of .wav files
- Real-time analysis of sound pressure and sound intensity (2 FFT passes, 1/1 and 1/3 octave simultaneously) yielding autospectra, interspectra, coherence, active (Li), reactive (Lj) and free-field (SIL) sound intensities
- Sound power according to ISO 9614 parts 1 and 2
- Sound mapping
- Correction for phase difference and convolution
- Remote control for measuring probe
- Robot control for automated operation (option)

dBFA32

Options

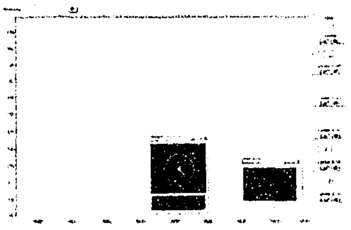

MAXIMUM LENGTH SEQUENCE (MLS)

This option is used for the MLS (Maximum Length Sequence) acquisition of the single or dual-channel impulse response (1 ms rate) of a "system". It is available as a complement to the "S3P" or the "RTP" configuration.

The MLS method is an efficient measurement technique for noisy environments with no powerful sound source and yields results that are more accurate than traditional methods. A convolution operator (calculation of system responses according to the measured impulse response), as well as the module to calculate the road surface absorption coefficient according to ISO 13472-1 are available as options.

ORDER ANALYSIS (OAM)

This option may be used in real time (RTP) or in post-processing (S3P) mode and provides the user with the display of overall levels of rotation speed orders, and of 2D and sonagram spectra for sound and vibration signals. Most steps in the process have been automated: tachometric signal processing, speed profile processing, analysis of successive run-ups and coast-downs. Non-integer orders are allowed. Dating of rotation speeds is accurate.

EXTRA POST PROCESSING PACK (E3P)

Available from the S3P or RTP configuration, this option features 4 new frequency operators (Pseudo Wigner-Ville, Wavelets, Capon and auto-regressive model) that allow to perform the time-frequency calculation of very short signals (shocks, sparks, etc.) with a time base down to sample. They provide results more accurate than standard multispectrum calculations based on FFT or 1/3 octave analyses.

Furthermore, this option includes a denoising operator based on wavelets (increase of the signal-to-noise ratio for noisy signals).

Other Options

1/3 octave real time and acoustic intensity only

- DDE Interface (Dynamic Data Exchange) for external programming

Post-processing

- Linked (bi-directional) with MATLAB data
- Importation of signals from more than 16 channels (SONY, TEAC)

Minimum PC configuration

Post-processing	PC Pentium, 32 Mo RAM, all Windows operating systems
Acquisition	PC Pentium III - 600 MHz, 128 Mb RAM, operating software depending on acquisition front end (see below). For the multi-channel system MELODIE, performances depend on the PC used.

Operating system (OS) according to the acquisition front end (version 4.3)

OS/Platform	Win 95	Win 98	Win NT 4.0	Win 2000
JAZZ	Available	Available	Post-processing only	Post-processing only
SYMPHONIE	Available	Available	Post-processing only	Post-processing only
HARMONIE	Available	Available	Post-processing only	Post-processing only
MELODIE	Available	Available	Available	Available

Operating mode according to the hardware (Version 4.3)

Recording, real-time and post processing modes are all available regardless of the acquisition platform (JAZZ, SYMPHONIE, HARMONIE, MELODIE), except for the real-time mode on JAZZ.

Audio recording performances according to the hardware

JAZZ / SYMPHONIE	1 to 2 channels 20 kHz (sampling 51200 Hz)
HARMONIE	1 to 4 channels 20 kHz (sampling 51200 Hz)
MELODIE	1 to 16 channels 20 kHz (sampling 51200 Hz)*

* *carried out on PC (PIII 600 mini - 128 Mb)*

FFT real time performances according to the hardware

SYMPHONIE	1 to 2 channels 20 kHz-800 lines. Independent of the PC.
HARMONIE	1 to 4 channels 20 kHz-3200 lines*
MELODIE	1 to 8 channels 20 kHz; 1 to 16 channels 10 kHz-3200 lines*

* *carried out on PC (PIII 600 mini - 128 Mb)*

1/3 octave real time performances according to the hardware

SYMPHONIE	1 to 2 channels 20 kHz. Independent of the PC.
HARMONIE	1 to 4 channels 20 kHz*
MELODIE	1 to 10 channels 20 kHz*; 1 to 16 channels 10 kHz* (20 kHz if using a 1 GHz Pentium)

* *carried out on PC (PIII 600 mini - 128 Mo)*

Please refer to the specific product data sheet of JAZZ, SYMPHONIE, HARMONIE, MELODIE for detailed technical data.

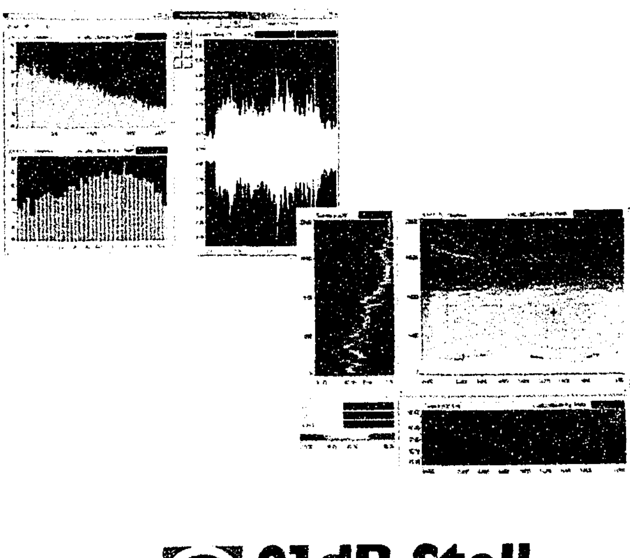

01dB-Stell
MVI technologies group

dBFA32

Benefits

- Multi acquisition front end PC-based system
- Audio recording
- Real-time frequency analysis
- Order and transient analysis
- Time-frequency transforms
- Multi-tasking processing
- User-friendly

France (Head Office)
565, rue de Sans-Souci
F-69760 Limonest
Tel. +33 4 72 20 91 00
Fax. +33 4 72 20 91 01

Italy
Tel. +39 49 920 0966
Fax. +39 49 920 1239

USA
Tel. +1 315 685 31 41
Fax. +1 315 685 31 94

Brazil
Tel. / Fax. +55 11 4992 3600

Asia Pacific
Tel. +60 3 73 22 633
Fax. +60 3 73 18 633

Web: http://www.01db-stell.com
Mail: infogb@01db-stell.com

Rev. 01.2002

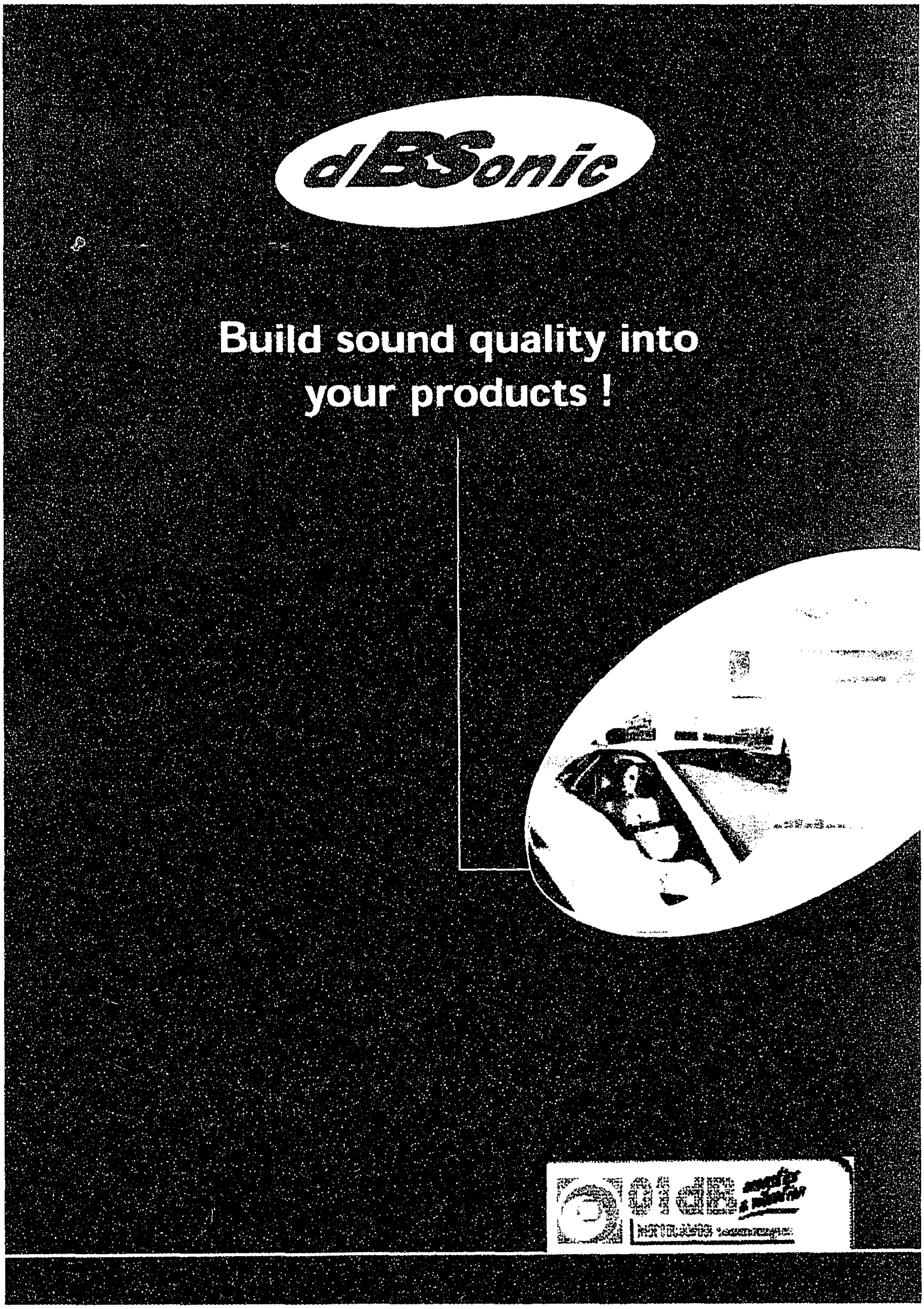
dBSonic
Build sound quality into
your products !
01dB

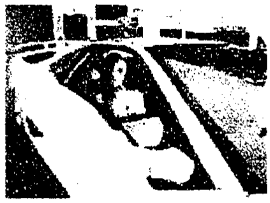

dBSonic is an off-line sound analysis software designed to fulfill the various needs of technical centers, laboratories and industrial engineering offices for performing efficient sound quality analysis.

dBSonic benefits from the long experience acquired with the CORTEX Acoustic Workstation which started in 1989 as the first digital psychoacoustics measurement system with real-time loudness analysis worldwide and the first digitally equalized Binaural Recording Head MK1 in 1996. Leading-edge technology in Sound Quality has been continuously developed at CORTEX (now part of the 01dB group) resulting in **dBSonic** strongest features:

- Ergonomic and innovative sound design
- Precise psychoacoustics and standardized measurements (IEC, DIN EN, ANSI, ...)
- Easy and intuitive operation
- Fast and flexible documentation

The Sound Quality system **dBSonic** is optimized for use with a manikin. Several other front ends are supported (Symphonie, Orchestra, ...) as well as Windows™ measurement systems.

The Sound Quality software package **dBSonic** offers a wide range of solutions to fit with general and specific customers requirements according to their application fields:

- Multipurpose sound analysis
- Engine noise analysis
- Acoustic design of industrial products
- Squeak and rattle
- Psychoacoustics R&D activities
- Musical acoustics
- Speech analysis and synthesis
- Education and training

With **dBSonic**, annoying sound components are easily analyzed, identified, documented and removed by creating targets sounds with its most innovative sound design tools PerceptualXplorer and FilterXplorer.

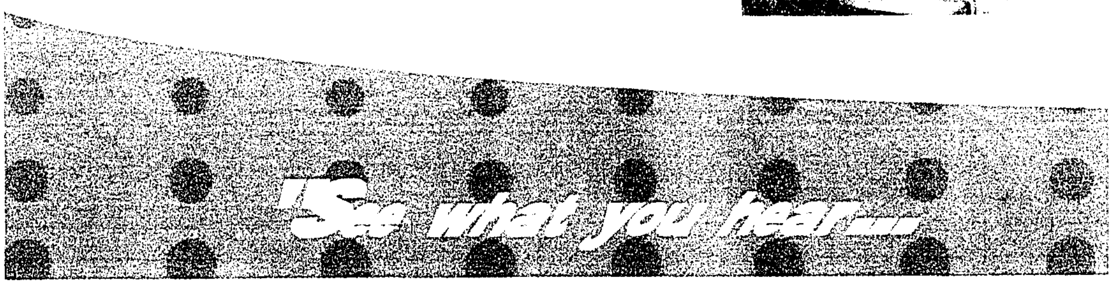

Innovative sound design

Powerful tools for the exploration of critical time variant and transient sounds.

Easy Creation of target sounds by intuitive editing and resynthesis of auditory spectrograms.

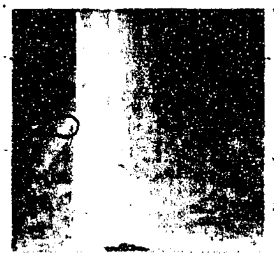

Auditory Analysis

- Whistling identification (circle)
- Clattering is caused by the fact that the sound consists of 3 single "events" within a short time

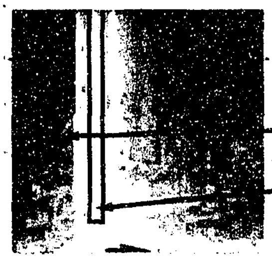

Synthesis of a target sound

1. Reduce level of whistling (arrow) by 18 dB (i.e. becomes less audible!)
2. Delete the second "event". After re-synthesis: the clattering has disappeared, but the sound is still too "hard".
3. Move the third event in the time domain (nearer to event 1).

Resynthesis:

The sound is softer, the two remaining events are not perceived separately any more.
The door sound provides a solid and quality impression.

Example: Modifying a Car Door-Slam-Noise

Hearing perception: weak initial whistling and clattering results in a poor quality sounding door slam

Comprehensive analysis

Standardized analysis capability order analysis, ...).

Accurate psychoacoustic metrics

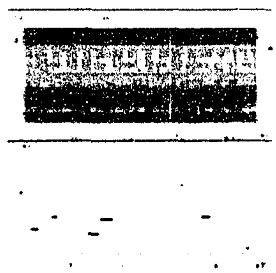

The time history of the loudness band at 2 kHz shows strong modulations, which are much more regular and distinct in the second part (diesel engine) of the recording.

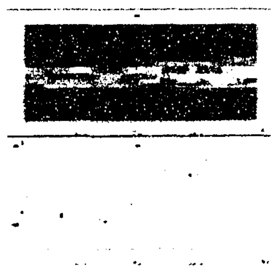

The Roughness analysis shows that the modulations in the second part of the recording cause an increase in perceived roughness.

Example: Comparision of Otto and Diesel

MAIN REFERENCES

Industrials:

- Bosch, DaimlerChrysler
- Kia Automotive, Rücker
- Siemens VDO, Tyco, Valeo
- Lufthansa, Blaupunkt, ...

(FFT, third-octave analysis,

and indicators.

Both engines show high Loudness values in the range of 2 - 3 kHz (13 - 16 Bark), but the diesel engine sounds much rougher.

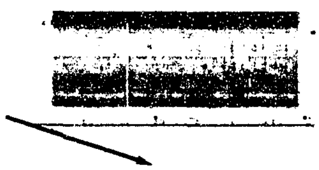

The Modulation analysis shows the strongest modulations in the frequency range around 2 kHz, with high modulations in the second part at 35 Hz and 70 Hz.

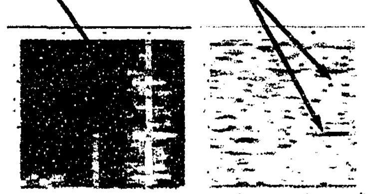

engine with identical third-octave spectra

Results inspection using Waterfall, Spectrogram, Spectrum/Slice Displays.

Ergonomic comparison of different results by dragging and dropping into the multiscalar and multispectra window.

Easy numerical export and adjustment of graphical features according to your individual needs.

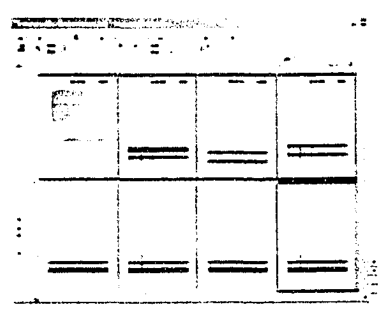

Fast calibrated recording, automated analysis, archiving of results in workspaces and projects, combined with fast and flexible documentation and recordings enables you to make **immediate measurements and complete reports.**

Report Wizard:
Step-by-step set-up of automatic reports for the selected workspace or project. Can be linked to MS WORD templates in order to create standardized reports.

Research centers and Universities:

- DLR Koln, Uni Oldenburg, Uni Hamburg
- FH Stuttgart, FH Regensburg, TU Cottbus
- Musik Hochschule Hannover, PTB Braunschweig
- Iuseong College Korea

System components

With artificial head: AES/EBU digital format

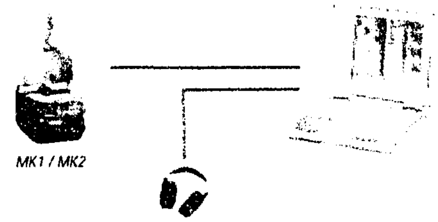

With Opus and digital sound conditionner

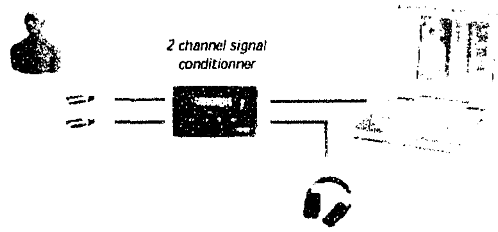

With multichannel front-end

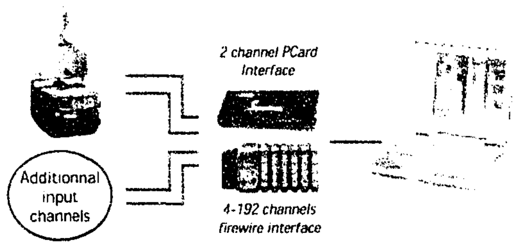

With USB-front-end

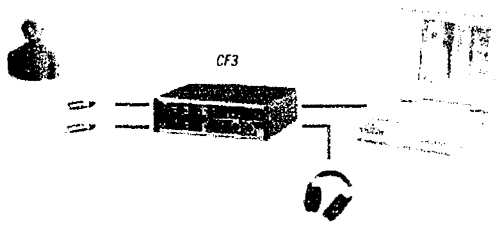

Easy calibration without adapter !
100 % repeatable calibration

Detailed ear and head shape
Provides excellent sound perception and most accurate directivity (according to IEC 951 standard)

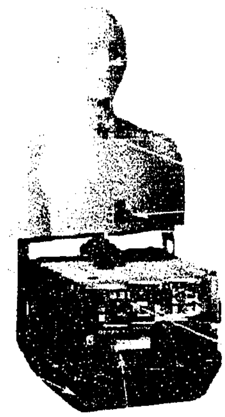

Digital processor units with :
24 bits AD convertors - DSP for equalization
Built-in calibration signal generator

Double tilting mechanism
Enables a realistic posture for correct measurement results

Optimal seat positioning
Safety belt holder - Robust and designed for drive test conditions

Front panel
Digital and analog outputs available simultaneously - RPM input and output

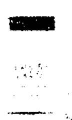

Remote control
For MK1 and optional DAT with RPM display

Optional DAT recorder

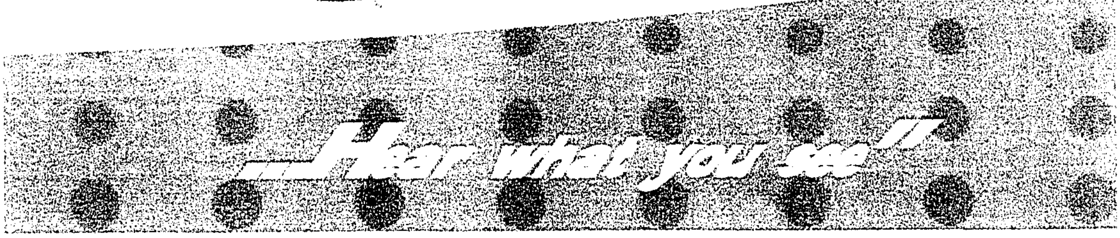

Technical specifications

dBSonic Sound Analysis Package (SAP)
- Sound signal recording and playback
- SPL-analysis according to IEC651 (DIN EN 60651) and ANSI S1.4-1983
- FFT and 1/3 octave analysis (IEC 1260 class 0 and ANSI S1.11-1986)
- Tonality and prominence analysis according to E DIN 45681-2002 and ANSI S1.13-1995
- Basic editing and filtering functions
- Workspace and Project management for multi-channel recordings
- Import of various data formats

dBSonic PerceptualXplorer (PXP)

The acoustic contribution of the individual components of a sound is not a secret any more! Intuitive exploration, editing, resynthesis of time and frequency components "millisecond by millisecond" or "Hertz by Hertz".
Includes: auditory spectrogram (ASP), spectral editor, time and frequency contours, detection of time varying tonal components (tracks), resynthesis.

dBSonic Psychoacoustics Analysis (PSY)

Audible differences between sound signals that you could not even measure in the past can now be expressed in numbers, displayed as spectra and compared exactly by means of psychoacoustics measurement methods.
Includes: "classical" psychoacoustic metrics loudness, sharpness, roughness, fluctuation strength, tonality in proven CORTEX quality, ...

dBSonic Sound Editor and FilterXplorer (SED)
- Cut, copy, paste, delete, trim, fade (in,out), change level, calibrated and hearing-based play back, resampling, import of various sound file formats.
- Graphical and numerical design of real-time and off-line filters. (up to 20 individual filters can be combined to a filter setup, each individual filter can be designed as equalizer, highpass, lowpass, bandpass, bandstop filter with Butterworth or Chebychev characteristics).
- Includes display of transfer functions (magnitude, phase, group delay for individual filters and for filter set) and influence on a reference spectrum.

dBSonic Extended Frequency Analysis (FXA)
- Modulation Analysis with display of modulation depth or level of the envelope versus time and versus modulation frequency for one frequency band or averaged over a time section for several frequency bands (with octave, 1/3 octave, Bark, ERB or freely selectable filter bandwidth)
- Includes Wavelet Analysis

dBSonic RPM Module (RPM)
- Order analysis based on resampling and order extraction
- RPM depending display for all analysis results (FFT, 1/3 octave, ASP, tracks)
- Simultaneous display of frequency vs. time/rpm or order vs. rpm with order cursor (scaled lin, log or in Bark)
- Multi-RPM/Order display for fast and effective comparision of orders from different recordings. RPM related A/B comparison
- Automatic recognition of a tacho signal in the LSB (16th bit) of a recording.
- Post-processing for tacho signal (smoothing, adjustment of prescaler)

dBSonic Documentation Module (DOC)
- Fast and easy documentation of selectable metrics by means of multiscalar and multispectra display
- Percentile calculation
- Workspace report and Report Wizard

dBSonic Difference Analysis (DIF)

Differences between two samples can be visualized in distance spectrograms for any analysis method of dBSONIC.
A/B Comparison of samples or marked sections, automatic sorting of the cliplist according to given categorical judgements.
Includes MEAN function and intuitive "clip-list" music box capability (jury)

dBSonic MATLAB® Interface (MAT)
- MATLAB® routines for importing dBSONIC files into MATLAB®
- Includes graphical user interface

MATLAB is a registered trademark of The MATHWorks Inc.

Benefits

- Leading-edge Sound Quality package resulting from more than 15 years of experience
- Easy and intuitive to operate
- Auditory spectrograms with high time and frequency resolution according to the human ear
- Accurate psychoacoustic metrics
- Innovative PerceptualXplorer enabling intuitive Sound design
- Fast and flexible documentation

France (Head Office):
200 chemin des Ormeaux
F - 69578 Limonest Cedex
Phone +33 4 72 52 48 00
Fax +33 4 72 52 47 47

Germany
Phone +49 7552 / 938 570
Fax +49 7552 / 938 571

Italy
Phone +39 049 920 0966
Fax +39 049 920 1239

USA
Phone +1 315 685 31 41
Fax +1 315 685 31 94

Brazil
Phone +55 11 55 79 6460
Fax +55 11 55 79 6610

Asia Pacific
Phone +60 3 563 22 633
Fax +60 3 563 18 633

Web: www.01db.com
Mail: infogb@01db.com

Rev. 10 2003

The presented characteristics are subject to change without notice.

APPENDIX D

D. Collected Noise Data

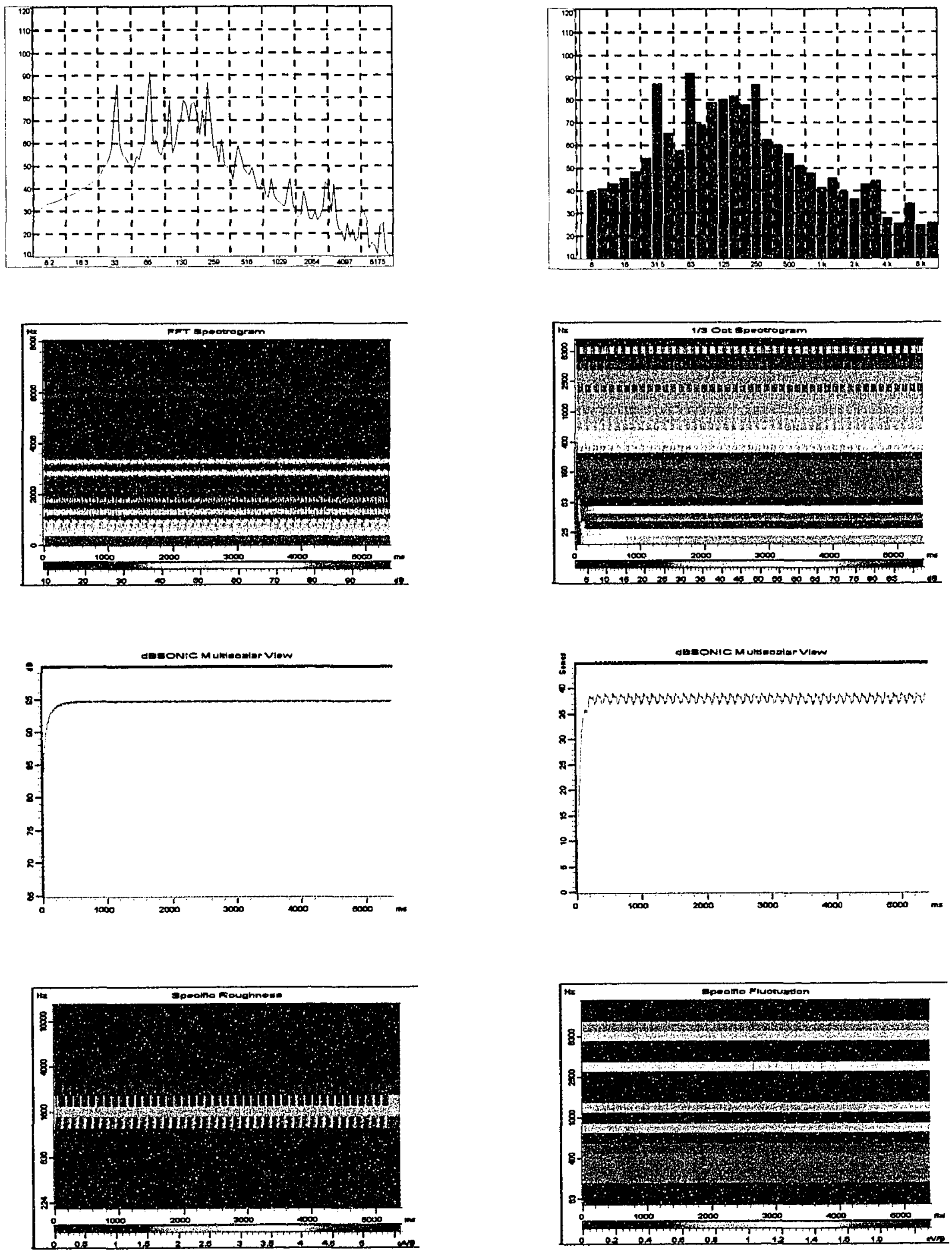

EXHIBIT D1 - Numerical Unmodified Results at 1000 rpm

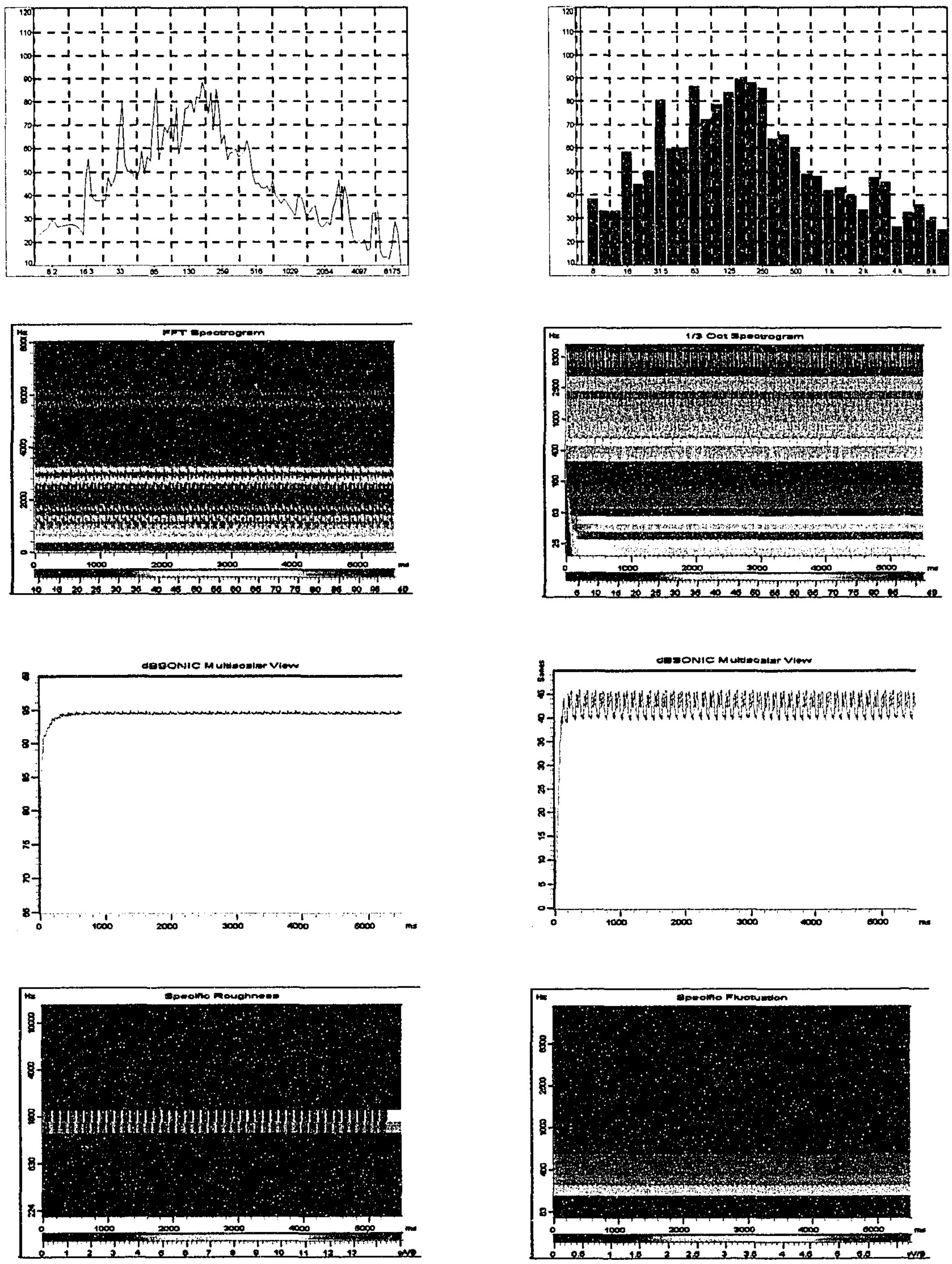

EXHIBIT D2 - Numerical Bridged Results at 1000 rpm

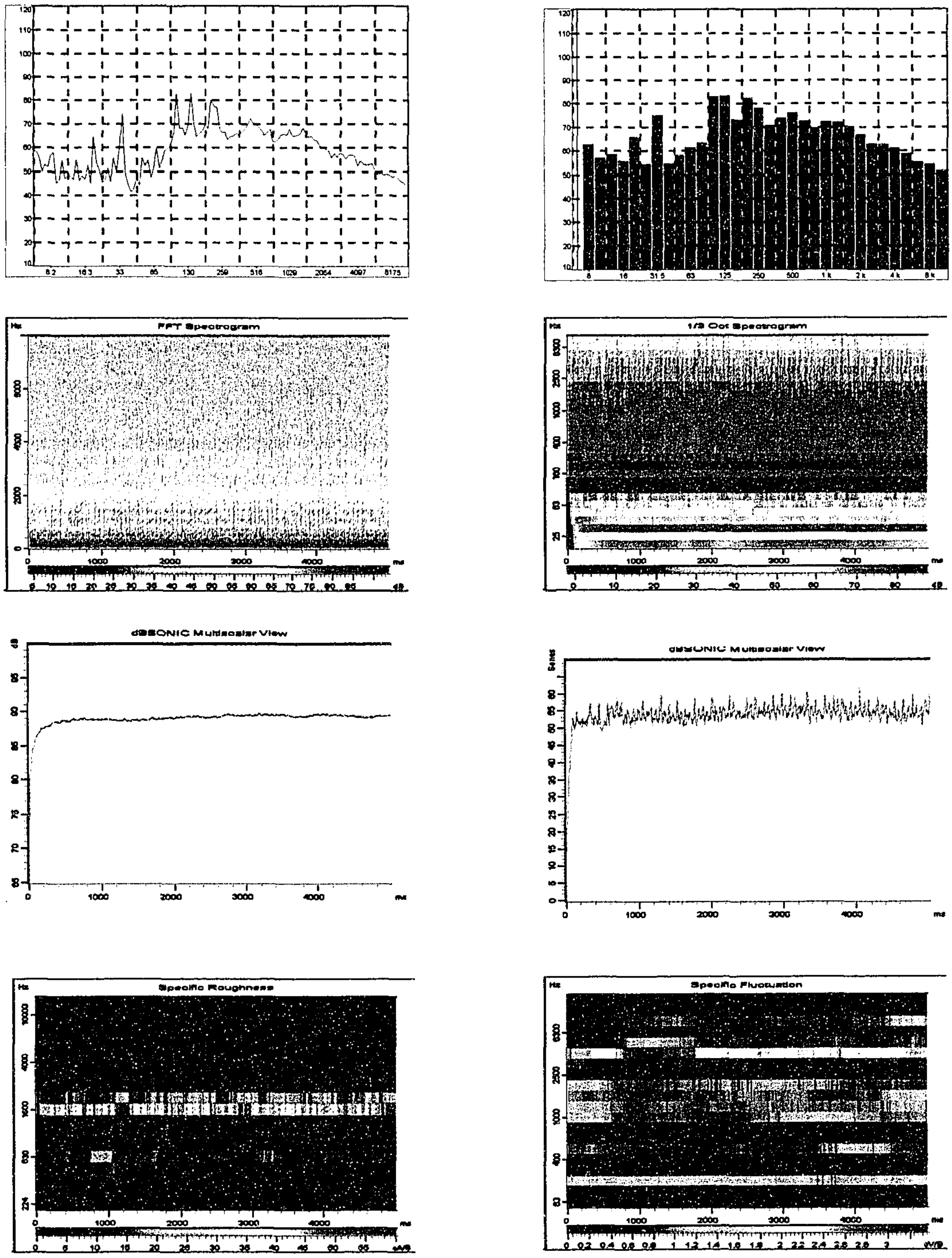

EXHIBIT D3 - Experimental Unmodified Results at 1000 rpm

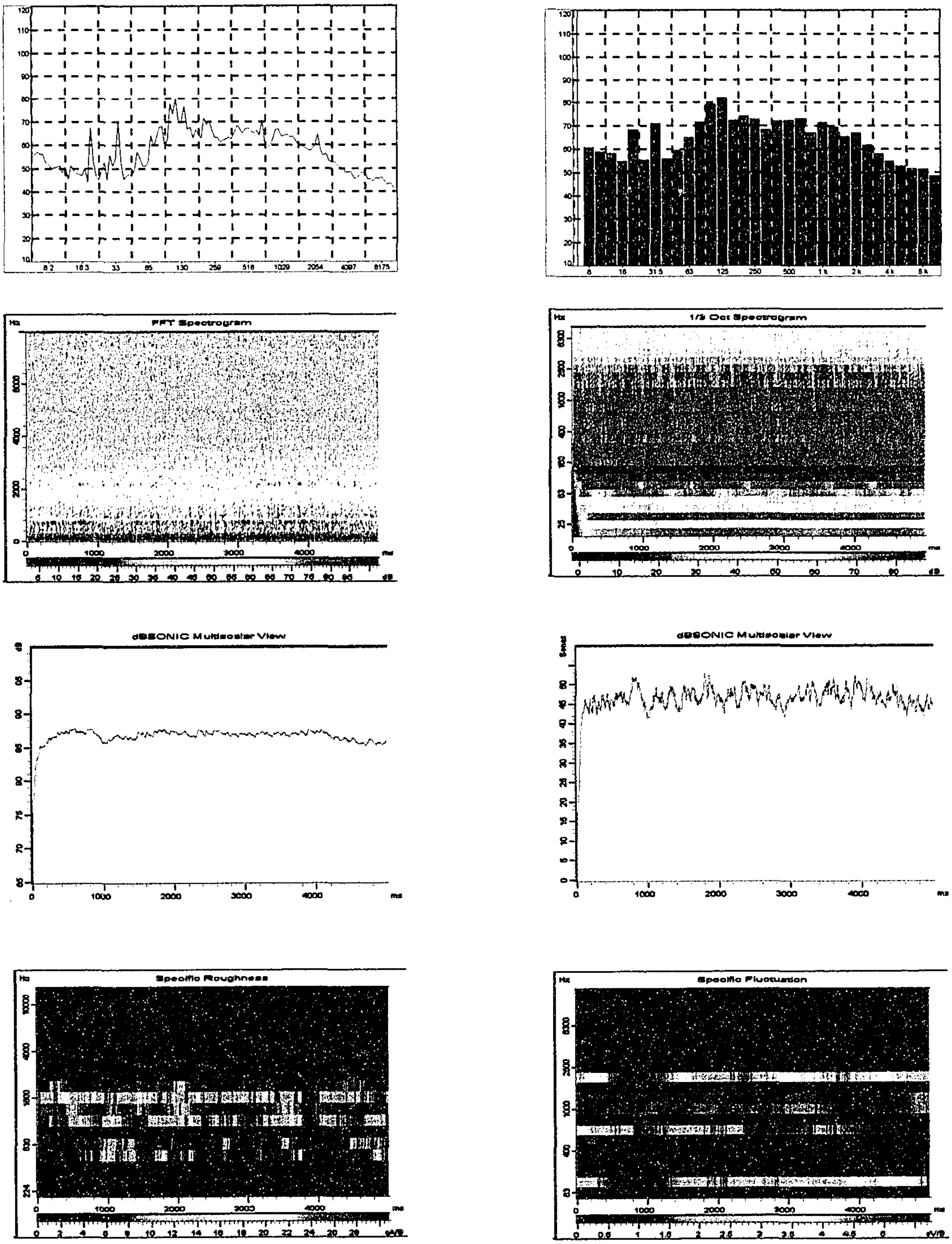

EXHIBIT D4 - Experimental Bridged Results at 1000 rpm

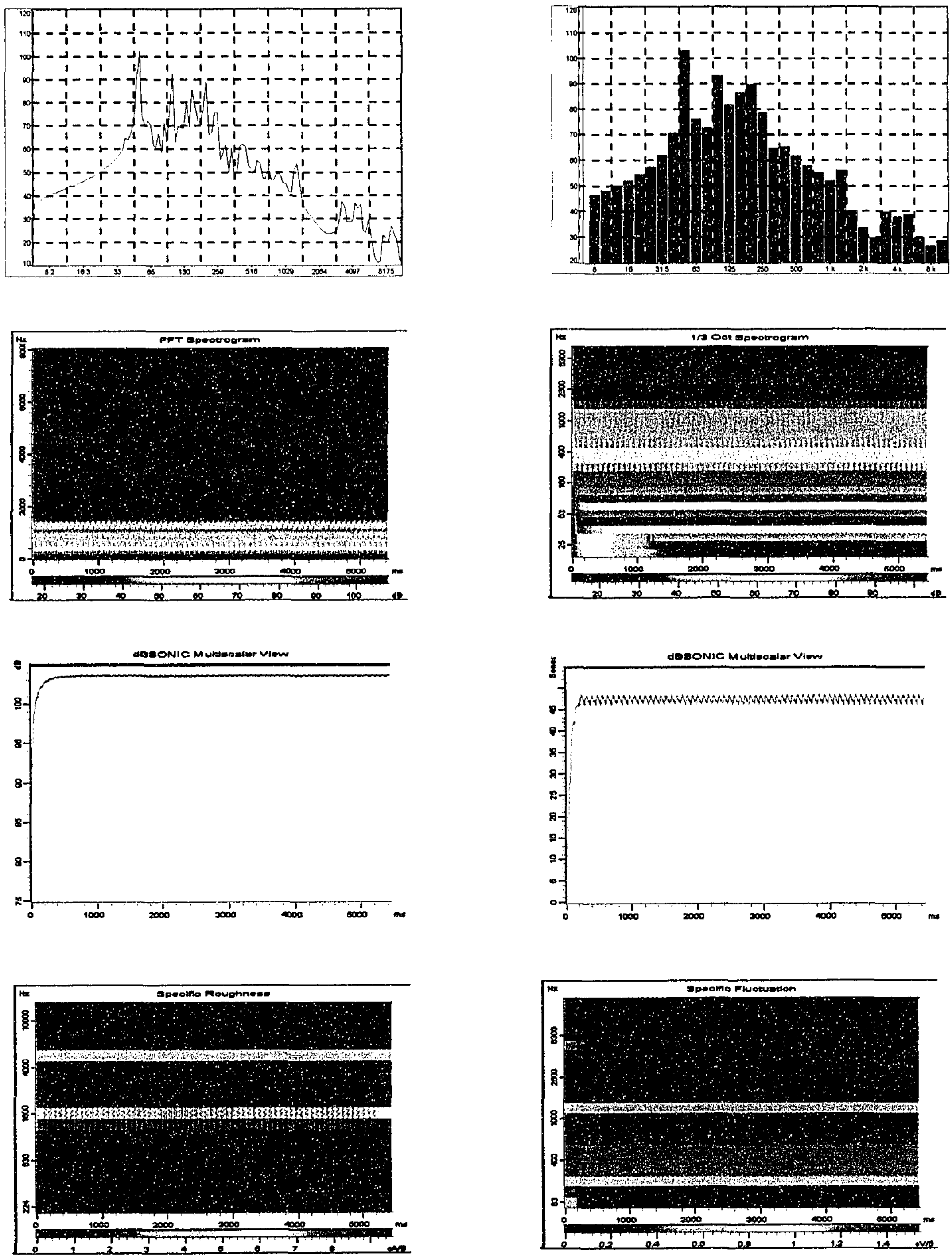

EXHIBIT D5 - Numerical Unmodified Results at 1500 rpm

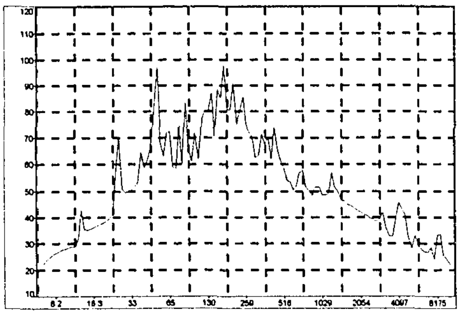

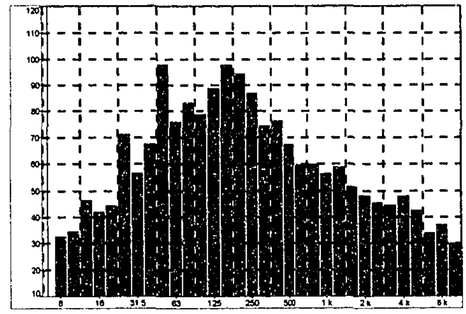

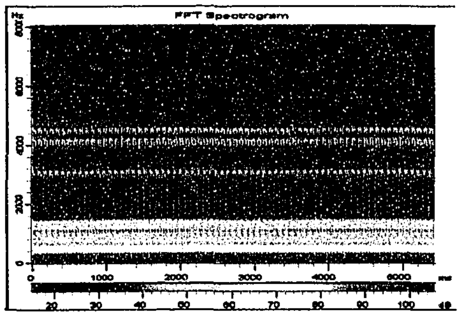

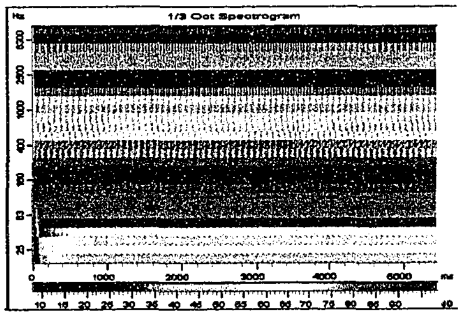

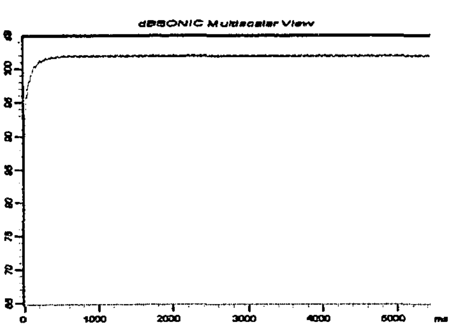

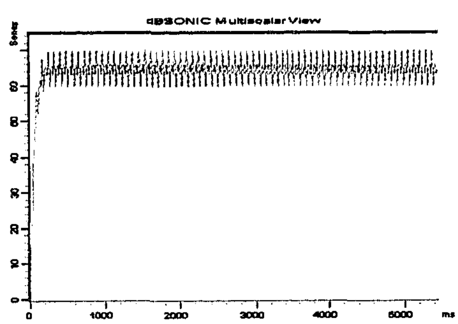

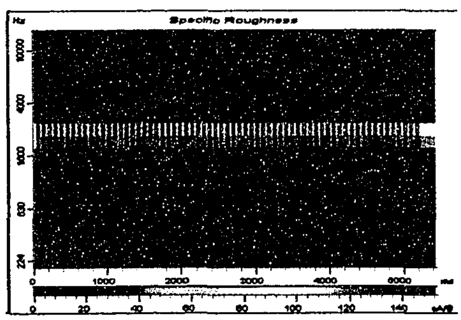

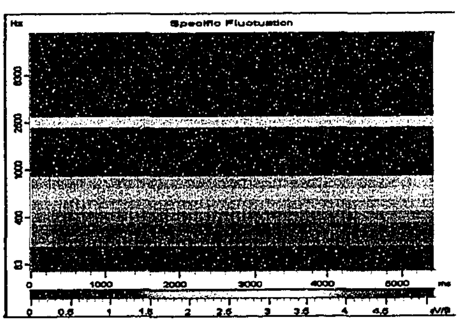

EXHIBIT D6 - Numerical Bridged Results at 1500 rpm

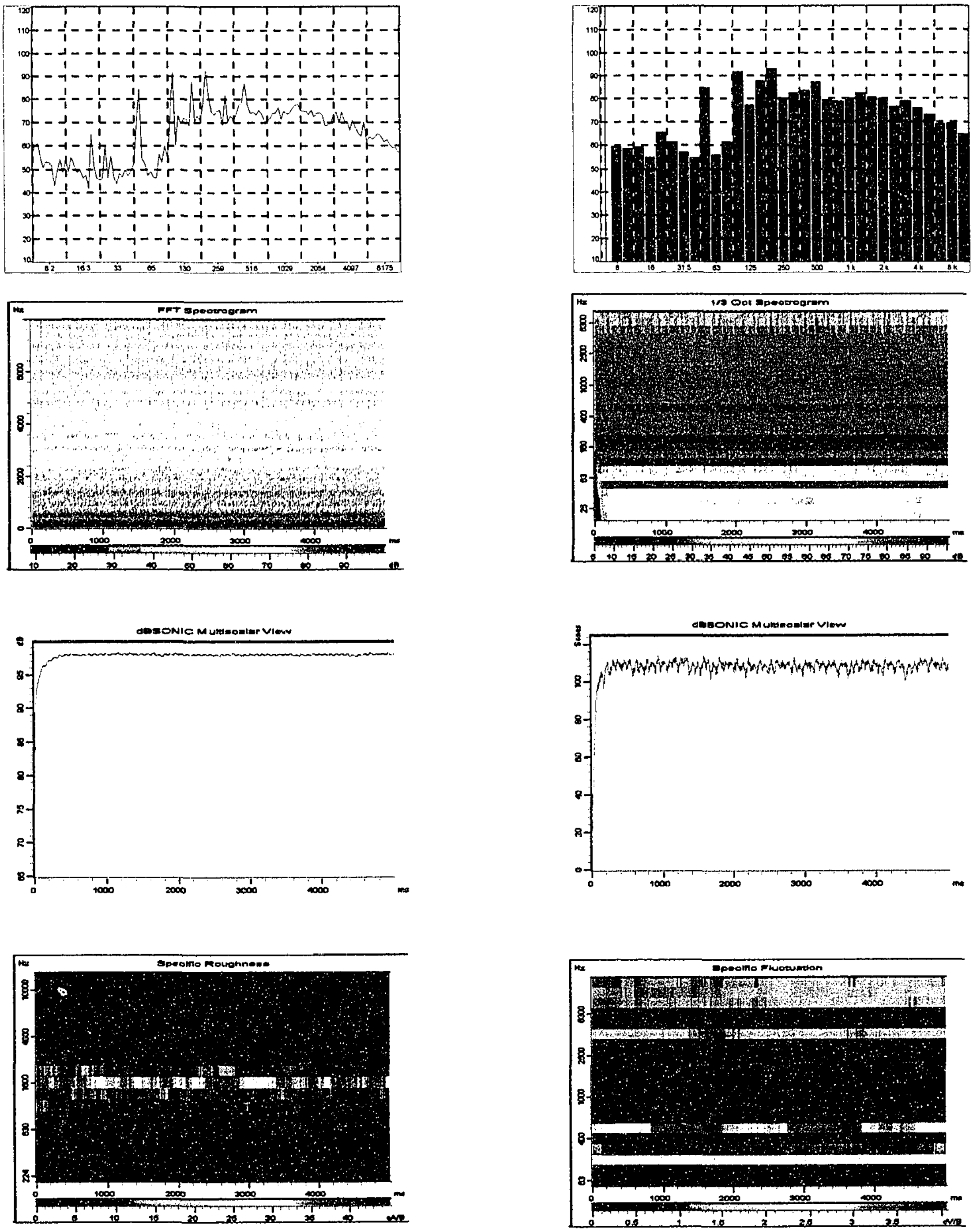

EXHIBIT D7 - Experimental Unmodified Results at 1500 rpm

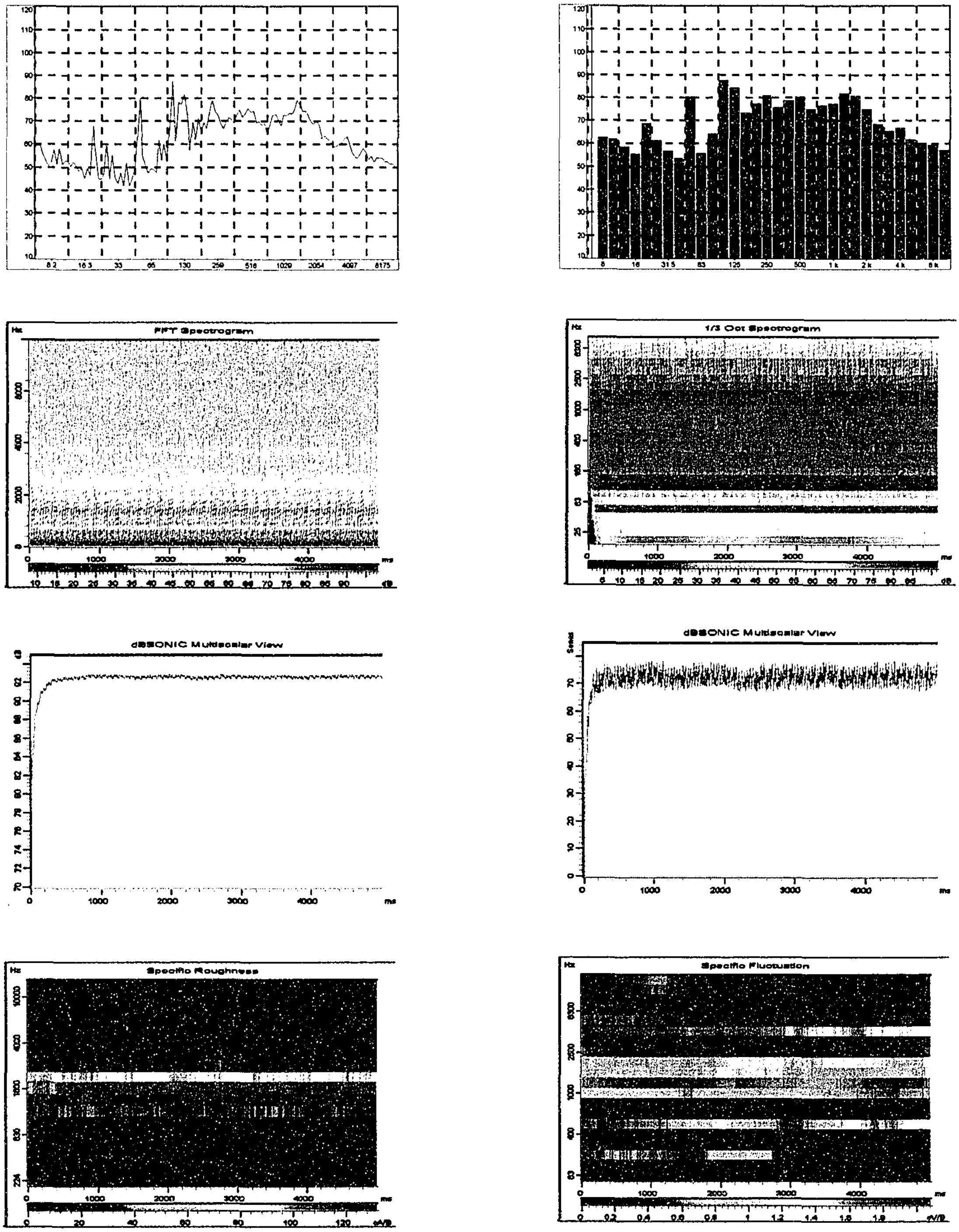

EXHIBIT D8 - Experimental Bridged Results at 1500 rpm

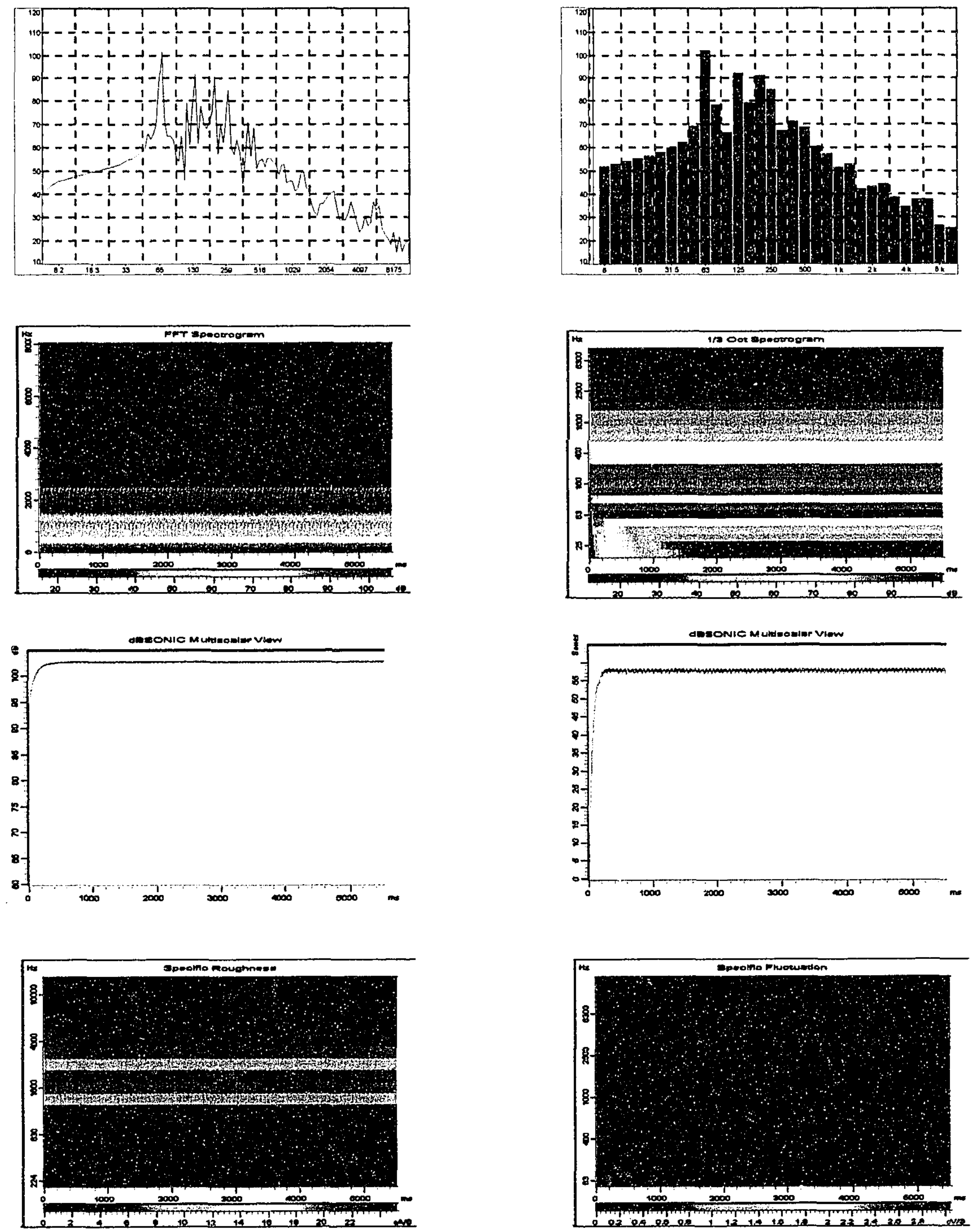

EXHIBIT D9 - Numerical Unmodified Results at 2000 rpm

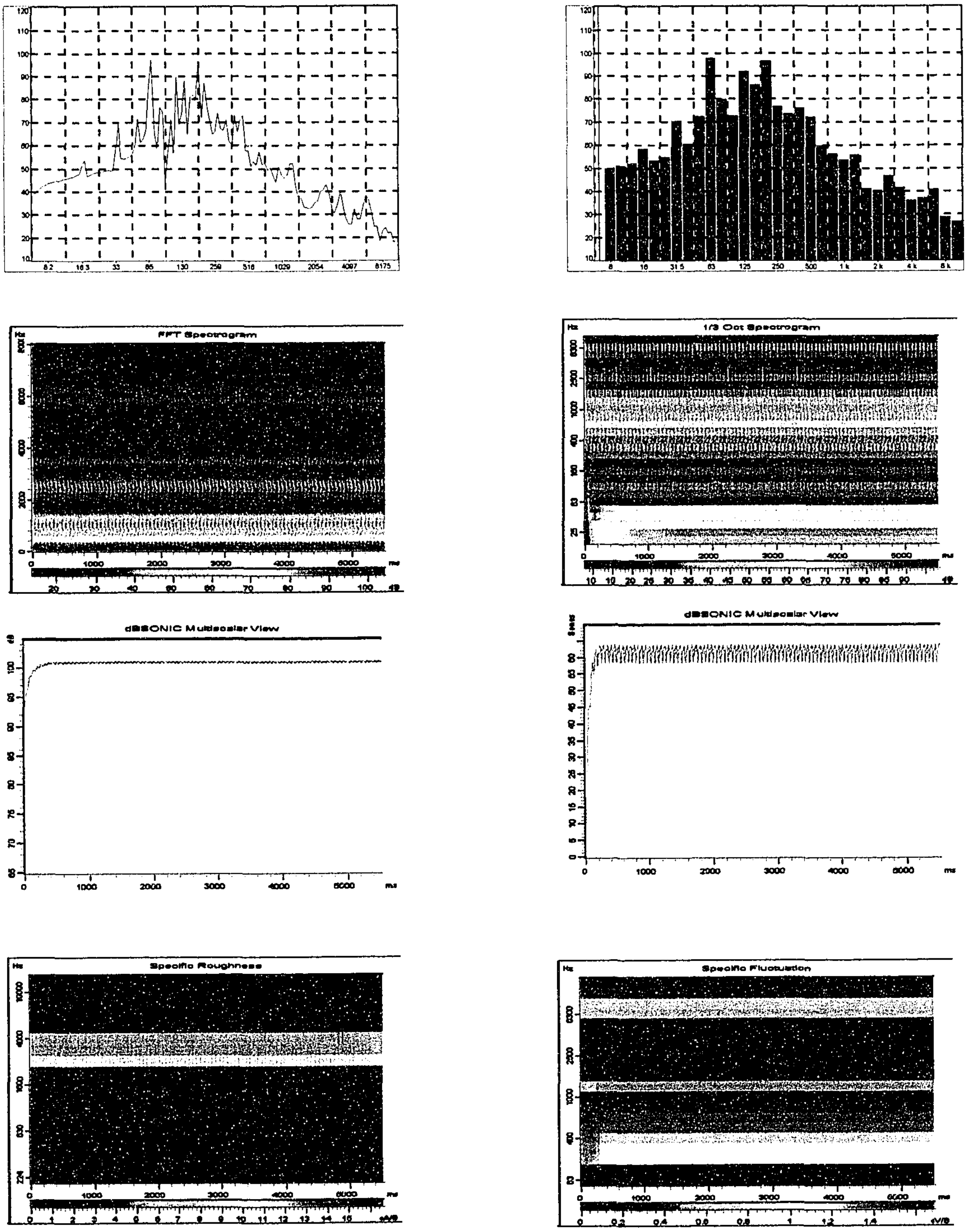

EXHIBIT D10 - Numerical Bridged Results at 2000 rpm

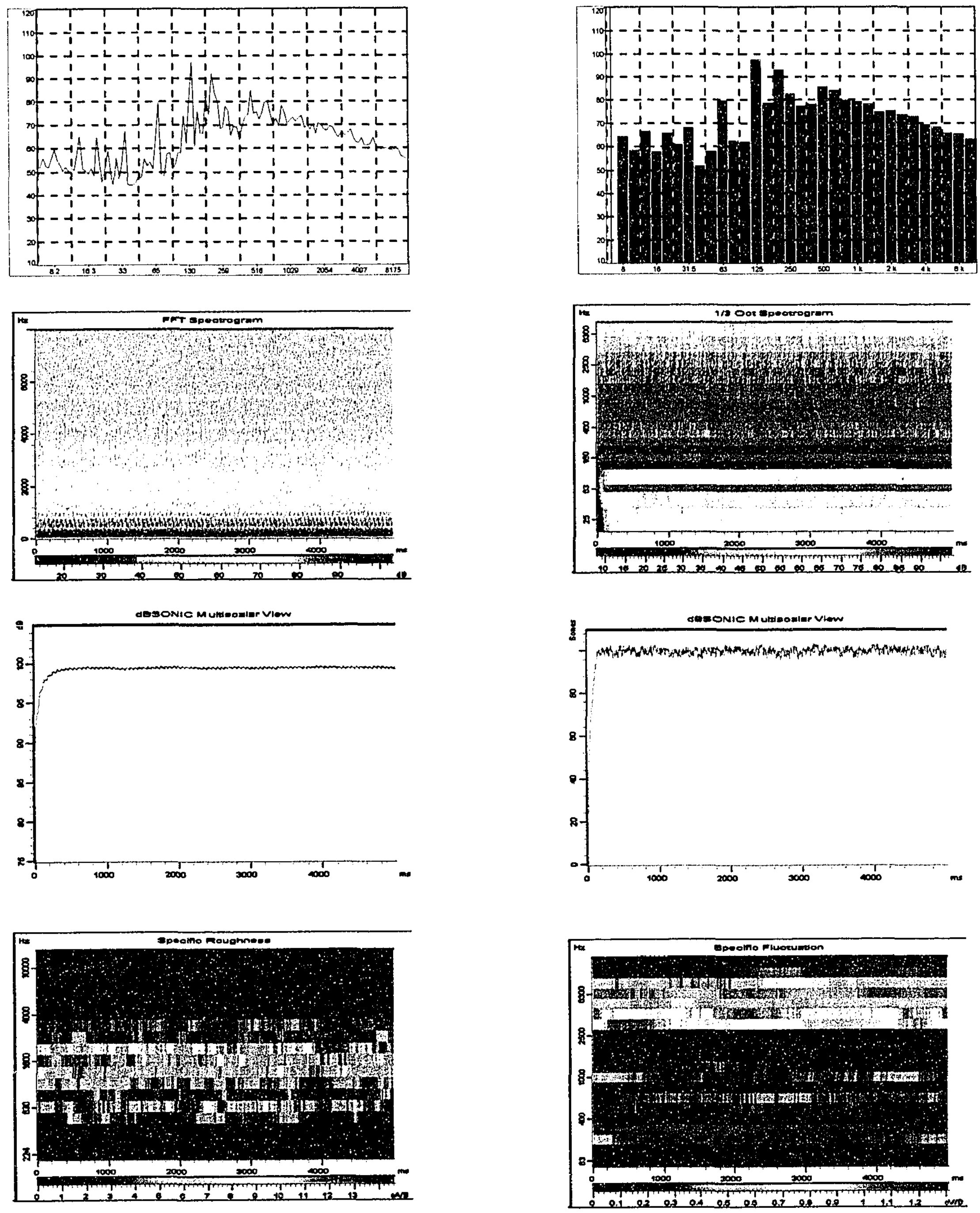

EXHIBIT D11 - Experimental Unmodified Results at 2000 rpm

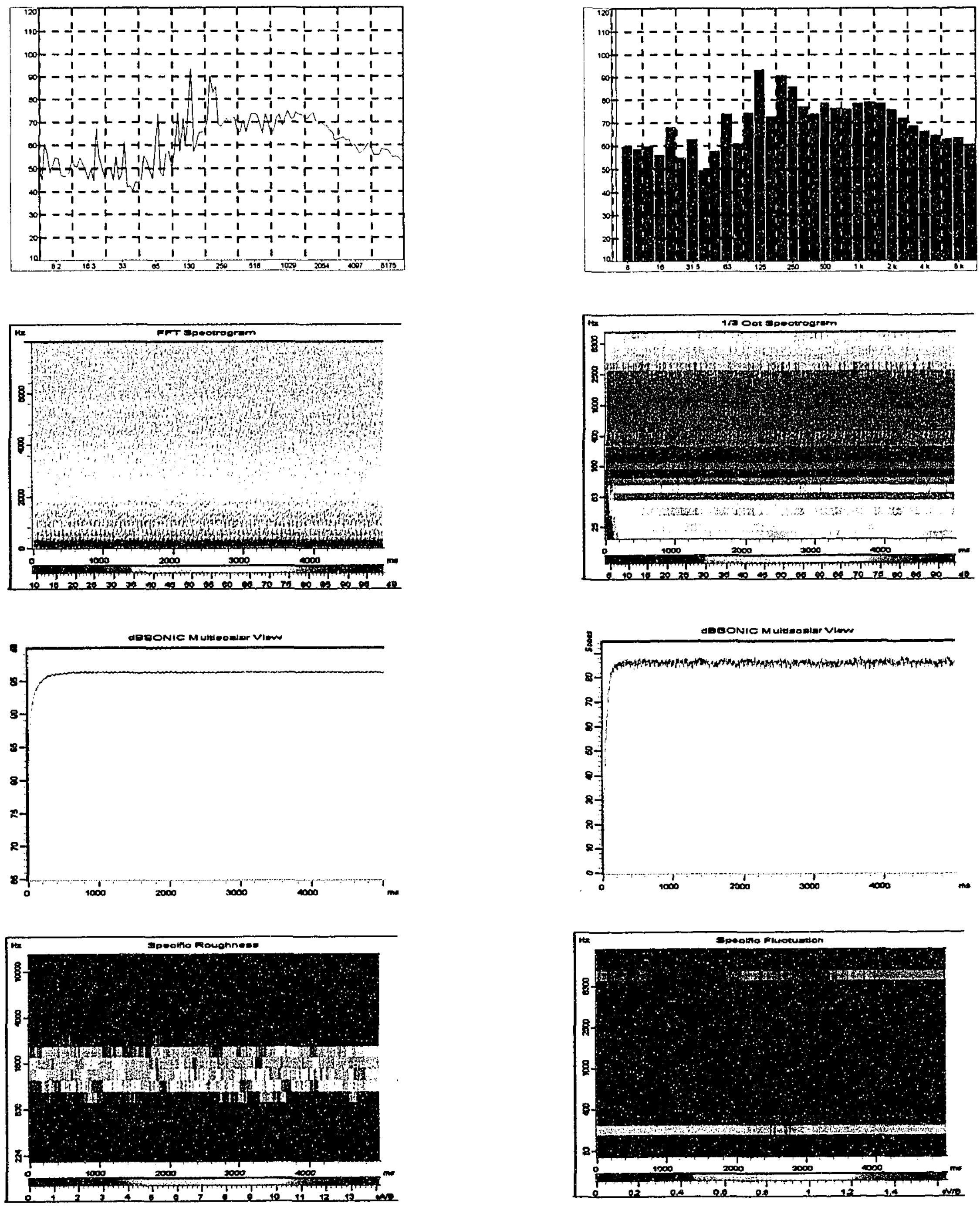

EXHIBIT D12 - Experimental Bridged Results at 2000 rpm

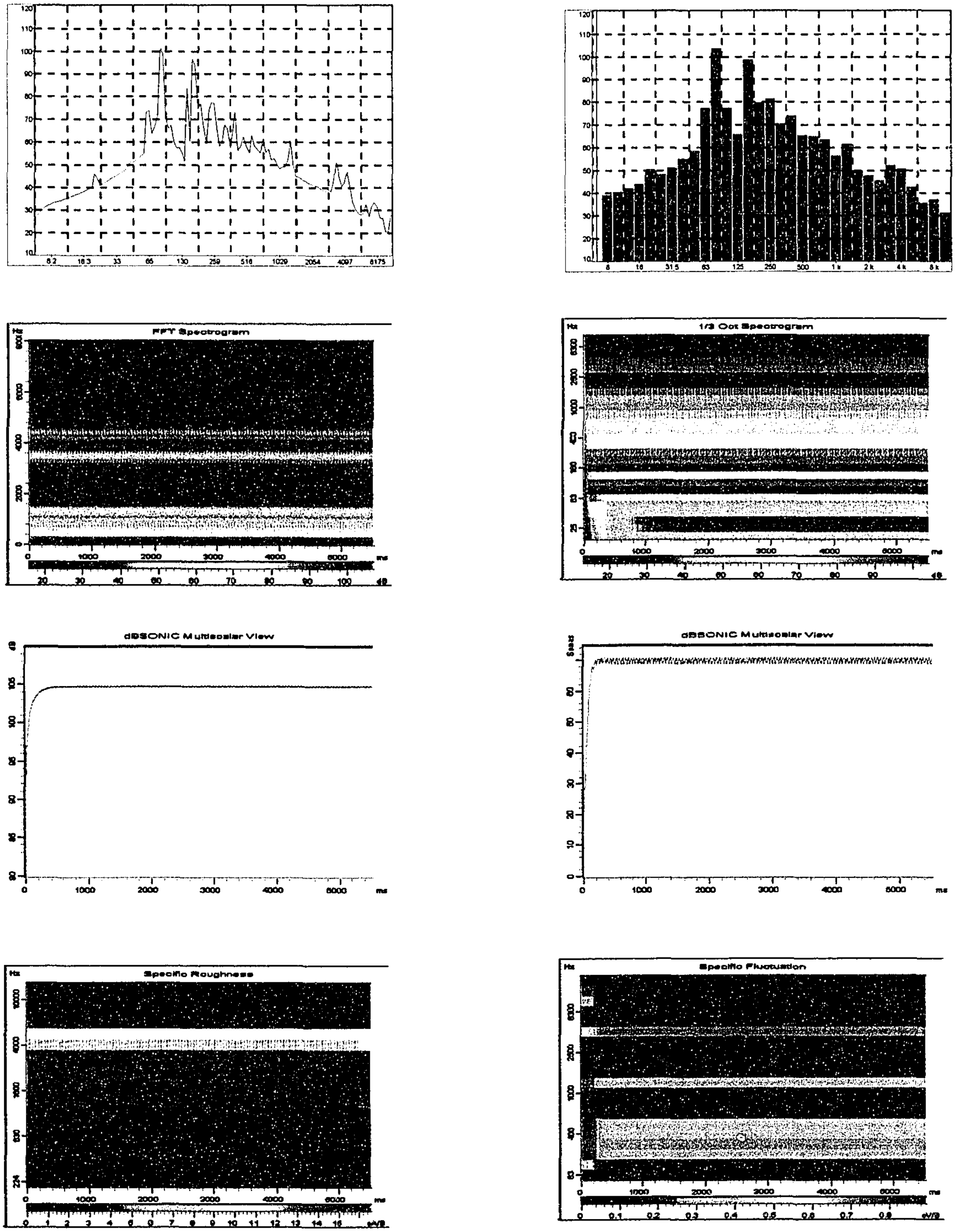

EXHIBIT D13 - Numerical Unmodified Results at 2500 rpm

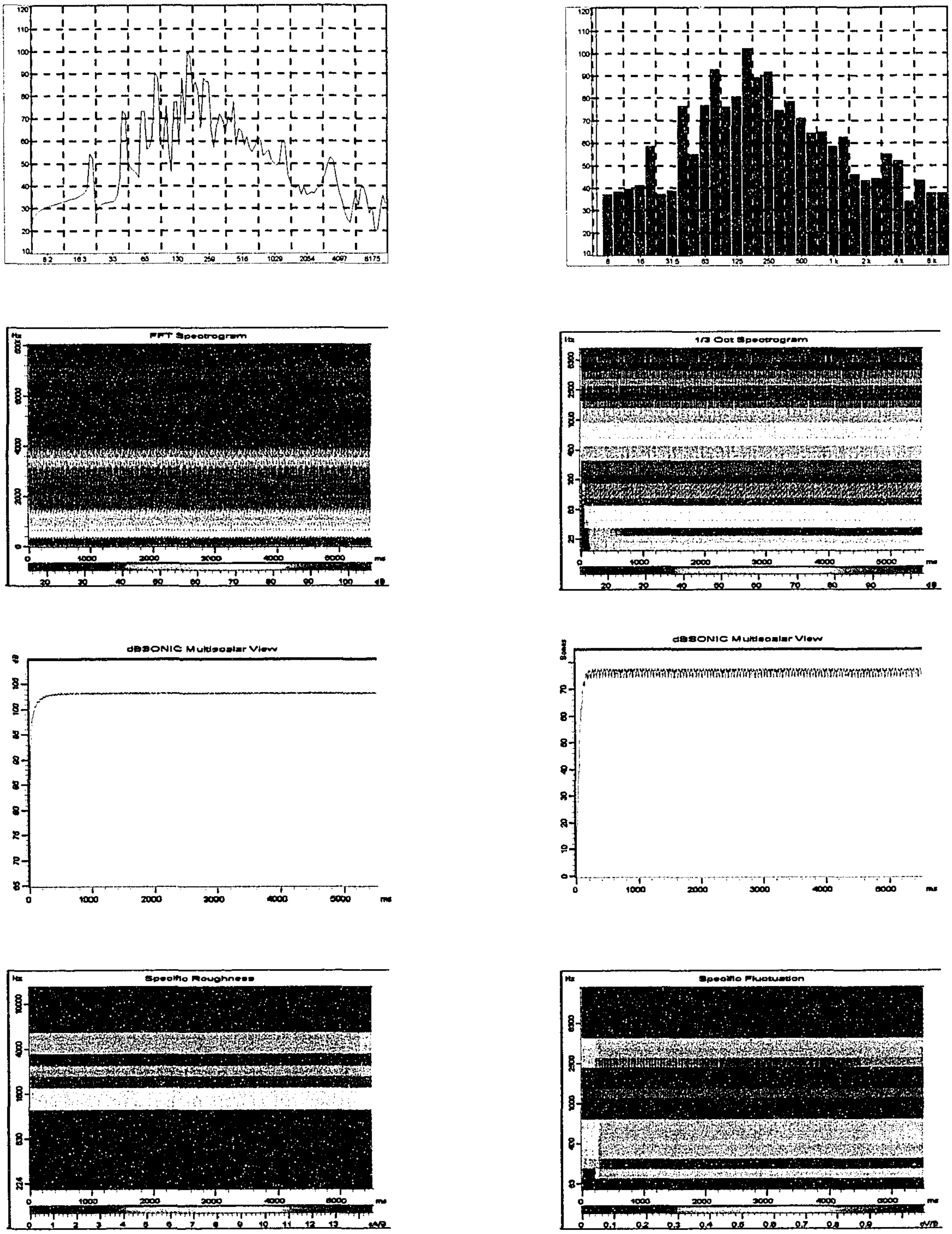

EXHIBIT D14 - Numerical Bridged Results at 2500 rpm

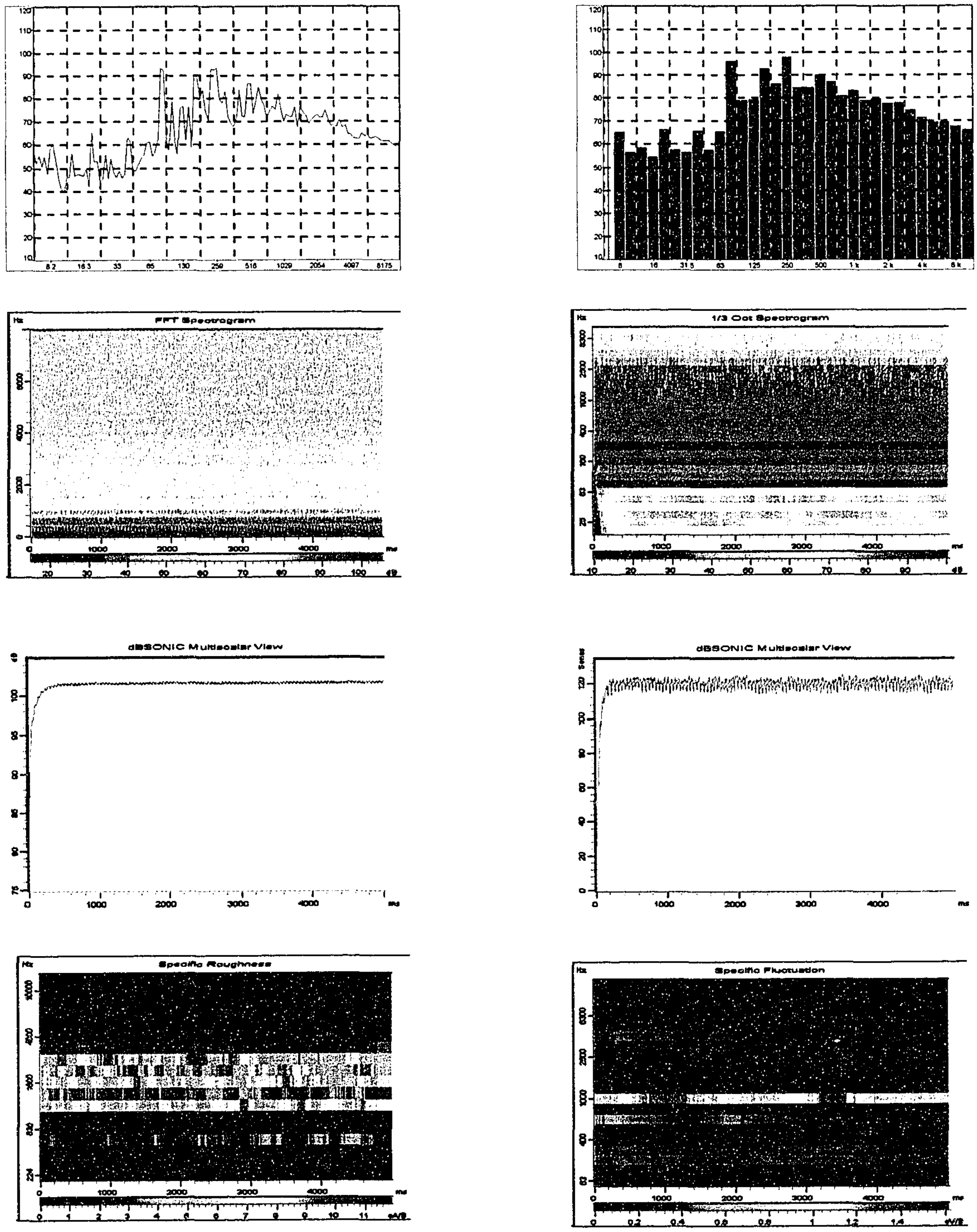

EXHIBIT D15 - Experimental Unmodified Results at 2500 rpm

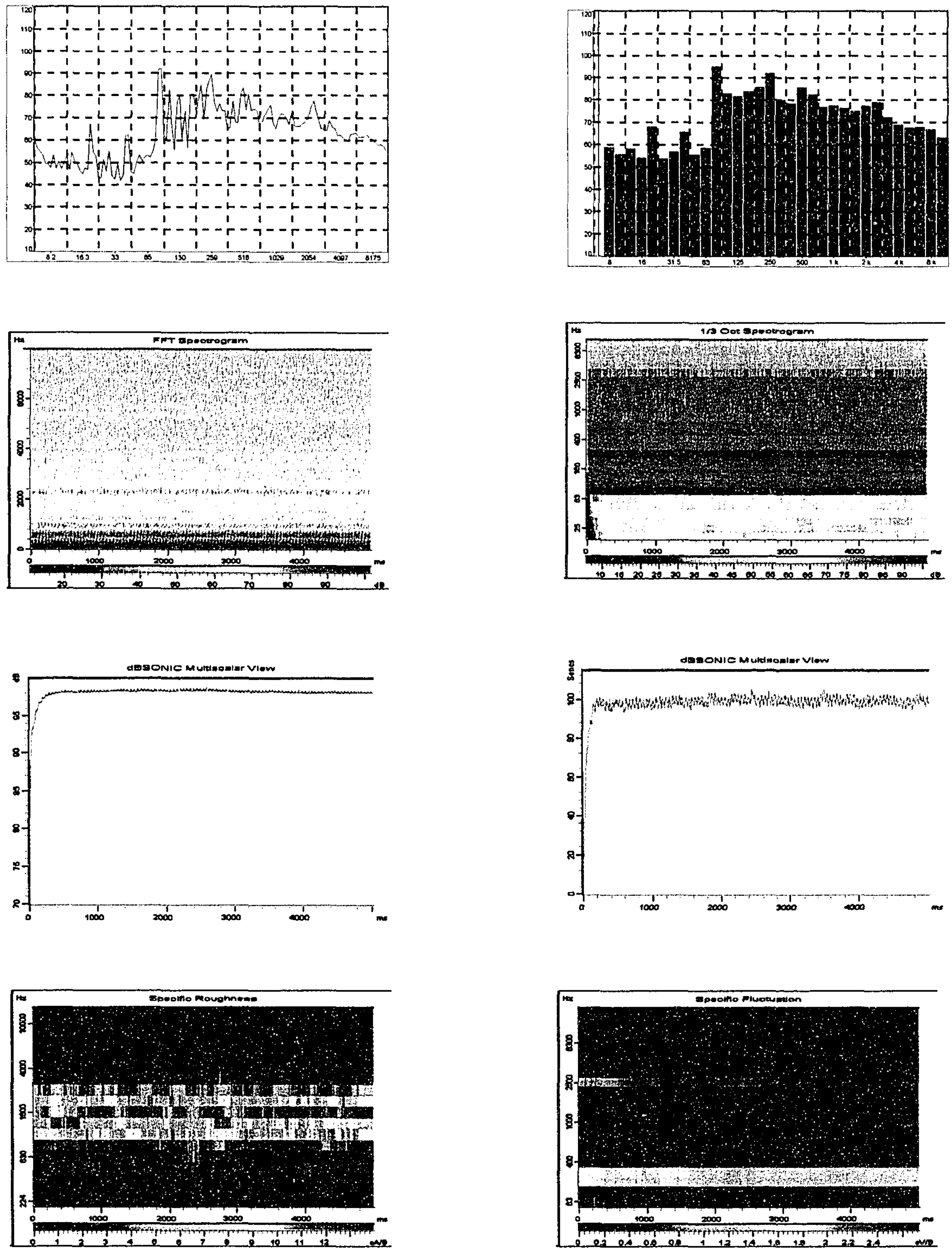

EXHIBIT D16 - Experimental Bridged Results at 2500 rpm

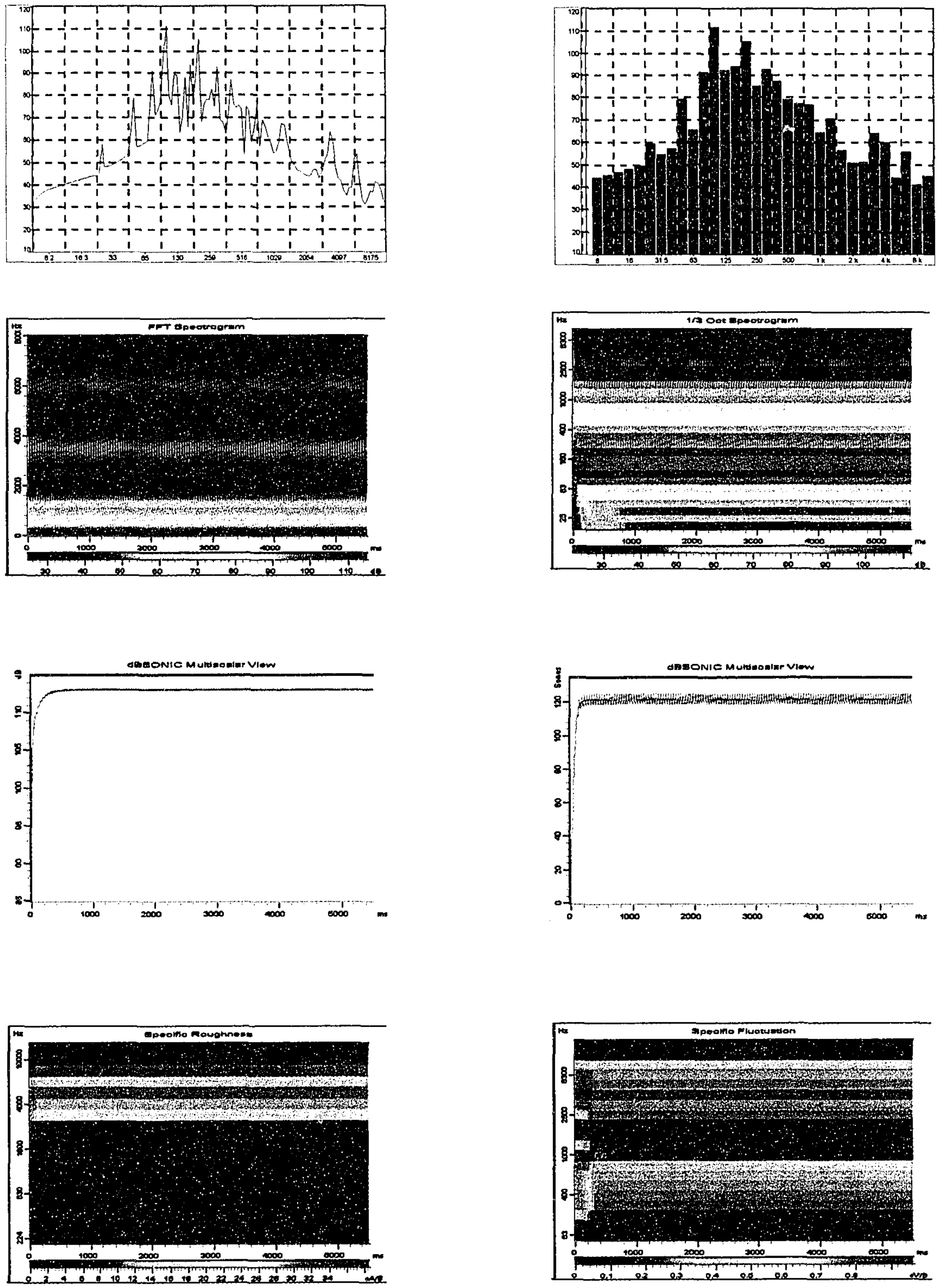

EXHIBIT D17 - Numerical Unmodified Results at 3000 rpm

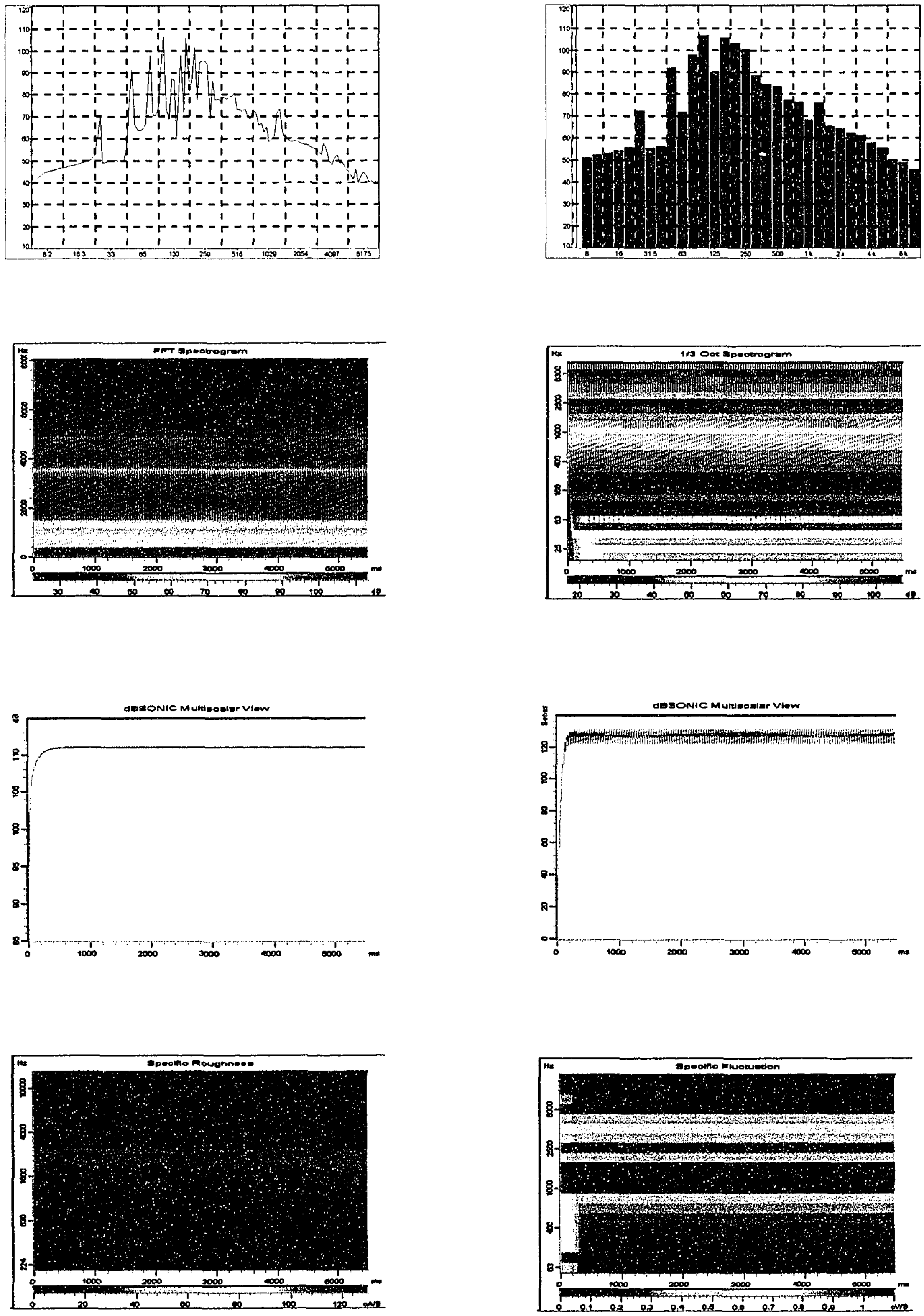

EXHIBIT D18 - Numerical Bridged Results at 3000 rpm

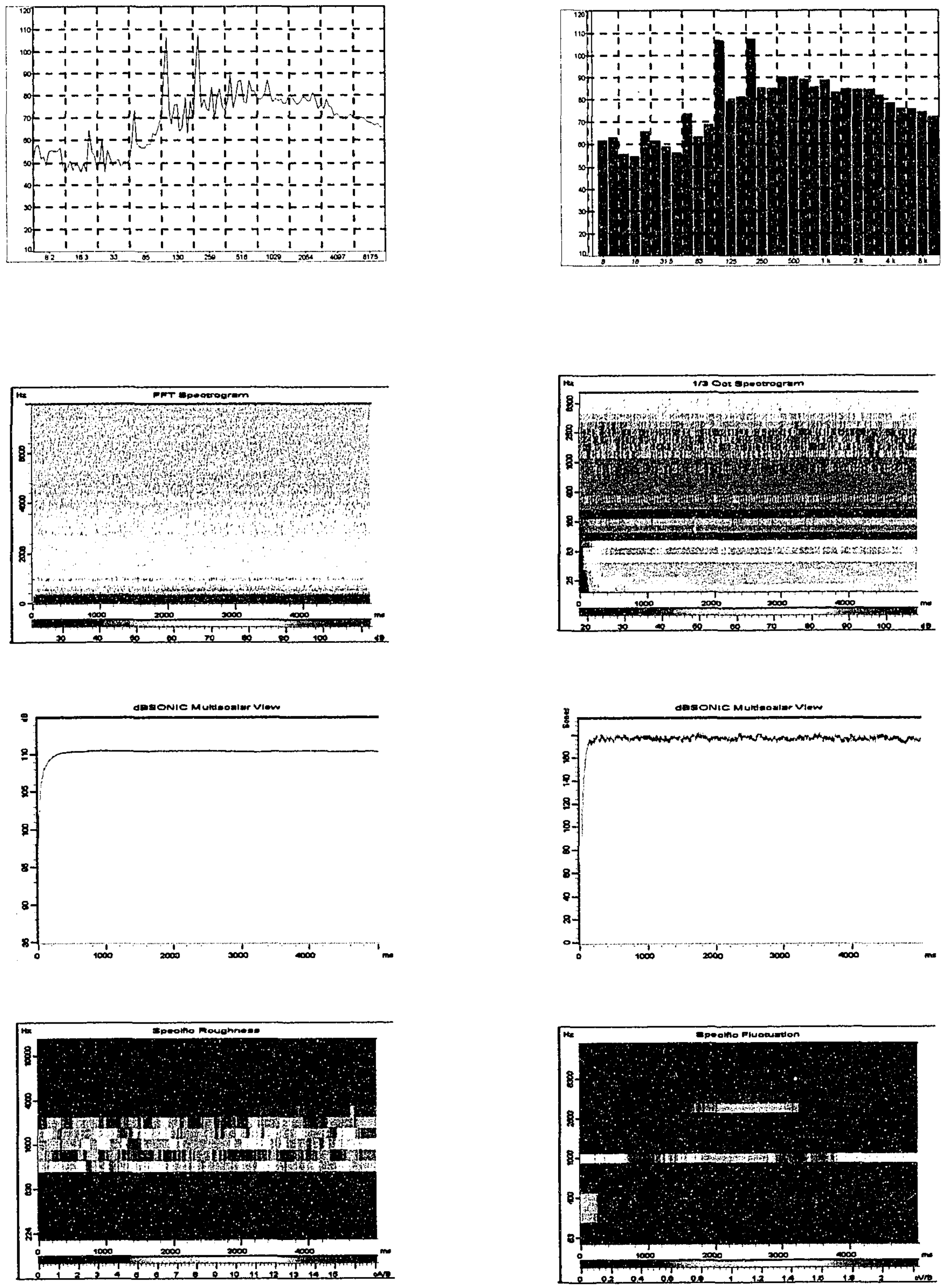

EXHIBIT D19 - Experimental Unmodified Results at 3000 rpm

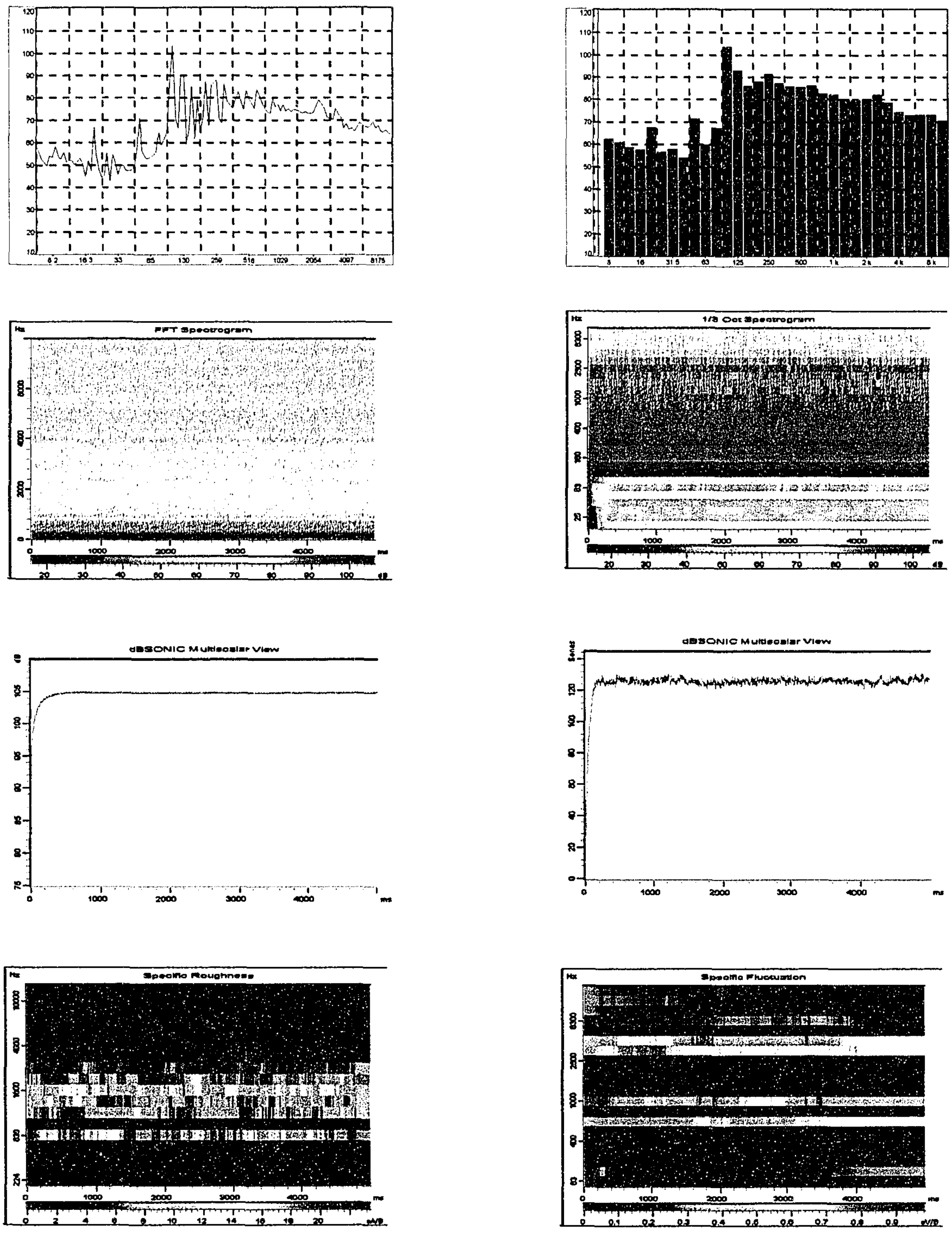

EXHIBIT D20 - Experimental Bridged Results at 3000 rpm

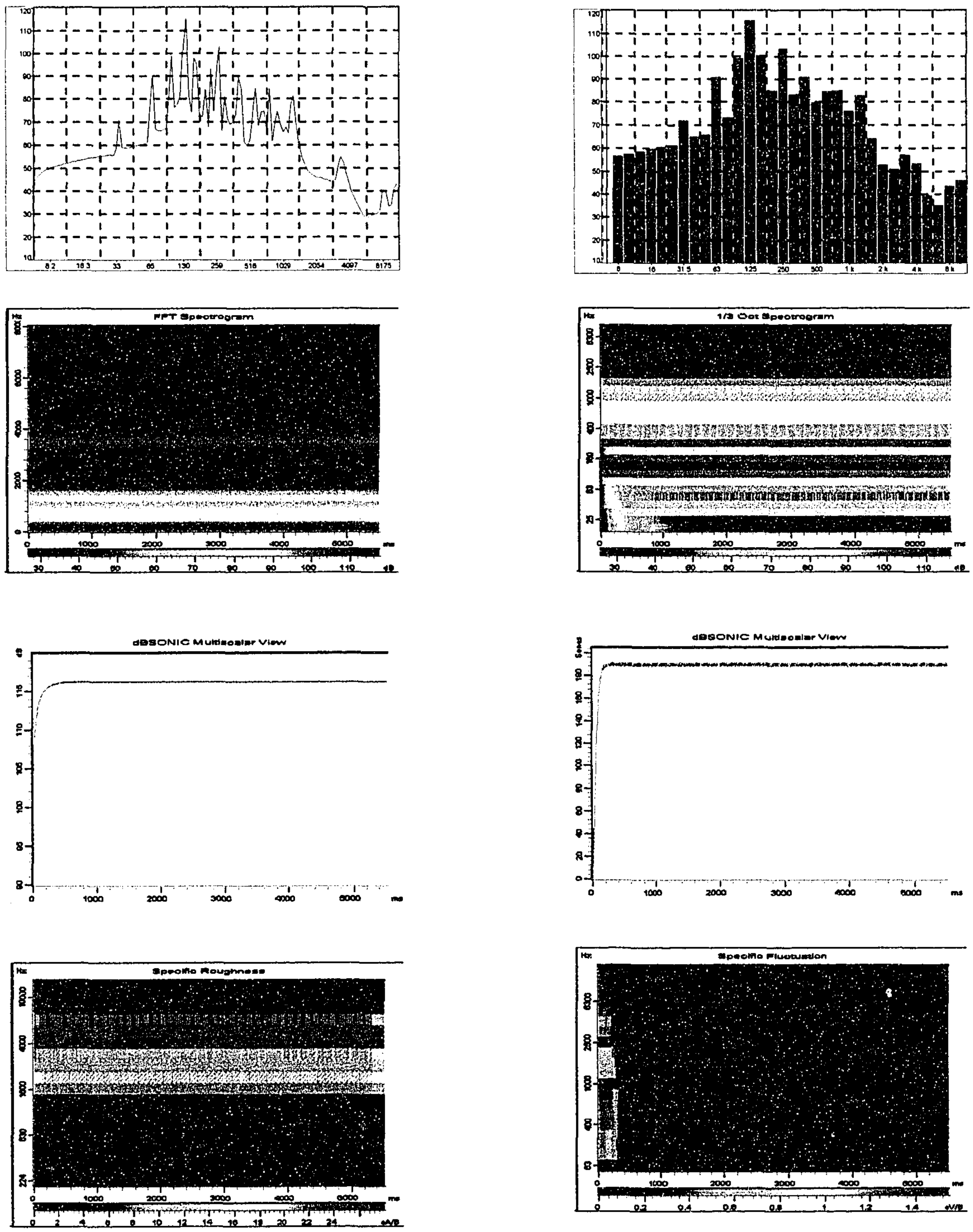

EXHIBIT D21 - Numerical Unmodified Results at 4000 rpm

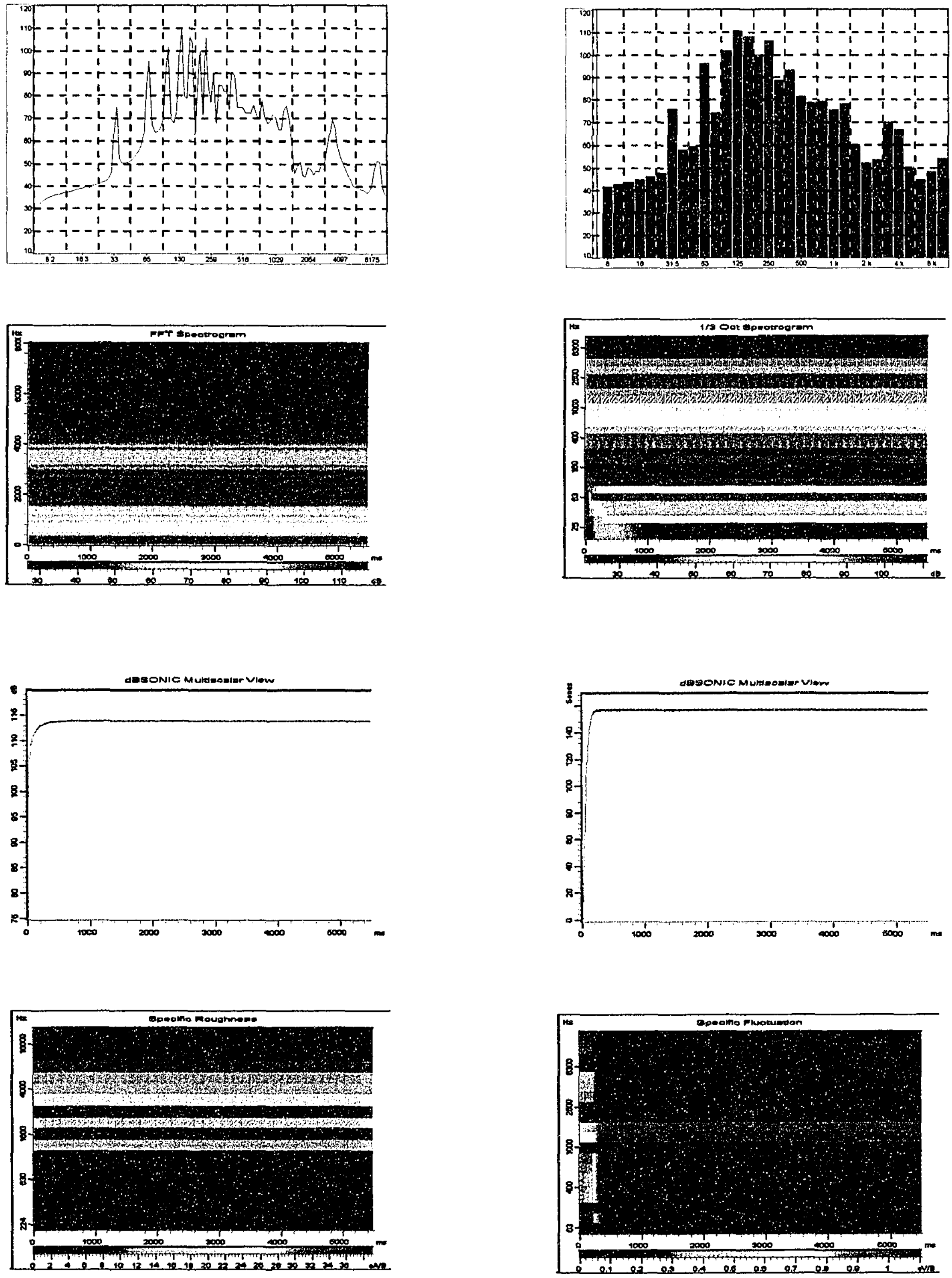

EXHIBIT D22 - Numerical Bridged Results at 4000 rpm

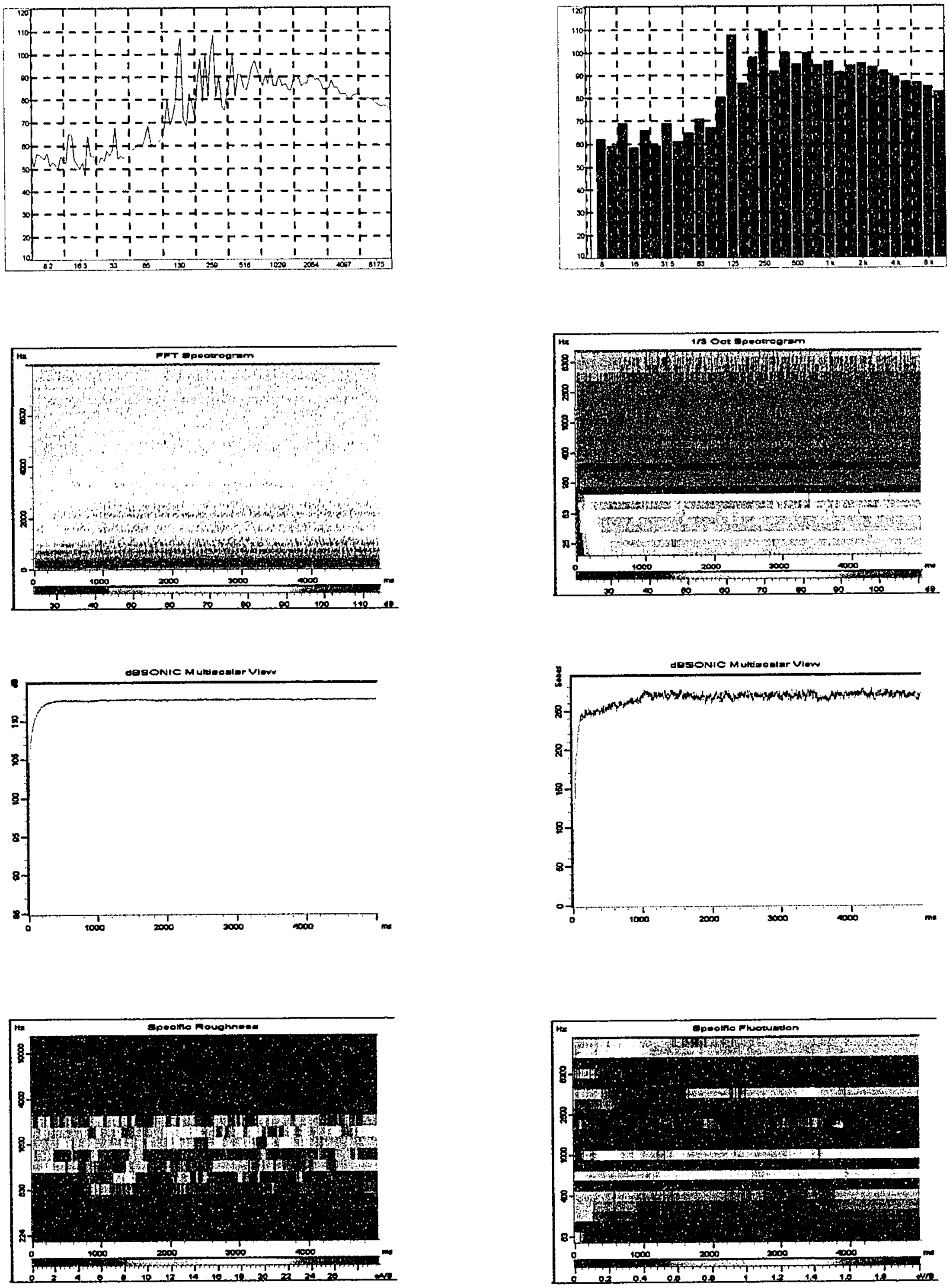

EXHIBIT D23 - Experimental Unmodified Results at 4000 rpm

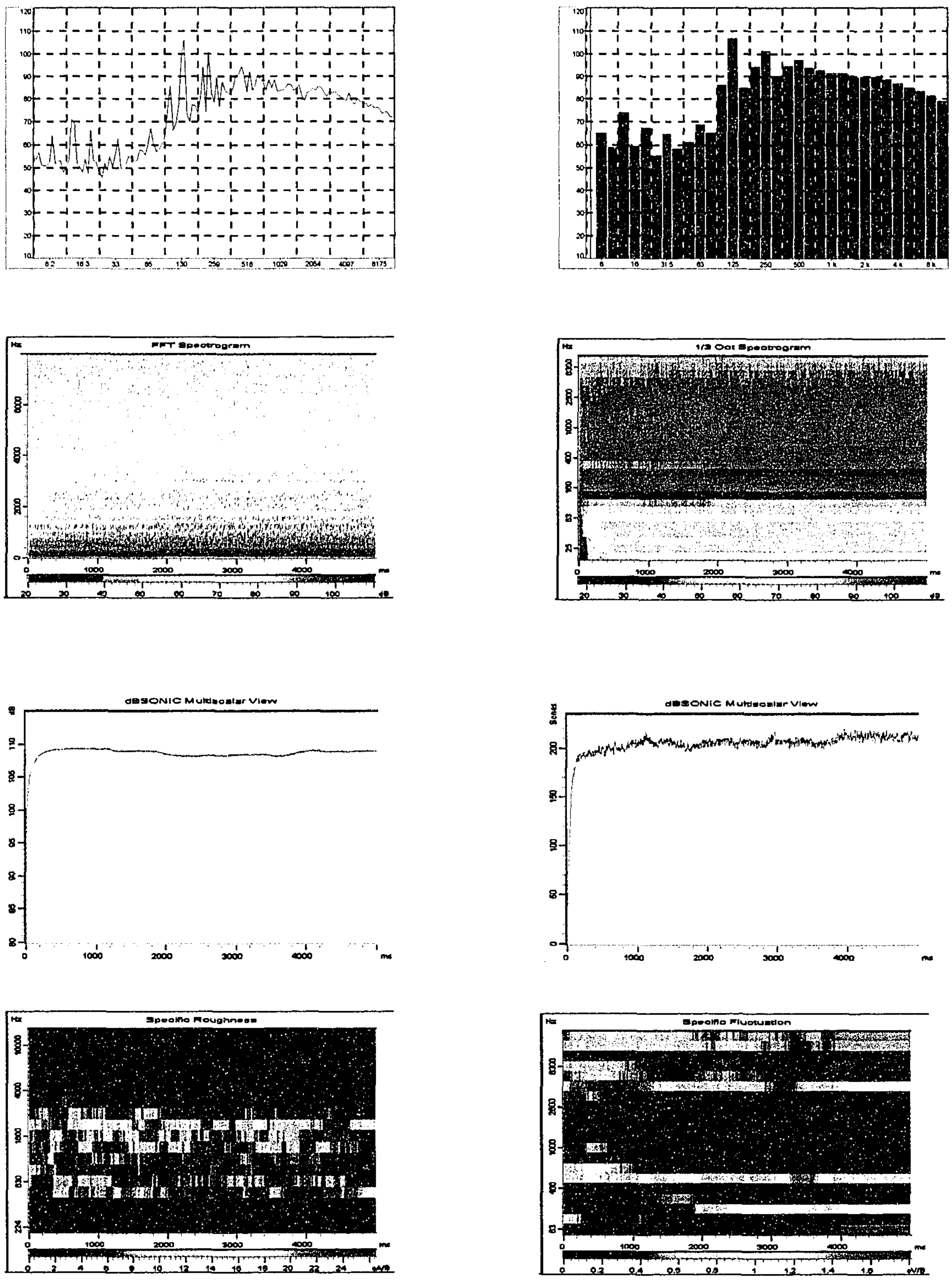

EXHIBIT D24 - Experimental Bridged Results at 4000 rpm

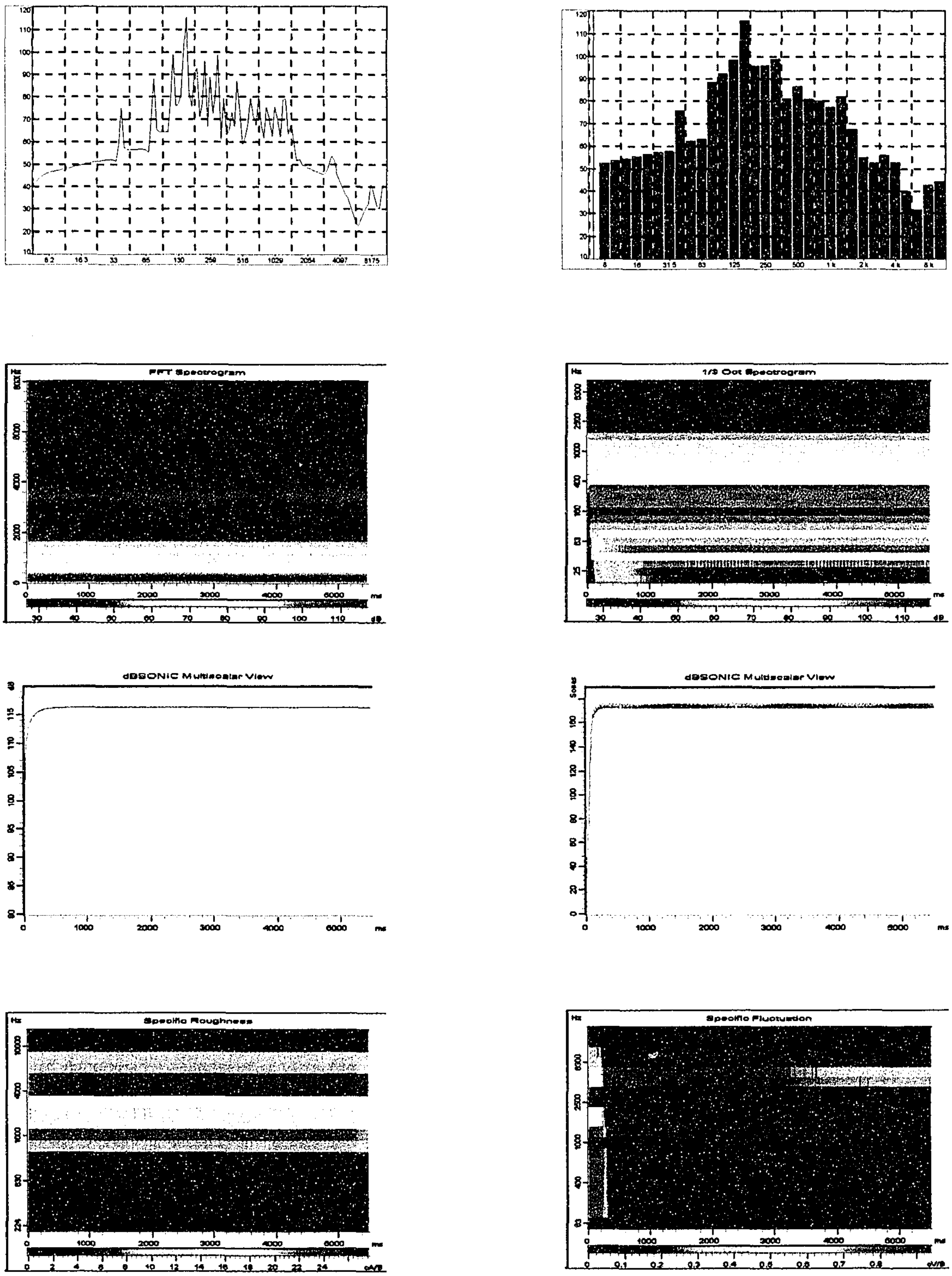

EXHIBIT D25 - Numerical Unmodified Results at 4500 rpm

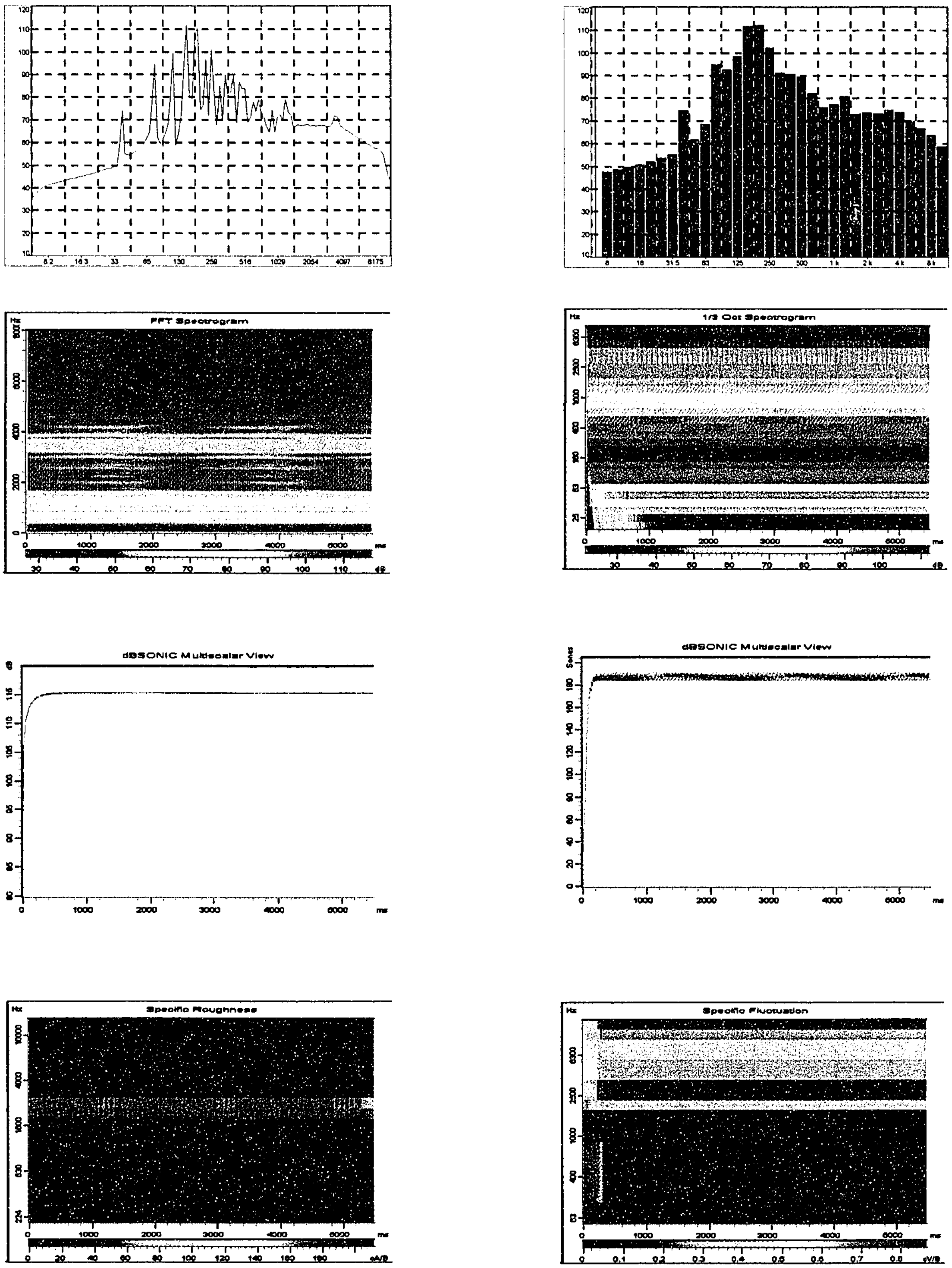

EXHIBIT D26 - Numerical Bridged Results at 4500 rpm

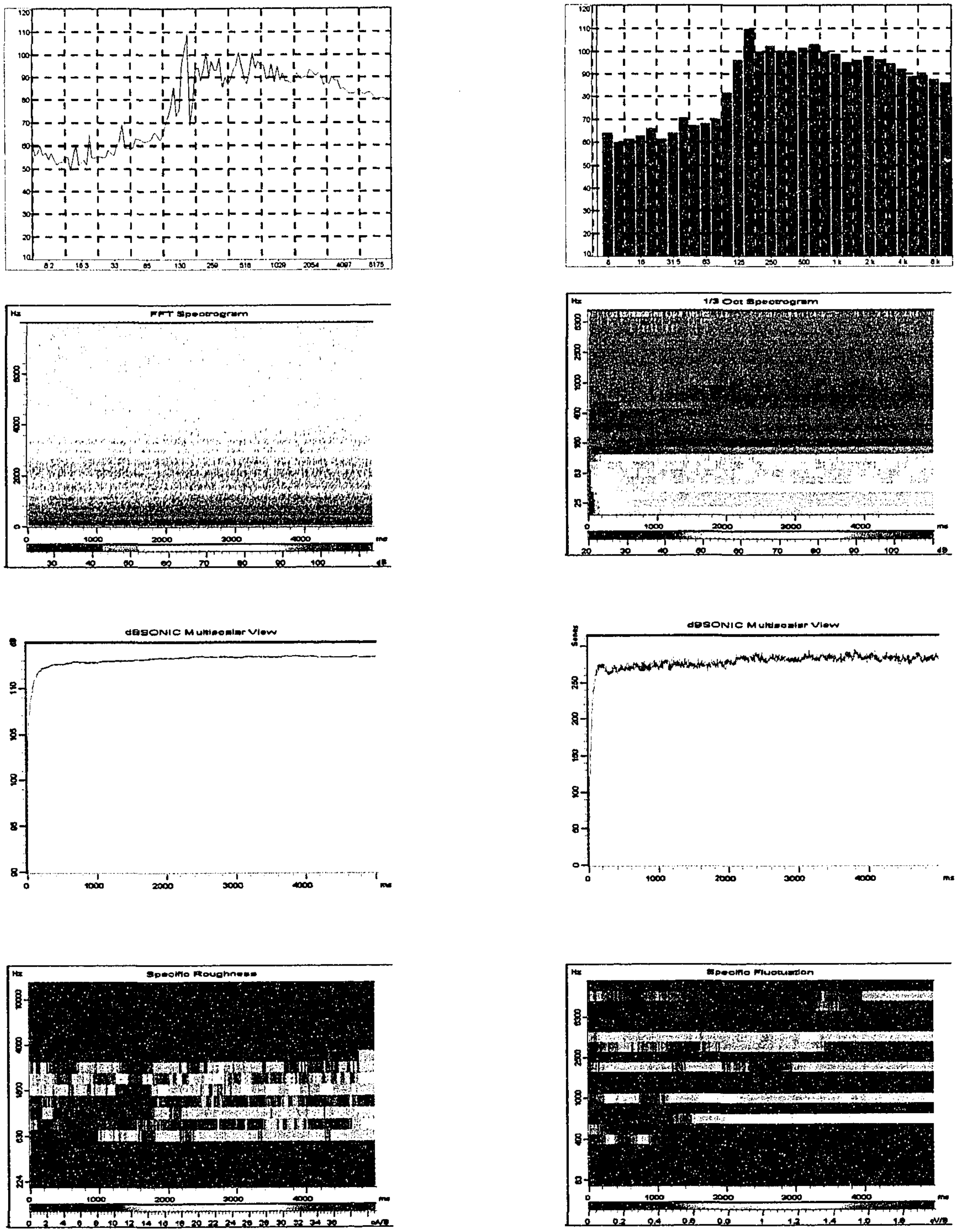

EXHIBIT D27 - Experimental Unmodified Results at 4500 rpm

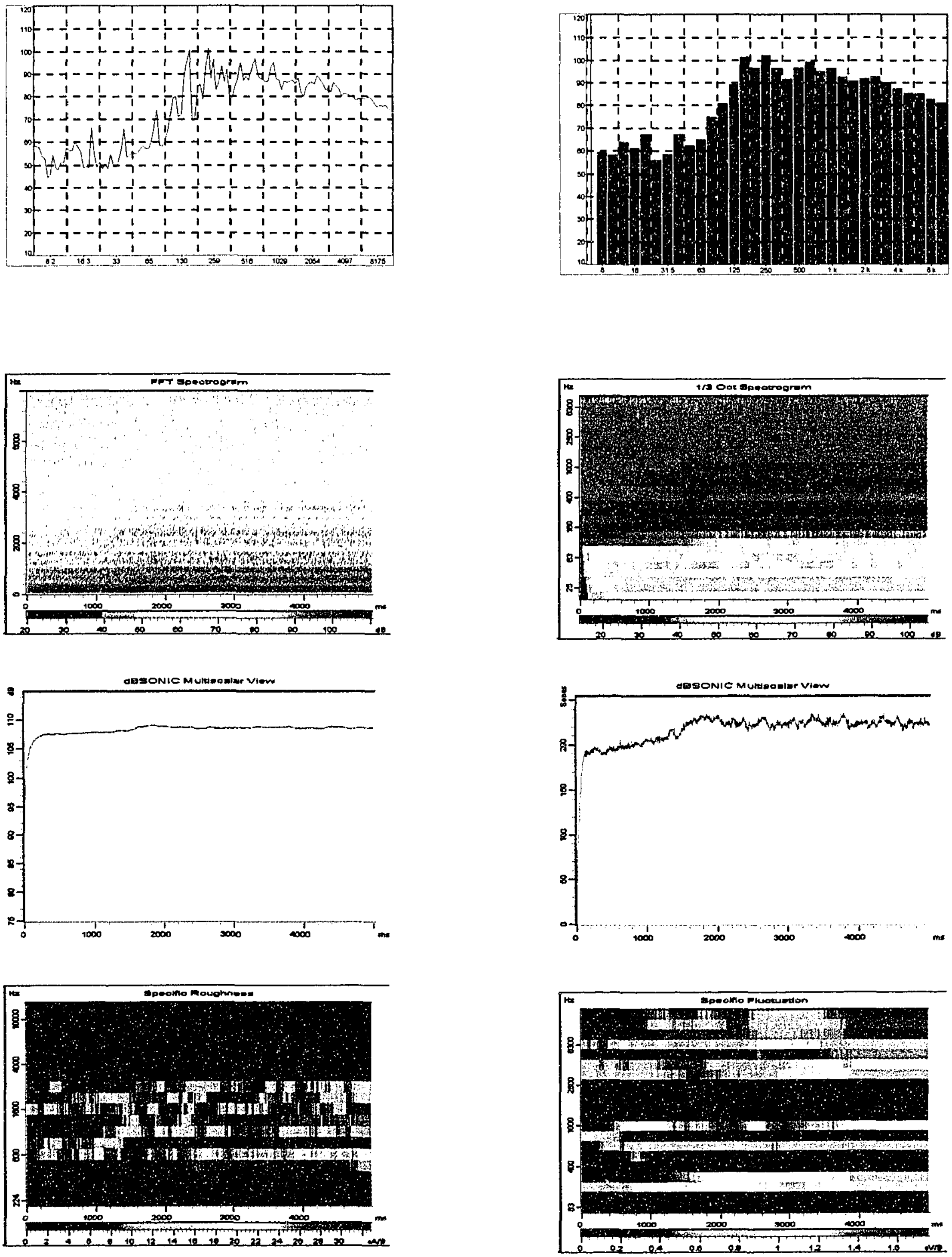

EXHIBIT D28 - Experimental Bridged Results at 4500 rpm

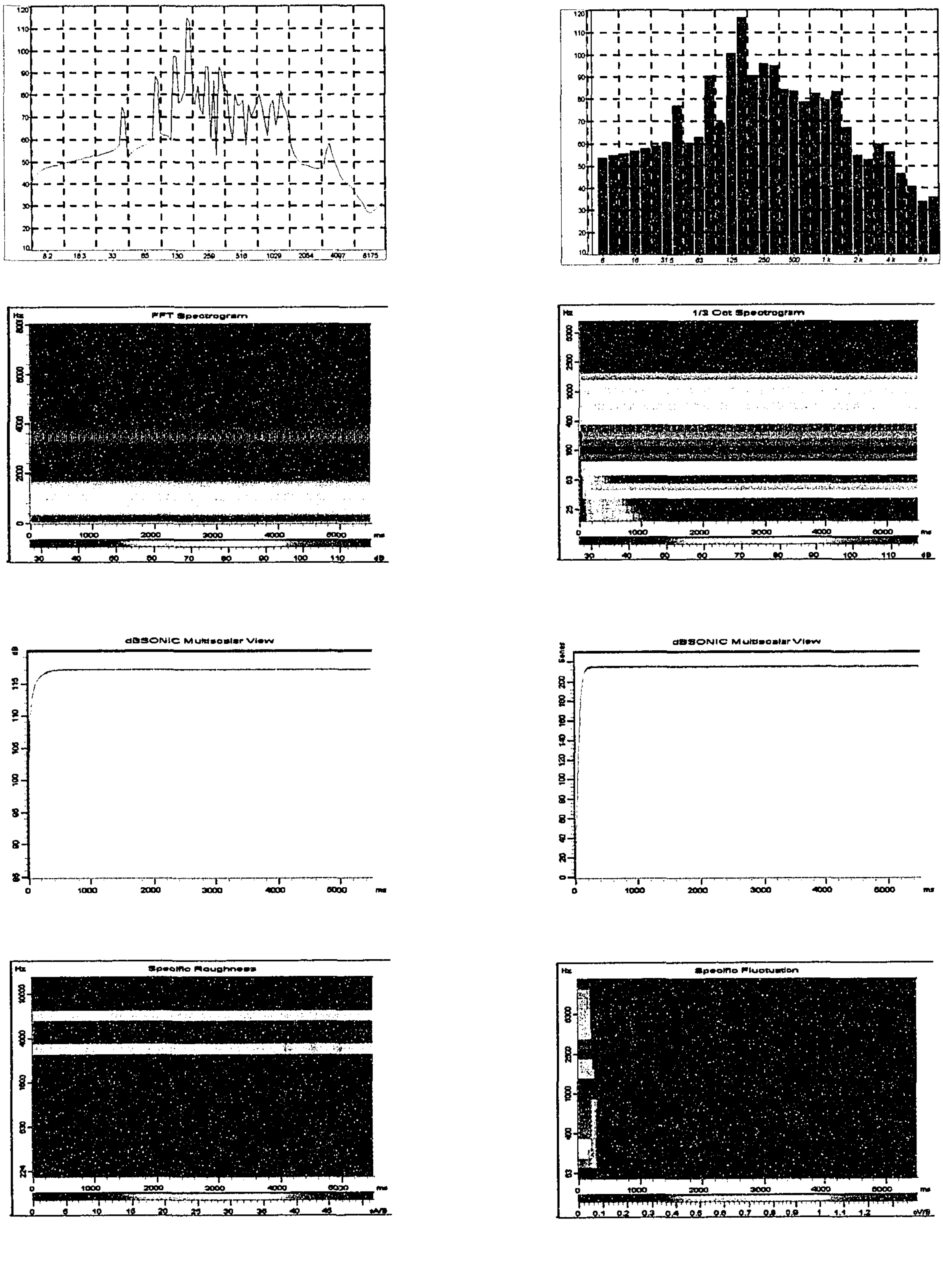

EXHIBIT D29 -Numerical Unmodified Results at 5000 rpm

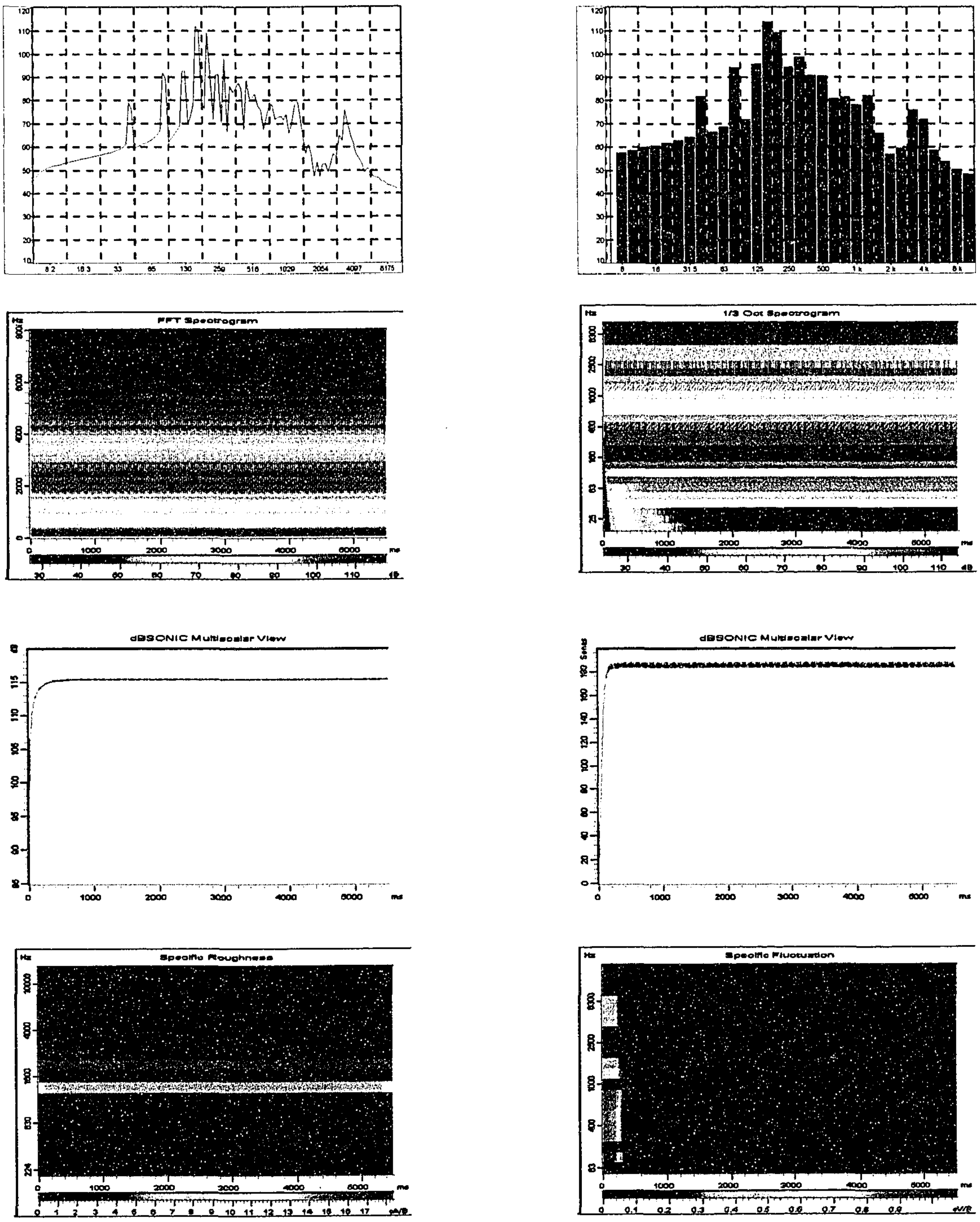

EXHIBIT D30 -Numerical Bridged Results at 5000 rpm

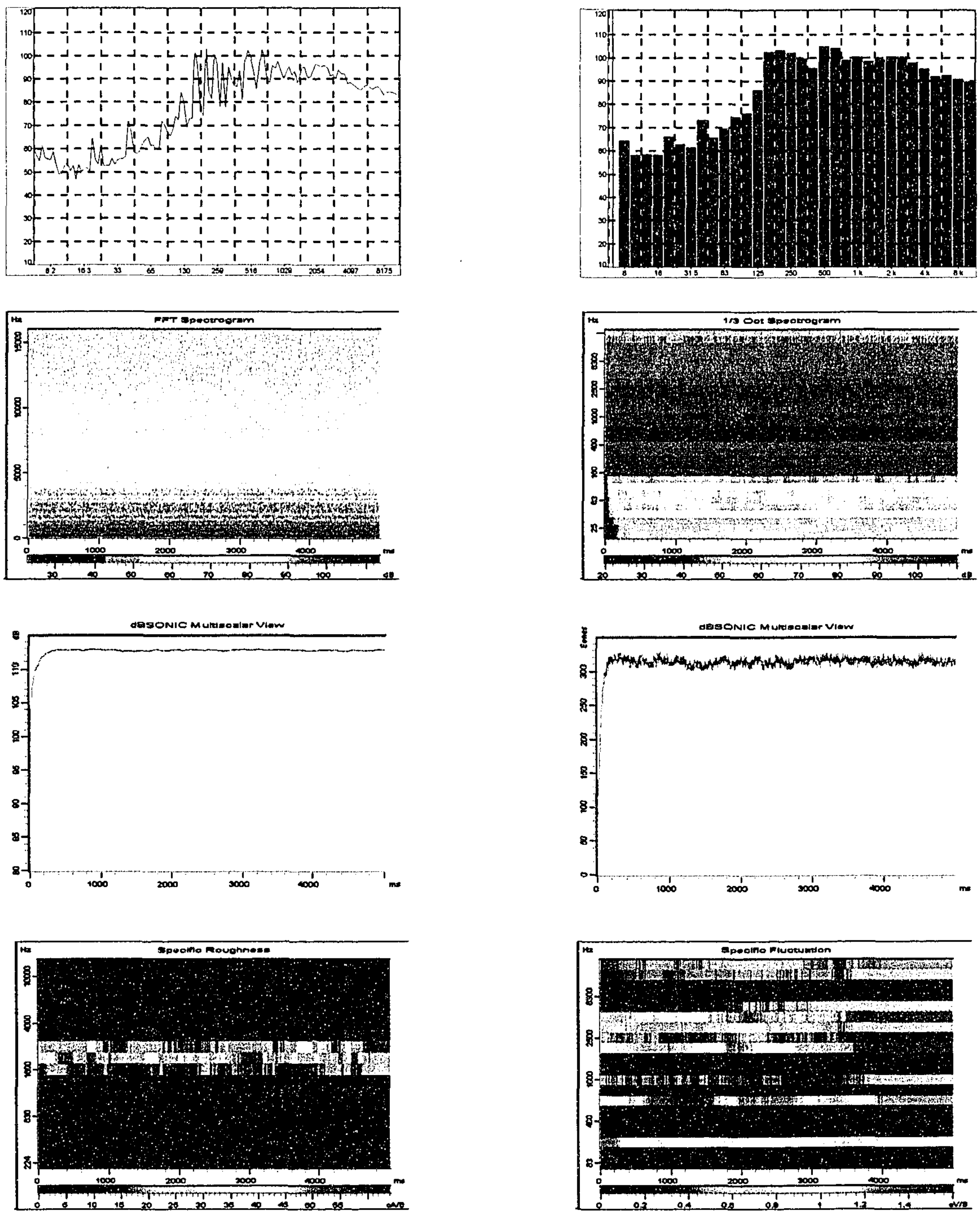

EXHIBIT D31 -Experimental Unmodified Results at 5000 rpm

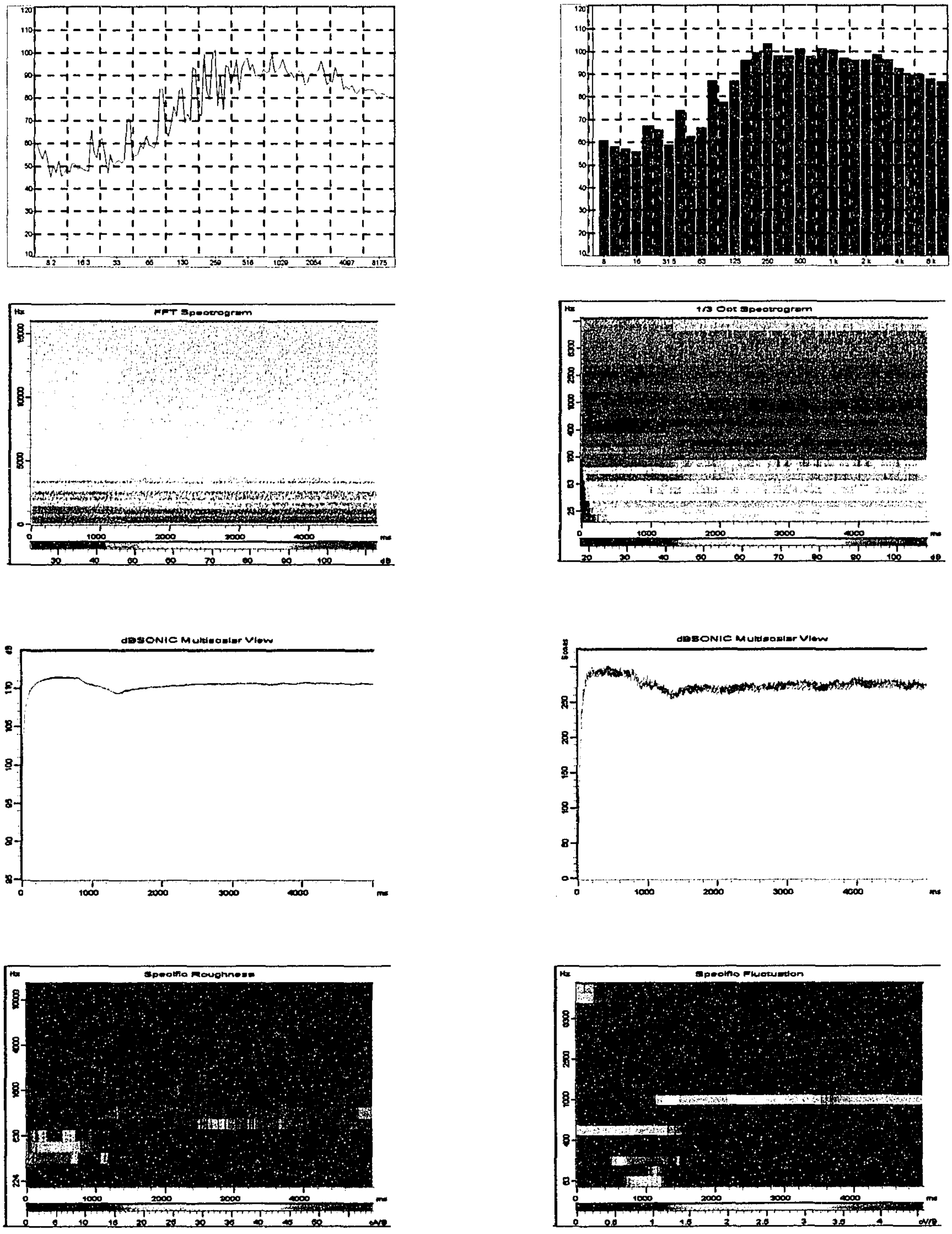

EXHIBIT D32 -Experimental Bridged Results at 5000 rpm

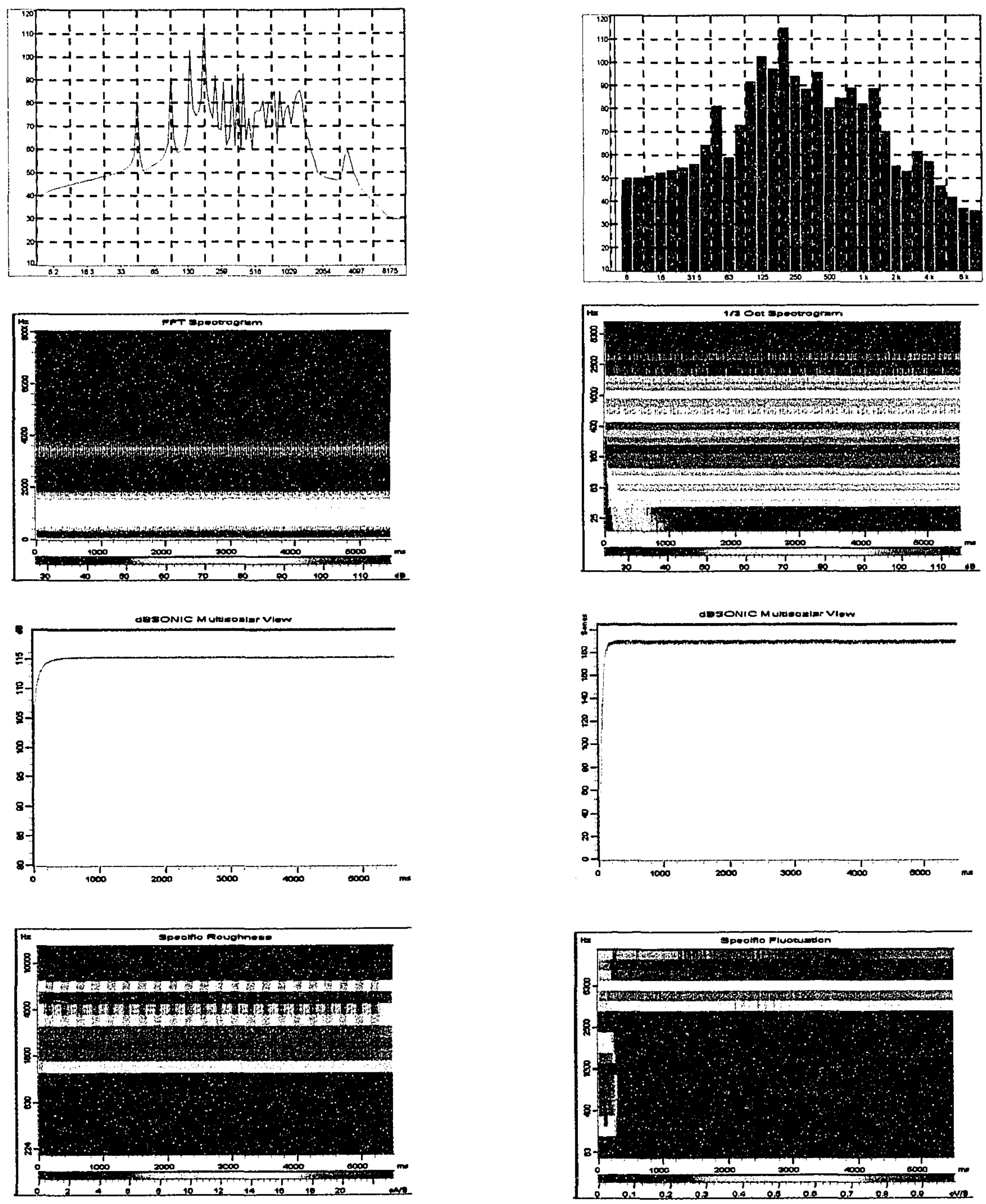

EXHIBIT D33 -Numerical Unmodified Results at 5500 rpm

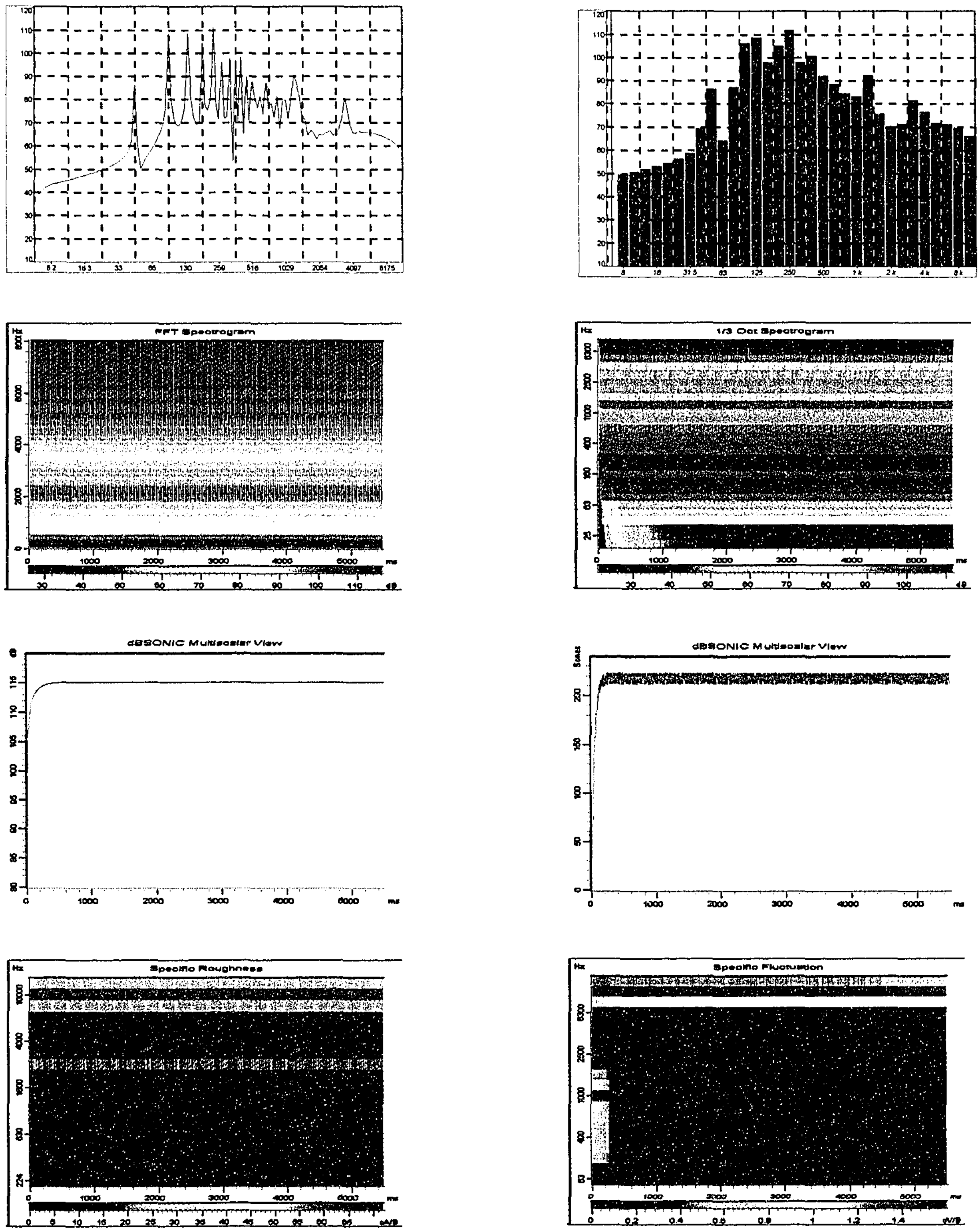

EXHIBIT D34 -Numerical Bridged Results at 5500 rpm

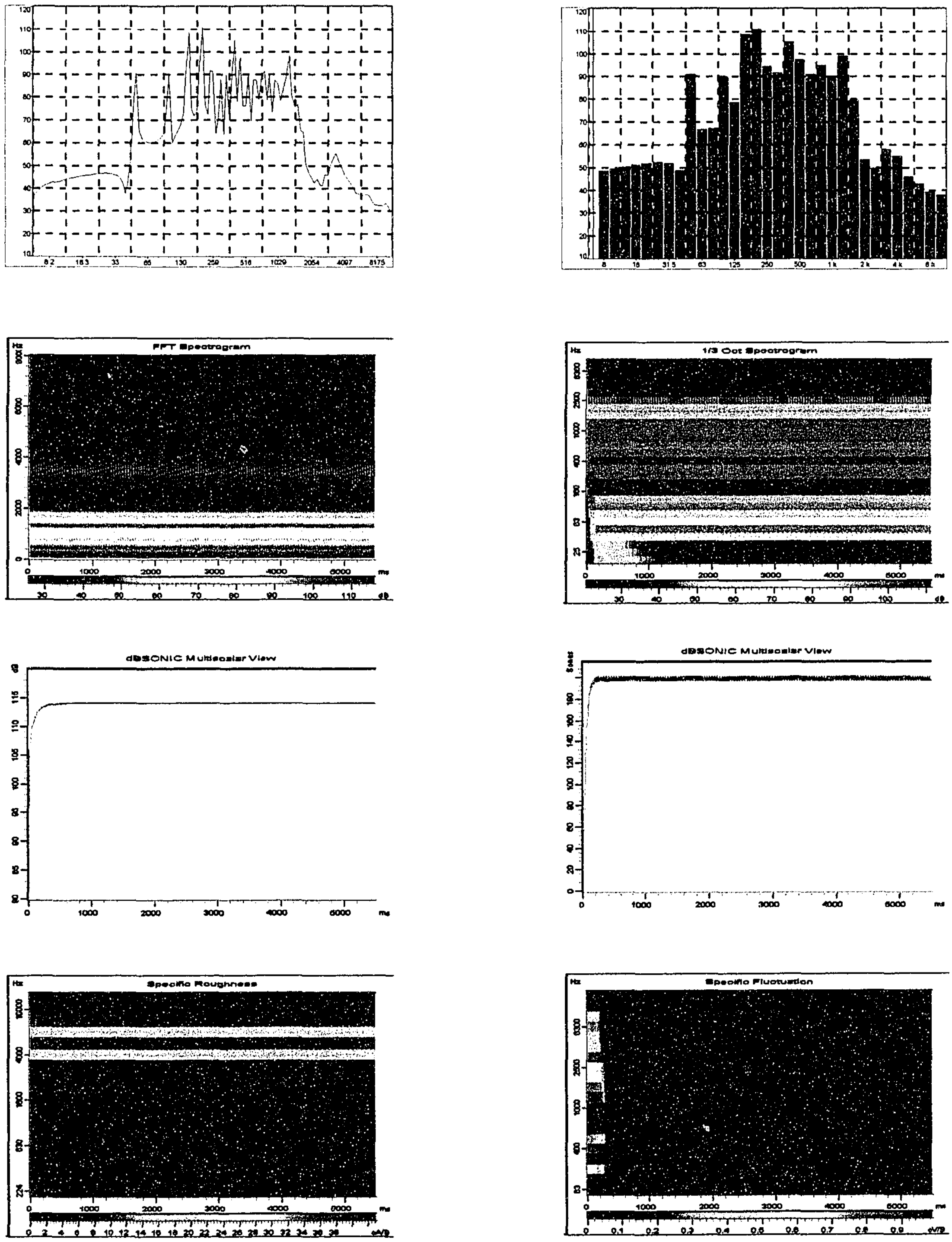

EXHIBIT D35 -Numerical Unmodified Results at 6000 rpm

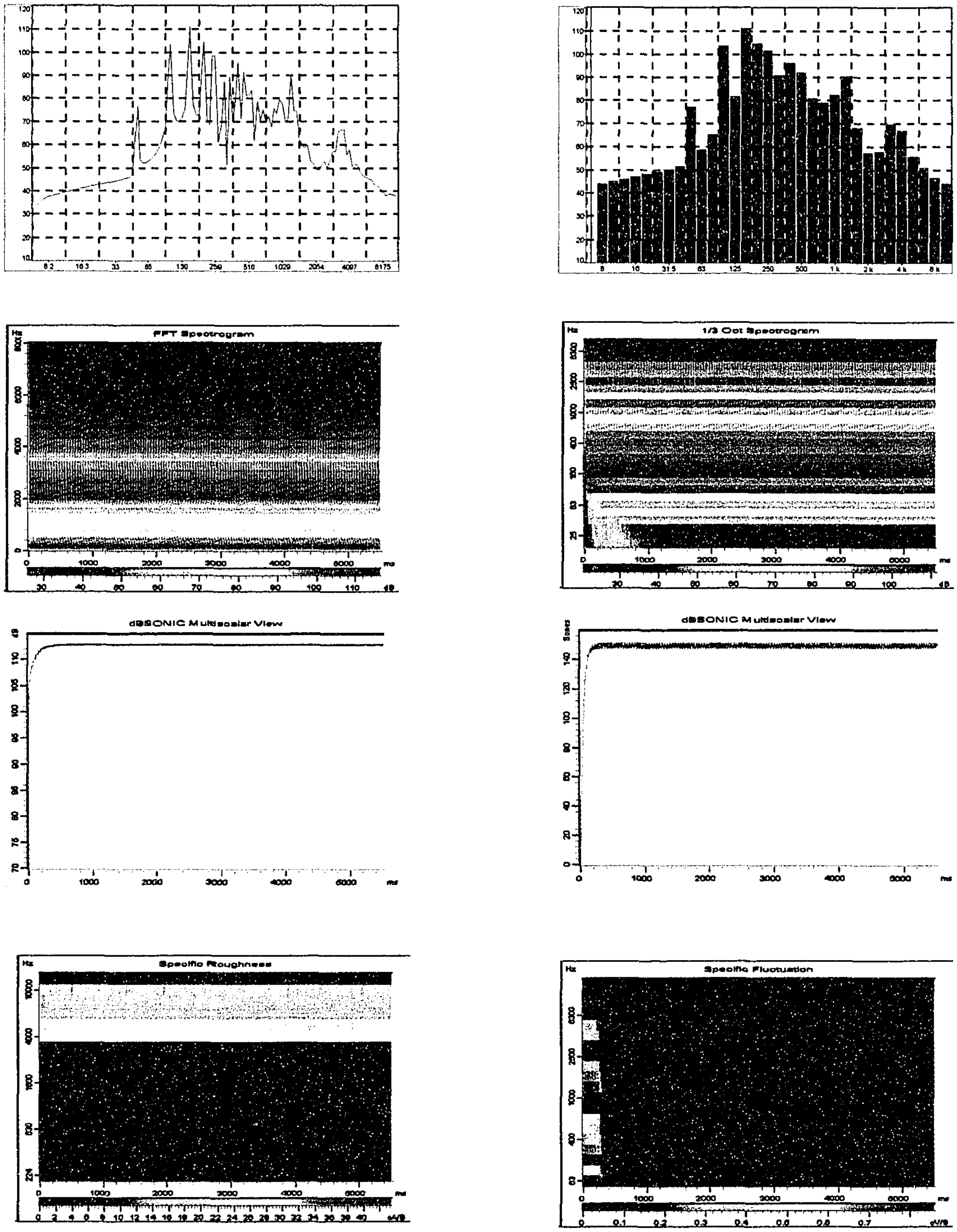

EXHIBIT D36 -Numerical Bridged Results at 6000 rpm

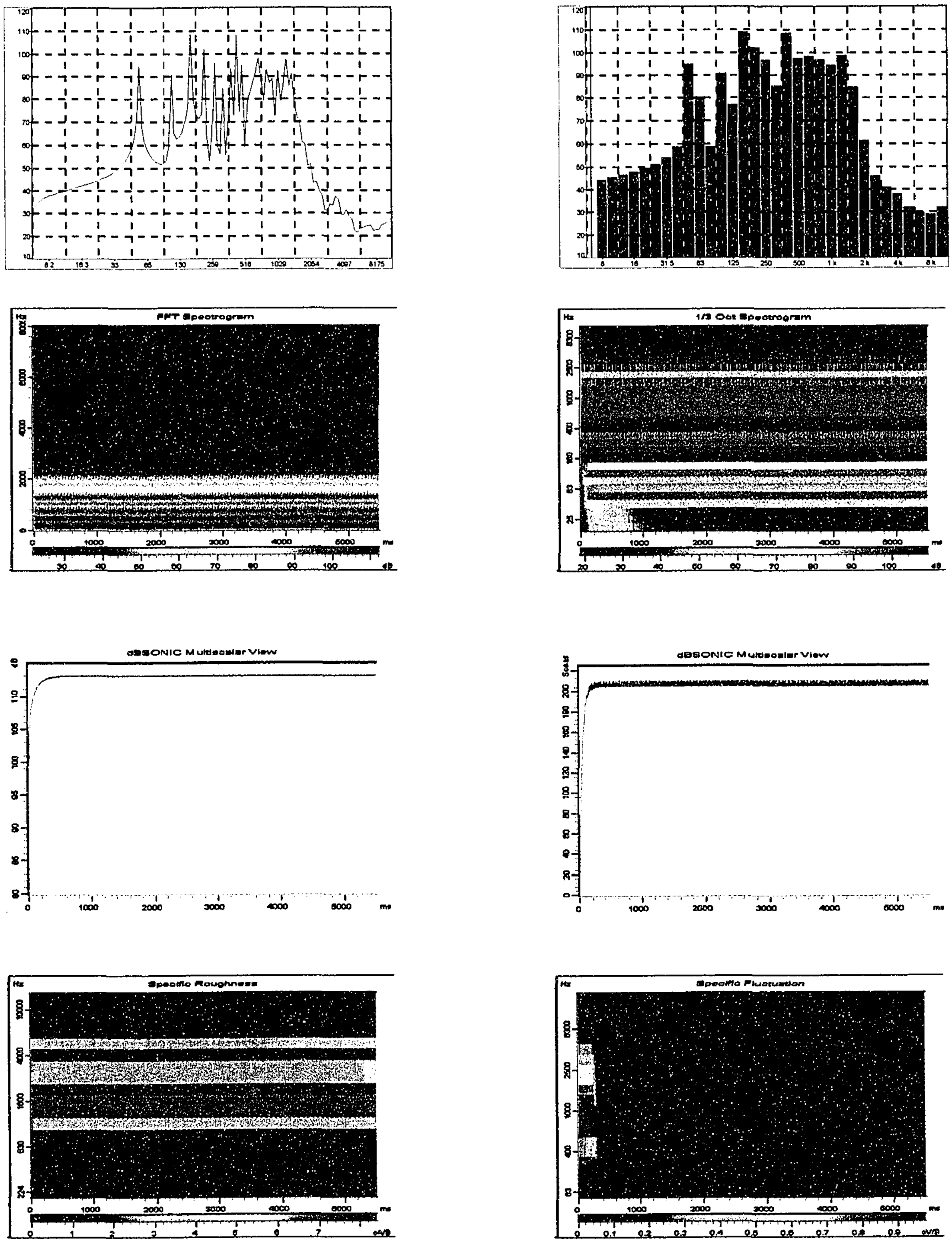

EXHIBIT D37 -Numerical Unmodified Results at 6500 rpm

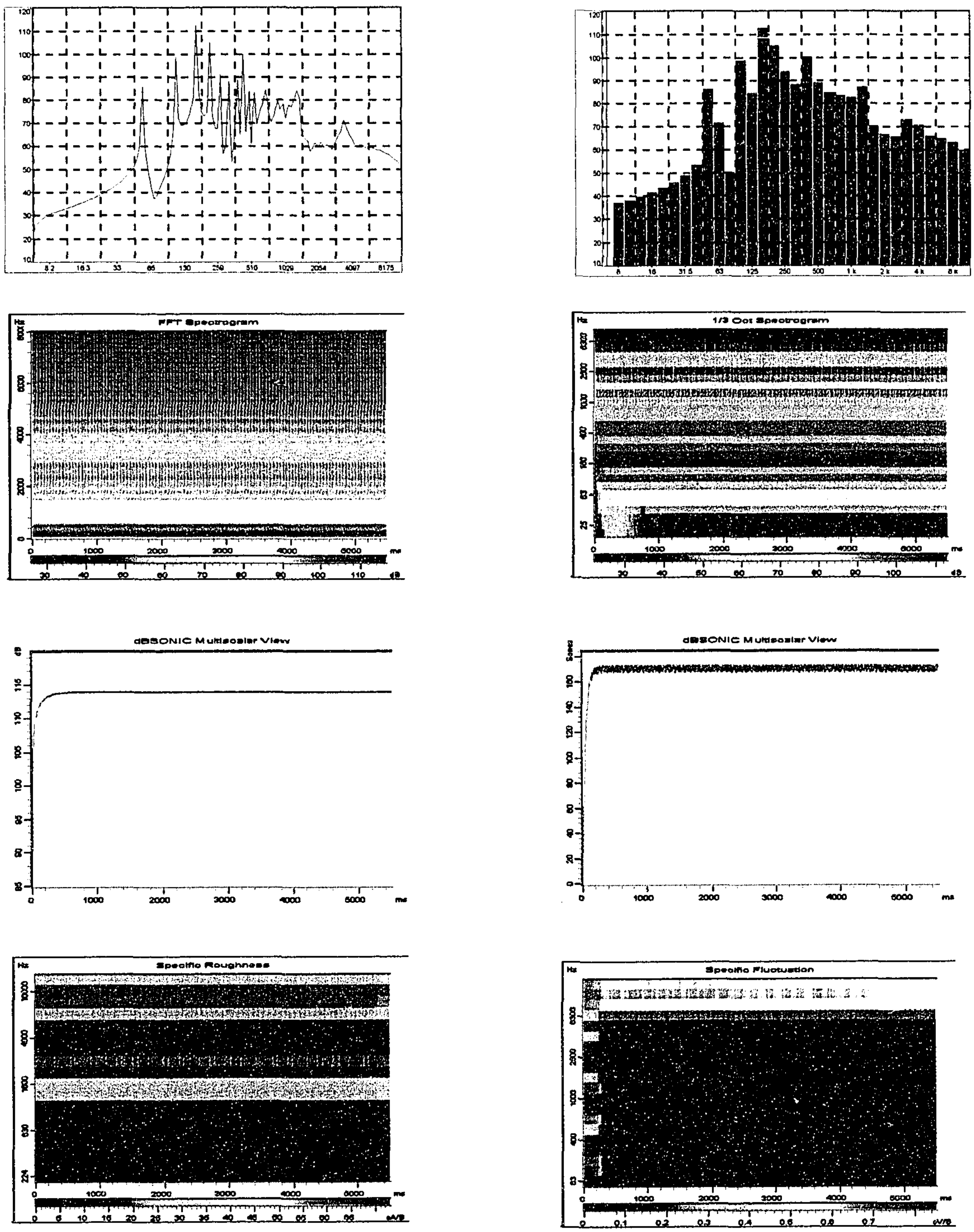

EXHIBIT D38 -Numerical Bridged Results at 6500 rpm

VITA AUCTORIS

1968	Born in Toronto, Ontario on February 20.
1987	Received OSSGHD from Brampton Centennial Secondary School.
1991	Received Degree of Bachelor of Applied Science from the University of Windsor, Windsor, Ontario.
1993	Received Professional Engineer Licence from the Association of Professional Engineers of Ontario.
1996	Received Degree of Master of Applied Science at the University of Windsor, Windsor, Ontario.
2003	Joined the Faculty of Engineering at the University of Windsor with the rank of Lecturer.
2005	Candidate for the Degree of Doctor of Philosophy at the University of Windsor, Windsor, Ontario.